



The
University
Of
Sheffield.

Gasification of Coal and Biomass Char Using a Superheated Steam Flame

By:

Thomas Edward Lakey, MEng (Hons), AMIChemE, GradEI

A thesis submitted in partial fulfilment of the requirements for the degree of
Doctor of Philosophy

The University of Sheffield
Faculty of Engineering
Department of Chemical and Biological Engineering

October 2016

Acknowledgements

I would like to thank my supervisors Professor Vida N. Sharifi and Professor Jim Swithenbank for the opportunity to undertake this research work, and their continued guidance throughout the project. Also thanks to Dr Yajue Wu for taking over supervisory duties after Professor Sharifi's retirement.

I would also like to extend thanks and gratitude to the technical staff of the University of Sheffield, in particular Mr David Palmer and Mr Mike O'Meara for their invaluable input in bringing this project to fruition.

Finally, thanks and appreciation are extended to the Engineering and Physical Sciences Research Council (EPSRC) for providing the funding which made this work possible and to Carbon Compost Co. for provision of softwood char material used in this experimental work.

Summary

Gasification of coal or biomass can produce hydrogen rich synthetic gas (syngas) for use in fuel cells, liquid fuels or chemicals. While coal gasification is well established, biomass gasifiers have been hindered by costs and difficulties such as tar and ash deposition. Ultra-Superheated Steam (USS) has been proposed as an economical method to maximise gasification temperatures and hydrogen yields. A novel entrained flow USS gasification system showed promise with coal in a previous investigation.

The main objectives were to investigate how a USS gasification system produced high hydrogen yields and feedstock conversion within a short residence time. Secondly, apply the system to biomass gasification for sustainable hydrogen production.

The principle tasks were to identify the factors affecting the product composition, and experimentally compare the conversion and yields from coal and biomass materials. Numerical software was used to investigate gas and particle behaviour inside the burner.

Coal and a unique high ash softwood char were successfully gasified. Char yielded up to 34.9%mol H₂ and 25.1%mol CO in the dry gas, demonstrating higher conversion and yields than coal despite lower feedstock heating value and feeding rates. Biomass ash was considered to catalyse char conversion. No detrimental effect was observed from ash deposition, which was dry and easily removed.

A fluid model mapped temperature distribution, showing good correlation with validation measurements and supporting the observation that wall temperature greatly affected particle conversion. Particle residence times were inversely proportional to particle diameter and density.

High ash biochar showed greater conversion than coal. Economic analysis revealed the system would be most competitive on an existing site with available feedstocks and steam. A longer reactor would increase time for homogeneous reactions to play a greater role. With further development this technology has potential to produce hydrogen competitively on a commercial scale.

Table of Contents

Acknowledgements	ii
Summary	iii
List of Figures	x
List of Tables.....	xiv
Nomenclature	xvi
Greek Letters.....	xvii
Super / Subscripts.....	xvii
Acronyms	xviii
1 INTRODUCTION	1
1.1 Global Energy Demand.....	1
1.2 Traditional Electricity Generation	2
1.2.1 Coal Power	2
1.2.2 Natural Gas	3
1.2.3 Nuclear Power.....	4
1.3 Renewable Energy Sources.....	5
1.3.1 Wind and Solar Power.....	5
1.3.2 Biomass Energy.....	5
1.3.3 Hydrogen Fuel.....	6
1.3.4 Waste to Energy Systems	6
1.4 Efficient Energy Use	7
1.4.1 Large Scale Energy Storage	7
1.4.2 Combined Heat and Power (CHP).....	8
1.5 Environmental Concerns	9
1.5.1 Global Warming	9
1.5.2 Observable Environmental Effects	10
1.5.4. Environmental Targets.....	11
1.6 The Cost of Power	11
1.7 The Hydrogen Economy	13
1.8 Objectives of Research	14
1.9 Layout of Report	15
1.10 Summary.....	15
2 LITERATURE REVIEW	17

2.1	Gasification Feedstocks	17
2.1.1	Coal.....	18
2.1.2	Biomass.....	21
2.2	Thermal Technologies	23
2.2.1	Combustion.....	23
2.2.2	Pyrolysis.....	25
2.2.3	Coal Gasification.....	27
2.2.4	Commercial Biomass and Waste Gasification Systems	34
2.2.5	Feedstock Preparation.....	36
2.3	Legislation.....	36
2.3.1	International Agreements.....	36
2.3.2	Carbon Capture and Storage (CCS).....	37
2.3.3	UK National Policies.....	38
2.4	Gasification Research	40
2.4.1	Tar Destruction Methods.....	40
2.4.2	Influence of Gasification Medium	41
2.4.3	Catalytic Aides for Gasification	43
2.4.4	Method of Heat Input.....	45
2.5	Summary of Literature	49
3	THEORY	51
3.1	General Gasification Chemistry	51
3.1.1	Thermodynamics of Gasification.....	52
3.1.2	Measures of Efficiency.....	56
3.1.3	Gasification Kinetic Theory	57
3.1.4	Kinetic Models.....	60
3.2	Flame Theory	60
3.2.1	Flame Fundamentals	60
3.2.2	Flame Structure	61
3.2.3	Flame Stabilisation Using a Burner Quarl	62
3.2.4	Adiabatic Flame Temperature.....	62
3.3	Steam Theory.....	63
3.3.1	Saturation and Superheat.....	63
3.3.2	Dissociation of Water	63
3.3.3	The Effect of Water Vapour on Hydrocarbon Flames	64

3.3.4	The Effect of Steam Addition on Burning Velocity	65
3.3.5	Ultra-Superheated Steam	66
3.3.6	Steam Reforming of Hydrocarbons	67
3.4	Heat Transfer	67
3.4.1	Radiative Heat Transfer	68
3.5	Analysis Methods	69
3.5.1	Gas Chromatography.....	69
3.5.2	High Temperature Thermocouple Error	69
3.6	Summary.....	70
4	PROCESS MODELS AND SIMULATION	71
4.1	Stoichiometric Equilibrium Model	71
4.1.1	Independent Equations for Stoichiometric Equilibrium Model	72
4.1.2	Solution of Independent Equations.....	73
4.2	Equilibrium Model using Process Software	74
4.2.1	Model Input Parameters.....	75
4.3	Equilibrium Simulation Sensitivity Analyses	76
4.3.1	The Effect of Steam Flow on Product Composition.....	76
4.3.2	The Effect of Temperature on Product Composition	77
4.3.3	The Effect of Steam/Carbon Ratio on Carbon Conversion	78
4.3.4	Simulation 1B Model Parameters	80
4.3.5	The Effect of Hydrocarbon Combustion on the CO ₂ Yield	81
4.3.6	Implications for Experimental System.....	81
4.4	Kinetic Process Model	82
4.4.1	Kinetic Model Flow Sheet	82
4.4.2	Configuration of <i>RPlug</i>	83
4.4.3	Results of <i>RPlug</i> Simulation	84
4.5	Computational Fluid Model.....	85
4.5.1	Constructing the Model.....	86
4.5.2	Mesh Independence Study	87
4.5.3	Selection of Model Parameters.....	88
4.5.4	Boundary Conditions	89
4.5.5	Results of Combustion Simulation	90
4.5.6	Particle Tracking	92
4.6	Summary of Simulations.....	97

4.6.1	Equilibrium Model Findings	97
4.6.2	Kinetic Model Findings	98
4.6.3	Computational Model Findings.....	98
4.6.4	Model Validation Measurements.....	100
5	EXPERIMENTAL PROGRAMME	103
5.1	Gasification System	103
5.1.1	Description of Gasifier	103
5.1.2	Steam Generator	105
5.1.3	Steam Flow Control and Metering	106
5.1.4	Feedstock Hopper and Screw Feeder	108
5.1.5	Gas Flow Control and Metering	110
5.2	Selection of Gasification Feedstock	111
5.2.1	Description of Analytical Tests	112
5.2.2	Results of Feedstock Analyses	114
5.3	Commissioning the Gasifier	116
5.3.1	Steam Supply and Dryness.....	116
5.3.2	Air/Oxygen Mixing Point.....	118
5.3.3	Replacement of the Burner Quarl	119
5.4	Gasifier Operating Procedures.....	120
5.4.1	System Start Up.....	120
5.4.2	System Shut Down.....	122
5.5	Experimental Procedure.....	123
5.5.1	Mass Flow Calculation	123
5.5.2	Mass Balance.....	123
5.5.3	Temperature Monitoring.....	123
5.6	Experimental Uncertainty.....	126
6	EXPERIMENTAL RESULTS AND DISCUSSION	128
6.1	Tuning Gasification Parameters.....	128
6.1.1	Runs I and II: Replicating Previous Work	129
6.1.2	Runs III and IV: Increasing the Equivalence Ratio	132
6.1.3	Runs V and VI: The Effect of Temperature.....	132
6.2	Effect of Fuel Gas	133
6.3	Gasification Feedstock Experiments	134
6.3.1	Gasifier Temperature Distribution	134

6.3.2	Results of Varying S/C Ratio.....	136
6.3.3	Mass Balance Results.....	138
6.3.4	Energy Balance Calculation.....	139
6.3.5	Gas Residence Time.....	142
6.3.6	Feedstock conversion	143
6.3.7	Gasifier Efficiency	146
6.3.8	Ash Deposition	147
6.4	Summary of Experimental Results	148
7	DISCUSSION AND EVALUATION.....	149
7.1	Equilibrium Model Discussion.....	149
7.1.1	Coal Conversion.....	149
7.1.2	Chemical Kinetics.....	150
7.2	Similar Superheated Steam Models.....	150
7.2.1	Ultra-Superheated Steam Composition.....	152
7.2.2	Operation with Sub-Stoichiometric Oxygen	152
7.3	Fluid Model Discussion.....	153
7.3.1	Detailed Modelling Approaches.....	154
7.3.1	Opportunities for Model Development.....	155
7.4	Sawdust Feeding Issues.....	156
7.5	Comparing Experimental Results.....	157
7.5.1	Char Gasification Using Present System	157
7.5.2	Large Scale Updraft Gasifier.....	159
7.6	Economic Analysis.....	160
7.6.1	Value of Products	160
7.6.2	Preliminary Costing of USS Gasification Process.....	162
7.6.3	Alternative Scenarios to Improve Competitiveness	163
7.6.4	Summary of Economic Analysis.....	165
7.7	Considerations for System Scale Up.....	166
7.7.1	Competing Technologies	168
7.7.2	Process Safety	169
7.8	Industrial Applications.....	170
8	CONCLUSION	172
8.1	Recommendations for Future Work	173
9	REFERENCES	175

10	Appendix A – Details of Models.....	191
10.1	Stoichiometric Equilibrium Model	191
10.1.1	Solution of Independent Equations.....	191
10.2	CFD model parameters.....	193
11	Appendix B – Feedstock Material Data	203
12	Appendix C - Supplementary Experimental Work	208
12.1	Gasification Feedstock Options	208
12.1.1	Wood Pellet Pyrolysis	208
12.1.2	Feedstock Analytical Testing.....	210
12.1.3	Comments on Analytical Tests	210
12.1.4	Selection of Feed Materials	211
12.2	Additional Experimental Raw Data	211
12.3	Review of Flame Analysis Methods.....	214
12.3.1	Temperature Measurements.....	214
12.3.2	Species Identification.....	214
12.4	Experimental Spectrometry.....	215
12.4.1	Optical Probe.....	216
12.4.2	Spectral Results	216
12.5	Summary of Flame Analysis.....	218
13	Appendix D - List of Publications	219

List of Figures

Figure 1-1: Population of the world, 1950-2100, medium variant projection (UN DESA, 2015)	1
Figure 1-2: Shares of world primary energy demand, forecast according to most likely 'base case' scenario (BP, 2016).....	2
Figure 1-3: Electricity generation in the United States by type in 2009 (IEA, 2011).	3
Figure 1-4: Estimated global final energy consumption in 2013 (REN21, 2015).....	4
Figure 1-5: Municipal waste treatment by European countries in 2012, data from Eurostat (CEWEP, 2012).....	7
Figure 1-6: (a) Global average temperature trend 1850-2015, (Met Office, 2016); (b) Atmospheric concentrations of greenhouse gases over the last 2,000 years, (IPCC, 2007).	9
Figure 1-7: Average power plant expenses for major US electric utilities (EIA, 2016a).....	12
Figure 2-1: Types of coal, relative abundance and their uses (World Coal Association, 2016)	18
Figure 2-2: 1973 and 2014 shares of world coal consumption (IEA, 2016)	20
Figure 2-3: Products from thermal biomass conversion. Reprinted from (Bridgwater, 2012) with permission from Elsevier.	27
Figure 2-4: Diagram of pressurised Lurgi gasifier. Reprinted from (He et al., 2013) with permission from Elsevier.	28
Figure 2-5: A schematic of the Winkler gasification process.	29
Figure 2-6: Koppers Totzek gasifier (Roland 1952) adapted from (Wikimedia Commons, 2010).....	31
Figure 2-7: Texaco gasification process.	32
Figure 2-8: E-Gas gasifier. Reprinted from (Higman and van der Burgt, 2008) with permission from Elsevier.....	33
Figure 2-9: Electricity generation by main renewable sources since 2000.	39
Figure 2-10: Effect of gasifying medium and temperature on hydrogen yield.....	41
Figure 2-11: Effect of catalyst on supercritical water gasification of sewage sludge. Reprinted from (Chen et al., 2013) with permission from Elsevier.	42
Figure 2-12: (a) Tar yield in product gas from different bed materials, (b) effect of bed materials on gas composition. Reprinted from (Erkiaga et al., 2013) with permission from Elsevier.	44
Figure 2-13: Burner nozzle showing three coal feeding locations. Reprinted from (Yoon and Lee, 2012) with permission from Elsevier.....	46
Figure 2-14: Carbon conversion and cold gas efficiency with feed location for the microwave gasifier. Reprinted from (Yoon and Lee, 2012) with permission from Elsevier.	47
Figure 2-15: (a) Steam/carbon ratio vs product gas composition. Points = experimental data; lines = numerically calculated results. (b) Numerically calculated gas composition vs height in the reactor. Reproduced from (Umeki et al., 2010) with permission from Elsevier.	48
Figure 3-1: Effect of pressure on syngas composition at 1000°C. Reprinted from (Higman and Van der Burgt, 2003) with permission from Elsevier.	53
Figure 3-2: Effects of temperature on syngas composition at 30 bar. Reprinted from (Higman and Van der Burgt, 2003) with permission from Elsevier.	54
Figure 3-3: Effect of equivalence ratio (ER) on the product gas composition. Reprinted from (Gao et al., 2008) with permission from Elsevier.	55
Figure 3-4: Effect of steam/biomass ratio on dry product gas composition. Reprinted from (Erkiaga et al., 2014) with permission from Elsevier.	56

Figure 3-5: The influence of particle size on required residence time for gasification of solid fuel. Reprinted from (Higman and Van der Burgt, 2003) with permission from Elsevier.	60
Figure 3-6: General description of laminar Bunsen burner flame. Reprinted from (Glassman and Yetter, 2008) with permission from Elsevier.	61
Figure 3-7: Burning velocities of 2:1 H ₂ -O ₂ mixtures at 100°C with diluents N ₂ (triangles) and steam (circles). Reprinted from (Koroll and Mulpuru, 1986) with permission from Elsevier.	65
Figure 4-1: Flow sheet of Simulation 1A. USS = Ultra Superheated Steam	74
Figure 4-2: Product gas mole fractions and steam temperature (TUSS) against steam flow. Mole fractions on wet basis; other inputs as per Simulation 1A.	76
Figure 4-3: Syngas exit temperature and composition against propane flow. O ₂ at stoichiometric requirement. Other inputs as per Simulation 1A	77
Figure 4-4: Hydrogen yield, syngas temperature and residual carbon and steam flow rates against propane/oxygen flow rates. CYIELD represents the solid carbon outlet flow rate.....	78
Figure 4-5: The effect of varying coal flow rate on gasifier temperature and yield; all other inputs as per Simulation 1A.....	79
Figure 4-6: Effect of varying propane flow rate in Simulation 1A, with carbon feed rate adjusted to 9 kg/hr.	79
Figure 4-7: Syngas yield on wet basis for Simulation 1B against propane flow rate.....	80
Figure 4-8: Kinetic model flow sheet with plug flow reactor.....	82
Figure 4-9: (a) The burner viewed from below, showing each inlet; (b) the CFD model geometry	86
Figure 4-10: Effect of grid density on temperature and axial velocity in the region of interest. M1, M2 are monitoring points. T= temperature, Ax= axial velocity	87
Figure 4-11: Contour plots of (a) temperature [K] and (b) mole fraction of CO ₂ for methane combustion in synthetic air along central axis of symmetry	90
Figure 4-12: (a) Velocity vectors [m/s] and (b) temperature contours [K] in plane with a synthair jet	91
Figure 4-13: Contour plots of mole fraction of (a) CO ₂ and (b) O ₂ in plane with a synthair jet	91
Figure 4-14: Single 70 µm coal particle residence time and temperature against gasifier length	92
Figure 4-15: Five stochastic paths for single 70 µm coal particle, showing particle temperature against residence time.....	93
Figure 4-16: Particle temperature vs residence time for ten 300 µm particles of (a) particle density 1550 kg/m ³ , (b) particle density 300 kg/m ³ . Gravitational force included.	95
Figure 4-17: Velocity magnitudes (m/s) for 20 particles of 300 µm, (a) 1550 kg/m ³ , (b) 300 kg/m ³ ...	96
Figure 4-18: Turbulent intensity against Y coordinate along the X=0 axis of symmetry. Y=0 represents the top of the burner and Y= -1300 mm is the reactor outlet.....	99
Figure 4-19: Representation of suction pyrometer inserted into quarl space	101
Figure 5-1: Experimental gasification system flow diagram, showing major equipment and safety control valves.....	104
Figure 5-2: Diagram of the experimental gasifier with dimensions in mm. T = thermocouple location	105
Figure 5-3: <i>Wanson Vaporax II</i> steam generator, with steam separator and feed water tank	106
Figure 5-4: The orifice plate removed from the experimental rig, showing damage from corrosion	107
Figure 5-5: The original screw shaft from the screw feeder, showing a reduction in shaft diameter at the lower end, leaving a gap between the shaft and the screw thread.....	108
Figure 5-6: Modified helical agitator extending to the hopper wall	108

Figure 5-7: Calibration of feed system for pulverised coal at various motor speeds, with linear trend line ($R^2 > 0.999$ in each case)	109
Figure 5-8: Screw feeder outlet, (a) the protrusion from the pipe, (b) agglomeration of coal through the screw feeder	109
Figure 5-9: Distributor attached to bottom of screw shaft to avoid coal agglomeration; (a) side view, (b) from below	110
Figure 5-10: Example of new rotameters installed.	110
Figure 5-11: Latvian char before sieving through 125 μm mesh for analytical testing	111
Figure 5-12: Perkin Elmer TGA 4000 used for proximate analysis	112
Figure 5-13: Parr 6200 Calorimeter used to determine gross calorific value	113
Figure 5-14: Particle size distribution of feedstock materials.....	115
Figure 5-15: Schematic of steam supply pipe work	116
Figure 5-16: Photograph of steam supply line	117
Figure 5-17: Data from steam line test, recorded by data logger.....	117
Figure 5-18: Temperature recorded at point (4) with gradual air introduction in steam test 3, recorded by data logger	119
Figure 5-19: (a) wooden mould used for quarl construction, (b) the completed replica quarl	120
Figure 5-20: The ABB PGC2000 gas chromatograph and carrier gas cylinders.....	121
Figure 5-21: Sketch of field of view from burner viewport	124
Figure 5-22: Schematic of suction pyrometer probe, incorporating a high temperature thermocouple within a refractory tube for gas extraction.....	125
Figure 5-23: (top) Suction pyrometer probe and (bottom) simple thermocouple mount for burner	125
Figure 6-1: Photograph of gasifier inside surface with ash deposits before and after sweeping with a brush.....	131
Figure 6-2: Run A1 gas temperature and yield against wall temperature.....	135
Figure 6-3: Diagram of R-type and K-type thermocouple positions, dimensions in mm	136
Figure 6-4: Dry product gas composition against S/C. Solid lines represent coal runs A1-3, dashed lines represent char runs C1-3. Mean of two runs shown with bars representing \pm one standard deviation.	138
Figure 6-5: Energy in and out of gasifier as a percentage of total energy input, from Table 6-9	141
Figure 6-6: View of gasifier inside wall from above, showing ash deposits. After passing a brush across the surface these deposits were easily removed as shown.....	147
Figure 7-1: Temperature distribution in pilot scale updraft gasifier. Reproduced from (Umeki et al., 2010) with permission from Elsevier.....	159
Figure 11-1: Example TGA curve for coal sample.....	203
Figure 11-2: Example TGA curve for softwood char sample.....	204
Figure 11-3: Example TGA curve for oak sawdust sample.....	204
Figure 12-1: Wood pellets as delivered	208
Figure 12-2: Diagram of the pyrolysis equipment (dimensions in mm)	209
Figure 12-3: (a) The pyrolysis unit, showing the feed trough and the end cap adjacent, (b) a sample of wood pellets after pyrolysis.....	209
Figure 12-4: Transmission against wavelength of known light source through glass viewport	215
Figure 12-5: Spectra from (red) propane-air and (green) propane-oxygen-steam flames, collected with probe at outer position.....	216
Figure 12-6: Close view of wavelengths up to 540 nm of Figure 12-5	217

Figure 12-7: Spectra of (red) propane-air, (green) propane-oxygen-steam and (blue) propane-oxygen-steam-coal flames, collected with probe at mid position	218
Figure 13-1: Conference paper presented at EUBCE 2016	220
Figure 13-2: Poster presented at ChemEngDay UK 2015	223

List of Tables

Table 1-1: Estimated Levelized Cost of Electricity (LCOE) for U.S. plants entering service in 2020 (2013 \$/MWh) (EIA, 2015).....	13
Table 2-1: ASTM classification of coals by rank (ASTM, 2012a).....	17
Table 2-2: Coal data by world region, data from (EIA, 2016b).....	19
Table 2-3: Life cycle emissions estimates for electrical generation by fuel type up to 2020. Data from (Weisser, 2007)	22
Table 2-4: Characteristics of biomass thermal treatment processes. Reprinted from (Basu, 2013) with permission from Elsevier.	25
Table 2-5: Typical product weight yields (dry wood basis) obtained by different modes of pyrolysis of wood. Reprinted from (Bridgwater, 2012) with permission from Elsevier.	26
Table 2-6: Summary of coal gasification technologies described.	34
Table 3-1: Principle gasification reactions.	51
Table 4-1: Normalised molar flow rates of the species entering the gasifier.....	72
Table 4-2: Predicted product gas yield from simple stoichiometric equilibrium model at 800 K.....	73
Table 4-3: Summary of input parameters to Simulation 1A	75
Table 4-4: Syngas yield from Aspen Plus simulation 1A compared to previous experimental results. Both are presented on a dry basis. Experimental data from (Shabangu, 2005).....	75
Table 4-5: Input flow rates to Simulation 1B	80
Table 4-6: Dry molar yield for simulations 1A and 1B. Run P1-A data from (Shabangu, 2005).....	80
Table 4-7: Carbon dioxide flow in USS and syngas streams in Simulation 1B	81
Table 4-8: Table of inputs to kinetic model, corresponding to Figure 4-8	83
Table 4-9: Reaction set specified for plug flow reactor	83
Table 4-10: Predicted dry gas yields from different methods.	85
Table 4-11: Input boundary conditions for CFD model. I = turbulence intensity, L = turbulence length scale.....	89
Table 4-12: Wall boundary conditions for CFD model	89
Table 4-13: Residence times for coal particles.....	94
Table 4-14: Residence times for 300 kg/m ³ 'char' particles. Complete tracks represent particles which reached the outlet within the permitted number of time steps. Std Dev = standard deviation.	94
Table 4-15: Residence time of injected particles, including gravitational force	96
Table 4-16: Gas compositions at pyrometer probe inlet from simulation and experiment (%mol dry basis).....	101
Table 5-1: Proximate analysis and calorific value (CV) of gasification feedstock materials ('d.a.f'=dry, ash free basis)	114
Table 5-2: Ultimate analyses of gasification feedstock materials; oxygen from balance of other elements	115
Table 5-3: Sizing results of gasification feedstock materials after sieving < 600 μm. D50 = median particle size.	115
Table 5-4: Results of BET analysis for coal and char samples	116

Table 5-5: Indicated composition of gas standard against measured composition, in %mol. Std. Dev.= standard deviation	126
Table 6-1: Summary of reactant flow rates and gas yields from model validation tests	129
Table 6-2: Synthetic air mixture compositions for Runs I-VI	129
Table 6-3: Reactant flow rates and dry product yields from Run I, Simulation 1B and from previous work (Shabangu, 2005).....	130
Table 6-4: Reactant flow rates (kg/hr) and gas yields (%mol) for methane control runs. ER = equivalence ratio. %O ₂ represents %vol of oxygen in synthair mixture.....	133
Table 6-5: Powdered feedstock experiment conditions; A= anthracite tests, C= softwood char tests	134
Table 6-6: Results of experimental runs A1-3 and C1-3 on a dry molar basis.	137
Table 6-7: Mass balances for coal tests (A1-3) and char tests (C1-3). Data is mean of two repeats.	139
Table 6-8: Heating value of product gas for each run on a dry basis. Data is mean of two repeats..	139
Table 6-9: Total energy flows in and out of gasifier for each run. Data is mean of two repeats. See text for details.	140
Table 6-10: Gas yields from C2 runs, on dry molar basis as recorded by the online GC; dry mass basis and wet mass basis.....	143
Table 6-11: Results of residual solids analyses for available samples. Data is mean of two repeats.	143
Table 6-12: Results of experimental run using low ash softwood char on a dry basis.....	145
Table 6-13: Cold gas efficiencies (CGE) and gross cold gas efficiency (G-CGE) for runs A1-C3. G-CGE includes energy in fuel gas and supplied steam as well as in the feedstock, as shown in Equation 6-2.	146
Table 7-1: Comparison of Ultra Superheated Steam temperatures calculated, simulated or measured across different works	151
Table 7-2: Product gas composition using wood char (Ryu et al., 2004),	158
Table 7-3: Estimate of annual operating costs for gasification system in current format.	162
Table 10-1: Calculation of equilibrium constants for reactions R1 to R3 using data from JANAF tables (National Institute of Standards and Technology, 2000).....	192
Table 10-2: Results of manually converged equilibrium model assuming equilibrium temperature of 800K.....	193
Table 10-3: Fluent input parameters (abridged).....	194
Table 11-1: Surface area statistics for main gasification feedstocks.....	205
Table 11-2: Latvian softwood char ash analysis. Reproduced with permission from NRM Laboratories	206
Table 12-1: Results of proximate analysis of various fuels, as received basis	210
Table 12-2: Results of ultimate analysis of various fuels, as received basis	210
Table 12-3: Example raw experimental data during process development using propane fuel gas. No data available where none presented. T5= gas temperature inside gasifier. T6= gas temperature at gasifier outlet.	212
Table 12-4: Raw data collected during one week (abridged). No data available where none presented. Motor %= percentage of feed motor capacity, used to calculate molar carbon flow by prior calibration. LIQ = liquid collected. Resid= solids collected. T3 = steam supply temperature. ..	213

Nomenclature

A	Pre-exponential constant	-
Bi	Biot number	-
c_p	Specific heat capacity	kJ/kgK,
CV	Calorific value	kJ/kg, MJ/kg
D	Pipe internal diameter	m
d	Diameter	m
E	Activation energy	J
F	Flame speed	m/s
G	Gibbs free energy	J
H	Enthalpy	J
h	heat transfer coefficient	W/m ² K
k	Rate constant	(various)
K	Rotameter correction factor	-
K_e	Equilibrium constant	-
K_w	Water dissociation constant	-
L	Length	m
m	Mass flow rate	kg/s
M	Third body catalyst	-
Nu	Nusselt number	-
n	Number of moles	-
p	Partial pressure	Pa
P	Pressure	Pa
Q, q	Heat	J
r	Reaction rate	mol/dm ³ s
R	Universal gas constant	J/molK
Re	Reynold's number	-
S	Entropy	kJ/kgK
S/C	Steam to carbon molar ratio	-
St	Strouhal number	-
T	Temperature	°C, K
u	Velocity	m/s
v	Volume fraction	-
V	Volume flow	m ³ /s
W	Work	J
x	Dryness fraction, or thickness	-
y	Mole fraction	-
Z	Vortex frequency	s ⁻¹

Greek Letters

α	Thermal conductivity	W/mK
Δ	Change in quantity	-
ε	Emissivity	-
η	Efficiency	%
μ	Viscosity	kg/ms
ρ	Density	kg/m ³
σ	Stefan Boltzmann constant	$5.67 \times 10^{-8} \text{ W/m}^2\text{K}^4$

Super / Subscripts

O	Reactant
$.$	Rate
$'$	Calibrated condition
$"$	Actual condition
c	Cold
e	Equilibrium
fw	Forward reaction
fg	Vaporisation
g	Gas / Vapour
H, h	Heat, hot
i	Reactant species
j	Product species
L	Laminar
l	Liquid
m	Mass
p	Constant pressure process
r	Reverse reaction
s	Solid
T	Turbulent
w	Wall

Acronyms

ASTM	American Society for Testing and Materials	HVDC	High Voltage Direct Current
BET	Brunauer-Emmett-Teller analysis	IEA	International Energy Agency
BFW	Boiler Feed Water	IGCC	Integrated Gasification Combined Cycle
CCGT	Combined Cycle Gas Turbine	IPCC	Intergovernmental Panel on Climate Change
CCS	Carbon Capture and Storage	IPGCC	Integrated Plasma Gasification Combined Cycle
CFC	Chlorofluorocarbon	KBR	Kellogg Brown and Root process
CFD	Computational Fluid Dynamics	LCOE	Levelised Cost Of Electricity
CGE	Cold Gas Efficiency	LCPD	Large Combustion Plant Directive
CHN	Carbon Hydrogen Nitrogen analysis	LDV	Laser Doppler Velocimetry
CHP	Combined Heat and Power	LP	Low Pressure
CPC	Compound Parabolic Concentrator	MEA	Monoethanolamine
CRC	Carbon Reduction Commitment	NPC	Non Premixed Combustion
daf	Dry, ash free basis	NO _x	Oxides of nitrogen
db	Dry basis	OFGEM	Office of Gas and Electricity Markets
DECC	Department of Energy & Climate Change (UK)	PA	Propane-Air flame
DEFRA	Department of Environment, Food and Rural Affairs (UK)	PAH	Polycyclic Aromatic Hydrocarbon
DH	District Heating	PDF	Probability Density Function
DOE	Department of Energy (USA)	PF, pf	Pulverised Fuel
DPM	Discrete Phase Model	PIV	Particle Image Velocimetry
EEA	European Environment Agency	PLIF	Planar Laser Induced Fluorescence
EMR	Electricity Market Reform	POS	Propane-Oxygen-Steam flame
EOR	Enhanced Oil Recovery	PRV	Pressure Reducing Valve
ER	Equivalence Ratio	PSD	Particle Size Distribution
EROEI	Energy Returned on Energy Input limit	RANS	Reynold's Averaged Navier Stokes
ETS	Emissions Trading Scheme	RDF	Refuse Derived Fuel
EU	European Union	RKS-BM	Redlich Kwong Soave with Boston Mathias modification
EWT	Enhanced Wall Treatment	RNM	Reactor Network Model
FGD	Flue Gas Desulphurisation	RO	Renewables Obligation
G.E	General Electric corporation	ROC	Renewables Obligation Certificate
GC	Gas Chromatograph	ROM	Reduced Order Model
G-CGE	Gross Cold Gas Efficiency	SO _x	Oxides of sulphur
GDP	Gross Domestic Product	UN	United Nations
GHG	Greenhouse Gas	UNFCCC	United Nations Framework Convention on Climate Change
HFC	Hydrofluorocarbon	USS	Ultra-Superheated Steam
HP	High Pressure	UV	Ultra Violet
HTW	High Temperature Winkler process	wb	Wet basis
		WGS	Water Gas Shift reaction

1 INTRODUCTION

This chapter gives a background of the energy industry with a particular focus on the UK, to introduce the context in which this project was undertaken.

1.1 Global Energy Demand

As of mid-2015, the United Nations estimates our global population at over 7.3 billion, growing at 1.18 percent per year. Figure 1-1 shows the medium variant projection of future global population, which is virtually certain to rise in the coming decades and likely to continue to rise throughout the century (UN DESA, 2015).

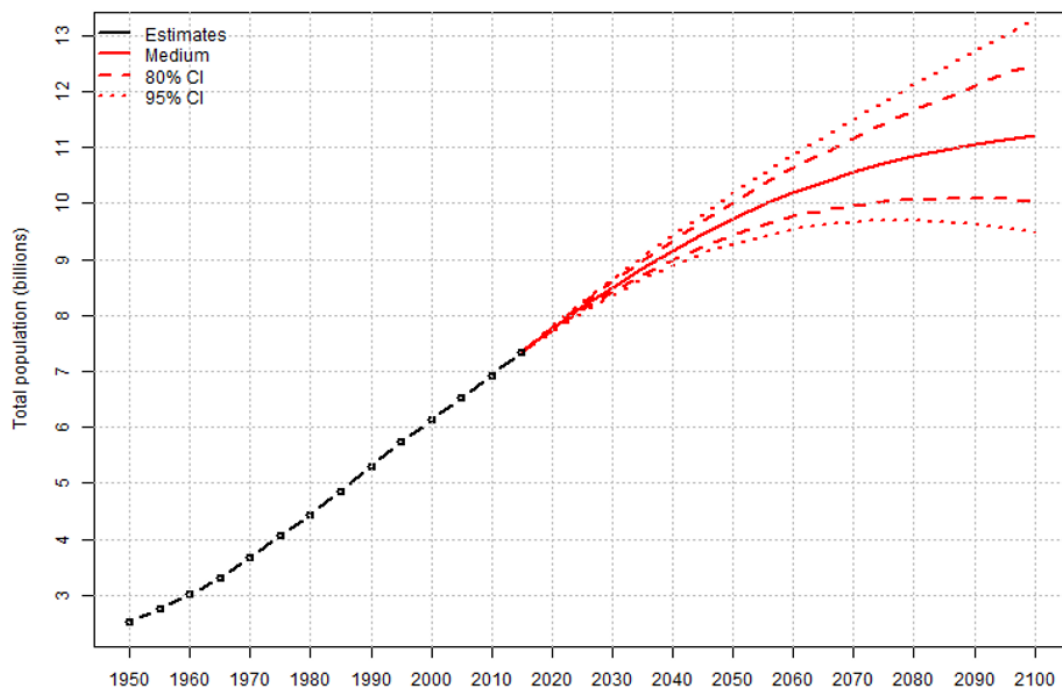


Figure 1-1: Population of the world, 1950-2100, medium variant projection (UN DESA, 2015)¹

The growing population will require additional energy for basic needs, including an increasing requirement for water desalination. Moreover with increasing Gross Domestic Product (GDP), a greater proportion will enjoy more affluent, energy intensive lifestyles. Industrial development in countries such as India requires rapid expansion of energy infrastructure to fuel growth and provide for their populations' improving quality of life (OECD/IEA, 2015). Currently most of this energy is obtained from fossil fuel reserves which are finite and cannot be relied upon indefinitely (Figure 1-2). The established method of producing electricity from such sources typically harnesses only

¹ Medium variant projection assumes a decline in fertility in countries where large families are prevalent; slight increase in fertility for several countries with less than two children per woman; survival prospects expected to improve in all countries. Confidence intervals demonstrate uncertainty in median trajectories (UN DESA, 2015).

1. INTRODUCTION

around one third of the energy available in the fuel. The effects of fossil fuel use on the Earth's climate are also of concern.

In the UK and other developed nations, many existing power generation facilities are reaching the end of their service lives and will require substantial rejuvenation or replacement within the coming years. The UK has pledged to generate at least 15% of its energy from renewable sources by 2020 (DECC, 2011). The contribution of coal to UK electricity generation has fallen from around 40% in 2012 to around 20% of the electricity mix in late 2015 (DECC, 2016a; UK Coal, 2012) due to plant closures and the gradual conversion of Drax power station from coal to biomass firing. Contributions from renewable electricity sources are expanding, but it is generally accepted that the UK and the world will continue to be reliant on fossil fuels for primary energy for several decades yet, due to the slower uptake of renewable sources for heating and transport, which constitute around one third primary energy consumption each (Figure 1-2).

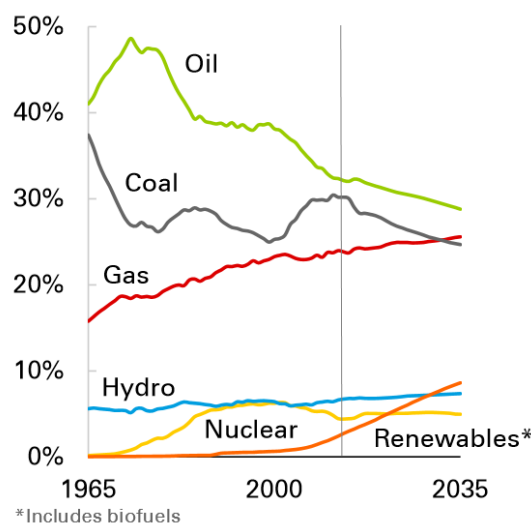


Figure 1-2: Shares of world primary energy demand, forecast according to most likely 'base case' scenario (BP, 2016)

1.2 Traditional Electricity Generation

The majority of world electricity is generated from coal and natural gas. In the last century, the nuclear power industry became a smaller but significant addition to the electrical mix, while renewable energy sources are an increasing contributor. A brief overview of some energy sources is given here, with further detail on coal and biomass given in a later chapter, with a focus on the UK.

1.2.1 Coal Power

Coal is the most abundant fossil fuel resource and has been mankind's primary source of energy since the late 1800s. It is also the most polluting due to its high carbon content which produces CO₂ when burned, and high sulphur and mercury levels compared to other fossil fuels (Bell et al., 2011). Nevertheless coal use remains high due to its abundance and affordability. It is the primary fuel in global generation, accounting for 43% of world electrical generation in 2014 (BP, 2016).

1. INTRODUCTION

Until recently, coal was the primary generation fuel in the UK. However several coal plants have recently ceased operating, either due to ageing infrastructure or the European Union's Large Combustion Plant Directive (LCPD). Plants which could not meet emissions limits were forced to cease operation by the end of 2015 (European Union, 2001). Historical coal plants were designed to produce power cheaply, with little regard for fuel efficiency or emissions targets. This makes it difficult for such plants to be competitive in the current age of increasingly stringent limits.

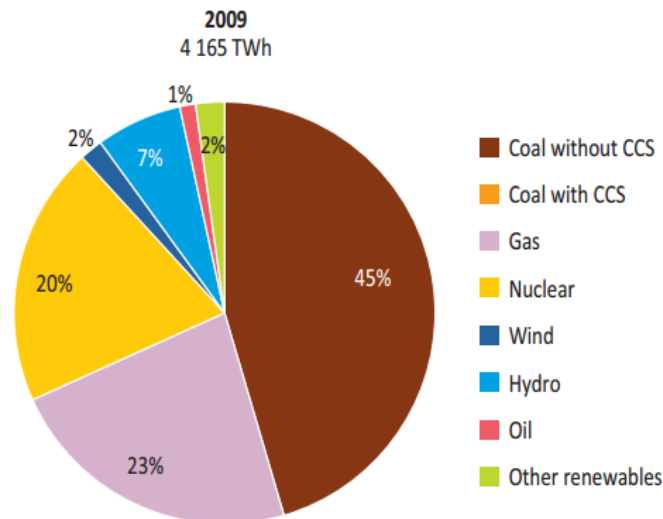


Figure 1-3: Electricity generation in the United States by type in 2009 (IEA, 2011)².

With such a global dependence on coal for primary energy, it is sure to remain a major contributor to the world energy mix for the foreseeable future. In order to reduce its environmental impact, new technologies to harness energy from coal more efficiently and cleanly must be identified. Some of these technologies, including carbon capture and storage (CCS) are discussed in Chapter 2.

1.2.2 Natural Gas

Natural gas can be used for power generation with higher efficiency and lower carbon emissions than coal. There has been recent investment in the UK into gas fired power stations, most recently Combined Cycle Gas Turbines (CCGT) which can operate at efficiencies approaching 60% (IEA/ETSAP, 2010; RWE, n.d.). These can be constructed more quickly than coal or nuclear facilities and are economically low risk compared to emerging unproven technologies.

Gas plants are susceptible to the volatile cost of natural gas fuel (Dawson and Spannagle, 2008), which can mean that they do not operate during times of low electricity sale price, but can quickly come online during peak demand. Natural gas reserves are finite, and though it is extracted from the North Sea the UK is a net importer of gas from large producers such as Russia. The reliance on imported fuel is a strong incentive to diversify national energy supply with sources which are more freely available to improve energy security.

Hydraulic fracturing or 'fracking' has freed up vast reserves of natural gas which were previously unavailable for extraction. There is currently much public opposition to this technology due to the perceived risk of earthquakes and gas surface leakage. In the USA shale gas extraction has boomed

² © OECD/IEA 2011, www.iea.org/statistics. Licence:www.iea.org/t&c

over the last decade and in 2010 accounted for over 20% of national gas production (Stevens, 2012). The technology may prevent traditional producers from dominating the gas export market; though estimations of its greenhouse gas (GHG) emissions vary. In the USA, emissions fell substantially in 2012, despite some estimates that the additional energy required for shale gas extraction results in more GHGs than conventional natural gas (Stevens, 2012).

1.2.3 Nuclear Power

The energy released by the fission of large atoms of Uranium is used for electrical generation in nuclear power stations. Nuclear power has very high capital cost offset by low running costs as fuel consumption is much lower than fossil fuelled plants.

Industrial disasters including Chernobyl mean public support of nuclear power is cautious, although it still features in the energy mix of many developed countries. France notably produces over 75% of its electricity from nuclear sources which, together with low operating costs, helps to make it the world's largest net exporter of electricity (World Nuclear Association, 2014). The 2011 Fukushima disaster exacerbated the safety concerns and public fear of this industry. Modern nuclear technology emphasises inherent safety and such a design would have averted the Fukushima meltdown by maintaining coolant flow (World Nuclear Association, 2015).

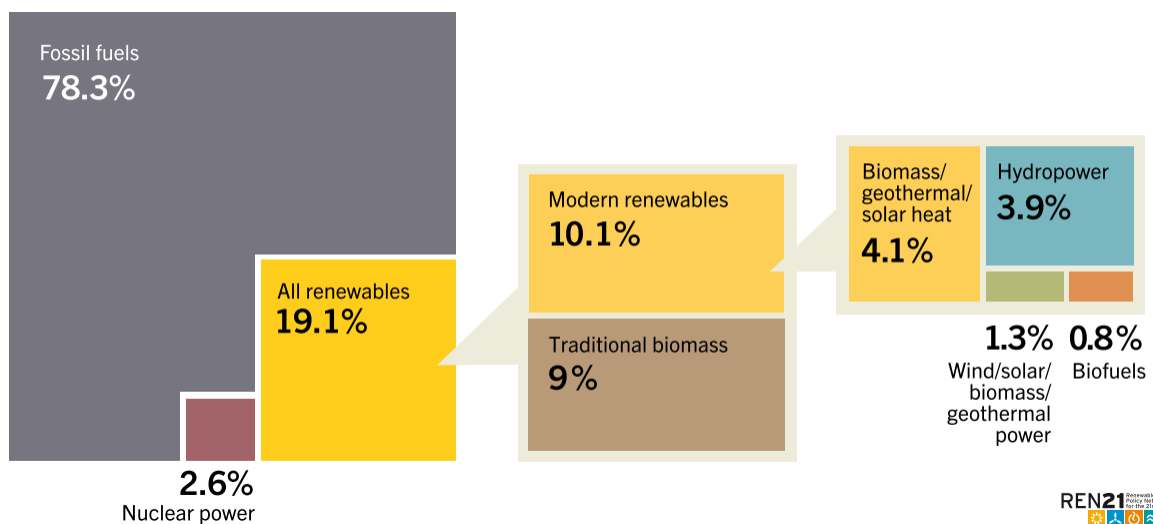


Figure 1-4: Estimated global final energy consumption in 2013 (REN21, 2015)

The UK is currently investigating the expansion of its nuclear capacity to provide energy security and meet CO₂ reduction obligations. At time of writing the debate over the cost effectiveness of the Hinkley Point C project is ongoing as a result of the agreed strike price being double current wholesale electricity prices (World Nuclear News, 2016), making new nuclear less competitive than renewable technologies. Further, the nuclear decommissioning industry is still in its infancy and is faced with the challenge of cleaning up the previous generation of nuclear power stations before new waste can be processed.

1.3 Renewable Energy Sources

This section outlines some of the renewable sectors which contribute to the energy mix. Some of these sources are already well established and offer a significant contribution to world energy supplies, while others are in various stages of development.

1.3.1 Wind and Solar Power

Wind power has seen the most commercial development in the last decade (REN21, 2015), particularly on the coastlines of Denmark and the Netherlands. The UK has great potential in terms of wind speeds and availability, due to its geographical location (European Environment Agency (EEA), 2009). Developments in technology include variable pitch blades which maintain a steady rotation speed in a range of conditions to increase availability of this resource. Offshore projects benefit from less landscape interference to give a more regular wind profile, but at greater expense.

Energy is only harvested between certain limits of wind speed and cannot be matched to demand, requiring a backup supply for periods with insufficient wind. The cost of keeping backup generation on standby should be considered with the cost of wind power. Equally, any electricity that is generated during high winds surplus to requirements is currently wasted. There is potential to combine this with energy storage to maximise availability (see Sections 1.3.3 and 1.4.1).

Solar technologies include photovoltaic (PV) and solar thermal systems. The former produces electricity from incident photons on semiconducting panels, while the latter relies on solar radiation for heating buildings or for use in specialised thermal power plants. In general, solar thermal technologies are cheaper than PV due to the materials required for semiconductor panels. These panels are also limited to around 20% conversion efficiency, though the development of novel materials is an area of ongoing research. As with wind, power is only produced during periods of appropriate intensity.

Collector efficiency can be increased using concentrating mirrors. Large schemes can incorporate many mirrors configured to track the Sun and direct light towards a central collector. Such systems require a large land area but have potential where land is cheap, for example in desert areas (MacKay, 2008). A system in North Africa, for example, could also be combined with sea water desalination, with the power transmitted via high voltage direct current (HVDC) cables to areas of high demand.

1.3.2 Biomass Energy

Wood is the oldest source of energy used by man. Wood fires were used for heat and power until forest areas could no longer support dense urban populations and were replaced by coal as the primary source of energy. Wood is still used as a cooking fuel in much of the world. There has been interest in producing electricity from biomass as it is described as carbon neutral; the carbon emissions from combusting biomass are offset by the CO₂ absorbed as it is grown. Wood is being used to partially or wholly substitute coal in some traditional coal fired power plants in order to comply with GHG emissions targets (Drax, 2014).

Biomass comes in many forms including forestry by-products and other organic waste streams. Using these as energy sources can both dispose of unwanted by-products and offset the use of fossil

1. INTRODUCTION

fuels (see Section 1.3.4). Sources such as straw have a much lower energy density which reduces the distance over which they can be economically transported. This limits their use to local areas. Energy crops are forms of biomass grown specifically for use as a fuel. They typically have a higher energy yield but often currently displace food crops.

Storage can be problematic as biomass typically has significant moisture content. This means it can begin to decompose, which can also cause an ignition risk if stored improperly. Moisture also limits the calorific value, such that it is often necessary to dry the material before combustion, adding to fuel treatment costs. Nevertheless, biomass is growing as a renewable energy source, both as a co-combustion material to offset coal use and through developments in algal energy crops and other emerging technologies.

1.3.3 Hydrogen Fuel

Hydrogen is the source of the Sun's energy via nuclear fusion. When combusted it yields no carbon emissions. Hydrogen power is currently being developed through fuel cells for vehicle propulsion, but there are a number of difficulties currently limiting its adoption. These include the production of renewable hydrogen on a commercial scale, and a storage method that is both safe and sufficiently dense to allow economical transportation.

Hydrogen is an abundant element but generally found bonded to other elements, such as oxygen in water (H₂O). It must be separated from these compounds before it can be used as a fuel. Using electrolysis, water can be separated into hydrogen and oxygen. However it requires large amounts of electrical energy to power this process. To qualify as a renewable source, the hydrogen must be produced using renewable means. Intermittent renewable sources such as wind turbines could be configured for hydrogen production by running a fuel cell in reverse. This means energy could be harvested and stored during times of abundance and deployed during peak demand, to maximise the operating hours of intermittent sources.

Another method of producing hydrogen is by gasification. Gasification is the process of converting carbon based material into gaseous carbon monoxide, hydrogen and carbon dioxide. This is achieved by heating to over 700°C with limited oxygen and/or steam. The resulting synthetic gas (*syngas*) was distributed as Town Gas in the 1800s before the widespread distribution of natural gas. This syngas can be further reacted to give a higher hydrogen purity or used in chemicals synthesis. Gasification technology is discussed in Chapter 2.

There is considerable interest in developing a suitable storage method for hydrogen in order to extend the application of hydrogen powered vehicles. Hydrogen suffers from low energy density by volume, requiring very large storage tanks compared to liquid fuels. There are also concerns regarding the safety of hydrogen vehicle fuel tanks. Various solutions have been suggested and are being developed; at present this is a significant challenge to the deployment of hydrogen vehicles.

1.3.4 Waste to Energy Systems

Energy can be generated from waste materials, such as municipal solid waste or industrial waste products. Several technologies exist for the extraction of energy from waste; most typical is direct incineration, suitable for solid waste of a dry nature. Gasification or pyrolysis of waste can be used to

1. INTRODUCTION

produce combustible gases and chars, while anaerobic digestion can be used for wet materials such as food waste and by-products from food and drinks industries; producing biogas as a product.

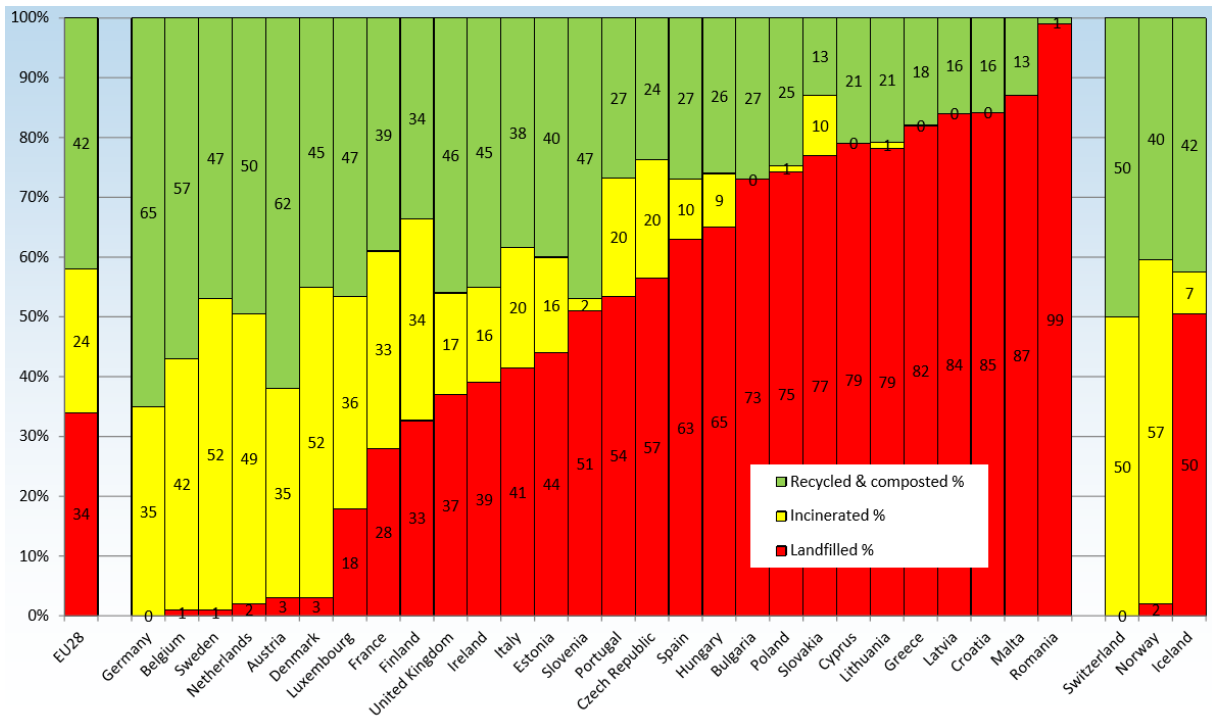


Figure 1-5: Municipal waste treatment by European countries in 2012, data from Eurostat (CEWEP, 2012)

Extracting energy from waste also reduces the volume sent to landfill, which provides an additional benefit. Where heat is produced, via incineration and other thermal treatments, efficiency can be amplified by combining them with a District Heating scheme (Section 1.4.2).

Figure 1-5 shows the average recycling and incineration figures for the EU28 countries. The UK was above average for quantities recycled and composted, while below average for incineration as of 2012. The countries which incinerate the highest proportions of waste include Sweden, Denmark and Estonia where heating demands are high; Denmark in particular has widespread use of district heating systems which benefit from the heat generated by incineration.

1.4 Efficient Energy Use

Large savings in fuel use and emissions can be made by using energy more efficiently. Typical coal fired plants, for example, have an efficiency in the region of 30-40%, which means that two thirds of the energy is dissipated via cooling systems. From both an environmental and an economic standpoint, the maximum energy recoverable should be harnessed to avoid additional fuel usage.

1.4.1 Large Scale Energy Storage

Storing excess electricity during times of low demand to be used at peak times would increase resource efficiency. A number of potential methods of storage are being researched, such as

1. INTRODUCTION

compressed or liquefied air, electrolysis of water to produce hydrogen (Section 1.3.3) and large scale battery technology.

Pumped storage hydroelectricity is the most established method, whereby water is pumped to a high reservoir one during hours of low demand and then allowed to flow back through a turbine during peak hours. This also has one of the fastest response times of any grid contributor. However large hydroelectric dams can significantly disrupt the local environment, as well as the water system downstream. The geographical requirements limit their application to sparsely populated mountainous areas, which are usually far from locations of high electricity demand.

Thermal storage methods are also under development. Large scale solar systems with sufficiently insulated thermal stores can supply a steam cycle on demand, using a technology such as molten salt storage (Herrmann et al., 2004). Countries such as Denmark with extensive intermittent wind power store excess electricity as heat to be distributed in their extensive district heating schemes (Danish Board of District Heating (DBDH), n.d.). Cryogenic storage uses electricity to condense a working fluid such as air which can be pressurised and evaporated using waste heat before expansion through a turbine on demand (Energy Storage Association, 2016).

1.4.2 Combined Heat and Power (CHP)

Power system efficiency can be increased by making use of heat energy that is otherwise exhausted to the environment. All thermal power systems expel heat via cooling towers, flue gases etc. which can be used to heat an industrial process or used offsite for low grade or domestic heating. The heat source must be located close to the target to minimise losses during transmission.

A heat source in a densely populated area can power a District Heating (DH) scheme. Thermal energy is fed through a network of pipes from a central producer to provide space and water heating. Heating networks can have multiple heat sources connected around the network (ADE, 2016). This improves space heating efficiency by making use of low temperature heat. A domestic central heating boiler burns fuel at around 1500°C to heat a room to 20°C. This large temperature imbalance makes for low fuel efficiency (Swithenbank, 2013).

DH system efficiency improves with the number of users served. Having a range of users allows the provider to maintain a regular output. A large network can also assist in balancing the grid contributions of intermittent sources, particularly if heat stores are installed. This means sources such as wind power can contribute district heat, which can be stored in the network and used at peak times to offset other fuel use.

Traditional power plants rely on economies of scale. They are typically located far from the end users and transmit power over long distances, incurring transmission losses. In de-centralised systems, compact facilities can be located close to the users, such as near hospitals, shopping centres, apartment buildings etc. which can benefit from the heat produced as well as the power. The downsides include the space requirement and the flue gas which must be thoroughly cleaned for release in an urban environment. CCGT technology boasts high efficiency but still a large footprint unsuitable for urban areas. Smaller engines such as marine gas turbines can be used for this purpose, which have an output around 50 MW suitable for powering a city district. If powered by hydrogen the local carbon and particulate emissions are avoided.

The UK's largest district heating scheme is in the city of Sheffield. An incinerator accepts up to 225,000 tonnes per annum of municipal waste to produce up to 21 MW of electricity and 45 MW of thermal energy (Veolia Environmental Services (UK), 2011). In Denmark 60% of the population is supplied with district heating, of which 23% was produced from waste sources as of 2005. The use of CHP reduced fuel consumption by 30% compared to separate heat and electrical production (Danish Energy Authority, 2005). A further advantage is the low water return temperature which allows for condensation of flue gas moisture, giving an extra boost to the system efficiency.

1.5 Environmental Concerns

Environmental motivations have led to efforts to reduce fuel consumption and emissions on a national and international level. Relevant policies and legislation are discussed further in the literature review.

1.5.1 Global Warming

Figure 1-6 shows the sharp increase in global temperatures over the last half century. Although there is continuing debate over the causes, it is generally accepted that anthropological emissions of greenhouse gases such as carbon dioxide have contributed to this trend.

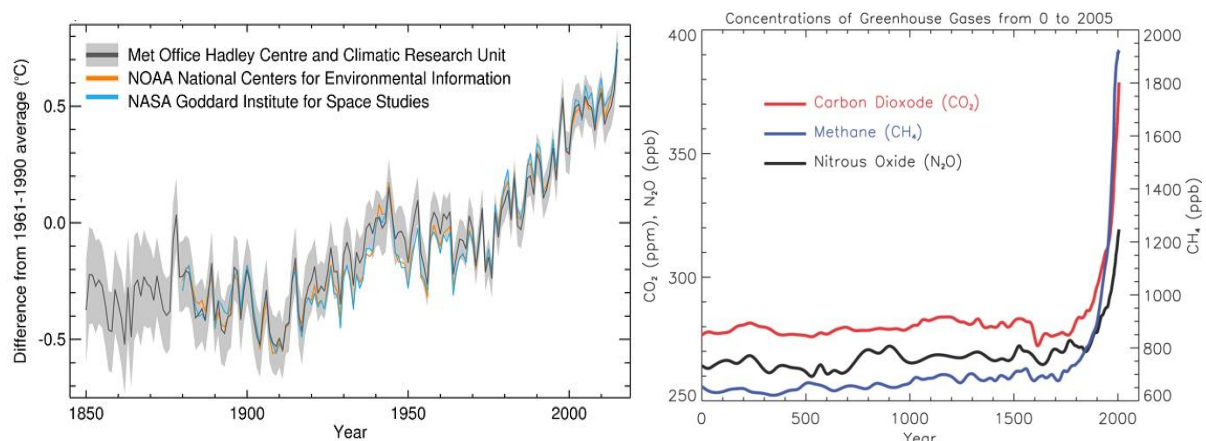


Figure 1-6: (a) Global average temperature trend 1850-2015, (Met Office, 2016); (b) Atmospheric concentrations of greenhouse gases over the last 2,000 years, (IPCC, 2007)³.

While these gases are also naturally occurring, they existed in balance with processes which released them (such as volcanic eruptions) and absorbed them (primarily photosynthesis by green plants). During the industrial revolution fuel combustion and large scale deforestation increased, as did the atmospheric levels of carbon dioxide. CO₂ is a high profile GHG as it is one of the most prevalent, though not the most potent; its atmospheric concentration has been found to increase sharply since the 1800s (Casper, 2010), see Figure 1-6. It follows that these emissions are contributing to the observed increase in global surface temperatures over the last two centuries.

³ (a) Contains public sector information licensed under the Open Government Licence v1.0. (b) "Atmospheric concentrations of important long-lived greenhouse gases over the last 2,000 years. Increases since about 1750 are attributed to human activities in the industrial era. Concentration units are parts per million (ppm) or parts per billion (ppb), indicating the number of molecules of the greenhouse gas per million or billion air molecules, respectively, in an atmospheric sample. (Data combined and simplified from Chapters 6 and 2 of this report.)" Quote and figure from (IPCC, 2007)

1. INTRODUCTION

The major incentive for controlling global warming is the damaging effect it can have on the Earth's climate. A difference in average temperature of even a few degrees would be enough to have a dramatic impact; forecasts predict severe heat waves in warm zones such as North Africa and an increase in the frequency and severity of tropical storms. Oceans will exhibit thermal expansion and increased volume from melting ice in Polar Regions, expected to lead to 0.5-1m rise in sea levels for a temperature increase of 4°C (Potsdam Institute for Climate Impact Research and Climate Analytics, 2012). This would have a devastating effect on low lying land areas such as the Netherlands and Bangladesh.

The effects of climate change would significantly impact the Earth as an ecosystem, altering habitats leading to the endangerment of species of plants and animals which are not able to adapt. Humans too would find their environment altered; water supplies and crop growing conditions disturbed making many areas uninhabitable.

1.5.2 Observable Environmental Effects

As well as the long term climate effects of anthropogenic emissions, there are environmental effects which are observable today. The most apparent in urban environments is smog. A combination of the words 'smoke' and 'fog', this describes the restricted visibility caused by burning large amounts of coal in densely populated areas. In 1950s London the effects were exacerbated by a temperature inversion that held the smog in place for several days, leading to 4000 deaths due to acid gases condensing in moist air (Met Office, n.d.). In the aftermath the UK Clean Air Act 1956 was established requiring residents to switch to smokeless fuels.

Modern day urban smog is also known as 'photochemical smog', incorporating the action of sunlight and is prevalent in warm, dry cities with high levels of sunshine such as Los Angeles. It is the product of a number of chemical reactions involving nitrogen oxides and unburned hydrocarbons released by motor vehicles; their interaction with UV light produces secondary pollutants such as ground level ozone, which is harmful to the respiratory tract.

While ozone is harmful in the troposphere, in the upper atmosphere it absorbs ultraviolet (UV) radiation from the Sun which is harmful to organisms on Earth. The ozone layer has been damaged by pollutants from human activities. Nitrogen oxides and organohalogenes such as CFCs break down ozone molecules to form chlorine and bromine radicals in the presence of the UV light. This has caused gaps in the ozone layer exposing the Earth to UV rays.

Acid rain is caused by emissions of sulphur oxides (SO_x) and nitrogen oxides (NO_x) reacting with atmospheric moisture and forming acids. It can also occur via dry deposition, when particles adhere to surfaces without moisture. Effects include damage to plant life by altering soil pH which harms microbes and leeches away nutrients and minerals. Acidification of waterways affects the hatching of fish eggs and depletes insect populations, which has an impact up the food chain. Acid rain damage is also visible on stone buildings and statues.

International treaties have been agreed to limit the amount of sulphur released into the atmosphere. Flue Gas Desulphurisation units are becoming more commonplace retrofitted on older combustion plants, particularly since the implementation of the Large Combustion Plant Directive in 2001, which imposed strict limits on permitted pollutant levels (European Commission, 2012).

1.5.2.1 Environmental Concerns of Combustion

Concerns related to the combustion process in particular include fly ash and thermal NO_x formation. Fly ash is the largest source of solid waste produced by coal combustion (Sajwan et al., 2006); it is also produced from waste incineration and other combustion sources. It consists largely of mineral matter from fuel which is not consumed by combustion, in the form of small particles entrained by the flue gas. These must be filtered out to avoid the release of potentially harmful trace elements.

Oxides of nitrogen (NO_x) are formed via three primary pathways known as fuel, prompt and thermal NO_x. Fuel NO_x is produced from the nitrogen within the fuel, and its rate of formation is a function of the degree of mixing between fuel and air. It can be controlled by minimising the amount of excess air introduced with the fuel, such that the fuel nitrogen is emitted as N₂ rather than NO_x. Prompt NO_x is formed by radical nitrogen and hydrocarbon species in the fuel, as is generally only significant in flames with a very high fuel to air ratio. It is formed during a very small time interval and is difficult to control, but has the smallest contribution of the three pathways. Thermal NO_x derives from nitrogen and oxygen present in the combustion air. Its formation peaks at the point of maximum temperature. As combustion efficiency tends to increase at higher temperatures, combustion systems are responsible for significant thermal NO_x formation (Petchers, 2003).

1.5.3 Environmental Targets

Since the 1960s there have been limits on pollution to protect the natural environment. These can be enforced on a national level; however pollution and nature do not respect national boundaries, so it is necessary to form international agreements. International legislation is generally based on voluntary agreements, such as the Kyoto Protocol concerning greenhouse gases. Most recently the COP21 agreement in Paris was adopted by all 190 nations to attempt to hold any global average temperature increase to below 2°C (COP21, n.d.). These are described in Section 2.3. Such agreements rely on voluntary participation.

Individual governments set individual targets, which are enforceable on a national level. The UK for example has the Renewables Obligation, pledging to produce 15% of the country's energy consumption from renewable sources by 2020. This includes electrical, heating and transport consumption targets. The Australian government had a similar scheme targeting 20% of electricity production from renewable sources by 2020 (Clean Energy Council (Australia), 2013). Such schemes allow governments to offer financial incentives to private sector firms to promote adoption of renewable energy in all sectors.

1.6 The Cost of Power

The major political drivers in maintaining an energy network include affordability, security and environmental impact (DECC, 2016b), which must be balanced sustainably to meet the needs of the users. The operating costs of major US electricity generators are compared in Figure 1-7, showing the effect of volatile natural gas prices. Since the shale gas boom the cost of natural gas in the USA has decreased substantially, making gas turbines competitive with traditional fossil steam plants.

Predictably, generators with little or no fuel costs such as nuclear and hydropower benefit from low operating costs. However the capital cost of nuclear facilities is comparatively greater, requiring higher upfront financing which discourages private sector investment. Hydroelectric facilities are

1. INTRODUCTION

reliant on suitable geography making them well suited to mountainous regions but limiting their use elsewhere. Nevertheless hydropower remains the largest global renewable electricity provider, with over 1000 GW of installed capacity (REN21, 2015).

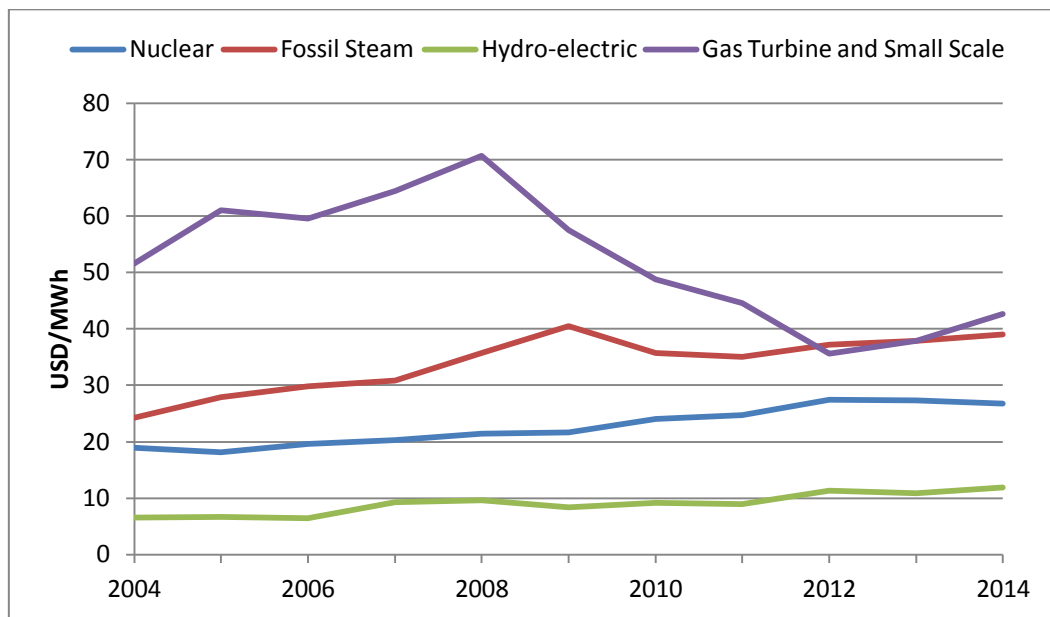


Figure 1-7: Average power plant expenses for major US electric utilities (EIA, 2016a)⁴

The cost of nuclear is demonstrated by the proposed construction of a new facility at Hinckley Point, UK. Due to be complete by 2025, the project is currently forecast to cost £18bn (BBC News, 2016). The vast expense is greater than a typical private company could afford, requiring collaboration between private companies and governments to raise the required funds. A minimum price for the electricity produced is also being agreed to provide investor confidence for the project to proceed.

Table 1-1 shows expected costs of future production from different sources. With recent reductions in capital costs, onshore wind is now cost competitive with new coal or gas fired generation per kWh (EIA, 2015; REN21, 2015). However backup capacity would be required for periods of low wind speed. Biomass shows a similar cost to conventional coal and advanced nuclear, but is dispatchable, renewable, geographically versatile and can provide electricity, heat and/or liquid fuels.

⁴ Expenses include operation, maintenance and fuel costs. Small scale includes internal combustion, PV and wind plants. Data from Federal Energy Regulatory Commission, cited in (EIA, 2016a)

1. INTRODUCTION

Table 1-1: Estimated Levelized Cost of Electricity (LCOE) for U.S. plants entering service in 2020 (2013 \$/MWh) (EIA, 2015)⁵.

Plant type	Capacity factor (%)	Levelized capital cost	Total System LCOE
<u>Dispatchable Technologies</u>			
Conventional Coal	85	60.4	95.1
Advanced Coal	85	76.9	115.7
Advanced Coal with CCS	85	97.3	144.4
Natural Gas-fired:			
Conventional Combined Cycle	87	14.4	75.2
Advanced Combined Cycle	87	15.9	72.6
Advanced CC with CCS	87	30.1	100.2
Advanced Nuclear	90	70.1	95.2
Geothermal	92	34.1	47.8
Biomass	83	47.1	100.5
<u>Non-Dispatchable Technologies</u>			
Wind	36	57.7	73.6
Wind – Offshore	38	168.6	196.9
Solar PV	25	109.8	125.3
Solar Thermal	20	191.6	239.7
Hydroelectric	54	70.7	83.5

1.7 The Hydrogen Economy

In order to decrease reliance on fossil fuels, new sustainable fuels must be embraced for electrical generation, heating and transport. Hydrogen is beginning to see application with development of fuel cells for small scale generation and vehicle transport; use as an energy vector to store energy from intermittent sources, as well as versatility to be used in localised small and medium scale gas turbines while avoiding carbon emissions at the point of use (Cotton et al., 2013).

As old coal fired plants close, it would take relatively little investment to convert them to gasification facilities in which coal or biomass can be converted into hydrogen gas. Hydrogen can be transported using pipelines as is currently practiced with natural gas, to densely populated areas to be used in compact gas turbines providing combined heat and power for local users. This approach could employ current technology that is sufficiently compact to operate in urban areas, with very high efficiencies if CHP and district heating are also employed. In suburban areas, hydrogen can again be distributed via existing natural gas networks into individual buildings, where fuel cell technology can produce CHP for maximum domestic generation efficiency. Hydrogen vehicles could be refuelled from home, work or any number of places currently supplied with natural gas. Such a scheme would make use of existing infrastructure wherever possible to minimise the cost of transition towards a hydrogen economy (Swithenbank, 2013).

⁵ Not including any government subsidy where applicable. Data from U.S. Energy Information Administration, Annual Energy Outlook 2015, April 2015, DOE/EIA-0383(2015) as cited in (EIA, 2015)

In July 2016 the publication of the H21 Leeds City Gate report outlined the plan to replace the natural gas network in the city of Leeds with 100% hydrogen. This ambitious project would use existing distribution infrastructure, with modifications to existing burners and boilers for minimum cost to the consumer. Hydrogen would be produced by steam-methane reforming in order to meet the high demand using proven technology, with inter-seasonal storage capacity in underground salt caverns. The conversion to hydrogen is expected to reduce carbon emissions by 73% by employing carbon capture and storage (CCS- see Section 2.3.2) at the point of hydrogen production (Northern Gas Networks et al., 2016). Establishing a large scale hydrogen network would provide additional incentive and markets for hydrogen vehicles and fuel cells. Demand for hydrogen would also allow new production methods to become competitive, including renewable sources.

1.8 Objectives of Research

The present work will build on initial research (Shabangu, 2005) in which a novel coal gasifier was developed based on ultra-high temperature steam. This gasifier was designed and built at the University of Sheffield, and operated to produce high yields of hydrogen and carbon monoxide from coal and other fossil fuel feedstocks. Due to the high temperatures and the highly reactive nature of the steam, the system was found to be non-slagging with no evidence of tar deposition under the conditions tested, showing promise for use with biomass fuels.

The aim of this project is to examine how the system yielded high fractions of hydrogen gas in the product stream. It will also investigate the application of this gasification system to biomass feedstocks, and compare the gas yields from coal and biomass sources in order to extend the application to other sustainable feedstocks. In particular, the steam mixture will be analysed and the burner arrangement simulated to investigate the effects of steam flame composition, reactant flow rates and feedstock composition on the product yield.

The objectives of the present work, addressed in this thesis include;

- To study the underlying theory of gasification, particularly steam systems. This includes gasification thermodynamics, kinetics and flame structure with respect to the Ultra-Superheated Steam gasification concept.
- Develop a numerical model of the gasification system to predict the effects of varying process input parameters such as the production of USS and optimise the gasifier yield.
- To upgrade and adapt the experimental system where necessary for reliable operation and improve control of reactant flows, particularly for biomass feedstocks. Establish a baseline USS composition with which gasification will be conducted.
- To investigate the suitability of the present system for renewable fuel generation, including characterisation of a specific waste biomass feedstock presented by an industrial contact. Investigate the suitability of this material for gasification using the USS system and compare the product yields with those of typical gasification feedstocks.
- Consider important economic aspects of the present gasification system to evaluate its viability and potential scale up. Highlight any wider industrial applications of the work.

1.9 Layout of Report

This report summarises work undertaken during a PhD programme beginning October 2013 and is structured as follows;

- Chapter 1 is an introduction to the current energy industry and challenges to meeting the future energy demand, providing a context for the research undertaken in this project.
- Chapter 2 provides a literature review of existing thermal technologies including gasification processes and current research being undertaken in this area for both coal and biomass feedstocks. General information on the properties of coal and biomass is presented alongside relevant emissions legislation which provides additional incentives for clean energy development.
- Chapter 3 is comprised of thermodynamic and kinetic gasification theory, as well as some relevant information regarding flame structure, steam characteristics and the effects of water vapour addition to flames, as relates to the present gasification system.
- Chapter 4 details the process modelling and CFD simulation work. Descriptions of model development are included with the general findings, which were used to plan the initial experimental programme. Empirical data was then used to extend and validate the models.
- Chapter 5 describes the experimental programme, including the classification of feedstock materials, modification of the experimental rig and details of experimental methods.
- Chapter 6 presents the experimental conditions and main results, comparing the effects of gasifier parameters, fuel gas and feedstocks. Mass and energy balances and feedstock conversion are discussed.
- Chapter 7 provides an overall discussion bringing together the findings from chapters four, five and six. The results are compared with similar literature works. An economic analysis of the system is presented with industrial applications of the results.
- Chapter 8 presents the conclusions drawn from the present work and recommendations for future work.
- The appendices contain additional data relating to the models and feedstock materials, as well as supplementary experimental work not included in the main chapters.

1.10 Summary

The population of the globe and energy consumption per capita are both forecast to rise. Energy demand in all sectors will be impacted. Existing infrastructure will struggle to cope and developments will be required in the fields of energy efficiency, new technologies and development of new fuel sources to meet global climate targets.

This must be achieved while simultaneously reducing environmental impact. Renewable energy sources are becoming increasingly important due to their emission free operation and independence from finite resources. National policies and international agreements are encouraging the phasing out of unsustainable power sources and harmful emissions, leading to more efficient fuel use. Projects such as combined heat and power and district heating schemes maximise the energy harvested from a fuel. Energy storage technologies will also allow energy to be stored and deployed during periods of peak demand, particularly from renewable intermittent sources, reducing the strain on the electricity supply network.

1. INTRODUCTION

Hydrogen gas has potential as a power, heating and transportation fuel. It can be combusted in a gas turbine and yields only water as a combustion product, providing energy without harmful emissions locally. Using hydrogen in the natural gas network offers opportunity to significantly reduce the carbon emissions from the heating sector and provides a market for renewable hydrogen generation.

One method of renewable fuel production is examined in detail in this thesis. Gasification of solid fuels has been used since Town Gas was produced from coal two centuries ago. While natural gas is currently the most economical option, rising costs and limited supplies will require an alternative fuel source in the medium term. A variety of technologies have been developed which can produce hydrogen and carbon monoxide from coals. The challenge is to produce hydrogen gas from low value feedstocks while minimising the production of harmful by-products which hinder the widespread use of biomass in power generation. An economical method of producing hydrogen from renewable sources could pave the way for an energy revolution.

2 LITERATURE REVIEW

This chapter offers an overview of coal and biomass feedstocks and thermal technologies, focussing on pyrolysis and gasification. Established gasification technologies are presented and compared. Relevant legislation for reducing emissions and increasing renewable energy adoption is discussed. The chapter concludes with a review of some current gasification research.

2.1 Gasification Feedstocks

This section introduces the coal and biomass feedstocks investigated in the experimental work. It addresses the forms in which these two fuels appear; their composition and their global distribution.

Table 2-1: ASTM classification of coals by rank (ASTM, 2012a)⁶.

Class/Group	Fixed Carbon Limits (Dry, Mineral-Matter-Free Basis), %		Volatile Matter Limits (Dry, Mineral-Matter-Free Basis), %		Gross Calorific Value Limits (Moist, ^B Mineral-Matter-Free Basis)				Agglomerating Character
	Equal or Greater Than	Less Than	Greater Than	Equal or Less Than	Btu/lb		Mj/kg ^C		
					Equal or Greater Than	Less Than	Equal or Greater Than	Less Than	
Anthracitic:									
Meta-anthracite	98	2	} nonagglomerating
Anthracite	92	98	2	8	
Semianthracite ^D	86	92	8	14	
Bituminous:									
Low volatile bituminous coal	78	86	14	22	} commonly agglomerating ^E
Medium volatile bituminous coal	69	78	22	31	
High volatile A bituminous coal	...	69	31	...	14 000 ^F	...	32.557	...	
High volatile B bituminous coal	13 000 ^F	14 000	30.232	32.557	
High volatile C bituminous coal	11 500	13 000	26.743	30.232	
					10 500	11 500	24.418	26.743	} agglomerating
Subbituminous:									
Subbituminous A coal	10 500	11 500	24.418	26.743	} nonagglomerating
Subbituminous B coal	9 500	10 500	22.09	24.418	
Subbituminous C coal	8 300	9 500	19.30	22.09	
Lignitic:									
Lignite A	6 300 ^G	8 300	14.65	19.30	} nonagglomerating
Lignite B	6 300	...	14.65	

^A This classification does not apply to certain coals, as discussed in Section 1.

^B Moist refers to coal containing its natural inherent moisture but not including visible water on the surface of the coal.

^C Megajoules per kilogram. To convert British thermal units per pound to megajoules per kilogram, multiply by 0.0023255.

^D If agglomerating, classify in low volatile group of the bituminous class.

^E It is recognized that there may be nonagglomerating varieties in these groups of the bituminous class, and that there are notable exceptions in the high volatile C bituminous group.

^F Coals having 69 % or more fixed carbon on the dry, mineral-matter-free basis shall be classified according to fixed carbon, regardless of gross calorific value.

^G Editorially corrected.

⁶ Reproduced, with permission from (ASTM, 2012a), copyright ASTM International, 100 Barr Harbor Drive, West Conshohocken, PA 19428.

2.1.1 Coal

Coal is a solid fossil fuel; a dark sedimentary rock formed by the deposition of organic matter in prehistoric peat bogs. These bogs experienced intense heat and pressure over millions of years of tectonic movement in the Earth's crust. Coal is found underground in layers or 'seams'. It has high carbon content as well as various fractions of hydrogen, oxygen, nitrogen and sulphur. Differences in volatile matter, moisture and composition differentiate coal into categories or 'ranks'.

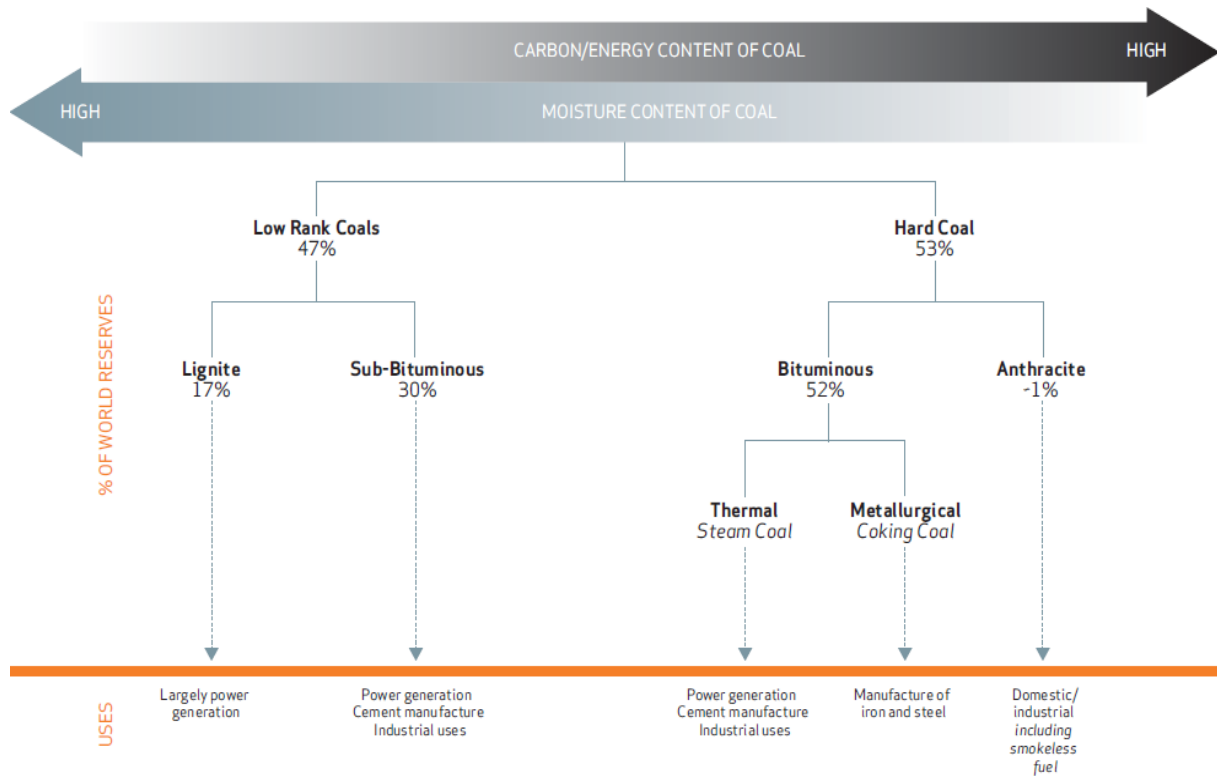


Figure 2-1: Types of coal, relative abundance and their uses (World Coal Association, 2016)⁷

The highest rank, corresponding to the highest calorific value, is Anthracite. Bituminous is the second highest and most abundant rank, accounting for around half of the world's reserves and is primarily used for power generation and metals manufacturing. Sub-Bituminous coal uses range from power generation to chemicals synthesis. Lignite is the lowest rank with the highest oxygen, hydrogen and moisture content. It has a lower calorific value than high rank coals, is softer and is used almost exclusively for power generation. Coal is broadly divided into 'hard coal' and 'brown coal', where hard coals include anthracite and bituminous types and brown coals include lignite and some sub-bituminous varieties (IEA, 2010).

2.1.1.1 Coal Composition and Properties

The classification of coal varies around the world. Even within a given rank there are observable differences; it is possible to distinguish between anthracitic coals, anthracites and meta-anthracites based on small differences in moisture and carbon content as well as the spatial ordering of organic matter (Bratek et al., 2002). To distinguish coal from peat requires a maximum moisture content of 75%, and a minimum energy content of 6.7MJ/kg on an ash free basis. These properties are determined by performing standardised tests such as ultimate and proximate analyses.

⁷ © 2016 World Coal Association

2. LITERATURE REVIEW

Proximate analysis allows comparison of fuels by measuring moisture, volatile content, fixed carbon and ash contents. Ash and moisture contribute to mass but not to the heating value. Ultimate analysis reveals the elemental constituents of a sample. Harmful elements such as chlorine and mercury can influence a coals suitability for a given purpose or the need for emission controls (Encyclopedia Britannica, 2014).

Coal has an apparent density in the range of 1.2 - 1.6 g/cm³. This property can be used to separate coal from other rock and was also used for exploration, as coal could be distinguished from other rock using drilling probes (ASTM, 1992).

The heating value (heat of combustion or calorific value) represents the amount of chemical energy in a fuel. All fuels contain some moisture, which is evaporated when the fuel is combusted. The higher heating (or gross calorific) value assumes that this vapour is condensed and the energy recovered from it, while the lower heating (net calorific) value assumes that this energy is lost (Quaak et al., 1999). The heating value depends on the rank of the coal and generally falls in the range of around 23-35 MJ/kg gross for coal for UK consumption (DECC, 2013a).

2.1.1.2 Coal Resources and Reserves

Coal is the most abundant fossil fuel, existing in almost every country worldwide. The largest deposits are located in the USA, Russia, India and China (World Coal Association, 2016). The presence of coal in any quantity is known as a resource. These include very diffuse or small quantities which may not be economically or practicably extracted. Those deemed extractable under current market conditions are known as reserves. Coal price and the current extraction technology determine a reserve's economic viability. For this reason quoted coal reserves can rise and fall with coal prices, but are a more meaningful representation of resource longevity (Bell et al., 2011).

Table 2-2: Coal data by world region, data from (EIA, 2016b).

	Production (P)	Consumption	Reserves (R)	Lifetime
	2012 data, per annum		2011 data	R/P
	Million short tons			Years
North America	1,106.5	955.7	267,411.0	242
Central & South America	110.0	51.5	16,138.9	147
Europe	773.6	1,026.7	90,743.4	117
Eurasia	606.5	465.0	251,364.5	414
Middle East	1.3	22.6	1,236.8	954
Africa	295.3	220.5	35,068.9	119
Asia & Oceania	5,794.1	5,444.0	317,827.2	55
World	8,687.3	8,186.1	979,790.8	113

Table 2-2 shows coal reserves and rate of production by region. By dividing these values an estimate of the reserve longevity is obtained, based on latest available data. Higher coal prices will allow previously uneconomical resources to be mined, expanding the feasible 'reserves'. At the point where the energy expended in extraction approaches the energy available in the coal, known as the Energy Returned on Energy Input limit, production will cease regardless of market value. It is however more likely that this trend will continue only up to a certain peak coal price, beyond which alternative energy sources will become more attractive than coal by comparison (Bell et al., 2011).

2.1.1.3 Coal Uses

Since the industrial revolution coal has been one of the top world energy sources due to its high energy density, making it more economical to transport than wood. By far the largest coal use is for electrical power generation. Pulverised coal combustion to generate steam was used in the earliest power stations and is still widely used today. Some improvements have been made to increase the process efficiency following the Carnot equation, where efficiency, η is given by;

$$\eta = \frac{\dot{W}}{\dot{Q}_H} = 1 - \frac{T_c}{T_h}$$

Equation 2-1 (Klein and Nellis, 2011)

Where \dot{W} is the work done by the system, \dot{Q}_H is the rate of heat transfer into the system, T_c and T_h are the temperatures of the fluids rejecting and receiving heat, respectively. Efficiency can be improved by increasing the temperature at which heat enters, T_h , or by reducing the temperature at which heat leaves the system, T_c . The latter is generally set by the temperature of ambient air or cooling water. T_h is limited by the materials of construction. Development of new high temperature resistant materials allows greater operating efficiencies to be achieved.

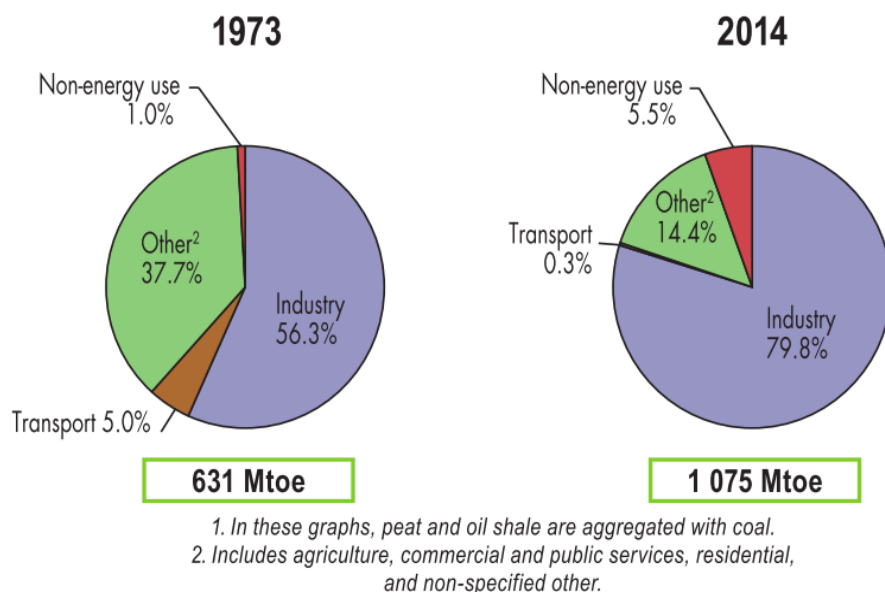


Figure 2-2: 1973 and 2014 shares of world coal consumption (IEA, 2016)⁸

Steel manufacture relies heavily on 'coking coal', a bituminous coal with a high carbon content that can be used to produce coke used in blast furnaces. Other uses include cement manufacture, requiring 20 kg of coal per 100 kg of cement; production of paper and chemicals and speciality products such as activated carbon and carbon fibre (IEA, 2010; World Coal Association, 2016).

2.1.1.4 Environmental Impacts of Coal Use

The atmospheric pollutants released from coal combustion include oxides of carbon, nitrogen and sulphur in large quantities; heavy metals such as mercury are emitted in smaller quantities. The scale of gaseous emissions from fossil fuels is around 11 tons per year for a typical British person; in

⁸ © OECD/IEA 2016, www.iea.org/statistics. Licence: www.iea.org/t&c

2. LITERATURE REVIEW

comparison the volumes of nuclear waste produced are approximately 0.84 litres per person per year from the ten nuclear reactors in the UK (MacKay, 2008).

Methane trapped within coal seams is often vented as it poses a safety risk during mining; methane is a greenhouse gas with 21 times the global warming potential of CO₂ over a 100 year period (IPCC, 1996). On average almost 7% of GHG emissions from hard coal extraction are associated with methane release (Dones et al., 2004). Lignite contains relatively little methane, contributing only around 0.6% of the total chain GHG emissions (Weisser, 2007). Acid rain is discussed in Section 1.5.2.

Mining consumes large volumes of water for washing and dust suppression. Heavy metals can leach from coal into the water requiring clean-up before discharge to the environment (US EPA, 2013). Coal dust can impair air quality, cause health defects and deposit onto vegetation and waterways. In addition, a 500 MW coal plant consumes 2.2 billion gallons of water per year during operation, equivalent to a city of 250,000 inhabitants (Biswas, 2009).

Land use is high with coal mining. Surface mining is favoured as it facilitates access and reduces the safety risks associated with underground mining. This means the overburden is removed to reveal the coal, displacing any wildlife or natural features. Responsible mine owners will account for rehabilitation of land after mining is complete (World Coal Association, 2016).

2.1.2 Biomass

Biomass has been used for cooking and heating since the origins of mankind. It is derived from organisms which used photosynthesis to turn solar energy into carbohydrates. Biomass encompasses a variety of materials with different properties. In general on a dry basis all biomass consists predominantly of carbon, hydrogen and oxygen (Vassilev et al., 2010).

2.1.2.1 Sources of Biomass

Wood is the most common biomass fuel, though there is a wide range in composition and heating value. Recycled wood can be distinguished from wood cut specifically for fuel use, and includes industrial sources such as pallets and construction waste. These are usually very dry materials which can be easily combusted. A comparison of some different types based on heating value was made by (Quaak et al., 1999).

Energy crops are fast growing plants which yield high energy output per area of land used and required energy input. Forestry produces biomass more slowly than energy crops but at lower cost (Biomass Energy Centre, 2011). Elephant grass and giant miscanthus have a higher energy yield than non-specific crops; however they often controversially displace food crops. This has led to research into algae for energy production. Algae have the fastest growth rate of any photosynthetic organism and can be cultivated on land unsuitable for agriculture using non-potable water (Leite et al., 2013).

Agricultural and forestry wastes include crop waste products; sawdust, and foliage which are often uneconomical to transport. The palm oil industry generates nine times more biomass waste than product oil in the form of empty fruit bunches and effluent from the oil extraction process (Foong-Kheong et al., 2014; Kelly-Yong et al., 2007).

Wet biomass sources include animal slurry, food wastes, sewage sludge etc. It has been estimated that in the UK one third of food produced for human consumption is discarded (Biomass Energy

Centre, 2011). These sources have a moisture content that is too high for combustion and are uneconomical for long range transportation. Many wet sources are composted and used as cheap fertilizer. Agricultural waste is prominent around the times of food crop harvests. Palm oil waste also has a high moisture content and is typically used as fertilizer (Piarpuzán et al., 2011). Organic wastes with high moisture can be treated by anaerobic digestion to produce a methane rich fuel gas.

2.1.2.2 Wood Pellets

The use of pelletised wood has seen recent growth for industrial co-combustion in coal power plants and for domestic heating. Industrial markets are largest in the UK, Belgium and the Netherlands promoted by government tariffs. Due to scarcity of local raw materials, most of the demand is met by Canadian imports. Domestic heating markets include Germany, Austria, Italy and the USA, using higher quality pellets. Pellets are used substantially in both industrial and domestic markets in Scandinavia, with Sweden being the leading consumer (Döring, 2012).

Wood pellets typically have a HHV around 18-20 MJ/kg (Roy et al., 2013), which can be increased by reducing moisture and volatiles content, such as via pyrolysis, to over 30 MJ/kg (Park and Jang, 2012). This is discussed further in Section 2.2.2 and demonstrated in Appendix C.

2.1.2.3 Environmental Impacts of Biomass Use

While biofuels offer GHG emission reductions over fossil fuels, there are risks associated with land use change including reduced biodiversity (Foong-Kheong et al., 2014). Biomass for electricity generation has many of the same environmental concerns as other fuels in terms of airborne pollutants. The major advantage is that biomass is often regarded as carbon neutral, in that the carbon dioxide emitted from its combustion is absorbed by the plant during its growth.

Table 2-3: Life cycle emissions estimates for electrical generation by fuel type up to 2020. Data from (Weisser, 2007)

Source	Current Emissions	Estimated Future Emissions	Comments
	(g CO ₂ eq/kWh _e)		
Lignite	1100-1700	>800	Variability in thermal efficiency & mode of operation; bulk emissions from combustion stage
Coal	950-1250	750-850	Upstream CH ₄ & coal transport contribute substantially to present emissions
Natural gas	440-780	<400	Potential improvements by reducing pipeline leakage & compression costs
Biomass	35-99		Wood based fuels only, assumed carbon neutral, emissions from raw materials harvest

Harvesting materials currently used as fertilizer, such as animal slurry, for energy use may result in additional use of synthetic fertilizers. These involve significant energy input and emissions from production such that the substitution may be more harmful in the long term (Biomass Energy Centre, 2011).

Wood pellets can offset fossil fuel use in domestic heating and power plants. However if they are transported over long distances their environmental impact is increased. Many pellets consumed in

Europe are shipped from Canada. By sourcing wood locally in Norway for pellet production using hydropower, CO₂ equivalent emissions were estimated to reduce by 23% (Sjølie and Solberg, 2011).

Table 2-3 compares the life cycle emissions from different fuels, based on literature sources. Lignite has the largest range due to different thermal efficiencies of lignite plants. Emissions from hard coal plant operation are lower; however there are considerable emissions from transportation due to greater distances between mines and power stations. Biomass values are based on woody sources only; the range of emissions arises from the feed type and upstream fuel cycle (Weisser, 2007). It was noted that carbon neutral does not necessarily imply GHG neutral, due to other emissions from combustion (Sjølie and Solberg, 2011).

2.2 Thermal Technologies

This section introduces the major technologies used to extract energy from fuels, focussing on coal and biomass. The technologies discussed include combustion, pyrolysis and gasification. Some commercial technologies for coal gasification are described and compared.

2.2.1 Combustion

Combustion is the most established method of liberating energy from a fuel. Combustion requires sufficient fuel and oxygen, as well as temperature and an ignition source for it to begin. The combustion process for solid fuels can be broken down into the following stages;

- Drying of the material as the moisture is driven off by evaporation
- Pyrolysis of the fuel as the volatile matter is liberated, leaving a solid char
- Combustion of the released volatile gases, which occurs rapidly
- Combustion of the solid char, which occurs relatively more slowly

Combustion heat is transmitted directly by radiation or transferred to the flue gases which can be used for heat exchange, usually with water to generate steam. Energy which does not follow this path is considered lost, including heat transfer through furnace walls or to the ash, or material that is incompletely combusted (Quaak et al., 1999). Combustion efficiency may be expressed as;

$$\text{Efficiency, } \eta = \frac{\text{Useful energy output}}{\text{Total energy input}}$$

Equation 2-2

High fuel conversion requires an excess of oxidant, i.e. air in addition to the stoichiometric air requirement (Quaak et al., 1999). The excess air factor or Equivalence Ratio (ER) represents the ratio of actual air supplied to the stoichiometric requirement. As the value increases, the fuel is more rapidly and fully consumed, but the flue gas is diluted by the additional air. Lower values of ER give a hotter, less dilute flue but risk failing to completely combust the fuel, reducing fuel efficiency.

For maximum heat transfer, flue gas enters at high temperature and exists at the lowest practicable temperature. The exit temperature is restricted if the gas contains acidic components such as sulphur oxides or hydrochloric gas. To avoid acid condensation the flue gas temperature should be maintained above the acid dew point, which presents an energy loss (Quaak et al., 1999).

2. LITERATURE REVIEW

Using oxygen instead of air increases the flue temperature by avoiding nitrogen dilution. In this case some flue gas is often recirculated to control the flame temperature and avoid melting metal components. Use of oxygen requires an air separation unit, presenting additional operating cost.

In general for combustion to progress good mixing of fuel and oxidant and sufficient residence time within the reaction zone are required.

2.2.1.1 Combustion Technologies

Combustion systems can be distinguished according to the design of the furnace bed. Among fixed bed furnaces are static, sloping or moving beds where the fuel is combusted. Primary combustion air is introduced usually from under the bed to react with char and devolatilise fuel as it is introduced. Secondary air is introduced above the bed to react with the volatile gases.

In fluidised bed systems fuel is introduced onto an inert bed material such as sand. Primary air is blown from underneath to fluidise the sand with the fuel, creating a well-mixed thermally uniform bed. At low air velocities this is known as a bubbling bed configuration. Increasing the air velocity above a critical point causes the bed material to be entrained with the air and separated by a cyclone at the gas exit. This is known as a circulating fluidised bed. Fluidised bed arrangements are suitable for fuels of variable quality and moisture content, as the thermal mass of the bed material can moderate some fluctuations in fuel heating value.

The most common source of electrical generation is the combustion of pulverised coal. This involves crushing the fuel into a fine powder before it is blown into the furnace with the combustion air. This technique makes use of the entire furnace volume for combustion, while the small particle size maximises fuel surface area allowing a high rate of reaction. This is necessary as the residence time of the fuel particles is limited by the height of the furnace.

Pulverised fuel combustion allows high controllability as fuel is present only in small quantities in the furnace at any one time. Disadvantages include the intensive grinding of fuel to the required particle size (Spliethoff, 2010). There are also concerns with the storage of pulverised fuel. It is possible to store high rank coals in pulverised form open to the atmosphere as they absorb little water and can be dried on entry to the furnace. However biomass sources will readily absorb moisture and swell in size. Pellets may disintegrate which can block feeding systems. Biomass sources can biodegrade and release heat, which can lead to auto-ignition. As such biomass should be stored away from sources of moisture, and monitored for signs of decomposition.

2.2.1.2 Biomass Co-Combustion

Co-combusting biomass in coal plants is used to meet environmental targets. It presents an effective means of reducing carbon emissions from coal plants and is one of the *“most efficient and inexpensive uses of biomass”* (Baxter, 2005). Addition of biomass typically has a small impact on the overall efficiency due to increased energy use in fuel preparation, higher moisture content and reduced pre-heating of combustion air. Co-combustion systems are often favourable compared to biomass only systems (Baxter, 2005).

In some cases co-firing is more expensive than using coal alone. Even where the biomass is of low value, the additional costs of transportation, preparation and handling can increase the cost per unit energy (Baxter, 2005). Co-combustion is more economical for smaller scale boilers with higher coal

costs compared to large users, particularly if located near a ready source of biomass fuel (Demirbaş, 2003). Carbon credits or other financial incentives may also favour biomass usage.

Co-firing also has the potential to reduce emissions of NO_x and SO_x (Basu et al., 2011; Demirbaş, 2003). However issues of increased slagging and fouling when high fractions of biomass are used, due to low ash melting temperatures etc., limit the amount of biomass fed in co-combustion to relatively low proportions of the fuel mixture.

2.2.2 Pyrolysis

Pyrolysis is the heating of a feedstock in the absence of oxygen, using thermal energy to decompose long hydrocarbon molecules. Unlike combustion, pyrolysis is endothermic requiring thermal energy input to drive off moisture and volatile matter. The gases can be cleaned and used as an energy source; the remaining solid char contains a high carbon fraction and can also be used as a fuel.

Table 2-4: Characteristics of biomass thermal treatment processes. Reprinted from (Basu, 2013) with permission from Elsevier.

Process	Residence time	Heating rate	Final Temp	Products
Torrefaction	10-60 min	Very small	280	Torrefied biomass
Carbonization	Days	Very low	>400	Charcoal
Fast	<2s	Very high	~500	Bio-oil
Flash	<1s	High	<650	Bio-oil, chemicals, gas
Ultraprapid	<0.5s	Very high	~1000	Chemicals, gas
Vacuum	2-30s	Medium	400	Bio-oil
Hydropyrolysis	<10s	High	<500	Bio-oil
Methanopyrolysis	<10s	High	>700	Chemicals

Pyrolysis can be broadly divided into the following processes;

- Torrefaction (mild pyrolysis)
- Slow pyrolysis
- Fast pyrolysis

Torrefaction is a low temperature pyrolysis treatment generally reserved for biomass or other wet sources. The material is heated to between 230-300°C in the absence of oxygen. Removing moisture increases the energy density which adds value and reduces transportation costs (Basu, 2010).

In fast pyrolysis, the feedstock is rapidly broken down to form mainly gases and aerosols. These can then be condensed to form a dark brown liquid fuel. Fast pyrolysis requires very fast heating rates which necessitates grinding the feed. High surface area is needed to overcome the typically low thermal conductivity of the feedstock, to ensure that the material reaches the desired temperatures with minimal exposure to lower temperatures which favour char production. Reaction at around 500°C maximises the liquid yield for most biomass sources, with a residence time of under 2 seconds to minimise secondary reactions. The char is quickly removed to avoid cracking the vapours.

Liquefaction is another technology available for biomass conversion. In a hydrothermal process the biomass is contacted with pressurised water at 300-350°C which effectively transforms the biomass

into a liquid fuel. This can also be performed through pyrolysis, gasification, supercritical water processing or other means (Basu, 2010).

2.2.2.1 Pyrolysis Yields

Pyrolysis yields are affected feedstock moisture and volatile contents, pyrolysis temperature and heating rate. Particle size affects feedstock heating times, devolatilization rates and yields.

Table 2-5: Typical product weight yields (dry wood basis) obtained by different modes of pyrolysis of wood. Reprinted from (Bridgwater, 2012) with permission from Elsevier.

Mode	Conditions	Liquid	Solid	Gas
Fast pyrolysis	~500°C, short hot vapour residence time ~1 s	75%	12% char	13%
Intermediate	~500 °C, hot vapour residence time ~ 10-30 s	50% in 2 phases	25% char	25%
Carbonisation (slow)	~400 °C, long vapour residence, hours to days	30%	35% char	35%
Gasification	~750-900 °C	5%	10% char	85%
Torrefaction (slow)	~290 °C, solids residence time ~ 10-60 min	0% unless condensed, then up to 5%	80% solid	20%

The effect of temperature is most significant. Low temperatures and higher residence times yield more solid char, while high temperatures and short residence times increase the gaseous yield. Intermediate conditions can be used to yield more liquid products (Bridgwater, 2012). A rapid heating rate leads to a greater volatiles yield, and a smaller yet more reactive yield of char by preventing secondary reactions which take place between char and volatiles (Mahinpey and Gomez, 2016; Rezaiyan and Cheremisinoff, 2005). Pyrolysis is considered slow if the time to heat the feedstock to reaction temperature is greater than the time held at the set temperature.

2.2.2.1 Pyrolysis Applications

Pyrolysis has been used in the production of charcoal since the 1700s. More recently it has seen commercial application for solid waste treatment, producing fewer emissions than incineration.

One example is the Mitsui Recycling 21 process. Waste material is pyrolysed at 450°C in a kiln, from which iron and aluminium are removed before the remaining solids are combusted with the product gases at 1300°C. Heat from combustion powers the pyrolysis process and generates steam for power generation. Another example in Hamm, Germany, pyrolyses 100,000 t/year of waste containing up to 50% plastic in two rotary kilns at up to 700°C. The products offset up to 10% of the fossil fuel in an adjacent power station (Rezaiyan and Cheremisinoff, 2005).

Another process produces oil via fast pyrolysis of biomass in a rotating cone reactor. Sand acts as a heat carrier and to break down and mix the feedstock. Vapours are removed and quenched in a condenser, while solids are blown into a fluidised bed where the char is combusted to heat the sand. Steam is also produced using excess heat. A system currently operating in Malaysia produces pyrolysis oil from empty fruit bunches, a by-product of palm oil industry (BTG-BTL, 2016).

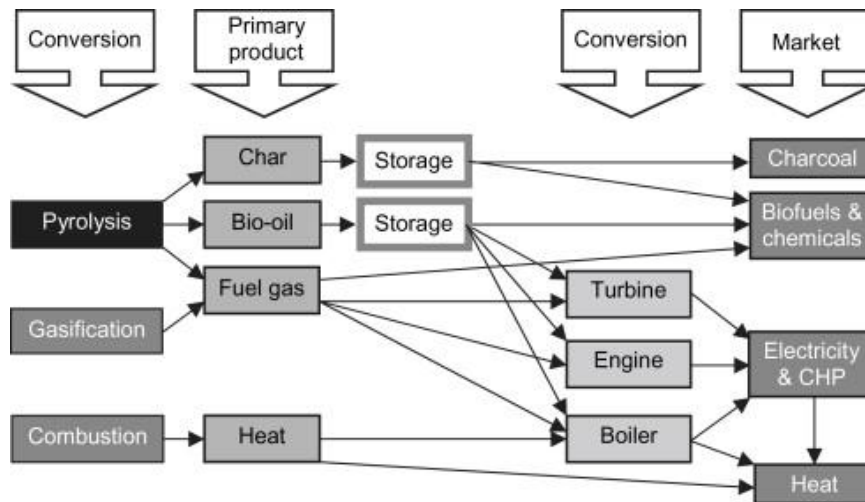


Figure 2-3: Products from thermal biomass conversion. Reprinted from (Bridgwater, 2012) with permission from Elsevier.

2.2.3 Coal Gasification

Gasification is the conversion of a carbonaceous feedstock into a fuel gas using high temperatures and the addition of a reactive gas. It is a continuation of the pyrolysis process whereby the residual char is reacted with a gasifying medium such as steam, air or oxygen at temperatures above 800°C to produce additional fuel gas rich in CO and H₂ (Bilitewski et al., 1997). The composition of the product synthesis gas (syngas) is determined by feedstock composition, the gasifying medium and the operating parameters such as temperature and pressure which influence the progress of the various chemical reactions. More detail regarding gasification chemistry is described in the Theory chapter.

Coal is currently the primary feedstock for gasification systems worldwide, with around four times as many gasifiers fed by coal as the next most prevalent feedstock, petroleum. Commercial biomass and waste fed systems are currently few but numbers are expected to rise in the near future. The dominant application for the coal gasification industry is chemicals manufacture, followed by liquid fuels. Planned future projects are most numerous for gaseous fuels (GSTC, 2016).

Commercial coal gasification processes can be categorised according to bed configuration and feeding methods. These include fixed bed (also known as moving beds); fluidised bed and entrained flow gasifiers. In dry ash systems the ash is removed as a solid while in slagging gasifiers it is melted and removed as a liquid. Coal is fed in lump or pulverised form, under pressure or as slurry. Established commercial technologies are summarised at the end of this section in Table 2-6.

2.2.3.1 Lurgi Process

The first commercial pressurised Lurgi process was developed in 1936. It is an autothermic process, meaning that heat for gasification is produced from the combustion of some of the coal. The process is a fixed bed, revolving grate technology usually fuelled by lump-fed lignite. It operates at pressures of 25-30 bar and temperatures around 620-760°C (Lee et al., 2007). For many years it was the only commercial pressurised process which contributed to its success (Higman and Van der Burgt, 2003).

The gasifying medium flows upwards in counter flow to the coal, being first preheated by the ash then heated in a shallow combustion zone up to peak temperatures before gasification occurs

above. The gasification products contact and dry the entering coal. Some pyrolysis products are thus entrained with the syngas before they can be reacted. These products include tars, phenol, ammonia and other hydrocarbons which must be removed by quench cooling after the gasifier exit (Higman and Van der Burgt, 2003). The typical syngas yield from this process depends on the feedstock and operating conditions.

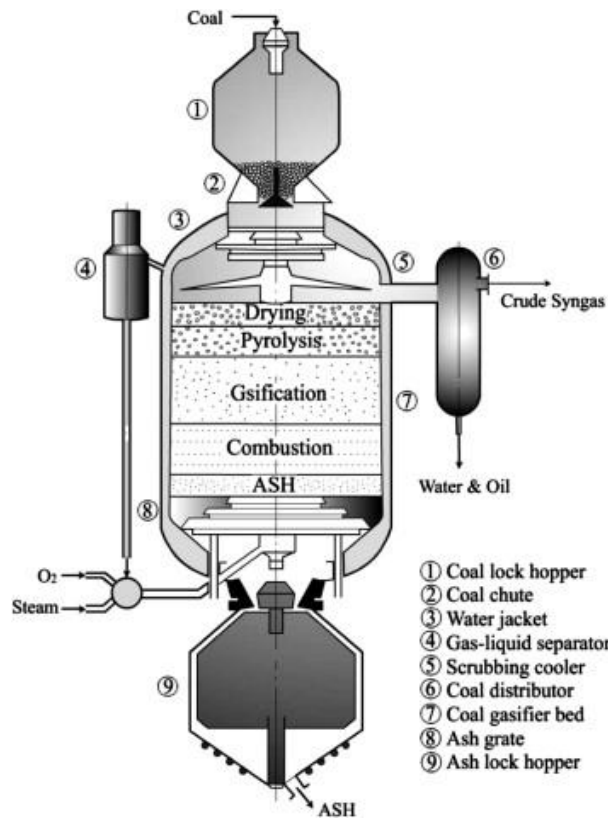


Figure 2-4: Diagram of pressurised Lurgi gasifier. Reprinted from (He et al., 2013) with permission from Elsevier.

An advantage of the Lurgi process is that the raw gas is further converted by passing over a catalyst, which promotes hydrogenation of higher hydrocarbons using leftover steam and facilitates gas clean-up without additional equipment (Schilling et al., 1981). The counter current arrangement gives a low oxygen requirement compared with other technologies; however the revolving grate system has more moving parts which require maintenance. The tar by-products also limit the use of the sensible heat in the product gas, reducing overall efficiency (Higman and Van der Burgt, 2003).

This process is recognised for its role in South Africa's Sasol complex. The product typically has a hydrogen fraction double that of carbon monoxide (Lee et al., 2007) and up to 50% in the raw gas (Rath, as cited in (Reddy, 2013)). However the high CO₂ content in the raw gas reduces its heating value.

2.2.3.2 The BGL Process

Developments into extending the fuel scope led to the British Gas/Lurgi (BGL) slagging gasifier, using bituminous coals and higher temperatures (1250-1500°C). As a result it became a molten ash process, requiring limestone addition to manipulate the slag flow and a redesigned ash removal system. Oxygen and steam are injected through ports in the side wall instead of under the bed.

This process was developed in the 1970s to produce synthetic natural gas from coal (Rezaiyan and Cheremisinoff, 2005). It aimed to increase CO and H₂ yields in a reactor suitable for coals with low ash melting temperatures and high levels of fines, while reducing steam consumption. During the 1990s the *Schwarze Pumpe* project in Germany, fuelled by lignite and municipal solid wastes, succeeded in increasing the fraction of CO in the syngas from 15 to 55% compared to the dry ash technology. The H₂ yield was reduced from 42 to 31.5%mol (Higman and Van der Burgt, 2003).

One further development was the Ruhr 100 process designed for operation at 100 bar. A pilot plant was built in 1979. The inclusion of a second coal lock hopper which halved the fuel pressurisation losses by operating alternately. By operating at such high pressure the throughput was effectively doubled and a greater fraction of methane was produced (Higman and Van der Burgt, 2003).

2.2.3.3 Winkler Process

The first Winkler process plant operated from 1925. This autothermal process uses oxygen and steam as the gasifying medium, as with all the technologies described in this section. This technology employs a fluidised bed at atmospheric pressure to contact the feedstock and gasifying agents. Due to the age of the technology and limited carbon conversion, almost all plants have ceased operation for economic reasons (Higman and Van der Burgt, 2003; Liu et al., 2009).

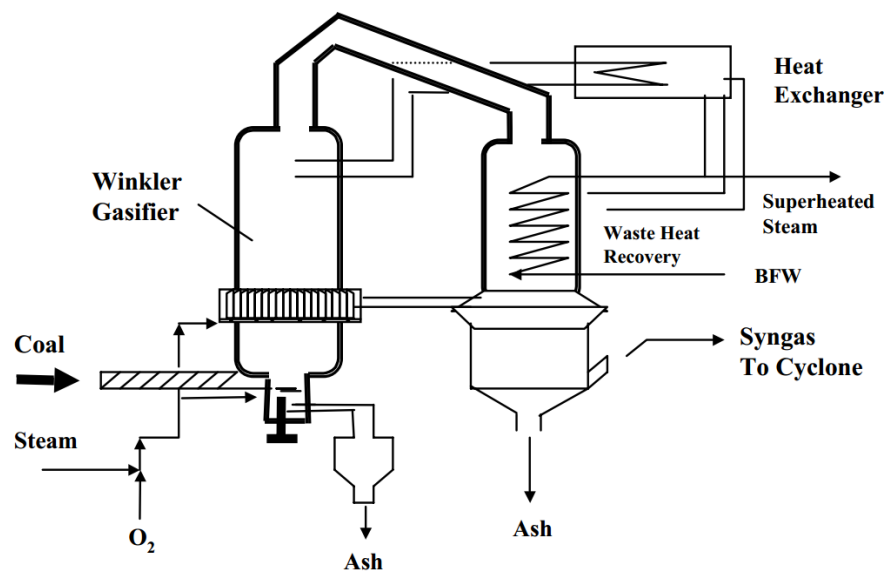


Figure 2-5: A schematic of the Winkler gasification process⁹.

Fluidised beds can accommodate a variety of feedstocks and are able to vary their load quickly, making them more versatile than other processes (Schilling et al., 1981).

Because small particles are entrained with the upward gas flow, secondary steam and oxygen are injected above the bed to improve carbon conversion and reduce the amount of tar produced. Ash must be removed to avoid being entrained. Some unreacted coal is also removed with the ash, reducing fuel efficiency. Even so, the raw gas leaves with a high dust content which requires comprehensive removal.

⁹ Republished with permission of Taylor and Francis, from (Lee et al., 2007); permission conveyed through Copyright Clearance Center, Inc.

The operating temperature is limited by the ash melting point, as soft ash can agglomerate and disturb the fluidisation regime (Higman and Van der Burgt, 2003; Schilling et al., 1981); however the low temperature and pressure limits the carbon conversion (Liu et al., 2009). Further developments led to a high pressure, high temperature Winkler process.

2.2.3.4 High Temperature Winkler (HTW) Process

Development of a higher pressure Winkler process allowed increased output and reduced product gas compression costs. The HTW process was developed by a German lignite producer in the 1970s and has been demonstrated at up to 30 bar (Higman and Van der Burgt, 2003). Higher temperature operation was made possible through the addition of limestone which raises the ash softening temperature and increased carbon conversion. The limestone addition also removes sulphur and makes the collected ash suitable for cement production (Schilling et al., 1981).

The dust in the raw gas complicates its purification. Cooling was performed using water tube coolers but fouling and corrosion problems were encountered; water scrubbing faced similar issues with blockages, leading to development of a hot gas filtration system (Rezaiyan and Cheremisinoff, 2005).

Further increases in gas velocity led to circulating fluidized bed systems and transport reactors. The Kellogg Brown and Root (KBR) is an example of a transport reactor in which the fluidisation velocity is sufficient to transport the whole bed around the reactor circuit at higher velocities and riser densities than circulating beds. This system benefits from up to 98% carbon conversion and higher throughput than HTW systems (Liu et al., 2009), but also significant operating costs for the circulation fans. The U-gas process is another similar fluid bed process.

2.2.3.5 Koppers Totzek Process

The Koppers Totzek process is an entrained flow system, whereby the feedstock and the gasifying medium travel co-currently, giving the fuel a residence time of only a few seconds within the gasifier. Such processes rely on fine feedstock particles and high temperatures to obtain sufficient conversion with short residence times (Higman and Van der Burgt, 2003). This process can accept dry pulverised solids or atomised liquids. The solid fuel preparation stage is intensive, limiting the moisture content to 2-8% and particle size <75 μ m (Schilling et al., 1981). There is also a high oxygen demand compared to other technologies, but the produced syngas is relatively clean, free of tar and available at high temperature (Higman and Van der Burgt, 2003).

The Koppers Totzek process was the first entrained flow slagging gasifier technology. It is operated at atmospheric pressure and commercial units were mostly built for ammonia production. Coal and gasifying medium are injected via opposite burners, with the raw gas leaving via the top and the slag exiting the bottom of the reactor. The ash is melted due to the high temperatures and collected as a liquid slag, quenched in a water bath beneath the reactor (Higman and Van der Burgt, 2003).

Unreactive fuels such as coke tend to yield a syngas high in CO and low in hydrogen, whilst the opposite is true of more reactive feedstocks such as lignite. Using natural gas as a feedstock was seen to yield 34% CO and 61.3% H₂ by volume (Schilling et al., 1981). If hydrogen is the desired product then a feedstock with a higher volatile content is most suitable.

High temperatures around 1500°C prevent the production of tar and phenol, which facilitates gas cleaning operations and is a great advantage over the other technologies listed. The high pressure

steam produced in the waste heat boiler is a valuable by-product with sufficient energy to power the air splitter for process oxygen (Schilling et al., 1981).

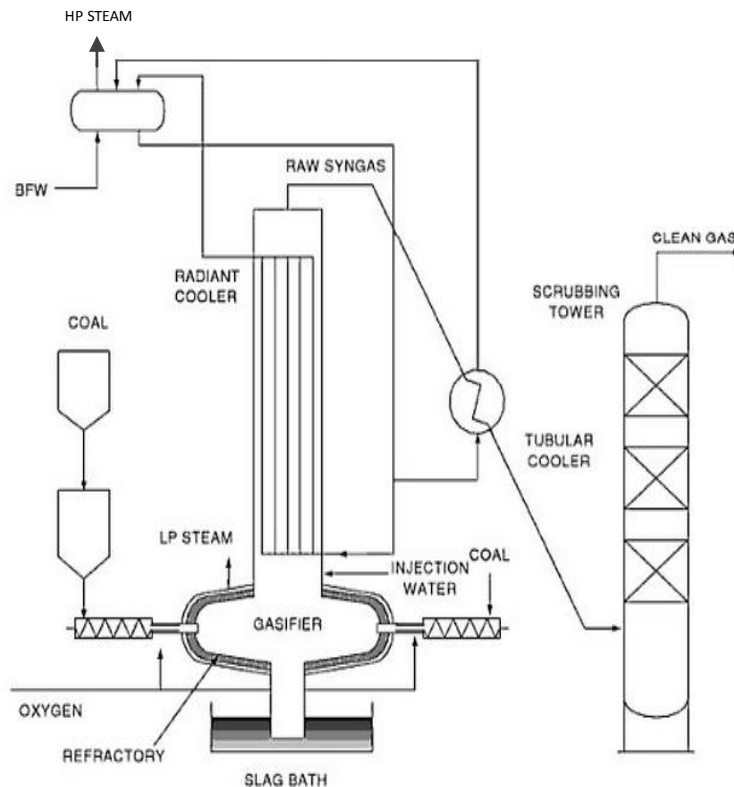


Figure 2-6: Koppers Totzek gasifier (Roland 1952) adapted from (Wikimedia Commons, 2010)

Such systems have the potential to rapidly vary their output from 60-100%, due to the small loading of fuel within the reactor at any given time. This process is able to shut down instantly and resume production in 30 minutes (Lee et al., 2007). There are also very few moving parts which reduces the maintenance requirements, particularly compared to moving bed designs. This gives entrained flow gasifiers high availability- often 95% or above (Higman and Van der Burgt, 2003; Schilling et al., 1981). The low pressure steam produced in the reactor jacket is more than that required for the process, which means the technology is self-sufficient in steam once it is running.

2.2.3.6 Shell Coal Gasification Process/Prenflo

These are both based on the Koppers Totzek process with the addition of pressurised operation. After initial collaboration, Shell developed the Shell Coal Gasification Process while Krupp-Koppers developed the *Prenflo* (pressurised entrained flow) process (Higman and Van der Burgt, 2003).

The feeding technology was key, using lock hoppers to pressurise the solid feed (Liu et al., 2009). Both feature diametrically opposed burners in the lower walls through which feedstock is injected for a residence time of 0.5-4 seconds before exiting the top of the reactor. These processes also operate above 1500°C at pressures of 30-40 bar. Additional steam is generated from the sensible heat in the product gas for additional power generation. The gas produced is typically around 66% CO and 33% H₂ (Higman and Van der Burgt, 2003; Lee et al., 2007; Liu et al., 2009; Manassah, 1981).

The exiting gas is quenched to 900°C to prevent the slag from sticking to downstream surfaces using recycled gas. Solids are removed by a candle filter (Higman and Van der Burgt, 2003).

The first commercial Shell process was an IGCC in the Netherlands built in 1993, which can process up to 2000 ton/day of coal. High rank coals require steam; sub-bituminous coals and lignite can operate without steam injection (Rezaiyan and Cheremisinoff, 2005).

The Shell process benefits from high conversion of a range of coals, thermal efficiency up to 80%, efficient heat recovery by producing HP steam and high throughput, as well as no significant by-product in the product gas (Lee et al., 2007). It uses 15-25% less oxygen than slurry fed systems as there is no requirement to vaporise feed water. However the solid feeding system is more complex which increases the capital expense, and injecting nitrogen or CO₂ with the feedstock has a negative impact on the syngas quality (Liu et al., 2009).

2.2.3.7 Texaco/G.E. Process

The Texaco process is another entrained flow system. A new preparation technique with slurry additives allowed this to become one of the most widely used technologies.

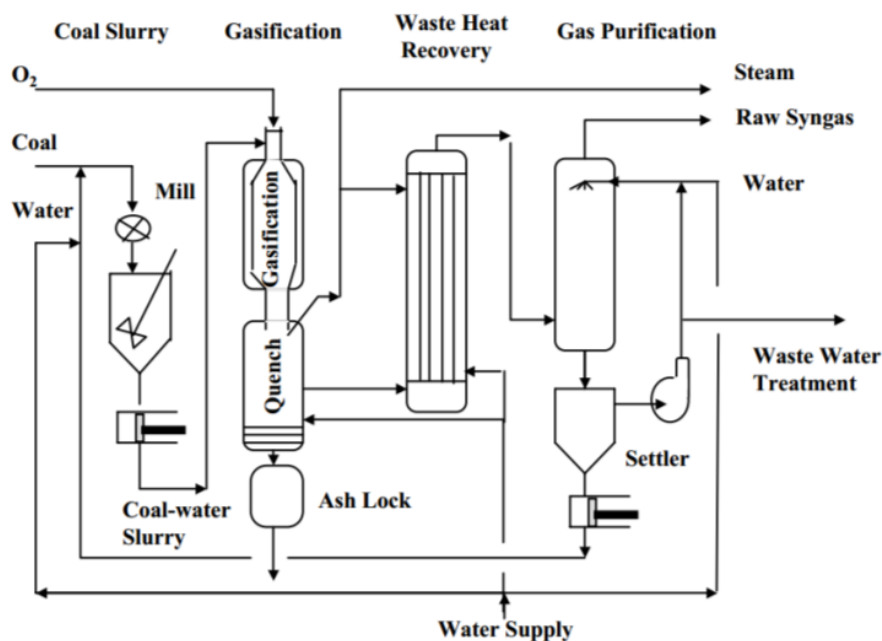


Figure 2-7: Texaco gasification process¹⁰.

In 2004 GE Energy acquired the technology formerly known as the Texaco or ChevronTexaco gasifier (Liu et al., 2009). Coal is fed as a slurry with water (48-55%wt coal), which replaces much of the steam injected in other processes. This water content imposes a high energy demand to vaporise it; as such this gasifier is best suited to energy dense feeds such as high rank coals (Lee et al., 2007). A liquid feed allows for easy pumping as opposed to batch compression of solid fuel in lock hoppers, which is typical of the other pressurised technologies described.

¹⁰ Republished with permission of Taylor and Francis, from (Lee et al., 2007); permission conveyed through Copyright Clearance Center, Inc.

2. LITERATURE REVIEW

The slurry is preheated up to 540°C before injection at the top of the gasifier. Operating pressure varies by industry; 20-30 bar for IGCC applications and up to 80 bar for chemicals synthesis (Lee et al., 2007). Operating temperature is around 1500°C, sufficient to melt the ash. This high temperature also inhibits tar and oil production, simplifying the gas clean up. By recovering heat from product gases, steam can be produced at up to 115 bar (Higman and Van der Burgt, 2003). This steam can be used in the process or for power generation.

The process can accept a variety of coals of different rank and operates at high temperature giving high carbon conversion compared to other early technologies. Disadvantages include the high O₂ requirement to maintain this high temperature, and a higher fraction of CO₂ in the product than processes with dry feeding (Liu et al., 2009). It is the least expensive design due to its simplicity but is described as the most maintenance intensive, at times requiring an installed standby unit, which cancels out the initial capital savings (Higman and Van der Burgt, 2003).

2.2.3.8 E-Gas/ ConocoPhillips Process

This pressurised coal slurry fed entrained flow process is distinguished from the Texaco process in that it incorporates two stages of operation. The technology has been owned by ConocoPhillips and most recently CB&I (NETL, 2013).

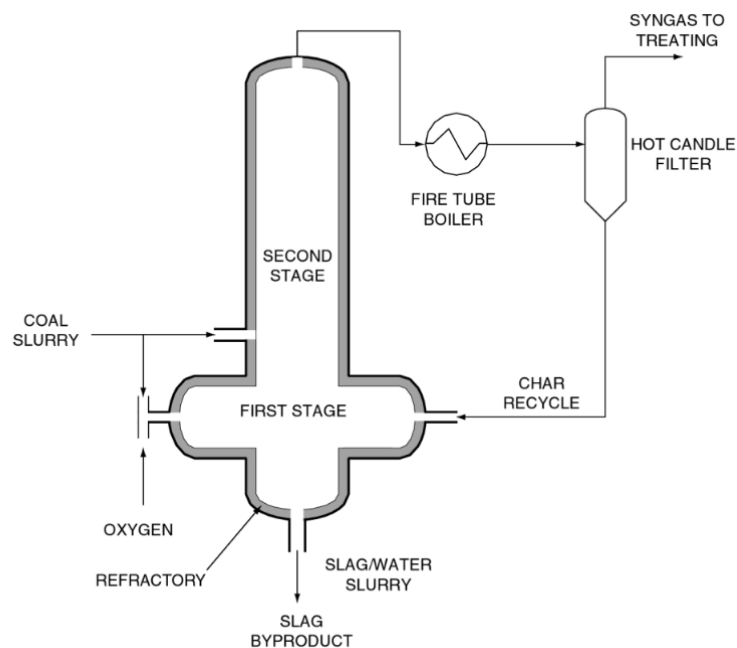


Figure 2-8: E-Gas gasifier. Reprinted from (Higman and van der Burgt, 2008) with permission from Elsevier.

Around 75% of the slurry is fed with oxygen into the lower section of the gasifier. Gasification occurs at 1400°C and up to 30 bar in the slagging stage. The cost of operating with liquid slurry and low rank coals is mitigated using the second stage, where the remaining slurry is injected into the hot gases from the first stage. This dries the slurry feed and provides heat for partial pyrolysis, and reduces the gas temperature to about 1050°C. The mixture passes through a fire tube cooler before being filtered to remove the remaining char. This char is then reintroduced at the first stage.

The second stage allows tuning of the syngas composition which can reduce downstream processing requirements. The process allows lower grade coals to be fed using the cold water slurry method while minimising the additional oxygen use and efficiency penalty. It also uses no lock hoppers for the slag removal (Higman and Van der Burgt, 2003; NETL, 2013).

2.2.3.9 Summary of Coal Gasification Technologies

Table 2-6 compares averaged data for different gasification technologies from various sources. It shows that fixed bed technologies have a high carbon conversion, likely due to the long residence times and low throughput compared with other processes. Fluid bed technologies have a lower carbon conversion due to the unreacted carbon removal with ash (Schilling et al., 1981). More reactive fuels such as lignite tend to yield a higher H₂/CO ratio, while unreactive fuels such as coke and anthracite yield more CO (Schilling et al., 1981).

Table 2-6: Summary of coal gasification technologies described¹¹.

Process Name	Lurgi	BGL	Winkler	HTW	Koppers-Totzek	Shell C.G./Prenflo	Texaco/GE	E-Gas/Conoco Phillips
Type	Fixed bed	Fixed bed	Fluid bed	Fluid bed	Entrained flow	Entrained flow	Entrained flow	Entrained Flow
Feed type	Lump coal	Lump coal	Ground coal	Ground coal	Pulverised coal	Pulverised coal	Slurry	Slurry, 2 stage
Temperature, °C	620-760	1250-2000	800-1100	800-1100	1400-1500	1200-1600	1200-1500	1400
Pressure, bar	25-30	20-30	(atm)	10-30	(atm)	25-65	20-80	20-40
Gas yield (%vol)								
H₂	40.0	27.9	37.7	33.4	31.0	28.3	34.4	32.9
CO	18.0	56.4	44.1	40.7	56.3	62.0	46.6	45.7
CO₂	31.1	3.7	15.9	12.1	9.8	3.0	11.2	15.6
CH₄	9.7	4.8	1.5	3.5	0.1	0.0	0.3	2.5
Inerts	1.0	3.7	1.0	1.1	1.1	7.0	1.3	2.8
H₂S etc	0.6	1.5	-	-	0.6	1.4	1.0	1.1
Carbon Conversion %	99.1	99.6	55-90	97.0	90-96	99.0	97.2	98.0

2.2.4 Commercial Biomass and Waste Gasification Systems

Biomass and waste gasification is an emerging market; some examples of commercial scale installations are given here. Many systems are built as demonstration plants; it is expected that more plants will be constructed as the technology matures.

The ten largest biomass gasifiers in the world are located in northern Europe (Vakkilainen et al., 2013); the two largest are in Finland including Kymijärvi II which produces 50 MWe and 60 MWth

¹¹ Data compiled from (Cortés et al., 2009; Higman and Van der Burgt, 2003; Lee et al., 2007; Liu et al., 2009; Manassah, 1981; Reddy, 2013; Schilling et al., 1981; Thyssen-Krupp Uhde, n.d.), Thumann, A (1981) as cited in (Liu et al., 2009) and Rath (n. d.), as cited in (Reddy, 2013)

2. LITERATURE REVIEW

from Solid Recovered Fuel. This consists of waste plastic, card and wood from domestic and industrial sources. The CFB air blown gasifier operates around 900°C producing primarily CO, CH₄ and H₂. The product gas is cooled to 400°C for cleaning to condense any alkali chlorides but avoid condensation of tars. The cleaned gas is combusted to raise high pressure steam for a turbine and for the district heating network (Lahti Energia, 2012).

The Energy Technologies Institute (ETI) recently ran a competition, offering funding for the best small scale waste gasification design with a net electrical efficiency over 25%. Three companies were shortlisted based on three different technologies; Advanced Plasma Power utilising a plasma torch for tar cracking, Broadcrown Ltd using thermal tar cracking and Royal Dahlman's MILENA segregated fluid bed design. The competition did not proceed beyond the initial stage due to a lack of funding by the company (ETI, 2016). One of the proposed sites in Tyseley, West Midlands, is now being developed as Birmingham Bio Power Ltd using Nexterra's fixed bed updraft gasification technology to generate 10 MWe from waste wood (Nexterra, 2014).

Energos technology is used in eight plants around Europe including on the Isle of Wight, UK. This process combusts all of the syngas to power the process and raise steam, so can also be categorised as two stage combustion of solid waste. It has a low electrical output of 1.8 MW, but the technology lends itself to production of heat for process steam or district heating (Energos, 2016).

2.2.4.1 Syngas Products (NEAT) Technology

The Syngas Products (formerly NEAT) gas-to-steam technology is used at the Avonmouth waste treatment facility near Bristol, UK. The energy recovery facility began operation in summer 2013 using Refuse Derived Fuel (RDF), which is biomass-rich non-recyclable waste from the adjacent waste treatment centre. RDF is treated by pyrolysis at >800°C followed by steam gasification of char. The gas products are combined and combusted to power the pyrolyser and raise high pressure steam for a turbine which generates up to 13 MWe (Syngas Products, 2016).

Due to the proprietary nature of the technology only basic details are available. The composition of the syngas is not stated, though the technology is designed to produce a gas with high calorific value for combustion as opposed to high hydrogen gas yield. Further advances are leading towards the use of a gas engine, which will allow generation of combined heat and power, further improving the efficiency of the process.

2.2.4.2 Air Products Renewable Energy Facility

Two 50 MW energy-from-waste units were to be built in Teesside, UK, to gasify 1000 tonnes/day of municipal waste using Westinghouse Plasma technology and Air Products gas processing technology (Air Products and Chemicals Inc, 2016a). Plasma gasification uses electric arcs through which air is passed to form plasma at temperatures around 5000°C. This plasma is then fed to the oxygen free gasifier for thermal decomposition of the feedstock. The gasification temperatures in the reactor are in excess of 3000°C, allowing treatment of a variety of feedstocks with high moisture content and inert materials such as glass and concrete. In addition, the gasifier is also charged with coke to provide a bed and crushed limestone to promote slag flow. Inert material is removed as vitrified slag, which can be used as aggregate.

A gas turbine imposes a tight specification for fuel gas, requiring sophisticated gas clean up prior to use (Westinghouse Plasma Corp, 2013). Deposits of alkali sulphates impede flow and cause corrosion

in the hot section of the turbine (Rezaiyan and Cheremisinoff, 2005). The high temperatures avoid the production of tars or higher hydrocarbons which hinder lower temperature gasification processes. The gas also requires compression before feeding to the gas turbine, which has a significant energy penalty.

After suffering several delays and cost overruns, Air Products cancelled the project in April 2016 citing “additional design and operational challenges would require significant time and cost to rectify” (Air Products and Chemicals Inc, 2016b).

2.2.5 Feedstock Preparation

Feedstock characteristics such as moisture and ash content, physical structure and metals content can determine the most suitable treatment method. Hard coals, being friable and having low moisture content, are suitable for grinding to maximise surface area for use in pulverised fuel combustion. Wet sources such as sewage sludge can be more suited to digestion due to the cost of drying. Woody biomass is unsuited to fine grinding due to its fibrous nature. Pyrolysis can improve the grinding characteristics of biomass as well as increasing porosity for high surface area. Hydrothermal treatment can also homogenise variable feedstocks such as municipal solid waste to produce a high CV powdery product similar to coal suitable for co-firing (Prawisudha et al., 2012).

2.3 Legislation

This section briefly describes policies, legislation and agreements which concern the energy industry. Air pollution control schemes are described, as well as solid waste concerns. In particular, UK governmental policies are identified which affect fuel and energy technology options.

2.3.1 International Agreements

Legislation and policies which have been internationally ratified set the benchmark for national targets and sanctions. The UK for example has a policy to ‘Support international action on climate change’ to lead the diplomatic effort to reduce climate change by negotiating with other governments and supporting developing countries in reducing their impacts.

2.3.1.1 Kyoto Protocol

The Kyoto Protocol was adopted in 1997 and first came into effect in 2005. It describes the need to reduce anthropogenic emissions of greenhouse gases to limit the effects of climate change. There were 192 parties to the protocol, of which 37 agreed to legally binding targets for the second phase of commitments, from 2013-2020. This ‘annex’ is made of up developed nations each with individual emissions targets (UNFCCC, 2013). The UK agreed to cut its carbon emissions by 12.5% based on 1990 levels by the year 2012. This target was successfully surpassed, and the UK now aims for 20% reduction by 2020. Notably, the USA chose not to ratify the Protocol; Canada also withdrew in 2012, so does not have targets for the second phase.

As a result of this protocol, governments are looking to reduce dependence on coal, by substituting less polluting sources such as natural gas and biomass. In the UK, modern combined cycle gas turbine (CCGT) plants can operate at close to 60% efficiency (Dawson and Spannagle, 2008; RWE, n.d.). However the cost of natural gas remains volatile and the UK is dependent on fuel imports. The

ability to synthesise a fuel gas which can substitute natural gas would allow these systems to be more economically competitive and secure as well as reduce their carbon emissions.

2.3.1.2 Montreal Protocol

The Montreal Protocol was one of the earliest environmental agreements that aimed to protect the ozone layer by limiting emissions of organo- halogens. These include CFCs and HFCs which at the time were in widespread use as coolants in refrigeration systems (EPA, 2010). As a result the use of CFCs and HFCs is now much more strictly controlled, and has seen a reduction in the levels observed in the atmosphere. The Montreal Protocol was ratified by 197 states, making it the most widely accepted agreement of its type.

2.3.1.3 Large Combustion Plant Directive (LCPD)

The LCPD was an EU directive which limited the emissions from plants with a thermal capacity over 50 MW, including power stations and energy intensive industries such as steel mills. The directive obliged plants that 'opted in' to reduce their emissions of NO_x, SO_x and particulates below prescribed levels. Plants incapable of complying could 'opt out' which limited their remaining operational hours before being forced to close by the end of 2015. The directive effectively forced governments and private energy companies to invest in 'Best Available Technologies' for emission mitigation or clean generation (European Commission, 2016).

The UK had a large number of plants affected by the LCPD. Of the 17 coal fired plants operating in the UK at the start of 2012, six opted out together with the three oil fired stations comprising over 25% of the UK's capacity at the time (DECC, 2015). Two of these plants converted to biomass fuel however they were still closed as their emissions of NO_x were above the threshold (DECC, 2013b).

2.3.1.4 Industrial Emissions Directive (IED)

In January 2016 the IED superseded the LCPD, imposing stricter limits on emissions from large combustion plants. Plants which are part of the Transitional National Plan can trade emission allowances with each other. Non-conforming plants have a limited lifetime derogation status and can operate for only 17,500 hours before forced closure in 2023 (European Commission, 2016).

2.3.2 Carbon Capture and Storage (CCS)

This is the concept of capturing carbon dioxide at sources such as power stations, to prevent it from entering the atmosphere. The gas is then compressed, transported and stored, trapping and effectively mitigating the carbon emissions from that source. The three principal categories of carbon capture are as follows;

- Post-combustion capture, in which the CO₂ is separated from the products of combustion;
- Pre-combustion capture, in which a fuel gas is produced from a feedstock from which CO₂ is more readily removed prior to combustion;
- Oxy-fuel combustion, in which fuel is combusted in pure oxygen in order to produce a flue of almost pure CO₂ and water vapour, allowing for easy separation.

Once the CO₂ has been separated from the other species to a suitable purity, it can be sold for use in food and drinks industries, sequestered for long term storage or used for enhanced oil recovery.

2. LITERATURE REVIEW

Post-combustion capture can be most easily retrofitted onto existing plants. The most common method uses monoethanolamine (MEA) to absorb CO₂ from flue gas. Although effective, the corrosive solvent is diluted with water to prevent damage to steel, increasing the solvent volume and the capture plant footprint. To regenerate the solvent it must be heated above 110°C, imposing a high energy penalty on the plant (Chalmers and Gibbins, 2007; Krutka et al., 2008).

The oil industry has for decades used CO₂ for enhanced oil recovery, by pumping it into wells to drive out additional resources (Global CCS Institute, 2013). Any usage requires the CO₂ to be cleaned, compressed and transported over long distances at significant cost. Uncertainty over the long term stability of sequestered CO₂ has also led to public resistance to the technology.

CCS has yet to become a firm UK policy due to the costs of establishing a CO₂ network. There is concern that the rate of development is too slow to impact on climate change (Global CCS Institute, 2013). The Norwegian government recently abandoned its *Mongstad* project due to overruns in time and budget. It was said that the economic recession and the low price of carbon credits resulted in reduced commercial interest in the technology (Patel, 2013). Research is underway to develop CO₂ utilisation processes, for chemical synthesis or to produce fuels, which would increase the value of carbon dioxide and provide an additional incentive for its capture (RSC, 2016).

The costs of post-combustion capture provide a case for fuel pre-treatments such as pyrolysis and gasification which facilitate pre-combustion capture. This can be more economical as CO₂ is present in higher concentrations, which facilitates the gas separation and reduces costs. Sulphur species can also be recovered as sulphur or sulphuric acid which are more valuable than the products of flue gas desulphurisation (Rezaiyan and Cheremisinoff, 2005).

2.3.3 UK National Policies

This section looks at the policies made on a national level in the UK. In particular policies which affect power generation and fuels are described.

2.3.3.1 2008 Climate Change Act

This was the world's first legally binding emissions target, which aims to reduce GHG emissions by 80% of the 1990 baseline by 2050. The EU Emissions Trading Scheme (ETS) allows polluters to buy carbon credits from users who have made efficiency savings, effectively spreading the cost of emission reductions (European Commission, 2013). The CRC Energy Efficiency scheme is a UK permit trading scheme for emissions not covered by the EU ETS. Participants that use over 6000 MWh/yr of electricity require allowances for every tonne of CO₂ equivalent emitted (DECC et al., 2013). The Act also reduces planning risks and supports a UK supply chain for the nuclear industry.

2.3.3.2 Increasing the Use of Low Carbon Technologies

The Climate Change Act also led to the introduction of this policy, which promotes renewable and nuclear energy. This is implemented through a number of schemes such as the Renewables Obligation, the Feed in Tariff, Renewable Heat incentives and Renewable Transport Fuel Obligation.

The Renewables Obligation (RO) was introduced in the UK in 2002 to promote large scale renewable electricity generation. Electricity suppliers in the UK must source a set amount of the power they provide from renewable sources each year. This is enforced using Renewable Obligation Certificates issued to renewable energy producers according to the quantity they generate. These certificates

are sold to electricity suppliers on top of the generated power, providing a premium above the wholesale electricity price for the renewable electricity. These certificates are used by the supplier to demonstrate compliance with their obligation. Biomass is one of several accredited sources of renewable electricity, which also includes onshore and offshore wind (DECC, 2013c).

The Feed in Tariff and renewable heat incentives provide financial support for small scale low carbon installations of electricity and heating, for example installation of solar panels on a domestic roof or investing in a biomass boiler. The Transport Fuel obligation requires that large scale fuel suppliers must source a percentage from renewable sources.

2.3.3.3 Renewable Energy Roadmap

The UK has a target of 15% of energy consumption from renewable sources by 2020, including electricity, heat and transport. It was recognised that the renewable electricity market is already strong with promising growth prospects, while renewable heat and transport fuels are less well developed. The Roadmap focuses on technologies that offer the greatest potential to meet the target economically and sustainably (DECC, 2011).

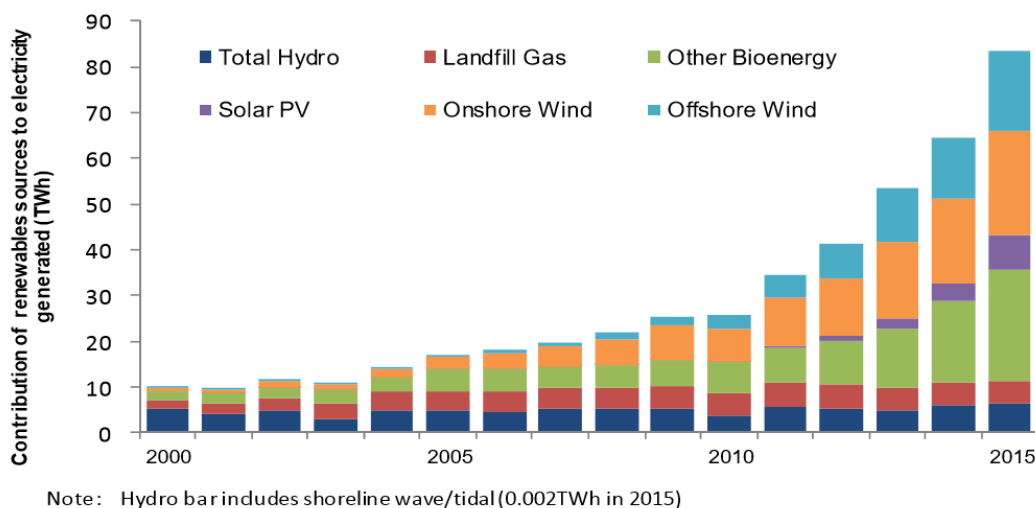


Figure 2-9: Electricity generation by main renewable sources since 2000¹².

The 2013 update summarises that renewable energy consumption rose from 3.8% in 2011 to 4.1% in 2012, with renewable electricity peaking at 15.5% of generation in Q2, 2013. High growth was seen in offshore wind, while use of biomass for electricity was limited. Biomass development is primarily in the generation of heat, such as CHP applications as defined in the Bioenergy Strategy 2012. Conversion of coal power plants to biomass is a low cost transitional means to rapidly reduce the carbon emissions from the electricity network (DECC, 2013d), though by itself may not be a sustainable long term solution.

2.3.3.4 Reducing and Managing Waste

This policy addresses waste production and management. As well as increasing recycling, the policy includes energy recovery from waste to provide economic opportunities and contribute to the renewable energy target.

¹² (Department for Business Energy & Industrial Strategy, 2016). Contains public sector information licensed under the Open Government Licence v3.0.

Anaerobic digestion is described as “*the best environmental option currently available*” (DEFRA, 2013) to divert waste from landfill while generating renewable energy and digestate as fertiliser. Investment during 2011-2014 fuelled substantial growth, particularly in waste food digestion. However in terms of electrical output per unit of waste, high temperature gasification has been calculated to give a higher yield (Gikas, 2014).

Incineration is included in the waste management policy and can reduce waste while producing heat and power which can be distributed through district heating networks such as in the cities of Nottingham and Sheffield. To qualify for an incineration permit, operators must recover energy wherever possible (Environment Agency, 2013). England currently incinerates 17% of waste, which is below the European average of 24% (see Figure 1-5). Public opposition to incineration makes it difficult for new units to gain permission. Advanced thermal treatments such as gasification may provide a more publicly acceptable solution to waste reduction with energy recovery.

2.4 Gasification Research

This section summarises some current research being undertaken in coal and biomass gasification, focussing on the treatment of solid materials. Current gasification research addresses the scale up of novel technologies, use of unconventional feedstock such as municipal solid waste, reduction of tar formation and improving carbon conversion.

Gasification can be used for hydrogen production. Hydrogen is not available naturally so must be produced from sources such as water. As such hydrogen can be described as an energy carrier with a similar function to electricity. It is seen as a promising energy vector for the near future, however around 95% of global hydrogen is currently produced from unsustainable fossil fuel sources (Balat and Kirtay, 2010; Mirza et al., 2009).

Gasification is one of several mechanisms used to produce energy from biomass. Compared with biological methods, thermal methods such as gasification benefit from higher overall efficiency and lower production cost (Balat and Kirtay, 2010). Biomass gasification is a viable route to hydrogen production, although not yet competitive with natural gas reforming (Balat and Kirtay, 2010; Udomsirichakorn and Salam, 2014).

2.4.1 Tar Destruction Methods

Much current research into biomass gasification uses fixed bed and fluidised bed technologies. These can be used at small scale and achieve high conversion of feedstock. However the production of tars presents the single largest challenge in any gasification commercialisation effort (Erkiaga et al., 2013; Nakamura et al., 2015). The definition of tar varies between authors, but it is generally understood to include largely aromatic organic species heavier than Benzene, produced from high temperature or partial oxidation treatment of biomass (Erkiaga et al., 2013; Milne et al., 1998; Stevens, 2001). These condense on contact with reactor walls and heat transfer surfaces, causing fouling which requires costly clean up. Tar production reaches a maximum at around 500°C before decreasing with increasing temperature (Bhutto et al., 2013; Lucas et al., 2004). Technologies for tar reduction are actively being researched (Acharya et al., 2013; Nakamura et al., 2015; Tuomi et al., 2015). Thermal cracking requires temperatures in excess of 1000°C to eliminate tar completely (Milne et al., 1998; Schmidt et al., 2011). The presence of steam is known to reduce high molecular

weight hydrocarbons via steam reforming (Mahishi and Goswami, 2007; Shen and Yoshikawa, 2013; Wei et al., 2007).

In high temperature steam gasification of waste plastics, the tar yield was observed to decrease rapidly with increasing temperature above 1000°C, particularly in the presence of steam owing to steam reforming of tar compounds. It was also suggested that high traces of metals in the feedstock may act as a catalyst for tar cracking (Kantarelis et al., 2009). See also Section 2.4.3.2.

2.4.2 Influence of Gasification Medium

Different gasification mediums are compared against hydrogen yield in Figure 2-10. Using oxygen instead of air as a gasifying agent produces a gas with a higher calorific value and hydrogen content, due to the absence of nitrogen dilution. Steam and oxygen mixtures yields a higher H₂ fraction again, and steam alone higher still (Udomsirichakorn and Salam, 2014). In many gasifiers a limited amount of oxygen is supplied to combust some feedstock to provide heat for the endothermic gasification chemistry. Where heat energy is provided externally by electric heaters etc. oxygen addition is not required. Similar results were also summarised by (Gil et al., 1999).

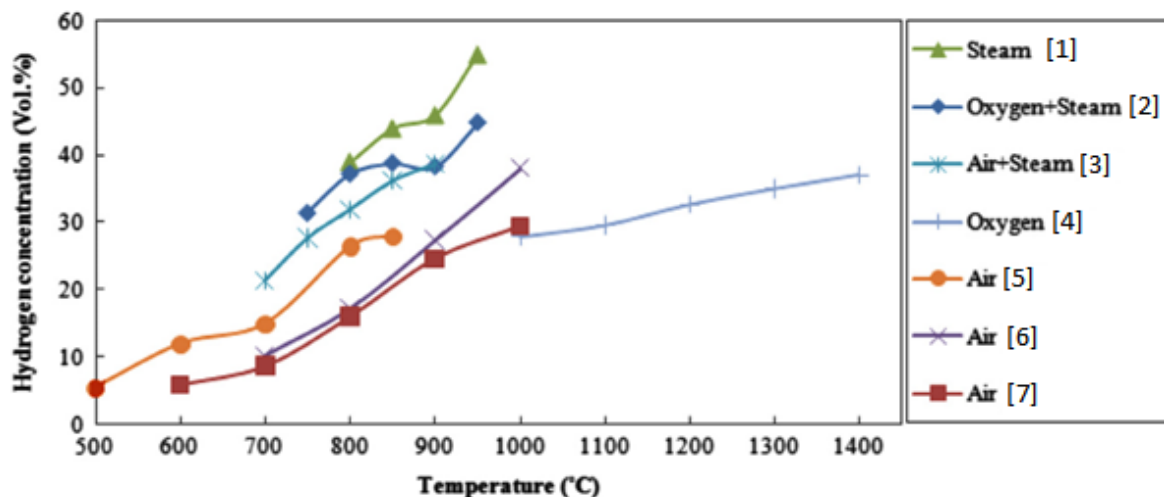


Figure 2-10: Effect of gasifying medium and temperature on hydrogen yield¹³.

It was suggested that when oxygen was introduced, oxygen reactions with carbon and hydrogen occurred in favour of water gas and water gas shift; decreasing the H₂ concentration compared to steam only applications (Gao et al., 2008). Steam only gasification was also found to yield greater quantities of hydrogen, as well as higher concentrations, on a mass H₂/mass biomass basis (Turn et al., 1998).

2.4.2.1 Effect of Gasification Temperature on Gas Yield

The effect of temperature on the product yield from biomass gasification has been studied in several works. In general, higher gasification temperatures yield higher concentrations of H₂ and CO, with lower concentrations of CH₄ and other hydrocarbons (Jin et al., 2010; Turn et al., 1998;

¹³ Data from [1] (Gao et al., 2008); [2] (Turn et al., 1998); [3] Lv et al, (2004); [4] Zhou et al, (2009); [5] Mohd Salleh et al, (2010); [6] Mohammed et al, (2011) [7] (Chang et al., 2011) as cited in figure by (Udomsirichakorn and Salam, 2014). Reprinted with permission from Elsevier.

Udomsirichakorn and Salam, 2014). Lower CO₂ content has also been reported with higher temperatures (Chang et al., 2011; Gao et al., 2008). A number of potential reasons for the increased H₂ yield at higher temperature have been reported, including improved conversion of biomass solid into product gas, additional heat provided to the endothermic char gasification reactions and cracking of heavier compounds and tars at elevated temperatures (Udomsirichakorn and Salam, 2014). The endothermic gasification reactions are discussed in the Theory chapter.

2.4.2.2 Supercritical Water Gasification

This technology utilizes water above 22 MPa (~220 bar) and 374°C as the gasifying medium, giving supercritical conditions. Properties of supercritical water such as high diffusion rate, low viscosity and miscibility with hydrocarbons make it a promising candidate for fast and efficient reactions. Moreover, lower temperatures can be used in comparison with combustion and other thermal technologies which reduce the formation of NO_x and SO_x while the closed system avoids particulate ash emissions (Jin et al., 2010).

A recent experimental work gasified bituminous coal in supercritical water. Coal was fed as a water slurry to a continuous fluidized bed reactor. It was found that with increasing coal concentration, the hydrogen concentration in the product decreased in favour of methane formation. A run at 24%wt coal in water was gasified continuously without plugging problems, and yielded on average 52% hydrogen in the product gas. Higher coal loadings resulted in incomplete gasification and plugging problems. The highest hydrogen yield was obtained for the lowest coal loading of 4%wt in water, giving a concentration of 63% H₂ in the gas at 580°C. With a large excess of supercritical water (circa 0.5%wt carbon in water) a hydrogen fraction of almost 70% was recorded. Varying the operating pressure from 230 to 270 bar had no significant effect on yield (Jin et al., 2010).

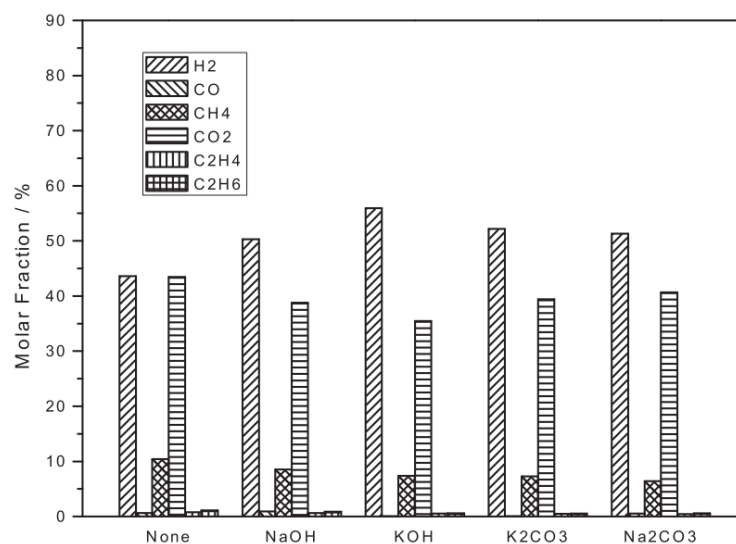


Figure 2-11: Effect of catalyst on supercritical water gasification of sewage sludge. Reprinted from (Chen et al., 2013) with permission from Elsevier.

A similar experiment was conducted using sewage sludge. This gasification method is well suited to this material as it avoids the need to dry the feedstock. High hydrogen yields typically require gasification temperatures above 600°C, but these temperatures have issues associated with tar formation and corrosion. As such a number of catalysts were investigated to suppress tar formation and promote hydrogen production. Similar trends were observed with respect to temperature

variation and concentration of feedstock as with the previous work. All the catalysts investigated were found to improve the H₂ yield; only Na₂CO₃ had an overall negative effect on the gasification efficiency (Chen et al., 2013).

In general the relatively low temperatures and high pressures used in supercritical water gasification appear to make this technique more vulnerable to solid deposition than other thermal methods, which impedes continuous operation, particularly with the tubular reactors used in high pressure applications (Jin et al., 2010).

A small batch system using RuO₂ catalysts in supercritical water has also been shown to be effective at producing methane from waste plastics (Onwudili and Williams, 2016a) and bio-oil (Onwudili and Williams, 2016b) at modest temperatures around 500°C.

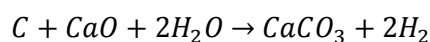
2.4.3 Catalytic Aides for Gasification

This section outlines some research in which catalysts are being used to enhance the gasification process, by promoting gasification chemistry or reducing the production of unwanted by-products.

2.4.3.1 CaO as a Sorbent for CO₂

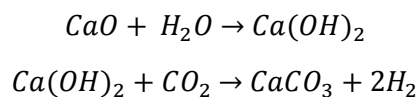
Research has been conducted on the use of CaO as a means of removing CO₂ from syngas. Steam gasification of coal produces a mixture of CO and H₂; additional H₂ is then produced through the water gas shift (WGS) reaction, which also produces CO₂. While steam gasification is endothermic, the WGS reaction favours lower temperatures, so these are traditionally performed in separate reactors under different temperatures. However if CO₂ could be removed during the WGS reaction, the equilibrium of this reaction will move to progress under higher temperatures and hence these reactions could be performed in a single reactor (Cotton et al., 2013; Lin et al., 2002).

The Carbon Dioxide Acceptor Process from the 1960s successfully reduced the levels of CO and CO₂ by around half, using CaO as a CO₂ sorbent. Using a single reactor as described, gasification and CO₂ capture are represented in one reaction as shown in Equation 2-3;



Equation 2-3 (Lin et al., 2002)

The reaction of CaO with CO₂ to produce CaCO₃ is highly exothermic, so higher pressures are required with increasing temperature. A possible intermediary reaction is of CaO with steam;



Equation 2-4

Equation 2-4 is substantially less exothermic than the one step reaction, which suggests that the addition of steam facilitates this reaction in high temperature environments. Nevertheless, pressures above 30 bar were necessary for this reaction to progress at 700°C (Lin et al., 2002).

In a continuous plug flow reactor the product gas was found to contain >70% hydrogen on a nitrogen free basis at 50 bar and 650°C. Atmospheric pressure tests were impeded by tar blockages and poor

absorption of CO_2 by CaO . Higher temperatures resulted in solid deposits. The experiment was found to run smoothly above 10 bar at 650°C . Lower H_2 yield compared to the batch reaction was associated with the shorter residence time of the gases in the continuous reactor (Lin et al., 2004).

Temperatures of 700°C caused $\text{Ca}(\text{OH})_2$ and CaCO_3 melting, which caused blockages impeding continuous operation. Decreasing the temperature to 650°C avoided the melting issue; however crystallisation of calcium compounds must be considered in reactor design and operation. The CaCO_3 can be thermally regenerated to CaO and a stream of near pure CO_2 (Lin et al., 2006, 2004).

Other researchers have investigated CaO as a CO_2 sorbent in biomass gasification. In a bench scale batch reaction of pine bark, CaO was found to increase the quantity of H_2 yielded by 48.6% compared to the case without CaO . The use of two reactors eliminated the need for elevated pressures (Mahishi and Goswami, 2007). Several research cases are summarised (Udomsirichakorn and Salam, 2014) in which hydrogen yields from biomass have been improved using CaO .

2.4.3.2 Use of Catalysts for Tar Reduction

In biomass gasification up to 20% of the feedstock can remain as unconverted char or be converted into volatile organic compounds including aromatic and heterocyclic species, in the form of tar (Hernández et al., 2013). Gaseous species containing sulphur and chlorine are also produced from biomass feedstocks. These by-products need to be removed to avoid contamination of the product gas, tar deposition and blockage of downstream equipment. The gas clean-up operations can account for 50 to 75% of the overall processing costs (Erkiaga et al., 2013).

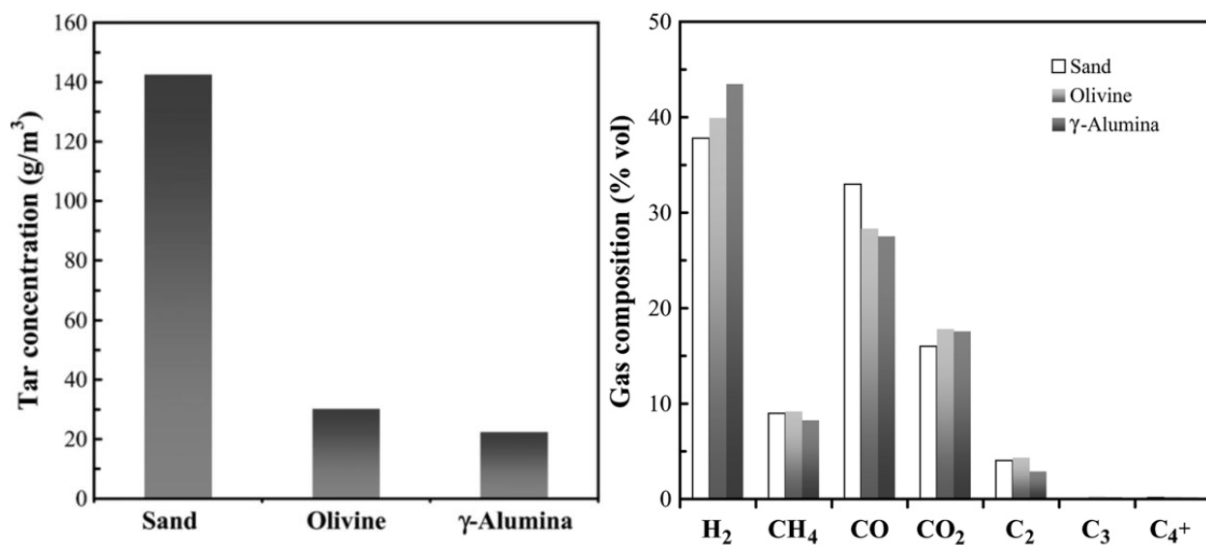


Figure 2-12: (a) Tar yield in product gas from different bed materials, (b) effect of bed materials on gas composition. Reprinted from (Erkiaga et al., 2013) with permission from Elsevier.

Tar reduction methods are broadly categorised as primary methods, which aim to reduce the tar formation in the reactor, and secondary methods to clean the tar from the product stream. Catalysts such as olivine and alumina have been shown to promote tar cracking in the reactor. Olivine ($(\text{Fe},\text{Mg})_2\text{SiO}_4$) is an inexpensive material and shares significant reforming capacity and high strength with alumina (Al_2O_3) (Erkiaga et al., 2013).

Olivine and γ -alumina were compared against silica sand beds to gasify crushed pine at 900°C. Both catalysts were found to substantially reduce the tar yield, as shown in Figure 2-12, and increase yields of H_2 and CO_2 . Reduced concentrations of polyaromatic hydrocarbons (PAH) and increased yields of light aromatics were associated to catalytic cracking of PAHs. It was concluded that the catalyst promoted the water gas shift reaction which explained the diminished CO levels compared to the sand case. Increased H_2 and CO_2 yields were associated to cracking tar compounds. Further, alumina appeared to promote the reforming of CH_4 and higher hydrocarbons (Erkiaga et al., 2013).

Metallic catalysts, particularly nickel based, have been shown to be effective at destroying tars and promoting reforming of methane, however they are insufficiently robust for use in fluid bed applications and suffer rapid deactivation leading to limited lifetimes (Dayton, 2002).

2.4.3.3 Ash Catalysis of Gasification Reactions

Char reactivity depends primarily on chemical structure, inorganic constituents and porosity (Di Blasi, 2009). Biomass chars tend to be more reactive than coal in both pyrolysis and gasification. Wood charcoals have porosities up to 50% with a pore size of 20-30 μm , while coals have porosities up to 18% and a pore size of around 0.5 nm (Dong and Borgwardt, 1998; Encinar et al., 2001).

In combustion systems fuel ash content is often undesirable, and processes such as acid leaching have been investigated to remove ash from coals. Trace elements in biofuels can form combustion residues which can cause technical and environmental issues, and can be difficult to monitor in gasification systems (Poole et al., 2007). However alkali metals, particularly sodium and potassium have been shown to catalyse oxidation reactions. Potassium has been shown to catalyse both biomass devolatilisation and char burn-out, as well as reduce primary tar formation in low temperature and flame environments (Jones et al., 2007; Nowakowski et al., 2007)

Oxides and salts of alkali and alkaline earth metals also catalyse steam and CO_2 gasification reactions (Chen and Yang, 1997; Di Blasi, 2009). Metal chlorides are particularly attractive as catalysts due to their low cost (Encinar et al., 2001). Conversely, the presence of silica decreases the catalytic activity of ash (Rizkiana et al., 2014; Zhang et al., 2008).

Soluble minerals have a greater influence than surface area on char reactivity (Di Blasi, 2009; Iniesta et al., 2001). In a study where charcoals were partially demineralised by acid washing, a six-fold increase in specific surface area was achieved but the samples exhibited much lower reactivity (Várhegyi et al., 2006).

2.4.4 Method of Heat Input

Various methods of providing heat to the endothermic gasification reactions have been studied. A distinction is made between *autothermic* and *allothermic* systems. In autothermic systems the heat energy is produced within the gasifier, usually by the addition of oxygen for combustion of part of the feedstock. Often a significant amount of the feedstock must be combusted; for a high rank coal this can mean as much as 35% of the feed (Piatkowski and Steinfeld, 2008). In an allothermic process heat is introduced from an external source such as electric heaters or auxiliary fuel. The gas yield from the feedstock is maximised however additional costs are incurred which vary with the heat source. This section describes some methods of providing heat for the gasification reactions.

2.4.4.1 Microwaves for Plasma Production

Plasma torches offer very high temperatures in pyrolysis and gasification, thousands of degrees higher than other entrained flow technologies. Plasma arc generator electrodes are sensitive to steam, often used as a gasifying medium. The use of these electrodes can be avoided by using microwave energy for plasma production, allowing steam to be used as a gasifying medium and plasma forming gas. This avoids nitrogen dilution and facilitates gas separation (Yoon and Lee, 2012).

In an experimental microwave steam plasma apparatus, mixtures of steam and air were tested as the gasification agent, to vary the oxygen/fuel ratio for gasification of coal and charcoal. It was found for both feedstocks that increasing the oxygen ratio had a negative effect on the hydrogen yield and increased the concentrations of CO and CO₂. In conventional gasification, combustion is required to provide heat for the gasification reactions. Where the heat is provided by microwaves, oxygen is not required for gasification to occur. Gasification performed without oxygen was found to yield the highest H₂ concentration of around 60% (Yoon and Lee, 2012).

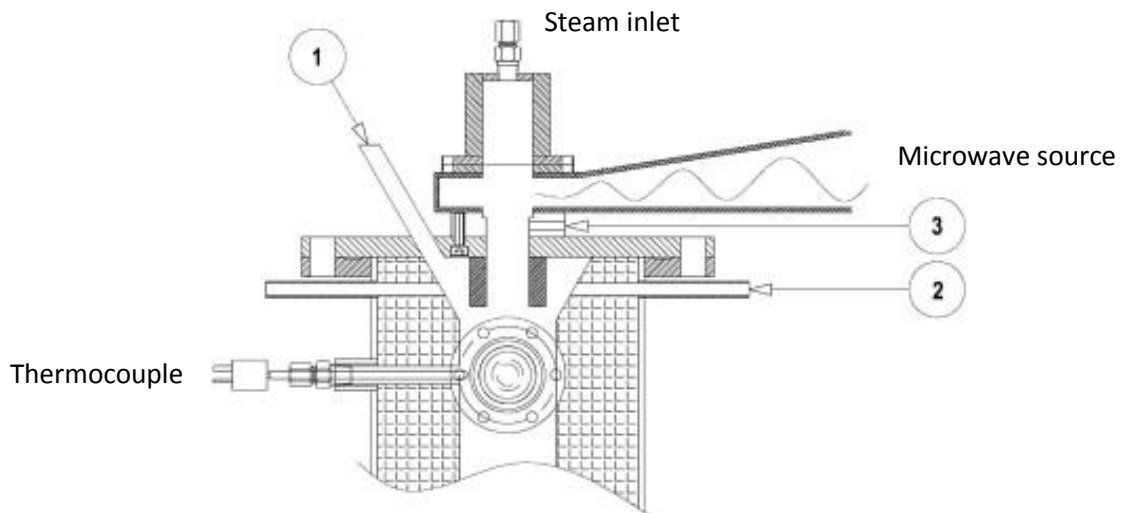


Figure 2-13: Burner nozzle showing three coal feeding locations. Reprinted from (Yoon and Lee, 2012) with permission from Elsevier.

Another finding was the effect of the coal feeding location. Figure 2-13 shows the reactor inlet with three feeding locations. It was found that the H₂ yield increased from 32 to 45% by changing the feeding location from point 1 to point 2, and decreased the CO₂ content from 35 to 25%. Location 3 gave comparable concentrations to location 2. The carbon conversions and cold gas efficiencies are shown in Figure 2-14. Both parameters were highest when using feed location 3. It was concluded that location 3 introduced the feedstock directly into the hottest central part of the plasma and subjected it to the longest residence time therein which increased the conversion. The syngas produced from feeding at location 3 had the highest H₂ concentration and the highest calorific value. Location 3 is close to where the plasma flame is formed and is narrower than the reactor diameter.

Carbon conversion increased with increasing oxygen in the plasma, due to increased combustion of feedstock. The yield of H₂ and CO was highest in low oxygen tests. There is therefore a compromise between syngas quality and quantity, expressed by the cold gas efficiency which peaked at an intermediate oxygen/fuel ratio of 0.272, where a ratio of 0.544 represented pure air with no steam.

2. LITERATURE REVIEW

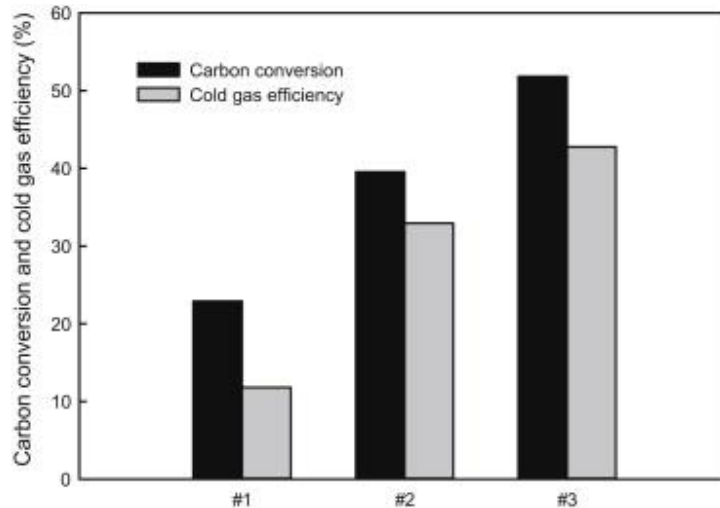


Figure 2-14: Carbon conversion and cold gas efficiency with feed location for the microwave gasifier. Reprinted from (Yoon and Lee, 2012) with permission from Elsevier.

In comparing coal and charcoal tests it was found that the carbon conversion and syngas yield from charcoal were significantly lower than for both coal samples tested. It was argued that because charcoal had a higher percentage of fixed carbon (70.37% compared to 57.32% and 34.78% in the coals) it was less reactive than the coal samples. Devolatilisation occurs followed by the char reaction; the latter requiring longer residence time. High carbon content means higher char fraction and low reactivity, hence requiring a longer residence time than afforded by this reactor resulting in low gas yield and poor conversion. The charcoal sample yielded higher CO_2 and lower H_2 and CO concentrations throughout the study (Yoon and Lee, 2012).

2.4.4.2 Cyclic Operation Using a Multi Compartment Fluidised Bed

Where external heating is supplied to allothermic fluidised beds, the external surface area is insufficient to provide adequate heat exchange. To improve the heat transfer, a reactor concept has been proposed utilising multiple compartments. The novel design divides the bed into adjacent compartments alternately used for gasification and combustion. Feedstock is introduced into gasification compartments fluidised by steam while the adjacent compartments were fluidised with air to combust the unreacted char and provide heat. Periodically the zones are switched to alternate gasification and combustion beds. Gasification products are removed separately from the combustion products, reducing the contamination of the syngas by nitrogen, oxygen or excess CO_2 (Iliuta et al., 2010).

Char conversion in combustion could reach up to 95% at 850-900°C. An increase in H_2 and CO yields and decrease in CO_2 and CH_4 with increasing temperature was observed, while simulation predicted a syngas yield of 35-40% H_2 , 17% CO , and 12% CO_2 on a wet basis, in fairly close agreement with experimental data of similar systems.

The alternating system was predicted to provide sufficient heat to preheat the bed material in 60 second cycles, which eliminated the need for auxiliary heating fuel. Where 20% heat losses from the system were simulated; it was reported that supplementary biomass may need to be fed in the combustion stages. The study demonstrates the feasibility of the alternating beds concept (Iliuta et al., 2010); a similar design is used in the MILENA system licenced by Royal Dahlen (ECN, 2011).

2.4.4.3 Solar Powered Gasification

Solar energy can be used to provide heat in place of combusting the feedstock which avoids combustion products in the syngas. Using concentrating mirrors, temperatures over 1000°C can be obtained.

Solar gasifiers can be broadly distinguished according to whether they are directly or indirectly irradiated. Direct systems expose the feedstock directly to solar radiation via a window, which offers efficient energy transfer but presents difficulties in keeping the window clean. Large windows result in thermal losses (Piatkowski and Steinfeld, 2008; Puig-Arnavat et al., 2013). Indirectly irradiated reactors rely on heat transfer by conduction through an opaque absorber surface.

Numerous types of reactor have been tested at laboratory scale. Most use CO₂ or steam as the gasifying medium. Few have been built beyond laboratory scale (Puig-Arnavat et al., 2013).

2.4.4.4 High Temperature Agent Gasification (HTAG)

In these systems the gasifying agent is heated prior to entering the reactor such that it acts as both reactant and heat carrier. A study found that the hydrogen yield increased with increasing steam fraction and increasing the temperature of the agent reduced tar formation and char residue, while increasing the heating value of the product gas (Lucas et al., 2004).

A demonstration scale updraft fixed bed gasifier using superheated steam was built to accept 1.2 tons/day of woody biomass and waste plastic. The updraft system was designed to increase char conversion by contacting the char with the hottest steam on entry to the reactor. This however caused significant tar content in the product gases. A reformer was installed and fed with limited oxygen for partial oxidation (Umeki et al., 2010).

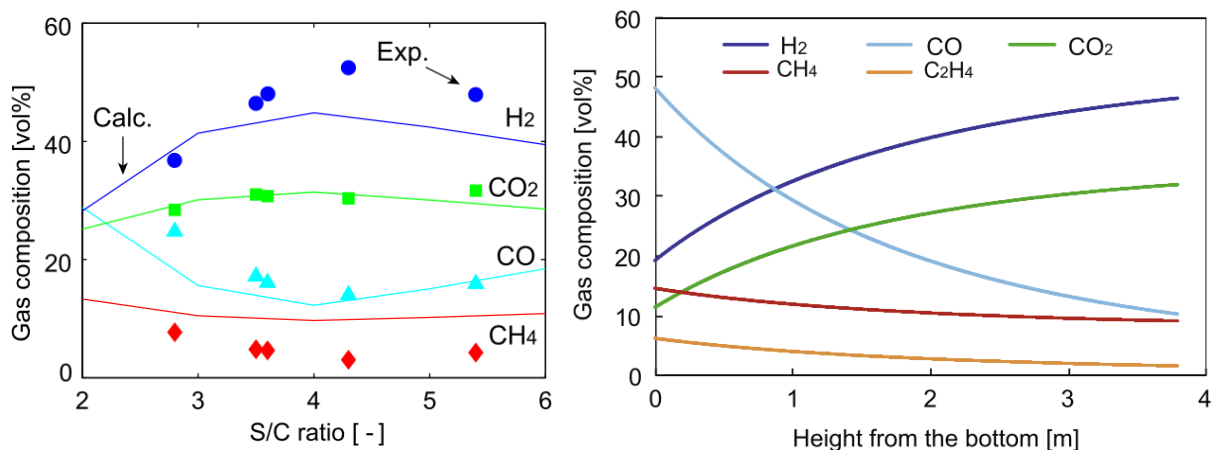


Figure 2-15: (a) Steam/carbon ratio vs product gas composition. Points = experimental data; lines = numerically calculated results. (b) Numerically calculated gas composition vs height in the reactor. Reproduced from (Umeki et al., 2010) with permission from Elsevier.

The authors noted a higher tar yield from steam gasification compared to oxygen blown gasification. A hydrogen yield over 40% was obtained in most experimental cases, as shown in Figure 2-15. The hydrogen concentration peaked at a steam/carbon (S/C) ratio of 4.3. Where steam is the heating medium and gasifying agent, the steam flow rate is directly linked to reactor temperature and residence time. At lower S/C ratios, increasing steam flow gave higher temperatures and increased reaction rate, resulting in increased H₂ yield. At high S/C ratios, the decrease in residence time

became dominant over the effect on reaction rate, causing H₂ concentrations to fall with increasing steam flow (Umeki et al., 2010).

This theory is further evidenced by Figure 2-15 (b). With increasing height in the up-flow reactor CO is consumed as H₂ and CO₂ are produced, while CH₄ and heavier hydrocarbons remain relatively unchanged. This implies that the water gas shift reaction did not reach equilibrium and has a greater effect on product composition than any other gas phase reaction at this stage.

This illustrates the compromise between reaction rate and residence time when both of these are determined by the gasifying agent. Similarly there is a compromise between product gas yield and heating value, as the highest volume yield at S/C ratio of 4.3 also contained a high fraction of CO₂, lowering the heating value. The study also observed increasing tar concentration with increasing steam ratio. This is contrary to other works and was explained by the fact that increasing steam flow reduced the residence time. In studies where the S/C ratio is altered by manipulating feedstock flow instead of steam, the greater residence time would allow for tar cracking (Umeki et al., 2010).

Another factor relating to residence time was observed in a batch reactor reacting waste plastic and steam. The hydrogen concentration increased with temperature and residence time up to a point, beyond which the concentration of H₂ was observed to drop slightly, which the authors associated with the methanation reaction of carbon with hydrogen to produce methane (Kantarelis et al., 2009). This suggests that there is an optimum residence time for hydrogen production from batch gasification reactions, subject to reactor conditions and the nature of the feedstock.

2.5 Summary of Literature

Coal is used in many industries for its high energy density and uniformity. Bituminous coals for power generation have energy contents in the range of 24-32 MJ/kg. It is a finite resource which will become less economically competitive as reserves are consumed. The environmental impact of coal combustion is causing governments to move towards cleaner energy sources, including novel 'clean-coal' technologies to reduce its impact.

Biomass has a wide range of forms and energy contents; wood pellets have a heating value in the region of 18 MJ/kg. The advantages of pyrolysis are the reduction in moisture and volatile matter which reduces the volume and weight of the material, simultaneously increasing the calorific value.

Thermal conversion processes yield a more uniform and reliable fuel leading to improvements in efficiency. Converting solids into gaseous fuel improves versatility and allows pollutants such as heavy metals to be removed prior to combustion. Flue gas typically must be cooled below 400°C for cleaning. Cooling combustion flue gas results in large energy losses while the penalty is lower for producer gas (Quaak et al., 1999). Fuel gas can be used in gas engines or turbines or converted into commodity chemicals. Biogas fuel is also more uniform and can be standardised, making it more valuable and marketable than solid feedstock (Basu, 2010; McKendry, 2002).

There are a variety of technologies available for commercial gasification of coal. The gas yield varies according feedstock, reaction conditions and plant application. Some technologies are calibrated for a specific feedstock while others are able to accept a wide variety of coals. Coal is the most common gasification feedstock, primarily used for chemical synthesis (GSTC, 2016).

2. LITERATURE REVIEW

Current environmental legislation has resulted in closures of many historic power plants. Gasification and pyrolysis provide opportunity for fuel production from biomass and waste materials, in line with renewable energy targets and waste management directives. Recent successes include the Syngas Products plant in Avonmouth (Syngas Products, 2016) and Empyro BV pyrolysis oil plant in the Netherlands (BTG-BTL, 2016).

To increase widespread adoption of these technologies there remain particular challenges to overcome, including the removal of tar for syngas to be used in gas engines. Reactor designs and operating parameters can be tailored to specific feedstocks and desired products, provided that the feedstock is uniform. Pre-treatment methods for variable quality feeds can facilitate this.

3 THEORY

This chapter covers the theory of gasification including the effect of reaction conditions and kinetics on the product yield, which will be demonstrated using the simulation work in Chapter 4. The system investigated in this work relies on a steam flame for the provision of heat and steam for gasification. Hence some discussion regarding the nature of high temperature steam and fundamental flame theory will be presented in relation to the experimental system used in this work. Heat transfer theory is covered briefly, emphasising the effect of radiative transfer at flame temperatures. Finally the theory of operation of some key equipment used in the experimental programme is described.

3.1 General Gasification Chemistry

Factors which affect the gas yield include temperature, pressure, choice of gasifying agent, feedstock properties and particle size, equivalence ratio, catalyst addition and gasifier type (Pereira et al., 2012). The principle gasification reactions are listed in Table 3-1.

Table 3-1: Principle gasification reactions¹⁴.

No.	Reaction Name		MJ/kmol
Heterogeneous (solid gas) reactions			
Equation 3-1	Combustion	$C + O_2 \rightarrow CO_2$	-393.8
Equation 3-2	Partial combustion	$C + \frac{1}{2} O_2 \rightarrow CO$	-110.5
Equation 3-3	Boudouard	$C + CO_2 \leftrightarrow 2 CO$	172.6
Equation 3-4	Steam-carbon 1 (water-gas primary)	$C + H_2O \leftrightarrow CO + H_2$	131.4
Equation 3-5	Steam-carbon 2 (water-gas secondary)	$C + 2 H_2O \leftrightarrow CO_2 + 2 H_2$	90.4
Equation 3-6	Hydrogasification (methanation)	$C + 2 H_2 \leftrightarrow CH_4$	-74.9
Homogeneous (gas phase) reactions			
Equation 3-7	Water gas shift (WGS) (CO shift)	$CO + H_2O \leftrightarrow CO_2 + H_2$	-41.2
Equation 3-8	Methanation	$CO + 3 H_2 \leftrightarrow CH_4 + H_2O$	-205.7

The heterogeneous reactions in Table 3-1 concern the reactions of carbon with various gas species. However, most fuels of practical interest contain species in addition to carbon, as described in Section 2.1. Wood contains significant amounts of oxygen and volatile species, while high rank coals

¹⁴ Reactions with a positive heat of reaction are endothermic (heat absorbing) and vice versa. Data from (Bhutto et al., 2013; Bulutoglu et al., 2016; Green and Perry, 2008; Lu and Wang, 2013; Pinto et al., 2010; Rakib et al., 2010; Rogers and Mayhew, 1995; Udomsirichakorn and Salam, 2014)

contain approximately one hydrogen atom for every carbon, as well as traces of sulphur and nitrogen. These species undergo side reactions and produce additional product species. These are usually in small enough quantities that they have a minor effect on gasification chemistry itself, but can be significant in the gas cleaning stage. For example nitrogen is generally inert, but at high temperatures can form nitrogen oxide pollutants.

Under gasification conditions any free oxygen is quickly consumed. Where carbon conversion is essentially complete, as in most industrial gasifiers, it is the homogeneous reactions (Equation 3-7 and Equation 3-8) which largely define the syngas composition (Higman and Van der Burgt, 2003). Factors affecting the progress of these reactions are outlined in the following sections.

3.1.1 Thermodynamics of Gasification

This section addresses the trends in the product yields obtained under different reactor conditions, such as at different temperatures and pressures. A later section will look at the reaction kinetics, which explains the routes by which these states are achieved.

3.1.1.1 Thermodynamic Equilibrium

For the reversible reactions shown in Table 3-1, the forward and reverse reactions take place simultaneously but at different rates. The rate of each is proportional to the concentration of reactants available; for example for the water gas shift reaction (Equation 3-7) the rate of the forward reaction, r_{fw} is proportional to the concentrations of CO and H₂O while the reverse reaction rate is proportional to the concentrations of CO₂ and H₂. The forward reaction can be represented as follows (Higman and Van der Burgt, 2003);

$$r_{fw} = k_{fw} [CO] [H_2O]$$

Equation 3-9

The rate constant, k_{fw} is dependent on temperature. Initially when the concentrations of CO and H₂O are much higher than those of CO₂ and H₂, the forward rate is much faster than the reverse rate of reaction. After some time under stable conditions the concentrations of products and reactants will begin to even out. At this point the forward and reverse reactions will proceed at the same rate and the reaction can be said to have reached the equilibrium state. The ratio of forward to reverse reaction rate constants at this point gives the equilibrium constant and can be expressed as follows;

$$K_e = \frac{k_{fw}}{k_r} = \frac{[CO_2] [H_2]}{[CO] [H_2O]}$$

Equation 3-10

The equilibrium constant, K_e varies with temperature but is independent of pressure, and can be used to predict the relative concentrations of the reactant and product gases at given conditions, provided equilibrium has been reached, via the following expression;

$$K_e = \frac{p_{CO_2} p_{H_2}}{p_{CO} p_{H_2O}} = \frac{v_{CO_2} v_{H_2}}{v_{CO} v_{H_2O}}$$

Equation 3-11

In this expression p_{CO_2} and v_{CO_2} represent the partial pressure and volume fraction of CO_2 in the gas mixture. Equation 3-11 also considers the gases to be ideal, but is found to give sufficiently accurate results for basic design purposes (Higman and Van der Burgt, 2003).

3.1.1.2 The Effects of Gasification Pressure

The major advantage of operating a gasifier under elevated pressure are the savings in operating costs from the need to compress the syngas, and a decrease in equipment volume which results in reduced capital costs. As such the gasifier pressure is often chosen based on downstream requirements in commercial units, rather than for its effect on the chemistry within the reactor; the economic benefit of compressing the reactants rather than the products often outweighs the effect on the chemistry. The advantages mentioned above are attained at pressures of around 20 bar. Operating above this pressure offers limited gains, while operational issues such as pressurising solid feedstocks have increasing influence (Higman and van der Burgt, 2008).

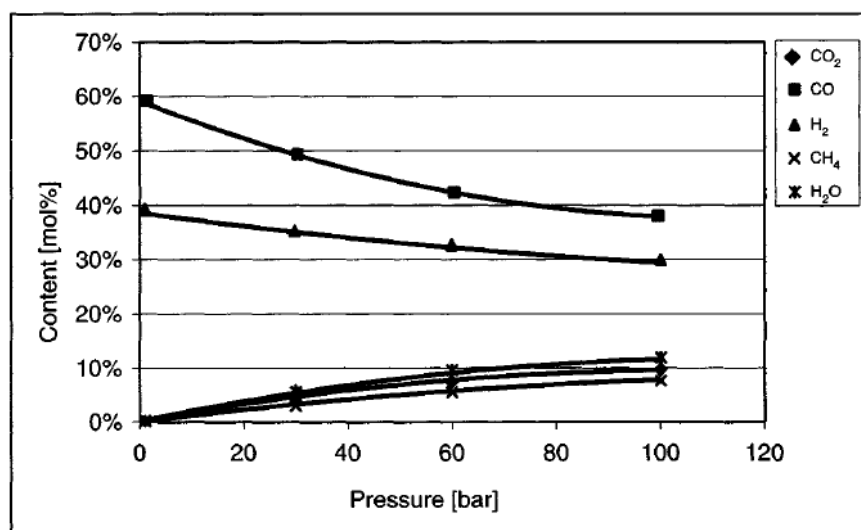


Figure 3-1: Effect of pressure on syngas composition at 1000°C. Reprinted from (Higman and Van der Burgt, 2003) with permission from Elsevier.

The effect of pressure on the syngas yield is demonstrated in Figure 3-1. It shows that with increasing pressure at constant temperature the H_2 and CO contents in the syngas decrease, while the proportions of CO_2 and CH_4 increase. This is because the hydrogasification reaction (Equation 3-6) progresses very slowly except at high pressures, while the water gas shift (WGS) reaction (Equation 3-7) shows little variation with pressure (Basu, 2010; Rezaiyan and Cheremisinoff, 2005). According to Le Chatelier's principle an equilibrium reaction responds to changes in pressure by favouring the state with the smaller number of moles for the smaller volume occupied. When the number of moles on each side is even, as in the water gas shift reaction, the effect of pressure is reduced. The increase in methane concentration brings an associated increase in the heating value of the gas, which can be beneficial for fuel gas applications.

Figure 3-1 describes the trends observed with varying pressure at a fixed temperature of 1000°C. At temperatures above 1500°C, the effects of pressure on gas composition follow a similar trend but the actual differences in product yield are almost negligible (Higman and Van der Burgt, 2003).

3.1.1.3 The Effects of Gasification Temperature

Choice of operating temperature is often influenced by the type of feedstock and ash behaviour, as well as associated costs such as oxygen consumption. For fuel gas systems where a high calorific value of product gas is desired, temperatures should be kept low to promote methane formation. However this is limited by the reactivity of the feedstock as temperature also influences the reaction rates, by altering the rate constants.

Low temperature operation tends to require longer residence times for equivalent conversion. This can mean larger equipment volumes are required, which increases the capital expenditure. For syngas production where CO and H₂ are the desired products, high temperatures are favoured (Dong and Borgwardt, 1998). As many commercial systems operate above 30 bar, temperatures above 1300°C are used to avoid high methane yields. This is illustrated in Figure 3-2.

The effect of increasing gasification temperature is a rising CO concentration and decrease in CO₂ and CH₄ concentrations. The H₂ content remains relatively steady, with a small decline at very high temperatures. The water gas shift reaction favours lower temperatures due to its exothermic nature; high temperatures would tend to promote the reverse reaction. However the increasing CO content is more likely due to the endothermic heterogeneous reactions. The steam-carbon and Boudouard reactions (Equation 3-4 to 6) are highly endothermic and favour high temperatures, yielding increased CO concentration at high temperatures (Rezaiyan and Cheremisinoff, 2005).

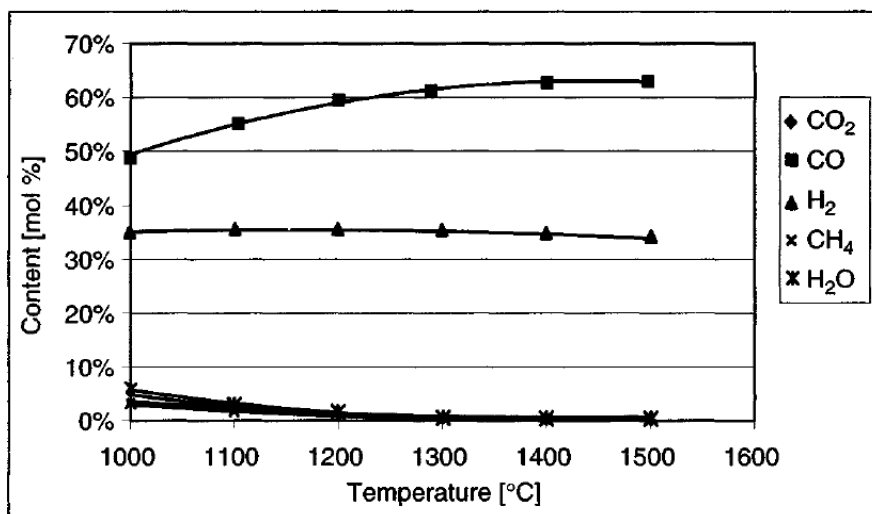


Figure 3-2: Effects of temperature on syngas composition at 30 bar. Reprinted from (Higman and Van der Burgt, 2003) with permission from Elsevier.

It is worth noting the interdependency of temperature with steam-carbon ratio for allothermal systems which use steam as the heating medium. A manipulation of the steam flow will influence reactant concentrations as well as temperature within the reactor; depending on the steam condition this may be higher or lower than the reactor temperature.

3.1.1.4 Equivalence Ratio (ER)

The equivalence ratio is defined as the ratio of air supplied in relation to the amount needed for stoichiometric combustion of the feedstock (Gao et al., 2008; Udomsirichakorn and Salam, 2014). As

mentioned in Section 2.2.1, this is also known as the excess air factor and is closely related to the air-fuel ratio used in engine management.

For gasification, the ER is applicable when air or oxygen is introduced for partial combustion of the feedstock. In contrast to combustion systems in which an ER of >1 should be used to ensure complete combustion of the feedstock, in gasification systems only a limited quantity of air/oxygen is introduced for partial combustion, usually an ER of <0.4 . Two effects can be observed by manipulation of the ER. Increasing available oxygen provides additional heat to the gasifier through the combustion reactions, which can improve the rate of the endothermic gasification reactions. However gasification feedstock is sacrificed for combustion and the additional combustion products will contaminate the product gas. Where air is used, small increases in ER will result in large increases in nitrogen dilution, which impair the cold gas efficiency (Section 3.1.2).

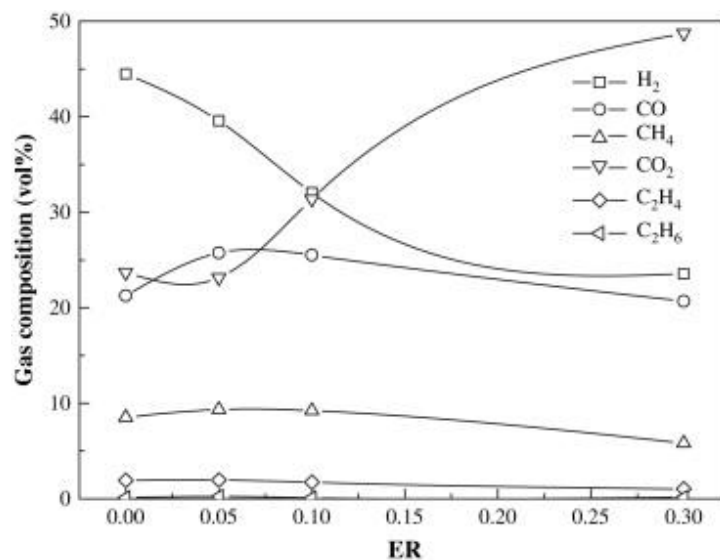


Figure 3-3: Effect of equivalence ratio (ER) on the product gas composition. Reprinted from (Gao et al., 2008) with permission from Elsevier.

The effects of ER on product yield are shown in Figure 3-3. It can be seen that even small increases in ER have a significant effect on the gas yield, as the hydrogen concentration falls sharply. It is possible that additional free oxygen initially reacts with H₂ when the hydrogen concentration is high to form steam. At ER = 0.05, it can be seen that the CO concentration initially increases as the CO₂ concentration decreases; this is likely due to the increase in reactor temperature and partial combustion (Equation 3-2). At ER above 0.05, a sharp increase in CO₂ is observed due to increased combustion. In the above study the optimum ER was found to be 0.05, though in allothermic cases where heat is input by other means, an ER of 0 is used to avoid combustion entirely.

3.1.1.5 Oxygen to Steam Ratio

Mixture of steam and air/oxygen are often employed as gasifying agents. In general lower oxygen to steam ratios increase H₂ and CH₄ production, while a higher oxygen ratio promotes CO and CO₂, as free oxygen readily oxidises available carbon in the feedstock. However it is not advisable to operate too lean in oxygen as small fluctuations in conditions can cause carbon deposition to occur (Higman and van der Burgt, 2008).

3.1.1.6 Steam Carbon Ratio, S/C

Steam as a gasifying agent produces a hydrogen rich syngas. Although biomass feedstocks contain a small degree of moisture, steam provides the major source of hydrogen atoms to yield H₂ gas in the product. A disadvantage of using steam is the energy demand in heating it up, and the endothermic nature of the gasification reactions have a substantial heating requirement (Erkiaga et al., 2014).

The results of one study which measured the effect of steam to biomass ratio (where biomass represents the carbon source) are shown in Figure 3-4. It was observed that increasing the steam to biomass ratio improved the yields of hydrogen and CO₂ while decreasing the yield of CO. This was attributed to the water gas shift reaction, as well as hydrocarbon reforming, which lead to a decrease in methane concentrations with increasing steam/biomass ratio.

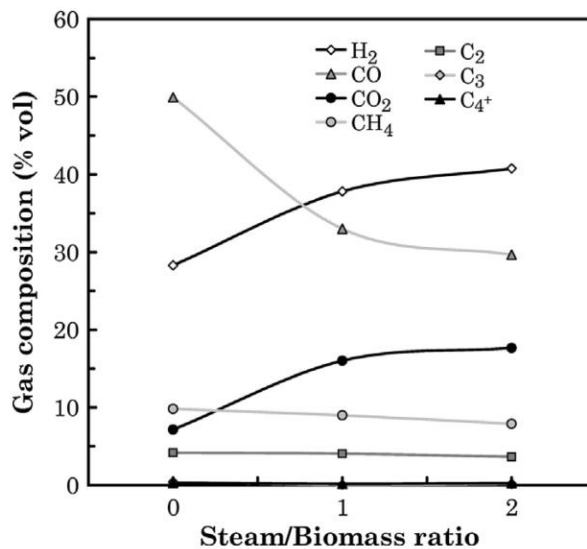


Figure 3-4: Effect of steam/biomass ratio on dry product gas composition. Reprinted from (Erkiaga et al., 2014) with permission from Elsevier.

This result is similar to a study (Umeki et al., 2010) described in Section 2.4.4.4, whereby the hydrogen yield increased and CO decreased with increasing S/C ratio. The study found that the effect reaches a maximum at an S/C ratio of around 4.3, after which the concentration of hydrogen began to fall. This was attributed to the trade-off between the increased reaction rate achieved with increasing steam flow, and the associated decrease in residence time. This only applied in cases where the water gas shift reaction was active but equilibrium was restricted (Umeki et al., 2010).

3.1.2 Measures of Efficiency

The *cold gas efficiency* is commonly used to describe the efficiency of operation of a gasification process. It is defined as follows (Liu et al., 2009; Probst and Hicks, 2006);

$$\text{Cold gas efficiency (\%)} = \frac{\text{Heating value of product gas}}{\text{Heating value of feedstock}} \times 100$$

Equation 3-12

The importance of this statistic varies according to the target application. For power applications the heating value of the product gas is paramount; and the different products of gasification each have

different heating values. Methane has the highest enthalpy of combustion per mole of the possible product gases, therefore high methane content in the product will increase the heating value and cold gas efficiency. However where CO and H₂ are the desired products, the cold gas efficiency is not representative of whether the process is achieving the required yields. In such situations the cold gas efficiency can be misleading; the yields of CO and H₂ should be read directly instead of the heating value. It is also important to be consistent in the use of higher or lower heating values.

Another measure of performance may be obtained from the carbon conversion efficiency;

$$\text{Carbon conversion (\%)} = \left(1 - \frac{\text{Carbon in residue}}{\text{Carbon in feedstock}} \right) \times 100$$

Equation 3-13

For economical operation it is important that the minimum amount of feedstock remains unreacted. The accepted conversion varies with reactor type, as discussed in Chapter 2; fluid bed reactors for example remove a portion of unreacted char with the ash from the bed to ensure smooth operation. The carbon conversion is an often quoted parameter by which to compare different reactor configurations.

3.1.3 Gasification Kinetic Theory

Reaction kinetics concerns the mechanisms and rates at which the gasification reactions may occur. In general this area is less well understood than the thermodynamics described previously, in which trends can be easily identified experimentally. The kinetics of heterogeneous reactions is complicated by surface structure and porosity effects, for example. As in previous chapters, the use of solid fuels is focussed upon here.

3.1.3.1 Devolatilisation of Feedstock

Feedstock devolatilisation is the first stage to occur after surface drying when coal or biomass is heated to moderate temperatures. Devolatilisation is proportional to the temperature and rate of heating and subject to feedstock particle size and other chemical reactions. For example in rapid heating applications devolatilisation and gasification may occur simultaneously, hence the rates of devolatilisation and gasification are interconnected.

At low heating rates the devolatilisation takes place before gasification, resulting in a build-up of volatiles in the gas phase. In counter flow gasification systems, this can result in volatile matter being removed with the product gas before it has reacted. This does not occur in co-current systems with high heating rates as concentrations of volatiles do not build up. Clean product gas can be removed without unreacted material using a relatively short residence time (Higman and van der Burgt, 2008). High heating rates usually require small particle sizes, to give a small Biot number. This is discussed in Section 3.4.

Elevated pressure hinders feedstock devolatilisation. Under a pressure of 30 bar, typically around 10% less feedstock weight loss is achieved compared to an equivalent atmospheric system (Higman and van der Burgt, 2008).

3.1.3.2 Gasification of Solid Char

The gasification of the solid phase remaining after devolatilisation is the slowest step in the process. Limited data exists on the gasification of volatile species however gas phase reactions are substantially faster than heterogeneous reactions between the solid char and gasifying agents, in which mass transport is significant.

The reaction rate (Equation 3-9) was shown to be proportional to the reactant concentrations multiplied by a rate constant, k . For heterogeneous reactions such as the Boudouard reaction (Equation 3-3) it can be assumed initially that the solid carbon is present in abundance, while the gas species is the limiting reagent. This means the kinetics can be modelled as those of a first order reaction as follows, with k_m as the mass related rate constant;

$$\text{rate} = k_m \times \text{concentration of limiting reagent}$$

$$k_m = Ae^{-E/RT}$$

Equation 3-14

In Equation 3-14 A is a pre-exponential constant, E is the activation energy for the reaction in question, and R is the universal gas constant. The above expression shows the dependence of the rate constant on temperature (Higman and van der Burgt, 2008).

The above expression is suitable when the products of the reaction are present in sufficiently small quantities that inhibition does not occur. If product inhibition is taken into account, the rate expression becomes a more complex function of the concentrations of reactants and products (Basu, 2010).

It has been suggested that a build-up of volatile species concentration has an inhibitive effect on char gasification, by dissociative chemisorption of H_2 over the carbon surface. The presence of hydrogen, light hydrocarbons and tar were thought to inhibit char gasification in a fluidised bed environment. The presence of a catalyst was found to overcome this (Bayarsaikhan et al., 2006).

3.1.3.3 Reactivity of Feedstock

Reactivity is the reaction rate under certain conditions of temperature, pressure and gasifying agent. There are a number of factors which can affect the reactivity of coal and char, including particle size and surface area, porosity including the inner structure and pore distribution, the structure of the fixed carbon, and catalytic effects of mineral matter.

The surface area of a particle can vary greatly with its porosity. A porous particle can have internal surface area orders of magnitude greater than its external surface alone. If these pores are accessible by a reactant gas then the internal surfaces are equally available for chemical reaction. The reaction rate based on the total available reaction surface is known as *intrinsic* reaction rate. The rate based exclusively on the external surface area of a particle is known as the *apparent* reaction rate (Basu, 2010).

Low rank coals have a larger specific surface area and higher reactivity in general than high ranking coals such as anthracite (Higman and van der Burgt, 2008). One distinction between coal and biomass chars is that the reactivity of coal decreases with conversion, while that of biomass char

3. THEORY

increases. That is to say the rate of conversion of biomass char increases as it is converted, which is beneficial for more complete char conversion, while the rate of conversion of coal tends to reduce as it is consumed (Basu, 2010).

The reactivity is also affected by pre-processing, for example thermal treatment will affect the porosity of the material and the extent to which it is converted prior to gasification. It has been shown that the pyrolysis temperature and residence time used to produce chars has a substantial effect on char reactivity. Typically lignite and coal chars produced by pyrolysis at high temperatures (>1000°C) or longer residence times tend to be less reactive than those produced at more moderate temperatures. This is because high temperature treatment reduces the number of active sites available for reaction. It was concluded that beyond a peak temperature which is characteristic of individual chars, the reactivity can decrease within a short time, leading to “dead-burning” where the char reaches a minimum reactivity. These effects were lower for high rank coals (van Heek and Mühlen, 1991). In coal, CaO is present and is sintered at high temperatures, which blocks some of the available pores. A similar effect has been observed for potassium and sodium in biomass char, whereby at moderate temperatures they have a catalytic effect and increase the char yield. However at high temperatures thermal annealing can block pores and active sites, reducing reactivity (Basu, 2010).

The mineral content in biomass ash is known to enhance reactivity (Higman and van der Burgt, 2008; Rizkiana et al., 2014). Studies have demonstrated that inorganic elements, particularly potassium, have a catalytic effect on biomass devolatilisation and char burn-out, while demineralised samples exhibited very long burn-out times (Jones et al., 2007; Nowakowski et al., 2007).

3.1.3.4 Influence of Mass Transfer on Reaction Rate

For a reaction to occur between a reactant gas and the char surface, the gas must be able to access the active carbon sites. The process by which the gas reaches the surface sites is by diffusion, after which the gasification reactions may occur. The diffusion process occurs at a limited rate. In situations where the chemical reaction proceeds much more rapidly than the diffusion process, the reaction is known as *mass transfer controlled*. If the rate of diffusion is faster than the rate of reaction, the reaction is known as *kinetically controlled*. In this situation the gas will diffuse initially onto the external surfaces, and also through the pores and onto the internal surfaces of the char (Basu, 2010).

The extent to which a reaction is kinetically or diffusion controlled will determine how factors such as particle size, porosity, reaction temperature and residence time affect the overall char gasification. An increase in temperature, for example, will tend to increase the rate of a chemical reaction, and may change a kinetically controlled reaction to a diffusion controlled one. It follows that in high temperature environments the majority of gasification reactions are diffusion controlled, and highlights the importance of mass transfer phenomena in attaining high conversion of feedstock. This is illustrated in Figure 3-5, which shows how the time required for gasification alters with particle size. Smaller particle size means a larger specific surface area available for reaction. Maximising the surface area provides many more active sites onto which reactants may diffuse and increase the overall reaction rate (Higman and van der Burgt, 2008).

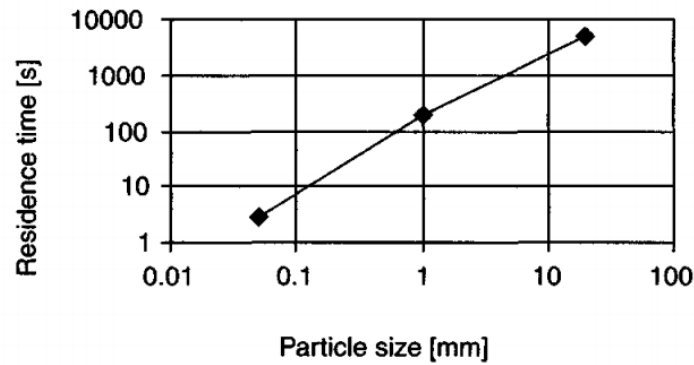


Figure 3-5: The influence of particle size on required residence time for gasification of solid fuel. Reprinted from (Higman and Van der Burgt, 2003) with permission from Elsevier.

This has also been supported by experimental findings, whereby smaller particles have been shown to yield greater quantities of gas. Smaller particles contribute to a higher heating rate of individual particles, as per Equation 3-24, which in turn produces more light gases and less char (Di Blasi, 1996; Udomsirichakorn and Salam, 2014).

3.1.4 Kinetic Models

An increasingly popular tool for the optimisation of gasification processes are kinetic models. These have been developed for a variety of reactor designs such as stirred tanks, fluidised beds and plug flow reactors. Developments in computing power and the understanding of the necessary chemical processes have expanded the use and sophistication of kinetic models, particularly in the area of computational fluid dynamics (CFD).

The wide variety of reactions inherent in gasification chemistry means that the reliability of these models depends heavily on the empirical data for each system. Combinations of experimental and simulation work can yield useful insights into gasification processes for optimisation purposes. This is demonstrated and discussed further in Chapter 4.

3.2 Flame Theory

The next section outlines some general theory regarding flames to provide some background to the burner arrangement used in the experimental work. As described in the Experimental Chapter 5, the gasifier investigated used a dual fuel burner to produce a steam flame which provided the energy for gasification to occur. To illustrate the phenomenon of a steam flame, some basics on typical flame characteristics and the nature of steam are presented in the following sections.

3.2.1 Flame Fundamentals

Not all flames are luminous, but common hydrocarbons do produce luminous flames. The colour of a flame depends on the fuel-oxidant mixture and the temperature. Chemiluminescence is a result of electronically excited species returning to their ground state by release of light. High temperature burned gases often glow red due to radiation from CO_2 and water vapour (Glassman and Yetter, 2008). The yellow colour of fuel rich flames arises from incandescence of soot particles due to their very high temperature (Glassman and Yetter, 2008).

A distinction can be made between premixed and diffusion flames. A premixed flame is one in which the fuel and oxidant are mixed before the flame front arrives, such as in a Bunsen burner with the air valve open. In a diffusion flame, the fuel and oxidant diffuse towards the reaction zone where they are mixed, for example in a candle (Borghetti et al., 1998).

3.2.2 Flame Structure

The structure of a laminar flame such as from a Bunsen burner is largely influenced by the burner geometry. The gas flow through the Bunsen tube is assumed laminar, fast in the centre and much slower at the tube walls, which contributes to flame stability (Glassman and Yetter, 2008).

In the 'dark zone' in Figure 3-6 the premixed gases emerging from the top of the burner are warmed by the heat of the flame. The majority of the reactions and heat release take place in the luminous zone. This is <1 mm thick and is the highest temperature point of the flame. There is a convective flow of reactant gases into the luminous reaction zone and a diffusion of radical species in the opposite direction towards the dark preheat zone. The recombination zone follows, where radical species recombine and release some additional heat (Westbrook and Dryer, 1984).

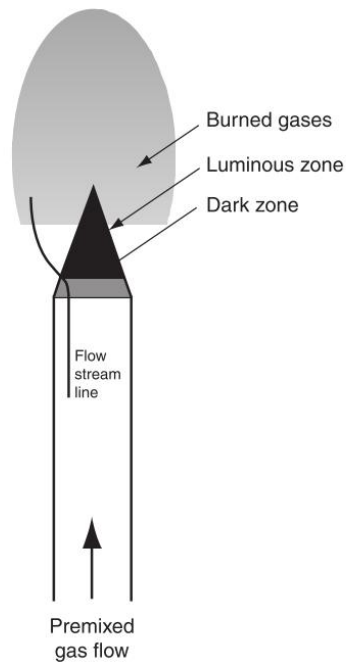


Figure 3-6: General description of laminar Bunsen burner flame. Reprinted from (Glassman and Yetter, 2008) with permission from Elsevier.

Mallard and Le Chatelier proposed that the heat transfer into the reactant gases was the controlling mechanism for flame propagation [(Mallard and Le Chatelier, 1883) as cited in (Glassman and Yetter, 2008)]. Later improvements identified that radicals' diffusion was the primary controlling factor in the flame. Concentrations of OH, H and O were found to be highest in the luminous reaction zone, while the concentration of HO₂ is highest in the pre-heat zone, formed by the diffusion of hydrogen atoms from the reaction zone (Glassman and Yetter, 2008).

Most burners of practical interest encourage turbulent mixing for rapid and efficient consumption of fuel. Under highly turbulent conditions the laminar structure disappears to give a distributed

reaction zone, in which the reactions occur in an area as opposed to a front. The general trends for turbulent flame speeds are that they are always greater than the laminar flame speed and increase with turbulence intensity (Glassman and Yetter, 2008).

This analysis suggests that the addition of water vapour to a hydrocarbon flame would tend to increase the concentrations of radical species, which would increase the burning velocity and intensify the reaction zone (see Section 3.3.3). A turbulent reaction zone area would offer a high concentration of radicals and rapid heating rates, which would produce a highly reactive area for gasification of feedstock particles.

3.2.3 Flame Stabilisation Using a Burner Quarl

A burner quarl or tile is a refractory lined space into which a burner is mounted, which acts as a preliminary combustion chamber to an industrial furnace. The fuel and oxidant are discharged into the quarl designed to increase flame stability by encouraging recirculation of hot gases towards the reactants inlet. These hot gases provide ignition energy to begin the combustion reaction, which proceeds out into the furnace (Monnot, 1985).

A quarl may be cylindrical or conical, with a taper that converges towards or away from the burner (Trinks et al., 2004). A cylindrical design is the simplest, and has been shown experimentally to stabilise a flame provided that the length of the quarl is greater than its internal diameter. It has also been shown that the temperature of the quarl walls does not significantly affect the stabilisation effect. The stabilising effect of a cylindrical quarl is enhanced as the jet impulse through the burner is increased (Monnot, 1985).

The gasifier burner was equipped with a burner quarl which was replaced during the experimental programme. The dimensions of the original were precisely replicated in order to maintain the stabilising effect.

3.2.4 Adiabatic Flame Temperature

Combustion energy increases the temperature of the products and the surrounding environment. In an ideal case no energy would be lost to the surroundings and the product gases would reach a maximum temperature known as the adiabatic flame temperature. For a general constant pressure process involving i reactants and j products;

$$Q_P = \sum_{j=1}^j n_j [H_{T_2} - H_{298}^0 + (\Delta H_f^0)_{298}]_j - \sum_{i=1}^i n_i [H_{T_1} - H_{298}^0 + (\Delta H_f^0)_{298}]_i$$

Equation 3-15 (Strahle, 1993)

Here the difference between the first two enthalpy terms gives the sensible heat of that species, with T_1 being the initial temperature of reactants and ΔH_f^0 giving the enthalpy of formation of that species at the standard state of 298 K. Enthalpy values for each species can be found from JANAF tables. In the ideal case $Q_P=0$; solving for T_2 gives the adiabatic flame temperature.

Due to the difficulty in accurately measuring flame temperatures, the calculated ideal adiabatic temperature is sometimes quoted for particular fuel mixtures or conditions. This was calculated for a range of flame conditions in the present work and compared with the temperatures measured experimentally. It was also used to compare the flame conditions with those from other similar works in Table 7-1.

3.3 Steam Theory

Chapter 2 established that most gasification systems use steam and air/oxygen to react with the carbon feedstock. Steam provides the major source of hydrogen atoms where hydrogen is a desired product. The experimental work in the following chapters centres around a super-heated steam flame, produced from combustion of fuel gas with a mixture of oxygen and steam. This section concerns how characteristics of steam as a reagent can affect flames and gasification environments.

3.3.1 Saturation and Superheat

These terms are used to define steam conditions in the experimental work. Steam is high temperature water vapour and is totally transparent, becoming visible in contact with cold air as droplets of condensation. Water and steam at boiling temperature are known as a 'saturated liquid' or 'saturated vapour' respectively. Further heating will increase the steam temperature above the saturation point to produce 'superheated' steam.

The latent heat of vaporisation for water is 2258 kJ/kg at atmospheric pressure (Rogers and Mayhew, 1995). This is orders of magnitude higher than the heat capacities of both water and steam, meaning the vaporisation stage has a greater energy demand than raising the temperature. Steam is commonly used as a heating medium in process industries as heat is given off at a constant controlled temperature. The saturation temperature can be manipulated by altering the pressure according to the needs of the process.

3.3.2 Dissociation of Water

Water molecules can spontaneously dissociate into H^+ (or H_3O^+) and OH^- ions. For pure water at room temperature the concentration of these ions is around two parts per billion. It is possible to produce hydrogen directly from splitting water molecules into $H_2 + \frac{1}{2} O_2$, though this requires substantial energy input. As discussed in Chapter 1, for hydrogen to qualify as a renewable fuel it must be produced using renewable energy. The work required is represented in Equation 3-16, assuming the reactants and products are at temperature T_0 ; water splitting occurs at T_h and ΔG and ΔG_0 are the free energy changes when the reaction occurs at T_h and T_0 respectively;

$$W_h = \Delta G = \Delta G_0 - \Delta S(T_h - T_0)$$

Equation 3-16 (Funk and Reinstrom, 1966)

Since ΔS does not increase significantly with temperature, it can be seen that the required energy input W_h decreases as temperature T_h is increased. At atmospheric pressure, $\Delta G = 0$ where $T_r \approx 4300$ K, at which point all of the water molecules are split. However at 3000 K only around a third of the water molecules are split and at 2000 K this drops to around 1% of molecules. Thus for any significant yield of hydrogen through direct thermolysis a temperature > 3000 K is required,

which presents difficulties due to material limitations. Also the hydrogen must be separated quickly to avoid recombination with oxygen (Grimes et al., 2008).

This shows that using heat alone, a small proportion of water molecules are spontaneously split into hydrogen and oxygen. In order to yield meaningful quantities of hydrogen at reasonably attainable temperatures, this energy demand must be reduced and the oxygen should be removed. This can be achieved through gasification by offering lower energy reactions and converting oxygen to CO.

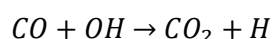
3.3.3 The Effect of Water Vapour on Hydrocarbon Flames

As stated in the introduction to this chapter, the present work is based on the concept of Ultra-Superheated Steam; steam injected into a flame and raised to very high temperatures described in Section 3.3.5. This addition is known to give a colourless flame with expected high concentrations of radical species (Lewis, 2007), though the effect of water on flames is not well understood.

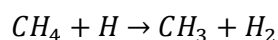
Water is used for fire suppression by removing heat through evaporation and diluting the oxidant with water vapour. However at certain ratios the addition of water vapour was shown to increase flame temperature, CO₂ production and O₂ depletion rates and reduce CO and soot production compared to cases without water addition (Suh and Atreya, 1995).

The addition of up to 30% water vapour in the oxidant was shown to increase the levels of OH radicals in the flame; beyond this level the OH concentration remained relatively constant. This was true for an oxidant consisting of 20%mol oxygen; though is likely to change with increasing O₂ content or flame temperature (Suh and Atreya, 1995).

It was suggested that CO reacted with the abundant hydroxyl radicals in high temperature flame zones to yield CO₂ and hydrogen as shown in Equation 3-17, as well as additional heat. This heat release compensated for the cooling effect of adding water vapour to the flame and resulted in a higher peak flame temperature.



Equation 3-17 (Müller-Dethlefs and Schlader, 1976)



Equation 3-18 (Suh and Atreya, 1995)

It was also suggested that the hydrogen atoms produced could react with methane fuel as in Equation 3-18. By increasing the concentration of H atoms the production of CH₃ radicals would also be increased leading to a more active flame (Suh and Atreya, 1995). This effect was only observed up to a concentration of 30% water vapour in the oxidant, indicating that there is a critical concentration of water vapour at which the enhancement effect reaches a maximum. Above the critical water content in the flame, the enhancement effect was lost and the flame was suppressed by the water vapour.

This critical water content is likely to be surpassed in the USS mixture, particularly for the synthetic air mixtures described in previous works. This analysis indicates that reducing the steam content in the flame would offer enhanced flame reactivity by avoiding suppression by excess water.

3.3.4 The Effect of Steam Addition on Burning Velocity

Another study investigated the effect of steam addition on the burning velocity of hydrogen/oxygen flames. Steam affected the flame in ways other than flame cooling and heat transport. When steam was used as a flame diluent in place of nitrogen, the burning velocity was increased at diluent fractions below 45%, as shown in Figure 3-7. This was in spite of the lower adiabatic flame temperature due to the heat capacity of steam (Koroll and Mulpuru, 1986). It was concluded that a more likely mechanism for this effect was that of steam as a *third-body catalyst*, particularly for the recombination reaction shown in Equation 3-19.

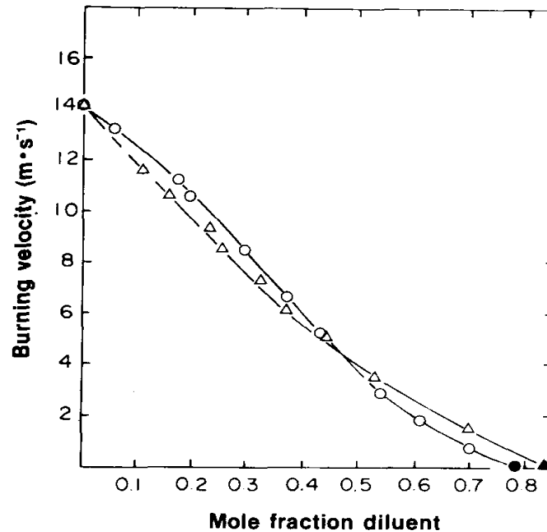
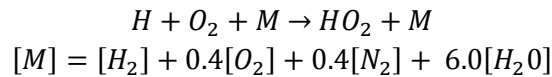
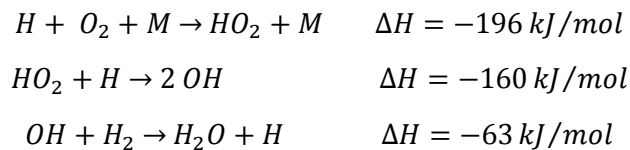


Figure 3-7: Burning velocities of 2:1 H₂-O₂ mixtures at 100°C with diluents N₂ (triangles) and steam (circles). Reprinted from (Koroll and Mulpuru, 1986) with permission from Elsevier.



Equation 3-19 (Warnatz, 1981) as cited in (Koroll and Mulpuru, 1986)

In this equation, *M* is the *third body* which is necessary to remove some of the energy from the reactants to stabilise the combination of H and O₂ (Glassman and Yetter, 2008). Several species can be used for this purpose. From the *[M]* coefficients it is seen that the third body efficiency of steam is very high compared to H₂, O₂ or N₂. This indicates that steam effectively catalyses the recombination of hydrogen and oxygen, and subsequently the chain of reactions involving HO₂ and OH radicals that follow, such as in Equation 3-20. The subsequent reactions are exothermic with low activation energies so provide a substantial source of heat in the flame (Koroll and Mulpuru, 1986).



Equation 3-20 (Koroll and Mulpuru, 1986)

The third body effect explained the higher burning velocities observed in Figure 3-7 when low mole fractions of steam were added. At higher diluent concentrations, the cooling effect of steam dominated over the catalytic effect, resulting in a lower burning velocity than for nitrogen.

The implications are that addition of water vapour in high temperature flames can increase the reactivity by catalysing the production of HO₂. This is in addition to increasing the concentration of OH radicals, contributing to a reactive gasification environment. The associated energy release would also provide additional heat for the endothermic gasification reactions.

3.3.5 Ultra-Superheated Steam

In contrast to the abovementioned studies which investigated small steam additions to flames, Ultra-Superheated Steam (USS) uses steam as the bulk material in the flame in place of nitrogen in a typical fuel-air mixture.

A method for producing USS was patented by F. M. Lewis and involves mixing water vapour or steam with oxygen in a ratio between 15-60%vol oxygen. This mixture is used to combust a fuel gas or oil in a high turbulence burner at a near stoichiometric fuel-oxygen mixture, to yield a gas mixture which is predominantly water vapour and carbon dioxide (Lewis, 2007). The omission of nitrogen from the oxidant means no energy is wasted in raising inert species up to high temperature, leaving more energy available for heating the steam.

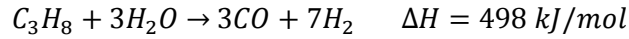
The adiabatic flame temperature of USS is considered to range between 1316-2760°C ignoring the energy conversion associated with free radicals formation (Lewis, 2007). The USS flame is clear and colourless, which is characteristic of the production of relatively high quantities of dissociation products such as high energy radicals. As described in Section 3.2, radical species play an important role in flame propagation and enhance the reactivity of a flame. Due to the high temperatures involved, all of the heat required for the endothermic gasification reactions could be supplied by the steam without the need for supplementary reactor heating. That is, combustion of the feedstock for heat supply is not required, nor is it necessary to externally heat the gasifier. The enhanced radical species concentration would also accelerate the gasification chemistry compared to lower temperature steam, meaning that less steam is required to gasify a given feedstock, improving the economics of the process.

Other advantages of USS gasification are that the high temperatures involved prevent the formation of tars, and that when operated previously the system was found to be non-slagging. This makes it particularly applicable to the treatment of biomass and other feedstocks which are known to be problematic in lower temperature operations due to the formation of tarry products which deposit on downstream equipment.

A possible disadvantage of the USS system is that CO₂ is present in the mixture when produced from the combustion of a hydrocarbon fuel such as methane or propane. In addition to the direct dilution of the product, this CO₂ will inhibit the desired gasification chemistry such as the water gas shift reaction by shifting the equilibrium position. This will inhibit H₂ formation which is otherwise favoured by steam-only gasification, but may promote the Boudouard reaction of CO₂ with carbon for CO production. The expected yields will be lower in H₂ and higher in CO compared to steam only gasification systems.

3.3.6 Steam Reforming of Hydrocarbons

As mentioned in Section 3.1, steam reforming is widely used for hydrogen production from natural gas. This is the reverse of the reaction in Equation 3-8 in Table 3-1 and can be applied to other hydrocarbons such as propane. Higher hydrocarbons can also be reformed to produce chemical precursors such as ethylene. In one study the addition of steam was found to prevent coke deposition onto the catalyst and the formation of tar-like products (Rane et al., 2004).



Equation 3-21 (Bulutoglu et al., 2016)

Equation 3-21 shows the steam reforming of propane gas. Comparing with Equation 3-8, the reforming of propane has more than double the molar enthalpy, making it more sensitive to temperature. As such this reaction would be promoted in high temperature environments with a high concentration of steam, such as the USS flame described in Section 3.3.5. This was found to be significant if propane is used to generate the steam flame, as described in Section 6.2. The patent outlines that the burner should operate as close to stoichiometry as possible to maximise the efficiency (Lewis, 2007). However in the event that the burner is operated in a fuel rich condition, or incomplete combustion of the fuel gas is observed, any excess fuel gas is likely to be reformed by the high temperature steam. This would lead to inefficiency if endothermic reforming occurs in place of exothermic combustion of the fuel gas, reducing the energy available for gasification chemistry and reducing conversion of the gasification feedstock. Moreover as the products of fuel gas reforming are identical to those of solid gasification, this effect may not be noticed unless specifically looked for except for lower than expected flame temperatures.

3.4 Heat Transfer

Detailed explanations of the three mechanisms of heat transfer can be found in various textbooks. Briefly, the heat transfer rate \dot{Q} for each process can be represented by the following equations;

$$\begin{aligned}\dot{Q}_{conduction} &= -\alpha A \frac{dT}{dx} \\ \dot{Q}_{convection} &= hA (T_h - T_c) \\ \dot{Q}_{radiation} &= \varepsilon \sigma A (T_h^4 - T_c^4)\end{aligned}$$

Equation 3-22 (Rathakrishnan, 2005)

In an industrial furnace conduction applies primarily to the walls of the furnace and is proportional to the thermal conductivity and surface area of the wall and the temperature difference across its thickness, x . For conduction through a cylindrical shell of length L Fourier's equation becomes;

$$\dot{Q}_{conduction} = \frac{2\pi\alpha L \Delta T}{\ln \frac{r_o}{r_i}}$$

Equation 3-23 (Lienhard, 2013)

This expression was used to calculate the heat transfer through the gasifier wall in the energy balance, Section 6.3.4.

3. THEORY

Regarding heat transfer to particles, the Biot number Bi which is a ratio of the resistance to heat transfer from the surrounding fluid to the particle surface by convection, to that of conduction within the particle (Bergman et al., 2011).

$$Bi = \frac{hL_C}{\alpha_s}$$

Equation 3-24

In Equation 3-24 L_C is a characteristic length of a particle, usually taken as the ratio of particle volume to its surface area, and α is the thermal conductivity of the particle. Small particles have a small characteristic length which, combined with high gas temperatures results in a small value of Bi . Where $Bi \ll 1$, particles can be considered isothermal with minimal temperature gradients between the particle surface and the bulk solid. This simplifies the consideration of particle temperatures in Section 4.5.6. The short residence times in pulverised fuel burners and entrained flow reactors requires small particle sizes, such that the solid material can be quickly brought up to reaction temperature.

3.4.1 Radiative Heat Transfer

At high temperatures radiation becomes very significant, owing to its dependence on the fourth power of temperature (Equation 3-22). In industrial furnaces as much as 90% of the heat transfer can be by radiation (Baukal, 2003).

Radiation from burners and flames comes in two main forms; radiation from hot gases (non-luminous) and from hot particles within the gas (luminous). Non-luminous radiation in flames and combustion gases is dominated by CO, CO₂ and H₂O which participate in radiation over specific wavelengths, while other gases are generally considered non-participating. The emissivities of these gases can range from around 0.01 for low concentrations in narrow geometries up to 0.5 for H₂O at high partial pressure and large path length (Baukal, 2003).

Luminous radiation is usually the result of incandescent soot particles as described in Section 3.2.1 and is responsible for much of the radiated heat from a typical fuel rich flame. The radiation emitted increases with temperature according to the Stefan Boltzmann law. The peak emission wavelength decreases with increasing temperature according to Wein's displacement law, approaching the visible spectrum and making the radiation increasingly visible with increasing temperature.

In many furnaces radiation from hot refractory walls may dominate the heat transfer (Baukal, 2003). Opaque solids tend to participate to a greater extent in radiative transfer, the more closely they resemble an ideal black body. Coal particles closely resemble this ideal model. The radiative interaction between two bodies will also depend on the view factor; where a small body is within a much larger isothermal environment this is taken as the emissivity of the smaller body (Lienhard, 2013).

This analysis was considered in the construction of the CFD model in Section 4.5.3 particularly relating to the radiation model and the emissivity of the coal particles and furnace walls.

3.5 Analysis Methods

Some relevant theory concerning the methods of operation of some measurement devices is presented briefly here.

3.5.1 Gas Chromatography

Determination of the composition of gas mixtures was central to the present research programme, which was performed using a gas chromatograph. The chromatograph in Figure 5-20 works by separating mixtures of gases into individual species for identification and their relative concentrations determined.

The chromatograph consists of a column containing a stationary phase, which may be a liquid or polymer. A gas sample containing a mixture of species is transported along the column by a carrier gas, often helium. The gas species will interact with the stationary phase according to their vapour pressures. High vapour pressure components will interact less and so traverse through the column relatively faster. Different species will emerge from the column after a characteristic period known as the retention time, separating the gas mixture into constituent species. A detector at the column outlet records the retention time and quantity of material eluded (Jennings, 2012).

Thermal conductivity detectors can identify gas species as components with a low atomic weight have a higher thermal conductivity than larger, heavier molecules. The gas sample is passed across a filament which is held at a constant temperature by controlling the voltage across it. As the gas passes, the filament will change in temperature and require a change to the voltage to maintain a constant temperature. The change in voltage is proportional to the change in temperature, which is proportional to the conductivity of the gas. This allows the gas species to be detected.

3.5.2 High Temperature Thermocouple Error

Thermocouples are used to measure temperature in a variety of environments, and were widely used in the present experimental programme. They are accurate over a wide range of temperatures according to their type, the most common being K type which are sensitive between -200 and 1350°C. However in high temperature environments where radiation is significant, some discrepancy in measured temperature can be observed due to radiative heat loss.

Considering a thermocouple placed in a flow of hot combustion gases within a furnace, the net heat transfer to the thermocouple will include convective transfer from the gases to the thermocouple, and radiative transfer from the thermocouple to the cooler furnace walls. Understanding that the thermocouple is much smaller than the surface area of the furnace;

$$Q_{net} = hA_s(T_g - T_s) - A_s\varepsilon_s\sigma(T_s^4 - T_w^4)$$

Equation 3-25 (Lienhard, 2013)

Where g represents the gas, s is the solid thermocouple and w is the wall, ε is emissivity and σ is the Stefan Boltzmann constant.

Where the thermocouple is in thermal equilibrium, the two heat flows will be equal and opposite. At high temperatures any discrepancy between T_s and T_w will result in substantial heat transfer owing

to the fourth power relationship. This will result in T_s remaining below T_g and giving a reduced reading for the gas temperature. The error can be quantified with knowledge of the emissivity and heat transfer coefficients. The effect can be reduced using radiative shielding, which obstructs the view of the walls from the thermocouple while allowing convective heat transfer by the passage of hot gases (Lienhard, 2013). This is the principle behind suction pyrometry, in which hot gas is pumped past a thermocouple housed within an isothermal probe which more closely approaches the temperature of the gas. This technique was used to measure the gas temperatures in the experimental burner, as described in Section 5.5.3, using a double-shielded thermocouple to reduce radiative losses.

3.6 Summary

Gasification involves a number of predominantly endothermic reactions requiring heat input to drive them. It follows that gasification progresses faster and to a greater extent under high temperature conditions, increasing the yields of H_2 and CO and decreasing those of CO_2 and CH_4 . Operation under increased pressure tends to increase yields of CH_4 .

Feedstock reactivity is a function of particle size, structure, porosity and mineral content. High rank coals have a lower specific surface area than low rank and biomass chars. Moreover the reactivity of high rank coal decreases with conversion, while for biochar it increases. Mineral content in ash, particularly potassium, has been shown to catalyse devolatilisation and char burnout.

Flames are characterised according to the mixture of fuel and oxidant. Unburned soot particles cause a characteristic yellow incandescence in a flame, while lean premixed flames are identified by blue chemiluminescence resulting from their higher temperatures. Most industrial flames of interest are turbulent, characterised by high degrees of mixing and are often stabilised by a burner quarl to encourage mixing of hot gases with reactants. This was observed in the fluid model, Section 4.5.5.

Small additions of water vapour have been found to enhance the flame temperature and propagation rate, due to the increased concentrations of high energy radical species. The patented Ultra Superheated Steam (USS) mixture is composed primarily of high temperature H_2O and CO_2 . Characteristics such as high temperature and high concentrations of radical species such as OH provide a highly reactive environment for gasification. The gases in question also participate in radiation over specific wavelengths and their high concentrations could result in high emissivity across an adequate optical length, leading to enhanced heat transfer to and from the gas mixture. This defines the method of heat input used in the present experimental work. Feedstock particles were injected directly into the high temperature flame zone where they were subjected to extremely high heating rates.

Heat transfer is driven by the temperature difference between two bodies or regions. At high temperatures, radiation is the dominant form of heat transfer owing to the dependency on the fourth power of temperature. Radiation from furnace walls can be significant in small experimental reactors where the walls are close and can have a substantial effect on the furnace load. This was investigated further using the CFD model in Section 4.5 and found to be significant in determining particle temperatures. This was further evidenced in Section 6.3.1.

4 PROCESS MODELS AND SIMULATION

This chapter introduces simulation of the experimental entrained flow gasification system described in Chapter 5. Since experimental and simulation work was conducted in parallel, these chapters should be considered together. Two software packages were used to investigate different aspects of the design. Aspen Plus was used to model the overall process and demonstrated the effects of manipulating some process variables and illustrated the theory explained in Chapter 3. The sensitivity analyses also identified suitable benchmark conditions for the early experimental work described in the following chapters.

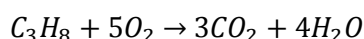
Following some experience with the experimental system, ANSYS FLUENT was used to simulate the reaction chamber in more detail. Models of the burner environment and the gasification chamber were produced to observe the material and temperature distributions, to help explain the experimental results and optimise the design.

To clarify the basis on which the equilibrium models operate, the initial approach was to construct a simplified stoichiometric equilibrium model using a spreadsheet. This simple model demonstrates the basics of the methodology used by the process simulation software.

4.1 Stoichiometric Equilibrium Model

A simplified model of the gasification system was created, based on a mass balance around the gasifier with a number of assumptions. The approach was that of a simplified stoichiometric equilibrium model as described in literature (Basu, 2010). For this method the input and output species are specified together with the set of chemical reactions which take place, as well as expressions for the chemical equilibrium of each reaction and the temperature and pressure of the equilibrium state (Cempa-Balewicz et al., 2013).

The initial model conditions were based on previous experimental work using this system (Shabangu, 2005). Inputs to the model included propane, oxygen, steam and coal. The molar flow rates of each were taken from run P1-A in the previous work. As the materials are introduced through a dual fuel burner, it was assumed that the reaction between propane and oxygen occurs instantaneously and to completion;



Equation 4-1

Coal in reality has a complex structure in the order of $C_{137}H_{97}O_9NS$ for bituminous coal (Bowen and Irwin, 2008). This structure varies between different coals and is difficult to define, so was simplified for this model to the fictitious composition CH, corresponding closely to anthracite. The molecular mass of CH was used to calculate the molar flow from the mass feed rate in the previous work.

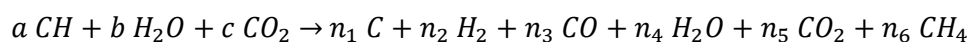
4. PROCESS MODELS AND SIMULATION

Thus, assuming complete conversion of fuel gas with oxygen and given the simplified coal structure, the species considered for the equilibrium model were reduced to CH, H₂O and CO₂. The molar flow of steam introduced directly to the burner was added to that produced from Equation 4-1. These were normalised for 1 mole of CH as shown in Table 4-1.

Table 4-1: Normalised molar flow rates of the species entering the gasifier

Species	Molar flow	Normalised molar flow	
CH	0.453	1.000	= a
H ₂ O	0.353	0.779	= b
CO ₂	0.0471	0.104	= c

An overall gasification reaction showing the reactants and possible products may be written as follows;

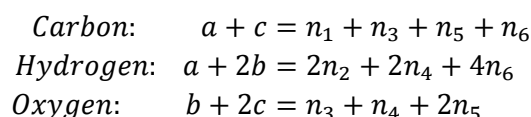


Equation 4-2

Equation 4-2 shows the possible product species considered in this model, with $n_1 - n_6$ as the total number of unknowns. The input parameters a , b and c are given in Table 4-1. To solve for six unknowns, six independent equations were required.

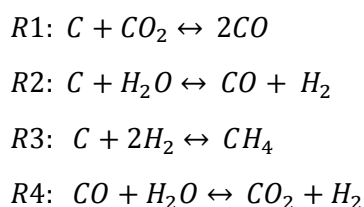
4.1.1 Independent Equations for Stoichiometric Equilibrium Model

An atom balance was performed for the three elements which feature in Equation 4-2.



Equation 4-3

Equation 4-3 gives the first three expressions which were used to create the model. Next, the chemical reaction set was specified. In reality there are many reactions that take place within a gasifier, as defined in Table 3-1, but for this model only those in Equation 4-4 were considered.



Equation 4-4

In this method $R4$ can be considered a subtraction of $R1$ and $R2$ such that $R1$, $R2$ and $R3$ can be considered alone (Basu, 2010). The equilibrium constants for these reactions are given below;

4. PROCESS MODELS AND SIMULATION

$$Ke_1 = \frac{y_{CO}^2 P}{y_{CO_2}}$$
$$Ke_2 = \frac{y_{CO} y_{H_2} P}{y_{H_2O}}$$
$$Ke_3 = \frac{y_{CH_4}}{y_{H_2}^2 P}$$

Equation 4-5

Here y_x represents the mole fraction of species x and P is system pressure (bar). By assuming 1 kmol of gas is produced and operation is at atmospheric pressure ($P = 1$), the mole fraction is equal to the number of moles of each gas in the mixture (Cempa-Balewicz et al., 2013).

An equilibrium temperature was chosen based on the reported syngas exit temperature in the previous work. Values for the equilibrium constants were calculated using enthalpy and entropy data at 800 K from the JANAF tables (National Institute of Standards and Technology, 2000), as detailed in Appendix A.

4.1.2 Solution of Independent Equations

The atom balances in Equation 4-3 and the values calculated for Ke_1 , Ke_2 and Ke_3 were used to solve for the six unknowns $n_1 - n_6$. The equations were solved in an iterative process until all the equations were satisfied to within 1%.

Table 4-2: Predicted product gas yield from simple stoichiometric equilibrium model at 800 K

Output parameter	Mole fraction
n1 (C)	0.100
n2 (H ₂)	0.333
n3 (CO)	0.266
n4 (H ₂ O)	0.089
n5 (CO ₂)	0.071
n6 (CH ₄)	0.111

The model predicts that the product gas would contain 33.3% hydrogen, 26.6% carbon monoxide and so forth assuming equilibrium was reached at a temperature of 800 K. The sum of the mole fractions in Table 4-2 is 0.97 owing to limitations in manual convergence of the model. The assumptions made for this model are as follows;

- Only the chemical reactions in Equation 4-4 were considered for this model
- Only the species listed in Equation 4-2 were considered as reactants and products
- Coal was represented as CH in order to simplify its structure
- The combustion of propane with stoichiometric oxygen was instantaneous and complete

A description of the solution method is included in Appendix A. Having demonstrated a method of solving equilibrium calculations, commercial modelling software was employed to improve the speed and rigour of the predicted gas yield.

4.2 Equilibrium Model using Process Software

From the simple stoichiometric equilibrium model it was shown that equations may be solved individually but not simultaneously, making the resolution of even a simplified model using only three gasification reactions laborious and of limited accuracy.

Subsequently, modelling software was used to simulate the gasifier system. Aspen Plus contains databases of characteristic data for each material involved in the reactions, and is able to calculate the interactions between them at specified temperatures and pressures.

An equilibrium model in Aspen Plus is based on the *RGibbs* function which calculates chemical and phase equilibrium. This tool uses minimisation of Gibbs free energy to calculate the equilibrium gas yield. This has an advantage over the stoichiometric equilibrium technique in that the reaction set does not need to be specified beforehand, meaning every possible interaction between reactants is considered. It is also beneficial for reactions involving biomass or coal whose chemical formula may not be exactly known, as an ultimate analysis can be used to specify these materials. An equilibrium model is only an approximation to a real system as it is independent of reactor size and shape, reaction kinetics and residence time (Basu, 2010).

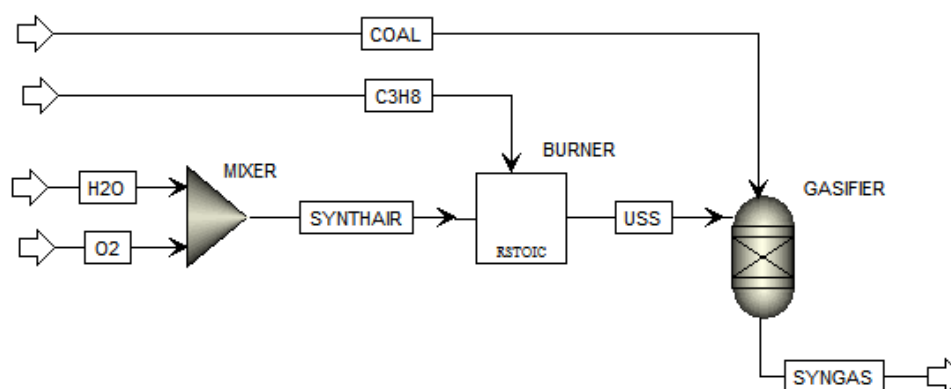


Figure 4-1: Flow sheet of Simulation 1A. USS = Ultra Superheated Steam

The flow sheet in Figure 4-1 incorporates a mixer unit for combination of steam and oxygen as in the experimental system described in detail in Chapter 5. The gasifier itself was modelled using two separate units; an *RStoic* block named BURNER to represent the initial stoichiometric combustion of propane in the synthetic air stream to produce the ultra-superheated steam (USS) as a product, and an *RGibbs* block to simulate the gasification chamber in which the solid feedstock reacts with the steam. In practice the burner is installed directly into the top of the gasifier such that these processes occur within one unit. This simulation was repeated without the burner block and found to give identical results, showing that the burner block is not necessary for the model. However it was useful for monitoring the adiabatic flame temperature of the steam mixture before reaction with the feedstock.

4.2.1 Model Input Parameters

The input flow rates were chosen based on the same data as the stoichiometric equilibrium model in Section 4.1 and summarised in Table 4-3. The previous work described the steam reaching the orifice plate at 420K (147°C) on average. The open end of the gasifier was assumed to reduce the steam pressure to just above atmospheric on entry to the burner.

Table 4-3: Summary of input parameters to Simulation 1A

	C_3H_8	Feedstock (graphite)	H_2O	O_2
Inflow kg/hr	2.488	21.204	18.792	9.000
Temperature (°C)	10	10	150	10

The property method chosen was the *Redlich-Kwong-Soave with Boston-Mathias modification* (RKS-BM) which is recommended for gas processing operations including combustion and gasification (Swanson, 2009). The solid feedstock was modelled as pure carbon (graphite) so as to define it as a conventional solid. As this idealised fuel contains no impurities and pure oxygen is fed instead of air, the only gasification products considered were water (steam), hydrogen, carbon monoxide, carbon dioxide and methane. The assumptions made in this model are listed below;

- Coal was modelled as carbon (graphite) containing no trace species such as nitrogen, sulphur etc. and no ash.
- The gasifier was modelled as an equilibrium reactor, in which the reactions are instantaneous. Reaction rates and residence times were not considered.
- The burner and gasifier were assumed adiabatic with no pressure drop and no heat losses.
- Combustion in the burner was instantaneous and complete.

The results of Simulation 1A are given in Table 4-4.

Table 4-4: Syngas yield from Aspen Plus simulation 1A compared to previous experimental results. Both are presented on a dry basis. Experimental data from (Shabangu, 2005)

Component	Simulation 1A mol%	P1-A mol%
H_2	45.12	37.4
CO	22.42	22.7
CO_2	27.14	32.6
CH_4	5.32	1.1

It can be seen that this model was in good agreement with experimental data, though the simulation over predicted the hydrogen yield and under predicted the carbon dioxide produced. The results of the simulation are limited as the system in reality would not reach equilibrium. However this case was used to examine the trends observed by varying reactant flow rates using the sensitivity analysis tool within Aspen Plus.

It was noted that in the simulation around half of the solid graphite introduced to the gasifier remained unreacted. The gasifier was charged with <6 g/s of coal in the experimental run but was

reportedly designed to gasify around 9 g/s according to initial design calculations (Shabangu, 2005). Such a high proportion of residual graphite suggests a large over feed of coal in the experiment. This is considered in Section 4.3.3 and discussed in Section 4.6.1.1.

4.3 Equilibrium Simulation Sensitivity Analyses

This section describes the effect of varying one reactant flow rate on the product gas composition using the sensitivity analysis function.

4.3.1 The Effect of Steam Flow on Product Composition

The steam flow in the initial simulation was 18.8 kg/hr; this was set to vary between 10 and 46 kg/hr and the effect on syngas composition observed. The results are illustrated in Figure 4-2, with the mole fractions presented on a wet basis. T-USS represents the adiabatic temperature of the steam entering the gasifier block, as per Figure 4-1.

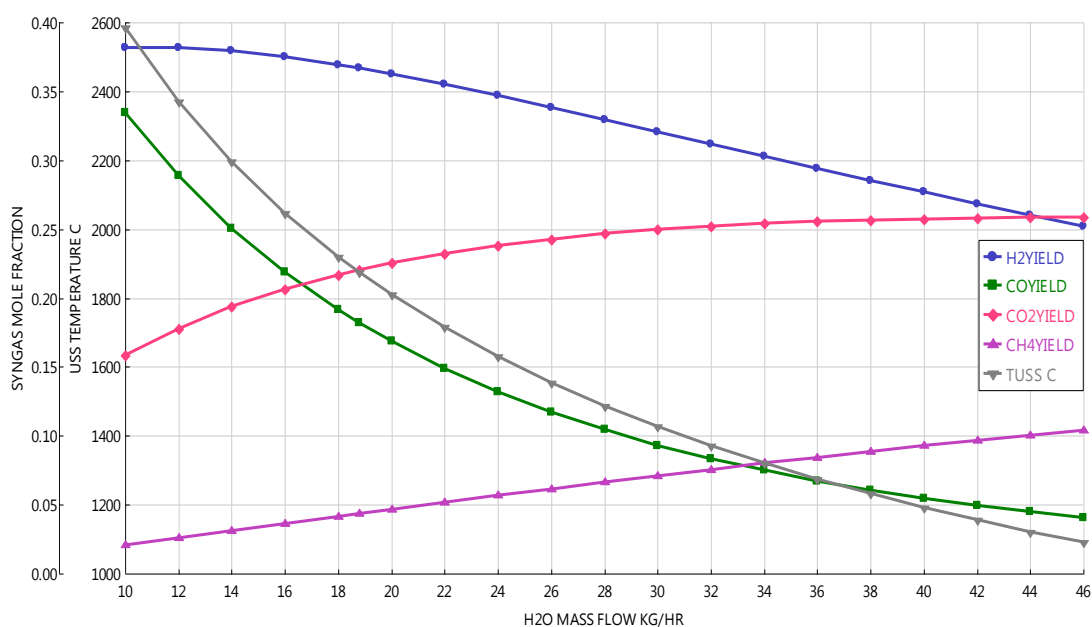


Figure 4-2: Product gas mole fractions and steam temperature (TUSS) against steam flow. Mole fractions on wet basis; other inputs as per Simulation 1A.

It can be seen that on an equilibrium basis, increasing the steam flow caused the mole fractions of H₂ and CO to reduce while those of CO₂ and CH₄ increased. This is expected as a greater steam flow through the burner resulted in a dramatic reduction in adiabatic steam temperature as shown. This reduced the gasifier temperature, favouring Methanation and inhibiting the steam-carbon and Boudouard reactions. The mole fraction of CO was seen to follow the curve of steam temperature almost exactly, suggesting a very close relationship between reactor temperature and CO yield.

Although the fraction of H₂ in the product was reduced due to the increased residual steam in the output, the actual flow rate of H₂ increases slightly owing to the increased availability of steam as a reactant. Lower reactor temperature would also mean slower reaction kinetics, which could affect the extents of the reactions attained within the reactor residence time. As mentioned previously, this was not considered in this simulation.

4. PROCESS MODELS AND SIMULATION

Due to the significant effect of steam flow on reactor temperature, these findings should be considered together with those of Section 4.3.2.

4.3.2 The Effect of Temperature on Product Composition

The heat source in the reactor is the combustion of propane in oxygen, which superheats the steam and provides energy to the gasification stage. The propane flow was manipulated to vary the temperature in the reactor. A calculator block was used to maintain the stoichiometric ratio by keeping the flow of oxygen at five times the molar flow of propane.

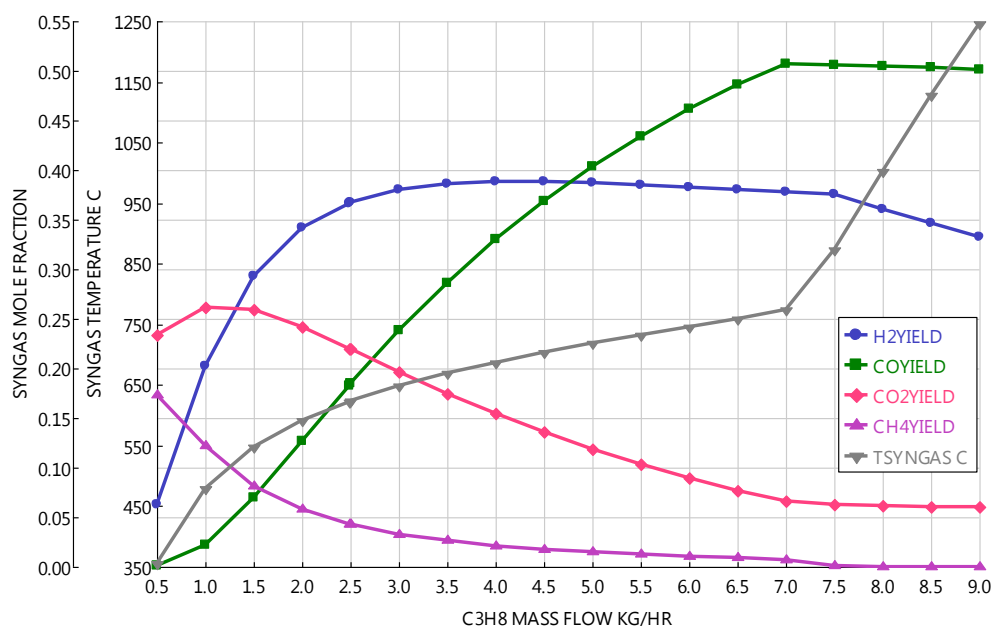


Figure 4-3: Syngas exit temperature and composition against propane flow. O_2 at stoichiometric requirement. Other inputs as per Simulation 1A

Figure 4-3 shows the effect of varying propane addition on the product temperature and yield. At low propane flows the temperature of the product (TSYNGAS) initially increased sharply with propane flow, and more gradually above the 2.5 kg/hr used in the experimental run. This suggests that the endothermic gasification reactions progress above a minimum temperature to absorb some of the additional heat. The hydrogen yield increased sharply at first while steam-carbon reactions were active due to abundant reactants. At higher temperatures the more endothermic Boudouard reaction is dominant. The water gas shift will also begin to consume H_2 in favour of CO at higher temperatures, causing the H_2 fraction to stabilise. The steam methane reforming reaction, which consumes methane to produce hydrogen and carbon monoxide, also favours high temperatures which accounts for the reducing methane concentration. The CO fraction increases with temperature until sufficient heat is provided for all of the carbon feedstock to be consumed. This is understood from the sharp rise in syngas temperature at 7 kg/hr propane addition.

Figure 4-4 also shows outlet flows of carbon (CYIELD) and H_2O (H2OYIELD). A propane flow of 7 kg/hr corresponding to an equilibrium temperature of around 760°C was sufficient to gasify all of the carbon in this mixture such that there was zero solid remaining. Increasing the propane flow beyond this point caused a sharp increase in temperature; as the carbon was fully consumed the

4. PROCESS MODELS AND SIMULATION

endothermic reactions stopped absorbing heat. The steam outflow increased as this is one of the products of propane combustion. From this analysis a propane flow of 7 kg/hr produced syngas with a high heating value, based on the low concentration of CO₂ and peak concentration of CO.

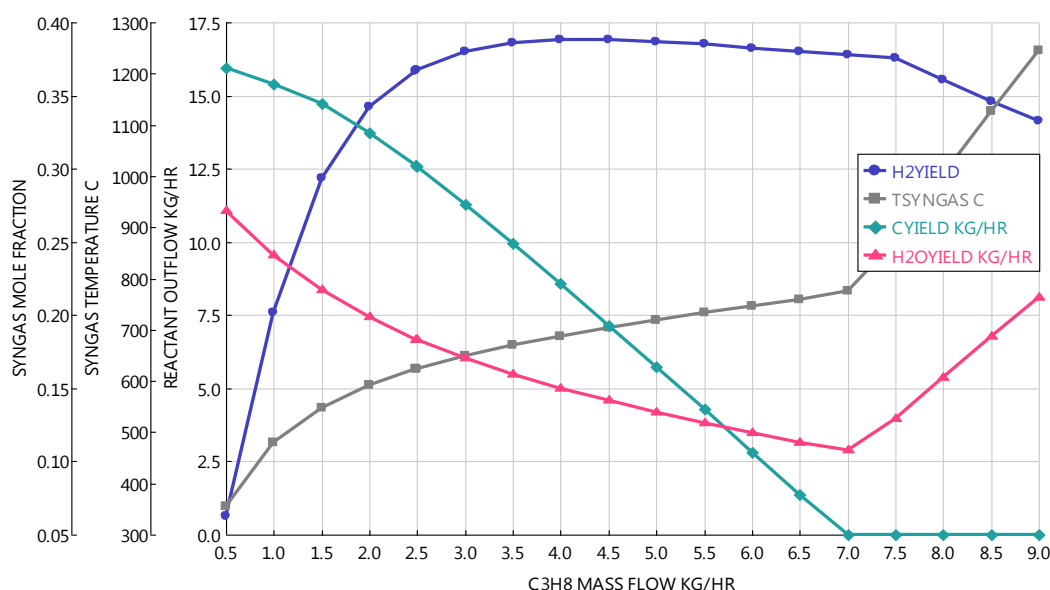


Figure 4-4: Hydrogen yield, syngas temperature and residual carbon and steam flow rates against propane/oxygen flow rates. CYIELD represents the solid carbon outlet flow rate.

4.3.3 The Effect of Steam/Carbon Ratio on Carbon Conversion

Figure 4-4 suggests that there was an excess of coal fed to the reactor under the experimental conditions given in Table 4-3. At the equilibrium temperature attained with 2.5 kg/hr propane, 12.5 kg/hr of carbon would fail to be converted. The original simulation used in designing the gasifier suggested a steam to carbon molar ratio (S/C) for complete conversion of 1.39. The ratio used in the experiment was $S/C = 1.04/1.765 = 0.59$ (Shabangu, 2005). This explains why so much of the introduced carbon remains unconverted in this simulation.

A sensitivity analysis was conducted around the mass flow of solid carbon. According to the simulation only 9 kg/hr were converted. Figure 4-5 shows the solid carbon outflow is nil below 9 kg/hr, after which it increases in direct proportion with the feed. This represents a steam to carbon ratio as follows;

$$S/C = \frac{1.04 \text{ kmol}}{\text{hr}} \text{ steam} \div \frac{9 \text{ kg/hr}}{12 \text{ kg/kmol}} \text{ carbon} = 1.39$$

Equation 4-6

This is in agreement with the equilibrium model used to size the gasifier. The hydrogen fraction peaks at 8 kg/hr carbon in Figure 4-5, corresponding to a steam/carbon ratio of 1.57. It can be concluded that a steam carbon ratio within this range should be used for maximum carbon conversion and hydrogen yield, assuming the reactor temperature is unchanged.

4. PROCESS MODELS AND SIMULATION

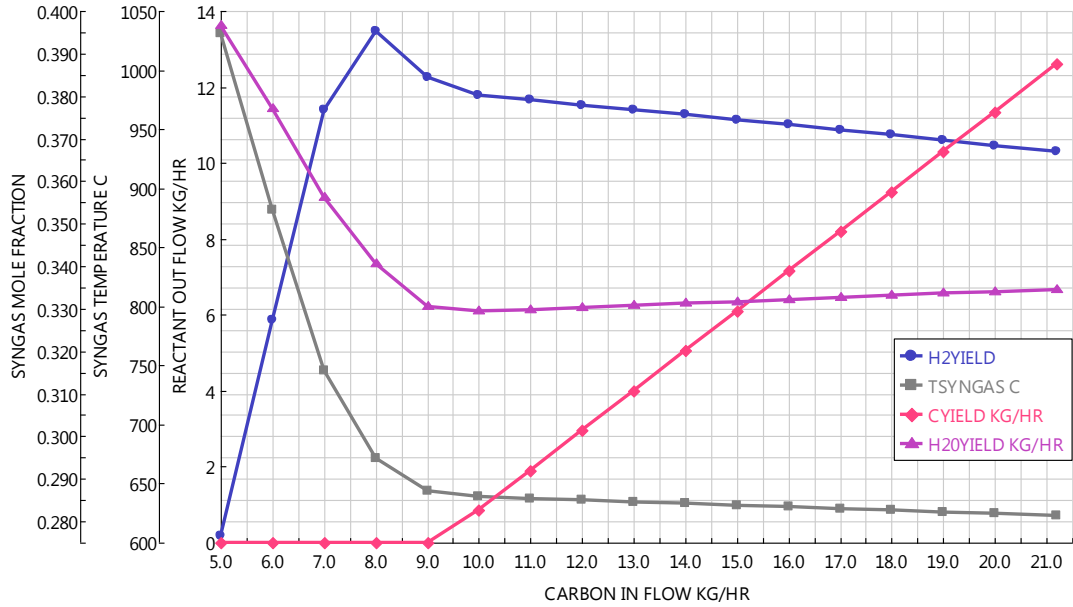


Figure 4-5: The effect of varying coal flow rate on gasifier temperature and yield; all other inputs as per Simulation 1A.

The S/C ratio can be altered by manipulating the flows of steam, carbon or both. It was found that a similar hydrogen fraction were predicted by either means, though increasing the steam flow increases the propane and oxygen requirements to achieve the necessary temperatures. Based on the size limitations of the experimental rig a lower flow rate configuration was simulated, reducing the coal inflow to give S/C of 1.39 while maintaining experimentally attainable flow rates.

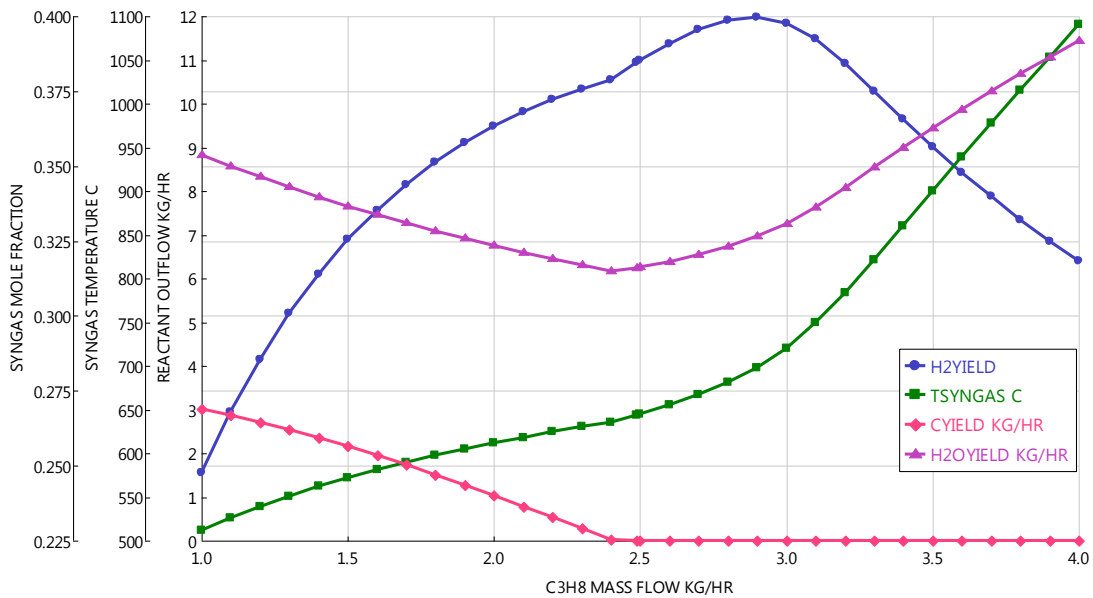


Figure 4-6: Effect of varying propane flow rate in Simulation 1A, with carbon feed rate adjusted to 9 kg/hr.

Figure 4-6 shows the mole fraction of hydrogen at various temperatures for the steam/carbon ratio of 1.39. This fraction peaked at 39.9 %mol on a wet basis at an equilibrium temperature of 700°C,

4. PROCESS MODELS AND SIMULATION

corresponding to a propane flow of approximately 3 kg/hr. These reactant flow rates were used to define an optimised Simulation 1B.

4.3.4 Simulation 1B Model Parameters

Based on the optimum propane flow and steam/carbon ratio found above, the simulation was adjusted to have the input flows as given in Table 4-5 to form Simulation 1B. The product yield is given in Table 4-6 and compared to that from experimental run P1-A and Simulation 1A on a dry, nitrogen free basis.

Table 4-5: Input flow rates to Simulation 1B

	C ₃ H ₈	Feedstock (graphite)	H ₂ O	O ₂
kg/hr	3.0	9.0	18.8	10.9
Temp (°C)	10	10	150	10

Table 4-6: Dry molar yield for simulations 1A and 1B. Run P1-A data from (Shabangu, 2005).

Component	Simulation 1A mol%	Experiment P1-A mol%	Simulation 1B mol%
H ₂	45.12	37.4	48.42
CO	22.42	22.7	30.65
CO ₂	27.14	32.6	20.43
CH ₄	5.32	1.1	0.50

Simulation 1B had higher fractions of H₂ and CO in the syngas and lower fractions of CO₂ and CH₄ compared to Simulation 1A. A sensitivity analysis around propane flow rate is displayed in Figure 4-7.

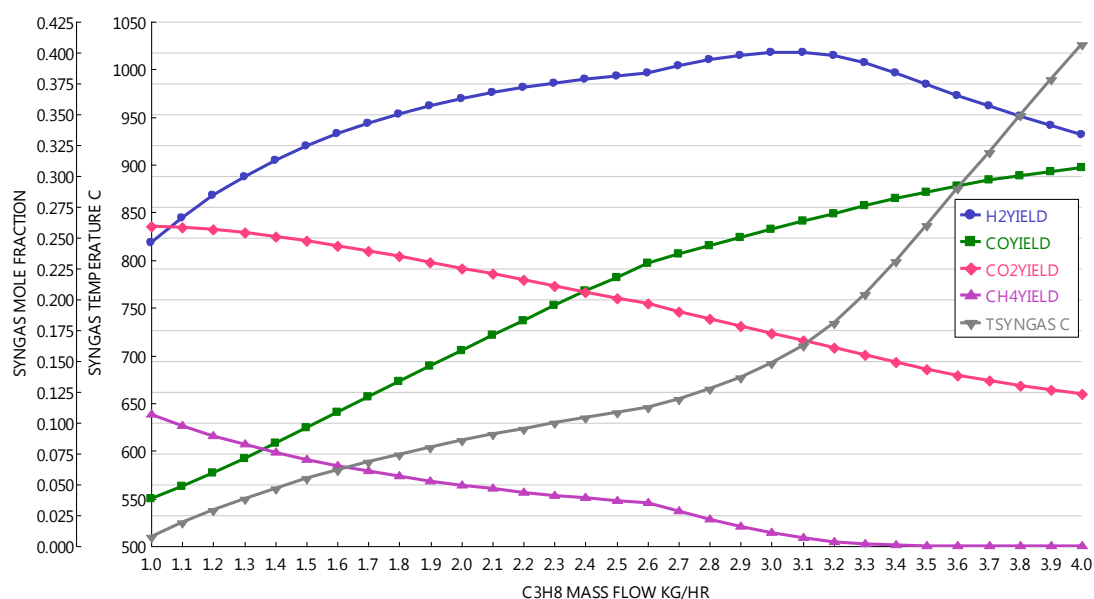


Figure 4-7: Syngas yield on wet basis for Simulation 1B against propane flow rate

4. PROCESS MODELS AND SIMULATION

Figure 4-7 shows that the hydrogen fraction peaked as expected at a propane flow of 3.0 kg/hr. Further increasing temperature leads to increasing CO and decreasing CO₂ fractions, showing that further optimisation can be made to the product heating value by sacrificing in part the hydrogen fraction. The model can be optimised differently depending on the target product. To determine whether continuing to increase the temperature is economical, the benefit of increasing the CO/CO₂ ratio should be compared with the increased cost of propane addition.

Given that increasing the amount of propane combusted will yield more carbon dioxide as a product, the next analysis investigated how much CO₂ is produced from propane combustion compared to from the gasification reactions themselves.

4.3.5 The Effect of Hydrocarbon Combustion on the CO₂ Yield

The simulation allowed an estimate of the source of carbon dioxide in the syngas. It is known from Equation 4-1 that combustion of propane in the burner stage yields carbon dioxide and water vapour as products with the release of heat for steam flame generation. By comparing the composition of the USS stream to the product stream, the amount of carbon dioxide produced in the burner compared to within the gasifier was obtained.

Table 4-7: Carbon dioxide flow in USS and syngas streams in Simulation 1B

		USS	Syngas
Total stream molar flow	(kmol/hr)	1.520	2.251
Mole fraction of CO₂		0.134	0.168
CO₂ molar flow	(kmol/hr)	0.204	0.378

From Table 4-7 it can be seen that over half of the CO₂ molar flow rate in the syngas stream originated in the burner as a result of propane combustion. This means that by substituting propane as the fuel for USS generation to an alternative fuel such as hydrogen, the flow rate of CO₂ in the syngas could be halved. This would result in a higher heating value syngas, and may facilitate the syngas separation and clean up.

4.3.6 Implications for Experimental System

These simulations facilitated an understanding of the equilibrium reactions occurring within a general gasification system and how these are affected by varying the input parameters. The simplified model demonstrated the expected trends rather than precise results. A practical system using coal or biomass in place of graphite will introduce additional species not considered in the simulations, which will participate in additional reactions. The physical dimensions and heat losses from a real gasifier will also have a limiting effect on the expected yield, such that conversion is expected to be lower in experimental runs.

Simulation 1B was used to guide the initial experimental work. The non-equilibrium effects of chemical kinetics were investigated in Section 4.4 following the collection of some initial experimental data.

4.4 Kinetic Process Model

An equilibrium model is advantageous as it does not require a reaction set to be specified *a priori*, but does not consider rates of reactions or the residence time in the gasifier. The model was extended to include some of these effects following some initial experimental work. The steam generation stage was included and the feedstock was modelled as coal instead of graphite.

4.4.1 Kinetic Model Flow Sheet

The steam generation stage included a water boiler, steam separator and a cooler to model heat losses. Having shown that the inclusion of a burner block made no difference to the simulation results it was excluded from this model. The equilibrium block was replaced with an *RPlug* block, representing a plug flow reactor that allowed the diameter and length to be defined. It also required a chemical reaction set and temperature profile to be specified. Kinetic data was also required for each kinetically controlled reaction.

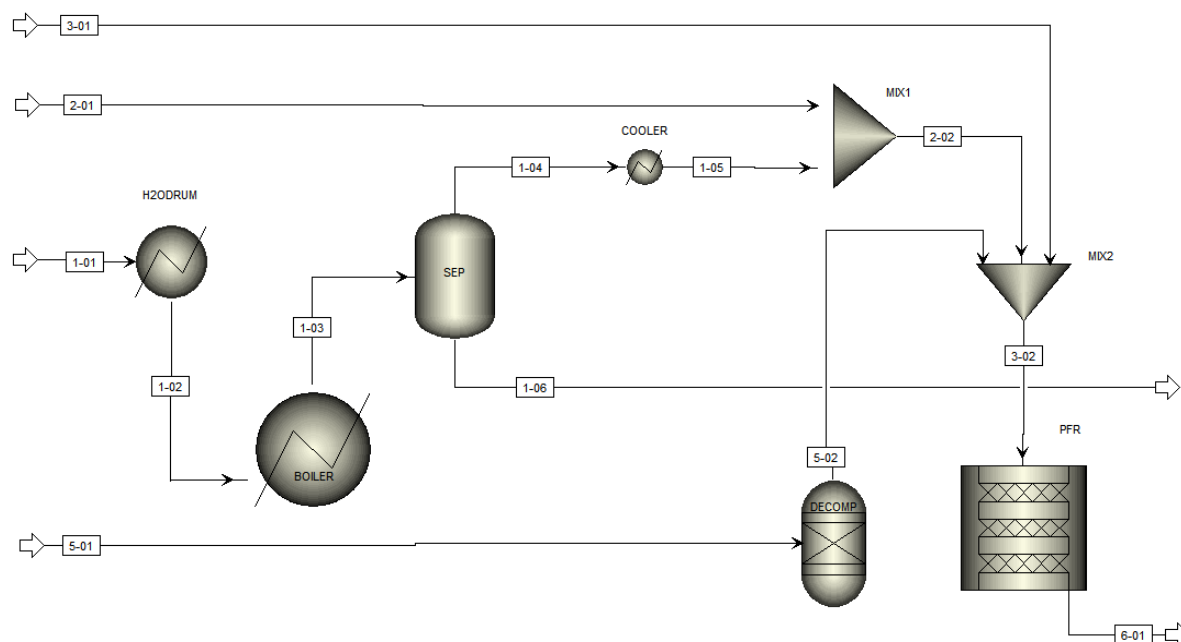


Figure 4-8: Kinetic model flow sheet with plug flow reactor

The component COAL was created based on data from the proximate and ultimate analyses of coal samples, to comprise 85%wt carbon, 7%wt oxygen, 3%wt ash, 2%wt moisture and 1.5%wt each of nitrogen and hydrogen. Sulphur was excluded at this stage. Because coal is an ‘unconventional’ component, a decomposition step was required to treat the COAL as a mixture of conventional components and model its reactions.

Unlike the *RGibbs* block, the *RPlug* reactor allowed only one input and output stream, which required an extra mixing block to combine the reactant streams prior to feeding. Stream 3-02 contained the sum of the components entering the reactor, though in the simulation no reactions occur until the mixture enters the gasifier.

4.4.2 Configuration of RPlug

Flow rates in this model were based on an experimental Run V-1, described later in Section 6.1. The input flows are specified in Table 4-8, with the condensate stream 1-06 from the steam separator.

Table 4-8: Table of inputs to kinetic model, corresponding to Figure 4-8

Stream	Material	kg/hr
1-01	Water	15
(1-06)	Water	0.6
2-01	Oxygen	14.6
3-01	Propane	3.2
5-01	Coal	6.9

Compared to Simulation 1B, a higher oxygen and lower steam flow were used to improve flame stability. A lower coal feed rate again was specified for controllability and to reduce waste.

4.4.2.1 Chemical Reaction Set

The reaction set specified for the plug flow reactor model is listed in Table 4-9. Although the reactions are reversible, under the reactor conditions these were assumed to progress in one direction only. The water gas shift reaction was entered twice to allow for the reverse reaction to take place.

Table 4-9: Reaction set specified for plug flow reactor

Rxn No.	Reaction Name	
1	Propane combustion	$C_3H_8 + 5 O_2 \rightarrow 3 CO_2 + 4 H_2O$
2	Boudouard	$C + CO_2 \rightarrow 2 CO$
3	Steam-carbon 1	$C + H_2O \rightarrow CO + H_2$
4	Partial char combustion	$C + \frac{1}{2} O_2 \rightarrow CO$
5	Water gas shift	$CO + H_2O \rightarrow CO_2 + H_2$
6	Reverse water gas shift	$CO_2 + H_2 \rightarrow CO + H_2O$
7	Char combustion	$C + O_2 \rightarrow CO_2$

The kinetic data applying to the Arrhenius equation shown in Equation 3-14 in the Theory chapter was obtained from literature, but was found to vary substantially between sources. One paper presents kinetic data as reported by four separate authors in which the cited data for the pre-exponential factor in reaction 7 varies by a factor of 10^5 and for reaction 3 by a factor of 10^9 , for example (Nikrityuk et al., 2013).

The variability arises from feedstock reactivity, reactant gas concentration and temperature. While it was expected that the kinetic data reflected differences in rank and reactivity of different coals, no clear correlation was found between coal type and reaction rate.

4. PROCESS MODELS AND SIMULATION

In some cases very long links of citations were followed before the original data was found (Nikrityuk et al., 2013). For the present model, data from Hla *et al* was chosen as it was not taken from other sources and was measured using the same coal type consistently. For the water gas shift reaction, the data was taken from Jones and Lindstedt (1988) and Wu et al (2009) for the forward and reverse reactions respectively, as cited in (Nikrityuk et al., 2013).

For propane combustion, various mechanisms have been proposed for the stepwise breakdown of the fuel. Up to eighty incremental steps have been proposed (Jachimowski, 1984). Kinetic data from one global reaction scheme was found to fully combust the propane (Jones and Lindstedt, 1988), which was assumed appropriate. Data for char combustion was taken from (Goldman et al., 1984).

4.4.2.2 Restricted Equilibrium

Aspen Plus allows different methods of modelling restricted equilibrium; by specifying a temperature approach or specifying the duty and exit temperature for which the approach temperature is calculated automatically. The initial experimental runs gave some insights into the temperatures achieved within the gasifier body and of the exiting syngas, which allowed the latter method to be used.

The temperature profile was manually assigned to the *RPlug* reactor. The adiabatic flame temperature of propane combustion in air is just under 2000°C; given that the heat capacity of steam is around double that of nitrogen gas at elevated temperatures, it was estimated that the flame temperature achieved was in the region of 1500°C which was set as the reactor inlet temperature. Initially the temperature was set to 900°C after 20% of reactor length, subsequently changed to 1150°C after 30% of the reactor length following further experimental measurement. The outlet temperature was set to 700°C.

4.4.3 Results of *RPlug* Simulation

The simulation was run at both temperatures. The product yield is compared with the equilibrium simulation and experimental Run V-1 on which the flow rates and conditions were based.

The temperature of the steam-oxygen mixture (stream 2-02) in the simulation was 90.5°C which is in the same range as the temperatures observed experimentally. The gas yield predicted by the *RPlug* model was generally in good agreement with the experimental yield, showing good correlation for H₂, CO and CO₂ and much closer agreement with the experimental yield than the equilibrium model. This result was expected as reaction kinetics limited the extent of gasification in the residence time allowed.

Table 4-10 shows that as the *RPlug* reactor temperature was increased, the fractions of H₂ and CO both increased while the concentrations of O₂ and CO₂ both decreased. This result suggests that the Boudouard and water gas reactions both progressed further at high temperature, which contributed to increased carbon conversion, with only 67% of the feedstock unreacted.

The high O₂ and low CO₂ in the product stream point to inadequate char combustion kinetics. The high hydrogen prediction may also suggest that H₂ combustion with O₂ should be taken into account. As the Methanation reaction was not specified in the reactor, there was no methane formation during this simulation.

4. PROCESS MODELS AND SIMULATION

The result was found to be sensitive to the peak temperature achieved at the reactor inlet, where a reduction of just 100°C gives a result similar to the low temperature case. This supports the previous conclusion that the reactor temperature is key to determining the progress of the gasification reactions.

Table 4-10: Predicted dry gas yields from different methods¹⁵.

	RPlug 900°C	RPlug 1150°C	RGibbs (equilibrium)	Experiment
	%mol			
O₂	18.38	12.52	11.47	0.31
H₂	24.54	33.70	36.99	22.2
CO	11.90	16.35	44.52	17.0
CO₂	44.50	36.94	7.02	58.4
CH₄	0.00	0.00	0.00	0.52
N₂	0.67	0.49	<0.01	1.61
Residual C	83%	67%	0%	~50%

This model gave some indications of the factors determining the product yield. Given that very fine tuning of the reactant conditions may not be replicable with the practical system, the simulation was not refined any further. For investigation of the behaviour of the gas distribution in the reactor, a more detailed study of the experimental burner and gasification chamber was undertaken using computational fluid dynamics, described in Section 4.5.

4.5 Computational Fluid Model

ANSYS FLUENT is a computational fluid dynamics (CFD) program that allows simulation of fluid flow around a two or three dimensional geometric domain. It operates by dividing the domain into a number of finite points at which the Navier-Stokes equations are solved in an iterative process based on some initial or boundary conditions. Simulations of flow patterns, temperatures and reaction yields for a chemical system can be performed for optimisations of burner and furnace designs, allowing system optimisation without the need for prototyping.

A CFD model of the gasifier was created to investigate the flows in the burner and gasifier. As with most furnaces and reactors, there is limited optical access to the experimental unit. The model was used as a method of visualising the mixing between fuel and oxidant flows, to observe the temperature distribution and the trajectory of feedstock particles. In order to gain useful outputs in a reasonable time frame some simplifications were made and the USS mixture was focussed on. For the purpose of this work the aims of the CFD model included;

- gain an understanding of the gas flow pattern and residence time inside the burner and gasifier

¹⁵ The kinetic model (RPlug) was run at both temperatures as described in the text, and compared with the adiabatic equilibrium model and experimental data. Residual C represents mass percentage of solid carbon feed remaining after test.

4. PROCESS MODELS AND SIMULATION

- simulate the heat release and flame zone to understand where the high temperature reaction zone is located
- observe the distribution of particles around the reactor, including their residence time in the high temperature reaction zone and temperatures achieved

4.5.1 Constructing the Model

The gasifier was created as a three dimensional domain as shown in Figure 4-9. The burner was a modified commercial model encompassing a coal distributor in the centre and fuel gas inlet annulus surrounding it. The synthetic air mixture was injected through the eight injection ports. The burner is housed in a 'quarl' or burner tile, the narrow section at the top of the geometry designed for flame stabilisation. This leads into the wider gasification chamber which is tapered at the exit. The dimensions of the experimental unit are detailed further in Chapter 5; the quarl zone diameter was 127 mm and the chamber diameter was 285 mm at the widest point. The total domain length was 1300 mm. The domain was constructed to represent half of the reactor with an axis of symmetry along the centreline as shown, in order to reduce the number of nodes and hence the computational demand.

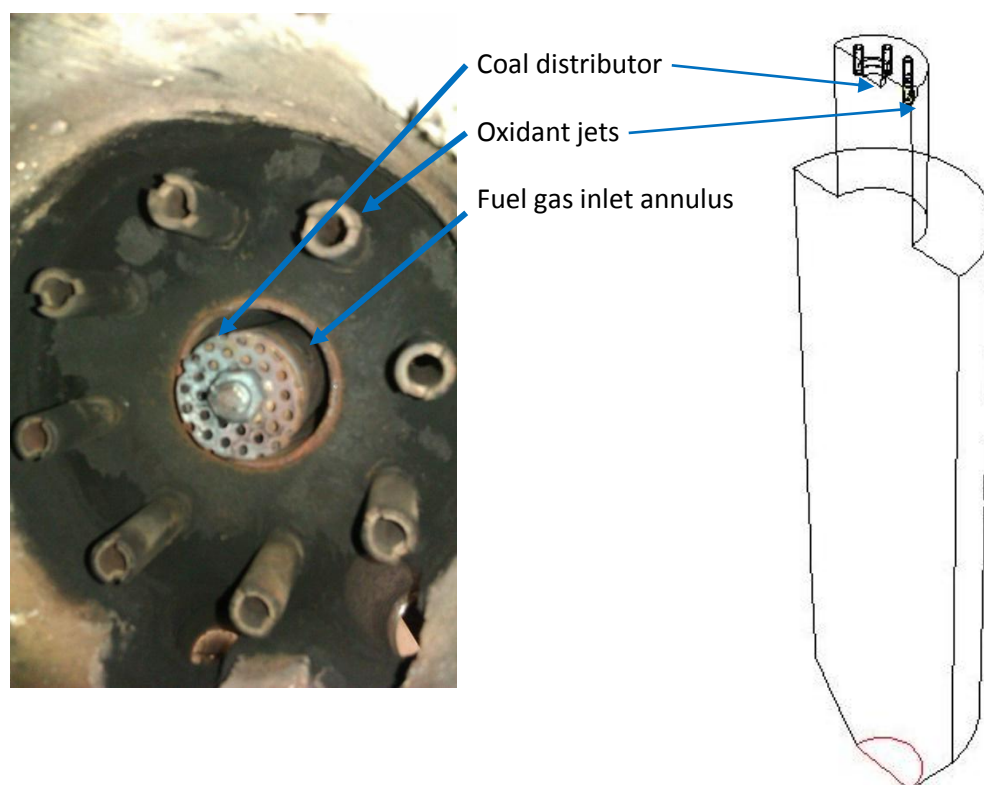


Figure 4-9: (a) The burner viewed from below, showing each inlet; (b) the CFD model geometry

The input flow velocities were calculated from the equilibrium simulation and the cross sectional area of each inlet port. Based on experimental observations in Section 6.2, the fuel gas was changed from propane to methane for this simulation, adjusting the flow rate to maintain the same energy input.

4.5.2 Mesh Independence Study

CFD simulations involve splitting a domain into a network of points or nodes at which the various equations are solved. The interconnectivity of each node creates a mesh of points around the domain. Where there is a rapid change in conditions, such as highly turbulent flows, it is important to ensure that the calculated solution is not limited by the number of calculation points. There should be sufficient mesh density to provide adequate resolution in regions of interest.

This can be tested by running a simulation in successively finer meshes until there is no impact on the calculated solution. From a preliminary model the region of interest was found to be in the burner quarl where the high velocity inlets are located. This was a highly turbulent region due to the mixing of the inlet species and heat release from combustion. A smaller domain consisting of the burner quarl region only was used for the mesh independence study. Monitor points were established within the region of interest below the synthetic air jets to record temperature and axial velocity, as well at the outlet temperature into the gasification chamber. The results of this study are shown in Figure 4-10.

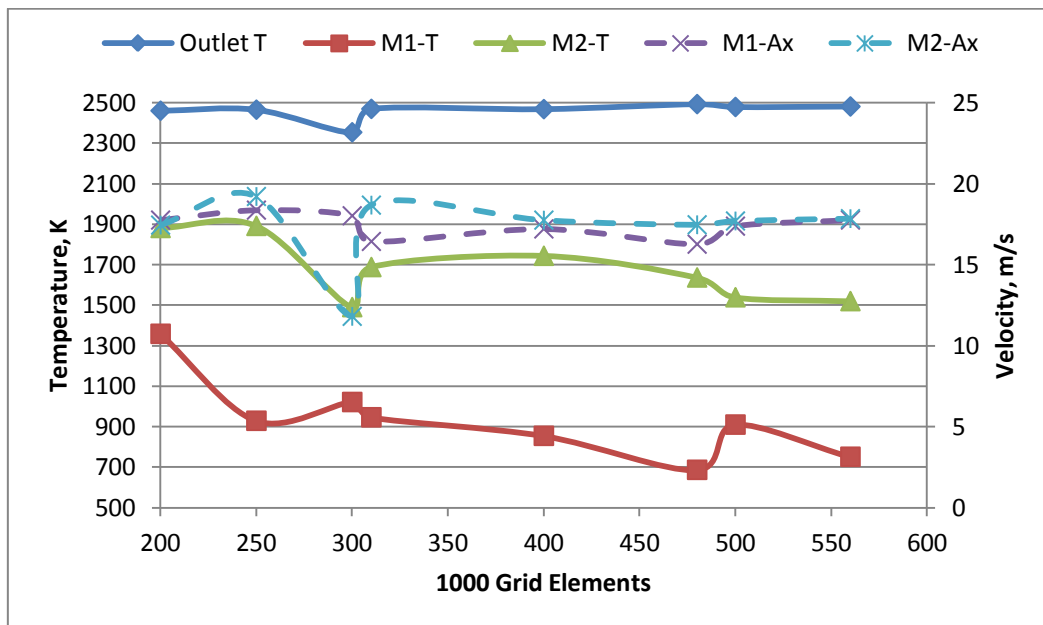


Figure 4-10: Effect of grid density on temperature and axial velocity in the region of interest. M1, M2 are monitoring points. T= temperature, Ax= axial velocity

It was found that the temperatures at the monitor points varied a little across different grids. As the flame zone represents a very steep temperature gradient across a small radial length, the displacement of the flame by even a few millimetres can have a sharp effect on local temperatures. As the velocity monitors and the outlet temperature remained stable across all the grids tested, it was concluded that the mesh of around 250,000 elements provided adequate grid resolution for this work. The same grid density was then used to mesh the burner in the full length geometry, with a lower grid resolution used for the gasification chamber where the flow velocity and turbulence were much lower. A gradual transition between the fine and coarse mesh zones was achieved using concentric spheres of gradually decreasing grid density centred on the highly turbulent region. The model parameters and boundary conditions used were the same in the mesh independence study as for the full length model, as described in Section 4.5.3.

4.5.3 Selection of Model Parameters

The viscous model selected was Realizable k- ϵ with Enhanced Wall Treatment (EWT). The k- ϵ model is an example of a Reynold's Averaged Navier Stokes (RANS) turbulence model using two transport equations, giving reasonable accuracy at economical computational demand. As such it is commonly chosen by researchers for combustion and gasification applications (Cuoci et al., 2010; Mayr et al., 2015; Mohamed Ismail et al., 2013; Roy et al., 2011). The Realizable k- ϵ model offers improvements in the turbulent viscosity and dissipation rates calculations, and is recommended over the standard k- ϵ model (ANSYS Inc, 2010a). The Enhanced Wall Treatment combines logarithmic and laminar layer formulations for a method that is applicable across the whole near wall region. It is recommended to use EWT wherever available (ANSYS Inc, 2010a; Yin, 2016).

4.5.3.1 Radiation Model

Due to the high temperatures expected in the burner, radiation will be a major form of heat transfer making the choice of radiation model important. The P-1 model is commonly chosen for its modest computational demand and applicability to complex geometries. It also is well suited to combustion simulations when the optical thickness is high. The P-1 model may suffer loss of accuracy at low optical thickness (ANSYS Inc, 2010b). Given that the steam flame is expected to be colourless, the Discrete Ordinates model was chosen as it can be used across all optical thicknesses at moderate computational and memory cost, and is popular for comprehensive combustion studies. The Weighted Sum of Grey Gases Model was used as a compromise between the simplified grey gases model and a detailed absorption model as it considers gases of interest without the need to calculate absorption at individual wavelengths (ANSYS Inc, 2010b; Baukal et al., 2001); similar such models for oxy-fuel combustion are under development (Yin, 2016). Scattering effects of combustion gases can often be neglected (Baukal et al., 2001).

4.5.3.2 Species Model

When choosing a species model, a number of approaches were compared. Combustion chemistry involves a great many intermediate steps, including the breakdown of fuel and oxidant into short lived species such as CH₃, CH and atomic C. A variety of reactions occur between these species before the formation of final species CO₂ and H₂O. In order to represent a simple combustion reaction such as methane and air, reaction mechanisms such as GRI-Mech involving 52 species and 325 reactions offer a comprehensive approach (Smith et al., 2000). Conversely the simplest approach was a methane-air 2-step model, which simplifies the combustion mechanism to two reactions. As the system in question does not involve air both of these were discounted.

For enriched oxygen flows it is most suitable to use the Eddy Dissipation Concept model for turbulence chemistry (Mayr et al., 2015) due to the high temperatures generated. At these temperatures dissociation reactions become significant, which are not accounted for in the simple 2-step models. These intermediate reactions and species absorb some of the energy of combustion and have been found to have a significant effect on simulation results (Cuoci et al., 2010). Additional reactions can be included providing appropriate reaction data is available; this has led to concentrated research efforts to improve the accuracy of kinetic data, for both coals and biofuels (Bhuiyan and Naser, 2016; Mohamed Ismail et al., 2013). A variety of models and sub models are under continuing development to balance kinetic detail with computational demand (Bibrzycki et al., 2016; Cheng et al., 2015).

4. PROCESS MODELS AND SIMULATION

An alternative approach is based on an assumed shape probability density function (PDF). The Non-Premixed Combustion (NPC) model operates without the need to specify a reaction set. Instead a PDF table is created from specified input species, from which the possible intermediate and product species are calculated by the software. The thermo-chemistry is then simplified to a function of mixture fraction, by assuming that ‘mixed is burned’ i.e. the chemistry is sufficiently fast compared to the rate of mixing that each small volume can be considered locally at equilibrium. The approach calculates the product species independently of individual reaction pathways, which is less accurate than a method using detailed kinetic mechanisms but gives a reasonable representation of combustion systems where the kinetics are rapid compared to the rate of mixing (ANSYS Inc, 2010a; Baukal et al., 2001). The NPC model was chosen in this case as a compromise that incorporates intermediate and radical species without the need for detailed and complex reaction kinetic data.

4.5.4 Boundary Conditions

The inlet boundaries were set using flow rates from the process model, with some adjustments based on experimental experience. The cross sectional area of the inlets was used to calculate inlet velocities. The synthetic air (*synthair*) input was set to 50/50 by mass of steam and oxygen.

Table 4-11: Input boundary conditions for CFD model. I = turbulence intensity, L = turbulence length scale

Input	m/s	T (K)	I (%)	L (mm)
CH ₄	2.6	300	10	3.5
Synthair	25	360	10	7.6

The outlet boundary was set as a pressure-outlet with appropriate turbulence parameters in case of reverse flow, which was generally not observed with the full length model. The axis of symmetry was set as a symmetrical boundary. The coal inlet was set as a wall at this stage, as coal addition would be simulated later using the DPM model described in Section 4.5.6. The gasifier walls were assigned the properties of the refractory material as listed in Table 4-12.

Table 4-12: Wall boundary conditions for CFD model

Parameter	Value	Unit
Heat capacity	1085	J/kgK
Density	3100	kg/m ³
Thermal conductivity	2.5	W/mK
Thickness	50	mm
Temperature	500	K
Emissivity	0.5	-

The heat transfer through the wall is proportional to the temperature difference, as represented using Fourier’s Law (Equation 3-27 in Theory chapter). In FLUENT the default options are a constant heat flux through the wall or a constant temperature wall. For walls with a non-zero thickness, the convention in FLUENT is that the “outer surface” is that adjacent to the fluid zone, while the “inner” surface is furthest from the fluid zone. In setting a fixed wall temperature it is the inner surface

4. PROCESS MODELS AND SIMULATION

which is set. This option was chosen as it approximates a rate of heat loss proportional to the fluid temperature and avoids cold spots appearing on the wall. Experimental data was used for the boundary temperature, and refractory properties taken from previous work (Shabangu, 2005). Emissivity values for refractory at elevated temperature are found from literature (Baukal, 2003). The surface of the burner itself, which was made of steel, was set to have zero heat flux to avoid instabilities arising due to the thin walls of the inlet jets.

4.5.5 Results of Combustion Simulation

The simulation was monitored at three point locations for fluctuations in temperature and axial velocity, as well as monitoring the distributions of the temperature contours and velocity flow pattern and the average temperature across the domain outlet. The simulation was considered stable when these monitors did not vary significantly over 500 iterations.

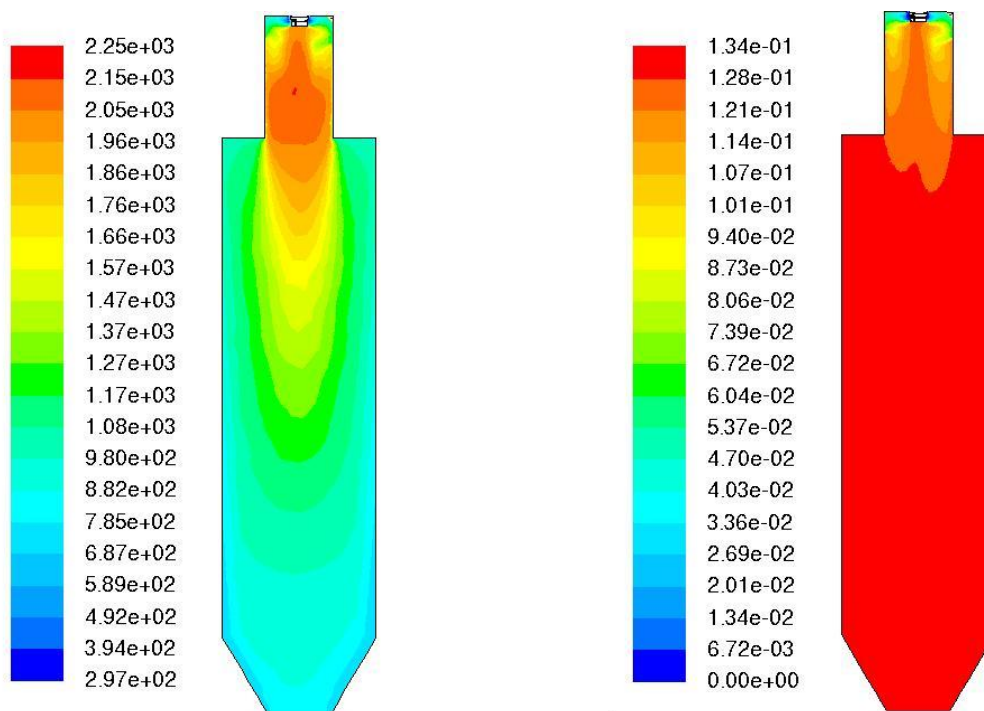


Figure 4-11: Contour plots of (a) temperature [K] and (b) mole fraction of CO₂ for methane combustion in synthetic air along central axis of symmetry

From Figure 4-11 it is apparent that the majority of heat release is in the lower part of the burner quarl before the expansion into the gasification chamber. The proximity of the hot refractory walls was found to contribute intense radiation in this region. CO₂ concentration rises sharply from under the synthair jets and is high along the central axis upwards flow region, stabilising at a maximum in the lower gasification chamber.

Figure 4-12 shows a two dimensional plane in line with one of the four synthair jets to show the region of interest directly below the jet. From the velocity profile the highest velocity is observed beneath the jet, which was set as a velocity inlet at 25 m/s based on the flow rate and cross sectional area, as specified in Table 4-11. A recirculation zone is visible in the centre of the burner in an upwards direction. This is expected as the purpose of a burner quarl is to promote recirculation of hot gases towards the reactant inlets to help ignition and maintain flame stability (see Section 3.5.2).

4. PROCESS MODELS AND SIMULATION

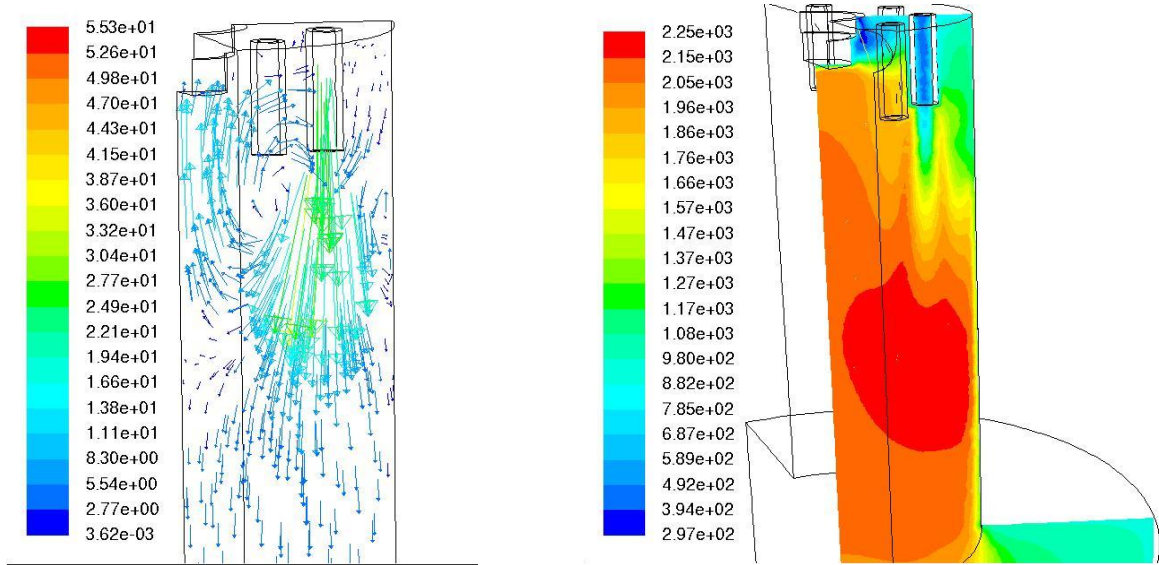


Figure 4-12: (a) Velocity vectors [m/s] and (b) temperature contours [K] in plane with a synthair jet

From the temperature profile it can be seen that the peak temperature is located where the synthair jet spreads out and the upward recirculation begins. The recirculation zone is characteristic of burners with high swirl numbers and is in agreement with the findings of a similar analysis of a downward firing gas burner in which the velocity profile was in close agreement with measured values and the temperature found to be over predicted by 2-400 K. Proposed explanations for this result included limitations of the two equation $k-\epsilon$ turbulence model and difficulty in simulating the exact ignition point, which would strongly affect the local flow pattern (Baukal et al., 2001). This is a limitation of using the NPC model which assumes that the chemistry is infinitely fast. Species distributions in the study supported this finding, as the CO_2 concentration was over predicted in the vicinity of the burner, while the concentration of oxygen was under predicted. This suggests that combustion in the simulation progressed more rapidly than was observed in practice.

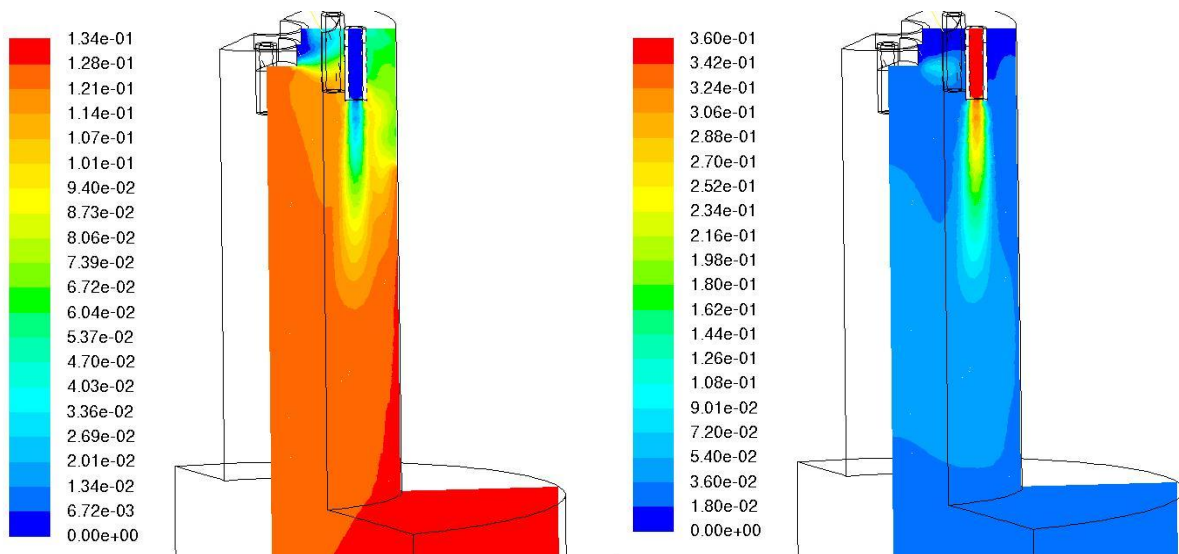


Figure 4-13: Contour plots of mole fraction of (a) CO_2 and (b) O_2 in plane with a synthair jet

4. PROCESS MODELS AND SIMULATION

Figure 4-13 shows mole fractions of CO₂ and O₂ in the jet plane. It is seen that CO₂ is circulated throughout the top of the burner with a high concentration along the axis, being drawn back into the jet stream. The O₂ concentration is quickly depleted with distance from the jet. Experimental validation is required to confirm any discrepancy caused by equilibrium chemistry as in the described study (see Section 4.6.4).

Using the volume of the domain from FLUENT as 0.0333 m³ and the flow through the lower outlet surface of 0.00888 m³/s, the mean gas residence time was calculated to be 3.75 seconds.

This study serves to demonstrate the gas flow pattern and turbulence in the burner and the region of heat release. The following section describes the addition of a solid particle into the gas stream and the conditions experienced by the particle.

4.5.6 Particle Tracking

To simulate the addition of coal particles the Discrete Phase Model (DPM) was used. This model allows injections of solid particles or liquid droplets and simulates their physical interaction with the continuous gas phase. It is appropriate for cases in which the discrete phase is dilute and occupies less than 10-12% of the volume fraction. Inter-particle interactions are not considered (ANSYS Inc, 2010a). The DPM model is suited to tracking individual particle trajectories through a domain and is capable of simulating combustion or specified surface reactions with the continuous phase. As additional reactions are limited to the particle surface only unless configured using a user defined function, gasification chemistry was omitted from this model for simplicity in satisfying the aims of the model. Coal was injected as inert particles for the purpose of tracking trajectory, temperature and residence time within the domain.

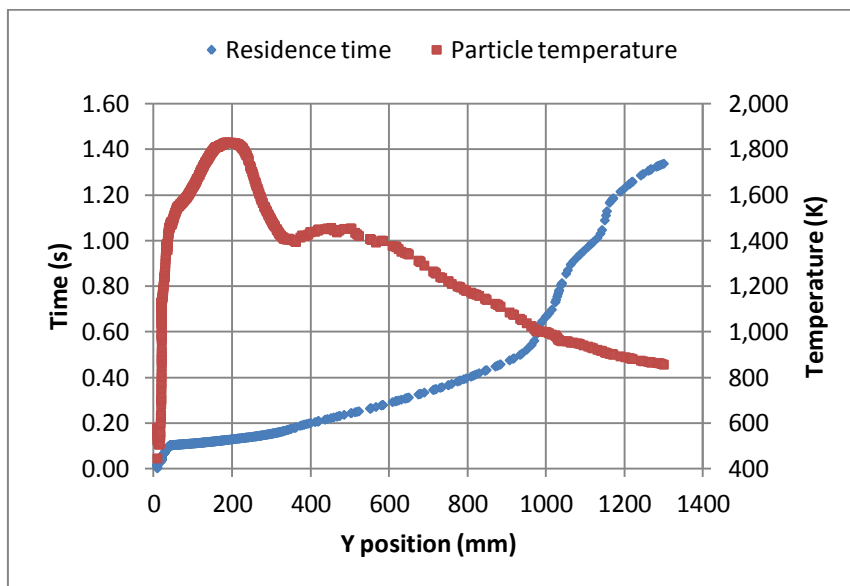


Figure 4-14: Single 70 µm coal particle residence time and temperature against gasifier length

The turbulent dispersion of particles is modelled using stochastic tracking to include the effect of velocity fluctuations on particle trajectories using the Discrete Random Walk (DRW) model. Each particle follows a statistically probable path calculated by the software (ANSYS Inc, 2010a). Optional physical models are available within the DPM; in the present work Particle Radiation Interaction was

4. PROCESS MODELS AND SIMULATION

activated to represent particle heating by radiation, and Thermophoretic Force to represent particle motion caused by temperature gradients which was found to be prominent in this model.

Because inert particles were not consumed within the simulation, a reduced coal flow rate was used to avoid overfilling the domain and exceeding the volume fraction limit. Initially a single particle injection was used. This was set as anthracite with density 1550 kg/m^3 , particle diameter 70 micron and sphericity set to 0.8 to represent a pulverised coal particle. The heat capacity was changed from the default constant value to a polynomial function of temperature using data from (Tomeczek and Palugniok, 1996). The trajectory of a single particle is shown in Figure 4-14.

From Figure 4-14 the particle motion can be understood; during the first 0.1 seconds after release it was suspended near the top of the burner; during the following 0.4 seconds it travelled almost 1000 mm along the reactor length, suggesting it was entrained by the synthair jet before slowing towards the reactor outlet at $y = 1300 \text{ mm}$. The particle temperature rose almost instantly up to a peak around 1800 K and gradually cooled with distance along the reactor. The location of the temperature peak corresponds to the peak gas temperature zone shown in Figure 4-11, lying between 150-300 mm along the reactor.

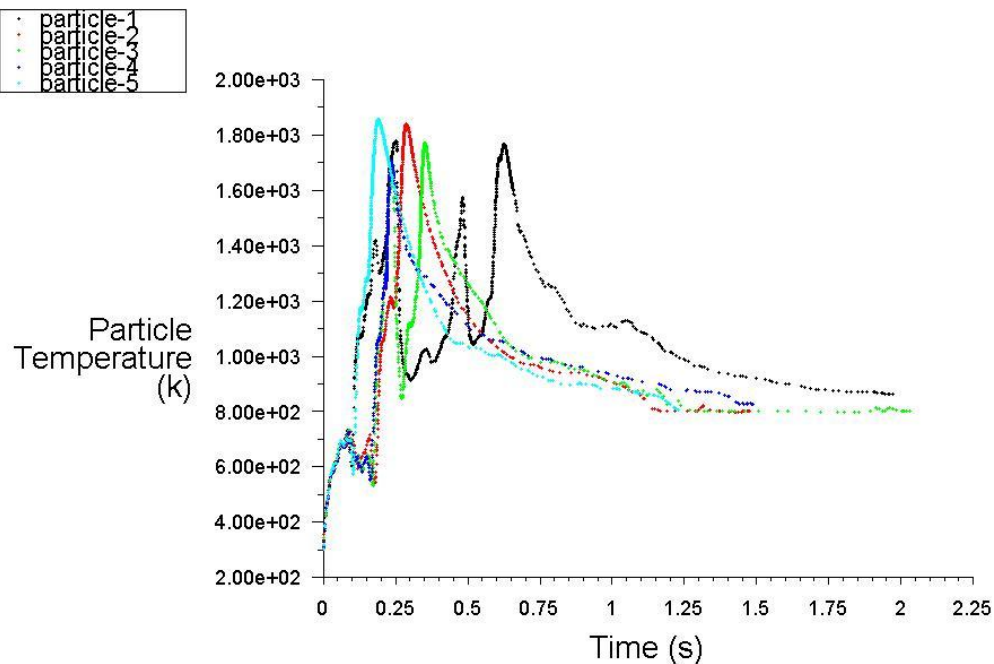


Figure 4-15: Five stochastic paths for single $70 \mu\text{m}$ coal particle, showing particle temperature against residence time

Due to the stochastic method used to calculate particle trajectories, considerable variation is observed with each calculation. Several particle trajectories are necessary to account for natural variations in residence time and particle temperature. This can be achieved by increasing the number of tries in the stochastic model, which computes additional trajectories for the same particle as shown in Figure 4-15. Here the variability is visible, with each track reaching peak temperature of around 1800 K in approximately 0.3 seconds. Two particle tracks experience more than one temperature peak due to being caught in recirculation flows in the burner and demonstrate a rapid rate of heating and cooling of the particle.

4.5.6.1 Effect of Particle Diameter

A greater number of particle tracks are necessary to obtain a statistically significant average temperature and residence time. The single particle injection can be expanded to a group injection to model a range of particle diameters or injection points. A comparison was made between different diameter particles, using 10 streams over 10 stochastic tries giving 100 particle tracks in each case. The residence time analyses of these tracks are given in Table 4-13.

It can be seen that the smaller particles were suspended for a longer average residence time in the reactor than the larger diameter particles. The largest particles also showed a much lower standard deviation, suggesting a more direct route towards the reactor outlet than the smaller particles which had a greater chance of being suspended in the reactor by the gas flow for longer periods.

Table 4-13: Residence times for coal particles¹⁶.

Diameter µm	No. complete tracks	Residence time (s)			
		Min	Max	Average	Std Dev
50	86	0.98	36.22	4.81	5.77
150	100	0.70	58.64	3.47	7.87
300	100	0.49	10.61	1.59	1.18

For the 50 µm particles 86 particle tracks were completed, which means 14 particle tracks did not reach the reactor outlet within the allowed time frame. These particles were sufficiently small to be entrained by turbulent gas flows indefinitely. To prevent these particles from distorting the residence time statistics they were abandoned by FLUENT after a prescribed number of time steps. For the larger diameter particles this did not occur, suggesting a lower probability of indefinite particle entrainment.

4.5.6.2 Effect of Particle Density

A representation of low density biochar was also investigated by changing the particle density in FLUENT from 1550 to 300 kg/m³ typical of softwood char (Gupta et al., 2002).

Table 4-14: Residence times for 300 kg/m³ 'char' particles. Complete tracks represent particles which reached the outlet within the permitted number of time steps. Std Dev = standard deviation.

Diameter µm	No. completed particle tracks	Residence time (s)			
		Min	Max	Average	Std Dev
50	83	1.12	19.06	4.42	3.99
150	90	0.99	38.75	5.01	7.07
300	100	0.87	39.25	3.76	6.57
500	100	0.74	24.28	2.48	3.25

¹⁶ Coal particle density 1550 kg/m³. 'Complete tracks' represent particles which reached the outlet within the permitted number of time steps. Std Dev = standard deviation

4. PROCESS MODELS AND SIMULATION

In this case a similar trend in average residence time with particle diameter was observed. The residence time of the small particles was comparable in both cases, with both 50 and 150 μm 'char' particles showing a similar residence time to 50 μm coal particles. The larger char particles showed less reduction in residence time with increasing size than in the high density case. This indicated that lower density particles were less sensitive to particle diameter than high density material, having a higher average residence time and standard deviation than for coal.

$$Q = mc_p\Delta T$$

Equation 4-7

Differences in particle heating were also investigated, as shown in the temperature plots in Figure 4-16. The dense particles take longer to reach peak temperature than the low density char particles, as the greater mass of these particles requires a larger amount of energy to achieve the same temperature change according to Equation 4-7, assuming equal rate of heat transfer, heat capacities and particle volumes;

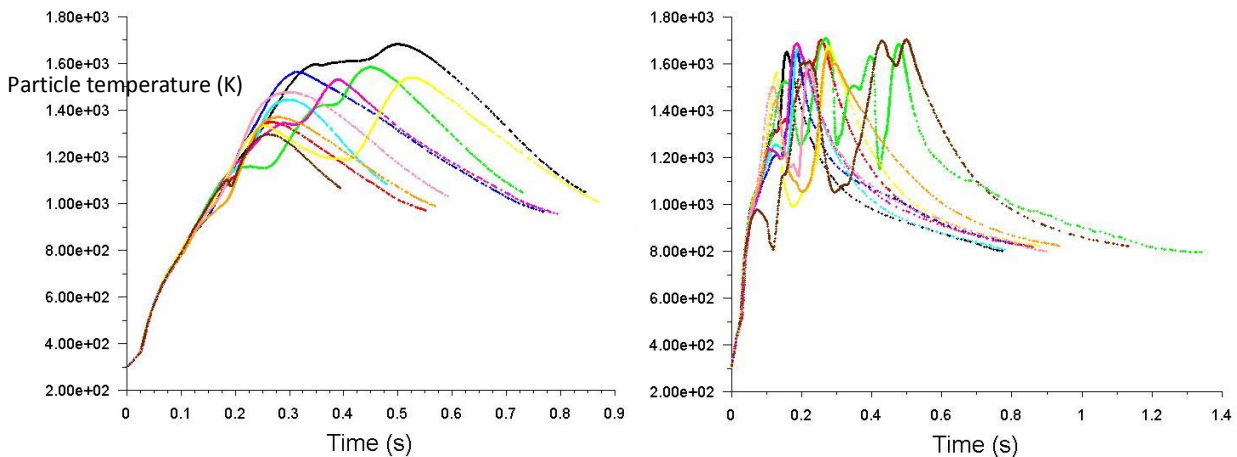


Figure 4-16: Particle temperature vs residence time for ten 300 μm particles of (a) particle density 1550 kg/m^3 , (b) particle density 300 kg/m^3 . Gravitational force included.

While the more dense particles take longer to reach peak temperature than the low density particles, the peak temperature reached is almost the same for both particle types. The difference in average residence time between the two particle types is also visible. This was investigated further with consideration of gravitational force on the same particles, as described in Section 4.5.6.3.

4.5.6.3 Effect of Gravity

Because the gas motion is dominated by the high velocity inlet jets and the thermal expansion by combustion, the force of gravity was not considered significant for the gas model. However with the addition of particles using the Discrete Phase model, the effect of gravity on particle motion was investigated.

Gravitational force was added as 9.8 m/s^2 in the $-Y$ direction. No impact was detected on the gas motion, with the gas residence time and velocity vectors being unchanged with this force. Particle average residence time however was substantially reduced for each particle condition in this case, as represented by the updated average residence times shown in Table 4-15.

4. PROCESS MODELS AND SIMULATION

Table 4-15: Residence time of injected particles, including gravitational force

Diameter μm	Particles completed tracks	Residence time (s)			
		Min	Max	Average	Std Dev
High density 1550 kg/m ³ coal particles					
50	99	1.34	6.11	2.24	0.96
150	100	0.58	1.38	0.87	0.16
300	100	0.39	1.25	0.72	0.16
Low density 300 kg/m ³ char particles					
50	89	1.43	10.65	3.38	1.98
150	100	1.10	3.84	1.66	0.52
300	100	0.68	1.53	0.96	0.18
500	100	0.49	1.21	0.75	0.16

The standard deviation in particle residence times was greatly reduced with the introduction of gravitational force. This implies that fewer particles were being entrained indefinitely by turbulent gas flows in the gasifier. This is supported by the increased number of complete particle tracks for the smaller diameter ranges. A visual representation of the difference between coal and char particles is shown in Figure 4-17.

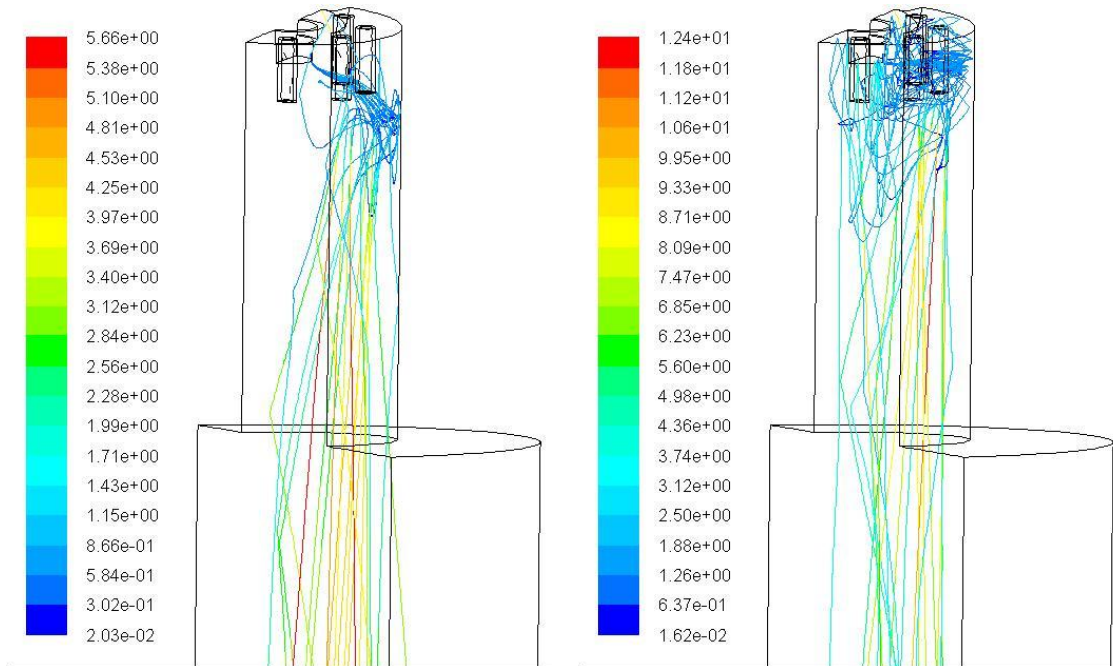


Figure 4-17: Velocity magnitudes (m/s) for 20 particles of 300 μm, (a) 1550 kg/m³, (b) 300 kg/m³

From the particle velocity tracks it is seen that high density particles are drawn more directly into the high velocity jets, spending only a short time in the top of the burner. The low density particles are seen to circulate in the top of the burner at low velocities, entrained by turbulent eddies before being drawn into the jets. The maximum velocity magnitude achieved by low density ‘char’ particles is around double that of the coal particles in the jets, demonstrating that low density particles are

entrained more easily with the gas flows reaching closer to the gas velocity. The effect on particle heating rate is seen in Figure 4-16 for the same particle tracks.

4.6 Summary of Simulations

Gasification involves a large number of possible reactions. Models can be used to predict the effects of varying parameters such as reactant flow rate and temperature. A stoichiometric equilibrium model is a simplified method that relies on reducing the reaction set and number of possible species in order to give a manageable number of variables for manual calculations. A basic equilibrium model was created first to describe the methodology, before being quickly superseded by process modelling software.

The equilibrium model was a simplified representation that did not consider reaction rates or residence times when calculating the product yield. The software considers the possible product species based on the reactants and reaction conditions, and uses the minimisation of Gibbs free energy technique to predict the output species. For simplicity the coal feedstock was modelled as graphite, to reduce the number of side reactions taking place.

4.6.1 Equilibrium Model Findings

The equilibrium model provided a useful starting point for the experimental work as it allowed rapid manipulation of reactant species and conditions to understand the expected trends. For example, increasing the fuel gas flow rate to increase reactor temperature tended to increase the fraction of CO in the output gas. This is in keeping with the trends predicted by the theory (Chapter 3) and the findings of other studies (Sections 2.4.4 and 3.1.1).

The results of the sensitivity analyses showed that increasing the steam flow rate gave a lower steam temperature. Generally higher temperature was favoured for syngas production and a molar steam to carbon (S/C) ratio of around 1.4-1.6 maximises carbon efficiency and hydrogen production under these conditions.

Unlike the equilibrium model, a practical reactor allows for only limited gas residence time and suffers heat losses with a steep temperature gradient between the burner and the gas outlet. This was investigated further using the computational fluid dynamics model.

4.6.1.1 Coal Overfeed

It was observed from the process model that much of the solid feedstock supplied to the gasifier remained unreacted at the equilibrium condition simulated. As this model was based on experimental flow rates from a previous work, it follows that a large amount of coal would have remained unreacted in those experiments. The reason for the low steam/carbon ratio used in that experimental work is not explained, but could include the practical difficulties in establishing a stable flame with high steam flows and obtaining the necessary coal flow rate with the available equipment. This is explained in Chapter 5 and discussed in Chapter 7.

The simulation was updated to reflect a lower solid feed rate to reduce the amount of unreacted coal in the product stream, described in Simulation 1B. It was found that using similar gas flows but reducing the coal feed by around 40% yielded a very similar product gas composition to Simulation

1A and the previous work. This dramatically improves the economics of operation and carbon efficiency. This finding was incorporated in planning the experimental programme for the present work.

4.6.2 Kinetic Model Findings

The finding of a reduced coal feed was taken into account for the extension of the process model. Incorporation of some kinetic data and an approximate temperature profile had a substantial impact on the predicted gas yields and feedstock conversion, giving a better representation of the experimental system and closer agreement in gas yield.

The increasing yields of H₂ and CO with increasing temperature are in agreement with the theory described in Section 3.1.1, further emphasising the importance of high temperature to improve gasification yield.

A further analysis showed that this model is highly sensitive to the activation energy of the Boudouard reaction. By reducing this from 69.55 to 68.0 kcal/mol the mole fraction of CO increases from 16 to 48%mol of the product gas.

It was noted that the reliability of this model was dependent on the reliability of the supplied temperatures and kinetic data. The empirical nature and variability inherent in the kinetic data was described in Section 4.4.2.1. To improve reliability it would be necessary to perform detailed kinetic studies on the specific feedstock materials, under the precise heating rates achieved in the experimental reactor which are still under investigation. The findings of this kinetic model were considered useful for progressing the experimental work at this early stage. Further development in tandem with the experimental programme would increase the value of this modelling approach.

4.6.3 Computational Model Findings

The grid independence study showed that the solution remained relatively steady at higher mesh densities, allowing a modest density to be chosen in order to prioritise computational speed.

Numerous model options exist for simulation of a burner environment. Several of these are discussed and compared in Section 4.5.3 with some justification for the parameters chosen in the current work; generally based on the trade-off between model rigour and computational demand.

The flow pattern in the burner was established and subsequently checked using a cold flow simulation and found to give the same recirculation pattern as shown in Figure 4-12. This supports the statement in Section 4.5.2 that the burner quarl will be the region of highest turbulence requiring the largest grid density. A plot of turbulence intensity against Y coordinate is shown in Figure 4-18, in which the Y coordinate is negative due to the frame of reference used in FLUENT. It is seen that the peak of intense turbulence exists along the upper 300 mm of the domain, representing the burner and region immediately below the quarl where the flow enters the gasification chamber, justifying the concentration of grid elements in this region.

4. PROCESS MODELS AND SIMULATION

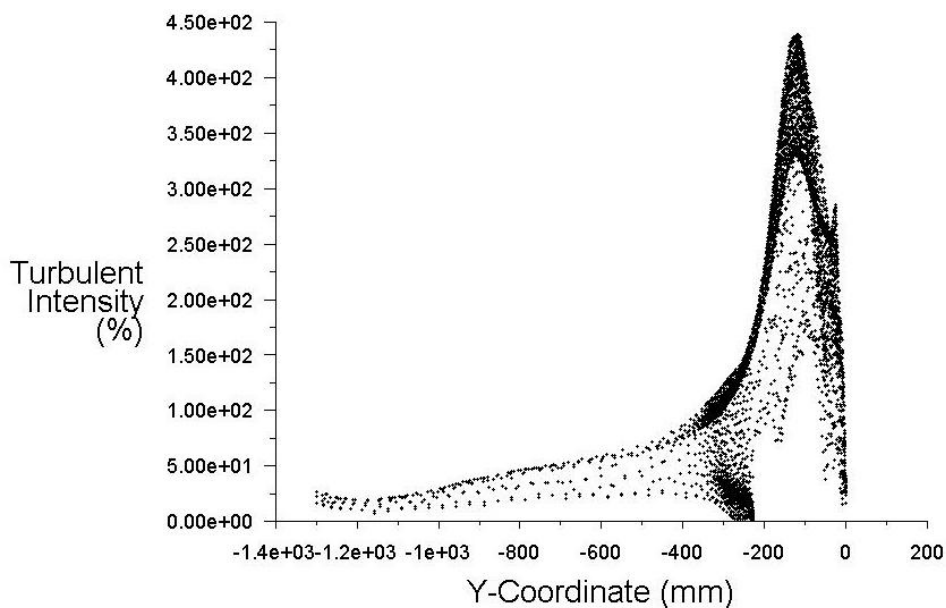


Figure 4-18: Turbulent intensity against Y coordinate along the X=0 axis of symmetry. Y=0 represents the top of the burner and Y= -1300 mm is the reactor outlet

4.6.3.1 Temperature Distribution

The adiabatic flame temperature for the mixture was calculated as 2550 K. The peak temperature in the model was around 300 K below this, as a result of formation of intermediate combustion species and heat loss through the walls. The region of highest temperature identified in Figure 4-12 corresponds well with the location of peak particle temperature in Figure 4-14.

The peak radiation temperature at the walls reaches 1400 K while peak particle temperature was around 1600-1800 K, both below the peak gas temperature of 2250 K. The higher temperature of the particles than the wall radiation indicates that particle heating is dominated by the gas phase rather than by radiation from the walls.

As with the process model there are inherent simplifications that will cause inaccuracies in the simulation, primarily the assumption of equilibrium chemistry in the NPC model (Section 4.5.3.2). The lack of chemical kinetic data in this model resulted in a more rapid rate of heat release in the model leading to higher temperature peaks than would be expected in the real system.

The rate of heat loss through the wall was also simplified using a fixed temperature for the outside wall temperature. In reality the rate of heat transfer is proportional to the temperature gradient across the wall, which will be non-uniform along the reactor length due to the heat release by combustion. This means the outside surface temperature will not be constant along the reactor length, however this method did allow for different inside surface temperatures without specifying a rate of heat transfer which was found to cause excessive cooling in some areas leading to cold spots and model instabilities.

4.6.3.2 Particle Behaviours

In modelling particle trajectories the following findings were observed. From Figure 4-15, Particle 1 exhibits three clear temperature peaks within one second. This shows that under intense heating the change in temperature is very rapid. This is related to the coal particle heat capacity, which varies

4. PROCESS MODELS AND SIMULATION

with temperature between 1-1.6 kJ/kgK but owing to the particle's small mass, results in a large temperature change according to Equation 4-7. This is also related to the Biot number (Equation 3-29) in that very small particles will have sufficiently small thermal gradients within them that they can be considered essentially isothermal. The high emissivity of the particles will also contribute to their rapid temperature change. Black particles of coal or char approach the ideal black body condition for radiation, with emissivity of 0.9 by default in FLUENT. This will result in the particle absorbing and emitting large amounts of incident radiation very quickly which explains the rapid temperature fluctuations.

It is expected that for a reacting particle the properties would be changed after the first temperature peak as the particle is consumed by gasification. This would alter both the composition and physical properties of the particle, which would likely cause it to behave differently. This is identified as a key area for future investigation, for the purposes of more detailed particle tracking as well as predicting gasification gas yields resulting from these reactions.

In comparing different particle diameters, larger particles were found to experience lower average residence times than smaller particles. This was expected as small particles were entrained to a greater extent by the swirling gas flows than larger ones. The simulation of discrete particle addition, particularly under the influence of gravity, has major implications for the expected conversion of feedstock introduced to this gasifier. The smallest particles which were easily entrained by the gas flow experienced an average residence time of 2 or 3 seconds, but this time decreases sharply with increasing particle size. This emphasises the importance of feedstock particle size not only for maximising surface area for reaction, but also for maximising hold up within the reactor to provide adequate time for conversion, as predicted in theory illustrated in Figure 3-5.

Low density particles were found to have longer average residence times for all particle diameters compared to high density material. Similar to particle diameter, this is reasoned to be due to the additional mass per particle giving greater inertia causing heavier particles to be entrained to a lesser extent by the circulating gas flow. The trajectories of these particles were dominated by the force of gravity and tended to fall in a direct path towards the outlet with relatively little entrainment or recirculation. The increased mass also resulted in a larger heat capacity demonstrated in Figure 4-16 where, in contrast to the smaller particles, a slower rise to peak temperature with little fluctuation is observed.

4.6.4 Model Validation Measurements

Some preliminary measurements were taken from the experimental system for model validation. The temperature measured at the gasifier outlet during experimental work was generally between 550-600°C, which is in good agreement with the 842 K (569°C) predicted by the fluid model as shown in Figure 4-11.

Chapter 5 describes an investigation using a suction pyrometer inserted into the top of the burner, extending into the centre of the burner quarl. The peak temperature recorded using this technique was 1420°C. In order to compare with the same location in the model, a monitor point was created at the coordinates of the probe aperture as represented in Figure 4-19. The insertion of the probe as shown is clearly intrusive and would affect the flow pattern in the burner. While this was unavoidable for the experimental measurement, in the simulation a virtual monitoring point was

4. PROCESS MODELS AND SIMULATION

created without the probe body to avoid disturbing the flow pattern. The image is for illustration only as the probe shaft was not included in the simulation.



Figure 4-19: Representation of suction pyrometer inserted into quarl space

At the coordinates of the probe aperture the temperature in the simulation was 2034 K (1761°C). This is around 340°C higher than the experimental measurement, showing a similar error to that recorded in the study described in Section 4.5.5 (Baukal et al., 2001) and considered to be in reasonable agreement given the simplifications inherent in the model.

The same position was used to find the predicted gas composition at the probe inlet, and compared with experimentally obtained gas composition from suction pyrometry. The gas compositions on a dry basis are shown in Table 4-16.

Table 4-16: Gas compositions at pyrometer probe inlet from simulation and experiment (%mol dry basis).

	H ₂	O ₂	CH ₄	CO	CO ₂	Total
Simulated	2.49	14.50	30.65	2.24	50.12	100
Experimental	29.4	0.2	16.4	20.0	31.1	97.1

Comparing the gas results in Table 4-16 it is seen that the simulated composition is much richer in fuel and oxygen than the experimental mixture, while the experimental sample was richer in partial combustion species such as CO. This is considered to arise from the time required to take experimental measurements. In suction pyrometry the gas is siphoned from the burner at very high temperature and cooled using a cold finger before being delivered to the online gas chromatograph. Several meters of pipework were required for this operation during which species in the gas mixture may continue to react with each other. Particularly while under high temperatures, it is reasoned that fuel would continue to react with oxygen or with steam to form CO through partial combustion or H₂ by reformation, as a mixture of these gases would be unstable at elevated temperature.

4. PROCESS MODELS AND SIMULATION

The syngas products, H₂ and CO observed experimentally in the burner region were not observed at the gasifier outlet during the same test. This suggests that these species were either formed in the burner reaction zone before being consumed further along the gasifier length, or that they were produced within the suction pyrometer apparatus as described above. The gas composition showed markedly less agreement between simulation and experimental results than the temperature results, which highlights an opportunity for further development of this model.

Further improvements in the detail and accuracy of the simulation would require additional and more precise measurements for validation. In the current work such measurements were limited by the restricted optical and physical access into the burner and gasifier bodies. The pyrometer probe measurements introduce a substantial impact on the burner environment due to its large intrusive nature, and the suction of gas from a relatively small burner volume will cause non-trivial changes to the local gas composition and combustion environment. This means errors introduced by the measurement methodology may be significant. These are discussed further in Chapter 7.

5 EXPERIMENTAL PROGRAMME

This chapter presents the experimental work conducted during this project. It includes a description of the gasification system; preparatory work including fuel sample preparation and analysis; and testing and development of experimental rig components such as the feedstock screw feeder and the steam supply. This is followed by experimental methods and results of various experiments.

5.1 Gasification System

The gasification system is illustrated in Figure 5-1. It is centred on a cylindrical gasification chamber which is fed by a steam generator, fuel gas cylinders and granulated feedstock from a hopper.

5.1.1 Description of Gasifier

The gasifier used in the following experimental work was developed in a previous research project, wherein its design and construction is described in detail (Shabangu, 2005). The gasifier consists of a cylindrical gasification chamber with a downward facing burner installed at the top. Methane was burned in a mixture of steam and oxygen to produce a steam flame using a patented methodology (Lewis, 2007). Powdered feedstock was introduced into the centre of this flame and gasification occurred as the reactants progressed down the length of the cylindrical reactor shown in Figure 5-2.

The gasification chamber has an internal length of 1300 mm and an internal diameter of 285 mm. The shell is made from mild steel lined internally with 50 mm fused alumina refractory giving high abrasion resistance and a maximum service temperature of approximately 2100 K.

5.1.1.1 The Dual Fuel Burner

The burner is a 6422-3 Fire-All Dual Fuel model manufactured by Fives North American Combustion, Inc. It was designed with a maximum capacity of 0.0322 m³/s air (Fives North American Combustion Inc., 2013; Shabangu, 2005). Dual fuel burners are typically used for co-combustion of gas and liquid fuels, comprising separate inlets for air, fuel gas and liquid fuel. On this burner the liquid inlet was adapted to accept granulated solid feedstock via a screw feeder, connected to a sealed feedstock hopper to prevent backflow of gas. The air feed, normally consisting of roughly 21% oxygen and 79% nitrogen, was replaced with a *synthetic air* mixture of oxygen and steam for production of the steam flame. The pilot burner was used for start-up only and did not affect the gasification process or products.

5. EXPERIMENTAL PROGRAMME

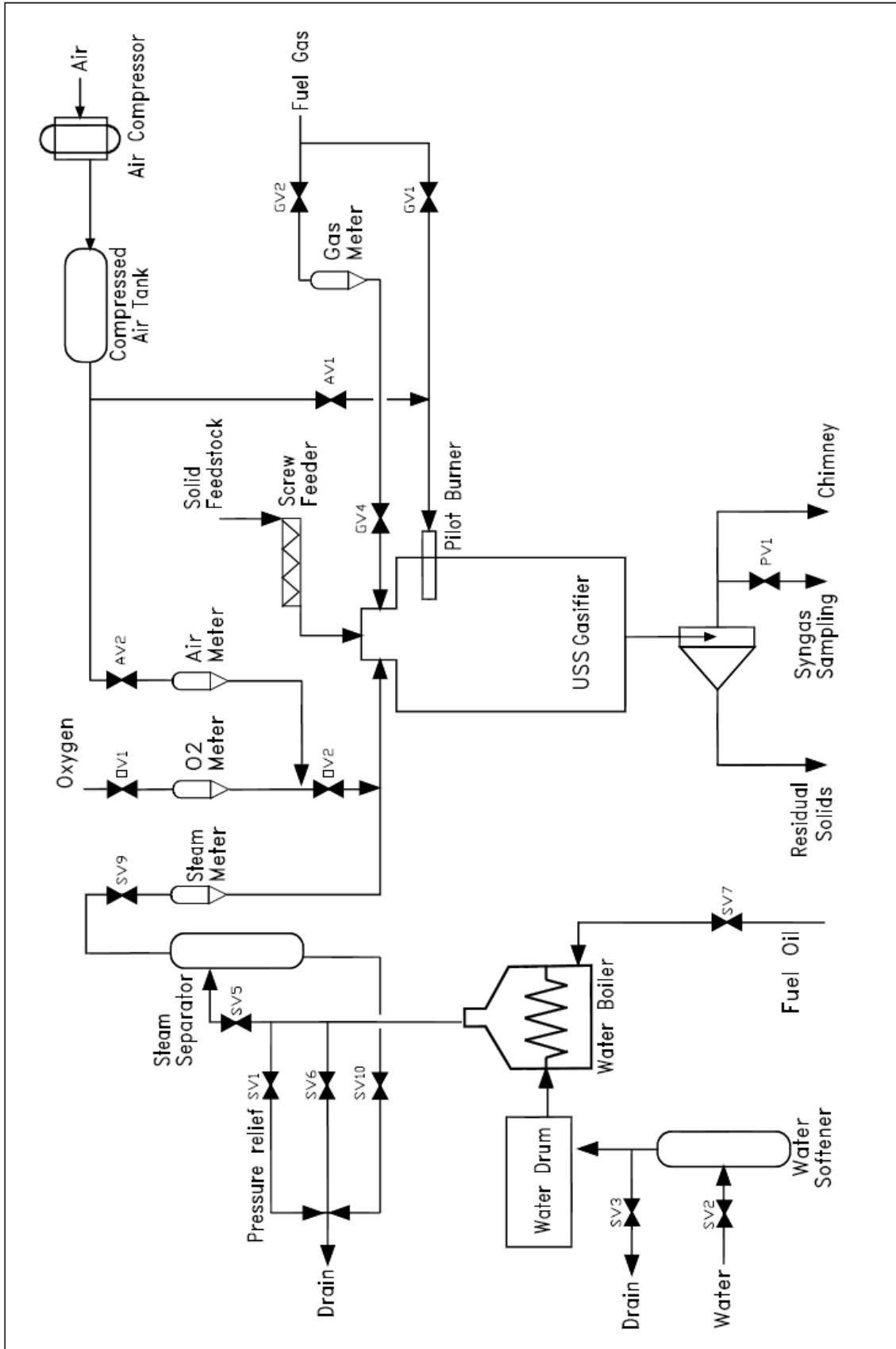


Figure 5-1: Experimental gasification system flow diagram, showing major equipment and safety control valves

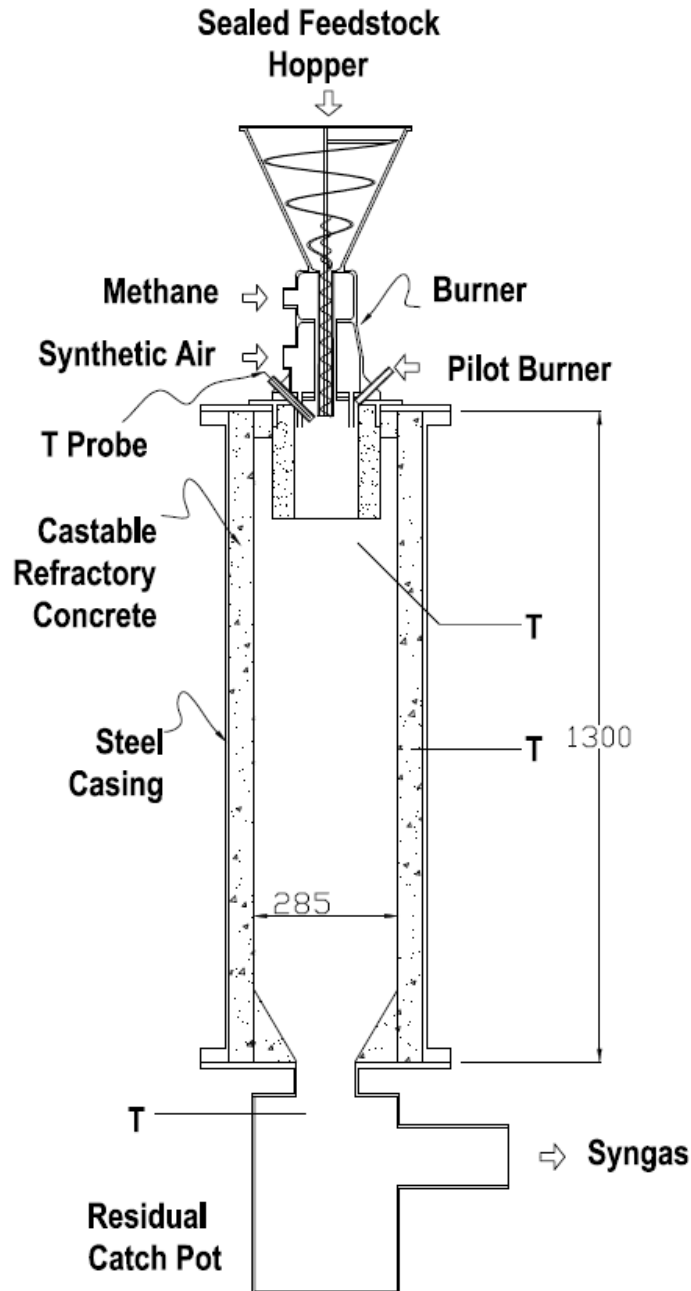


Figure 5-2: Diagram of the experimental gasifier with dimensions in mm. T = thermocouple location

5.1.2 Steam Generator

Steam is generated using a *Wanson Vaporax II* steam generator, which has a maximum working pressure of 38 barg and maximum output of 160 kg/hr saturated steam. Boiler feed water at 80°C is pumped to the coil which is heated by a fuel oil burner. During normal operation the output from the coil has a moisture fraction of around 10% to prevent dryout and overheating of the coil material. Excess moisture is removed by the steam separator before being supplied to the rig, at which point the steam dryness is nominally >98%.



Figure 5-3: *Wanson Vaporax II* steam generator, with steam separator and feed water tank

The supplied steam temperature was set by the saturation pressure. Because the gasifier was open to the atmosphere, high pressure steam was not required. The intermittent firing of the oil burner caused periodic fluctuations in output pressure which were dampened by a pressure reducing valve (PRV) located downstream.

5.1.3 Steam Flow Control and Metering

Steam flow can be calculated from the pressure differential across an orifice plate installed in the line. These are cost effective with no moving parts requiring little maintenance, but suffer from a limited measurable flow range. The turndown ratio is the ratio of the maximum to minimum measurable flow for a given accuracy. The best turndown ratio of an orifice plate is about 5:1, though typically a ratio of 3:1 is achievable (DeSá, 2001). For accurate measurement, the orifice edge must be well formed. Any burrs, rounding or irregularities around the leading edge of the orifice can result in large measurement errors (Howe and Lipták, 2003).

It can be seen from Figure 5-4 that the existing orifice plate sustained erosion and corrosion since its previous use. The nature of operation, whereby the rig was run for short periods and allowed to cool caused steam to condense within the pipes and has resulted in rusting of the metal surface. This alters the resistance to flow and the size of the orifice, leading to errors in the calculated flow rates. Similarly, any condensate appearing in the pipe upstream of the orifice would be trapped at the bottom of the pipe by the orifice, causing an additional restriction to steam flow and interfering with the measured flow calculation.

Accurate measurement across a wide range of flow rates and flow conditions was required to allow for the widest range of potential experiments. Low flow rates in particular present a metering

challenge, but can be measured using a vortex meter. The orifice plate was replaced with a state of the art vortex meter to measure the steam flow.



Figure 5-4: The orifice plate removed from the experimental rig, showing damage from corrosion

The vortex meter works using the von Karman effect. A blunt obstruction is placed within the pipe which creates a disturbance in the flow. The fluid passing the obstruction separates into areas of differential pressure known as vortices. By measuring the frequency of the vortices the velocity of the fluid can be calculated using the following equation;

$$V = \frac{Z \left(\frac{\pi D^2}{4} \right) d}{St}$$

Equation 5-1: (Emerson Process Management, 2009)

Where V represents volumetric flow rate (m^3/s), Z is the frequency of the generated vortices (s^{-1}), D is the inside pipe diameter (m), d is the width of the obstruction (or 'vortex shedder', m) and St is Strouhal number. The Strouhal number is a function of the shape of the vortex shedder and unique to each installation; it is dimensionless and remains constant over a wide range of Reynold's numbers and hence flow velocities.

Any high velocity condensate droplets in wet steam may impact on the vortex shedder and cause damage to the meter. To ensure that the steam is dry before it passes the vortex meter, the surrounding pipework was wrapped with rope heater elements to reduce heat loss. A bypass was also installed before the meter to vent wet steam prior to the start of the tests.

A pressure reducing valve (PRV) was used to maintain a stable steam supply pressure to the gasifier. As described in Section 5.1.2, steam was generated by passing pressurised water through a coil heated by a flame. The boiler fired periodically to maintain the output pressure within a target limit, but these fluctuations were found to be too large to sustain a stable flame in the gasifier. The PRV reduced the amplitude of fluctuations in steam flow rate to allow for stable continuous operation.

For accurate mass flows of steam, the temperature and pressure values from the data logger were used to find the density from steam tables as described in Section 5.5.1.

5.1.4 Feedstock Hopper and Screw Feeder

The powdered feedstock was fed to the gasifier from a conical hopper shown in Figure 5-2 via a vertical screw feeder. Within the hopper there is an agitator which rotated to prevent adhesion of fine powders to the hopper walls. During initial testing it was found that the motor used to power the screw and agitator had insufficient power to give the required range of feed rates. A higher powered motor was installed to accept a wider range of feedstock materials at variable feed rates.



Figure 5-5: The original screw shaft from the screw feeder, showing a reduction in shaft diameter at the lower end, leaving a gap between the shaft and the screw thread

The agitator and screw shaft were also re-designed. The existing shaft was found to reduce in diameter at the lower end, leaving a gap between the screw helix and the central shaft as shown in Figure 5-5. This caused some material to fall before reaching the end of the screw giving irregular feeding rates. The shaft was replaced with a consistent diameter for more even feeding.



Figure 5-6: Modified helical agitator extending to the hopper wall

The straight agitator in Figure 5-5 was replaced with a helical agitator shown in Figure 5-6. The hopper surface was painted to reduce adhesion of powdered feedstock to the walls. The refurbished hopper was found to run continuously and evenly without blockage or motor strain when filled with pulverised coal. The feeder was calibrated for coal as shown in Figure 5-7. The feeding rate remained

5. EXPERIMENTAL PROGRAMME

steady as the coal level in the hopper was reduced. Calibration was repeated for each material tested owing to differences in density and particle size.

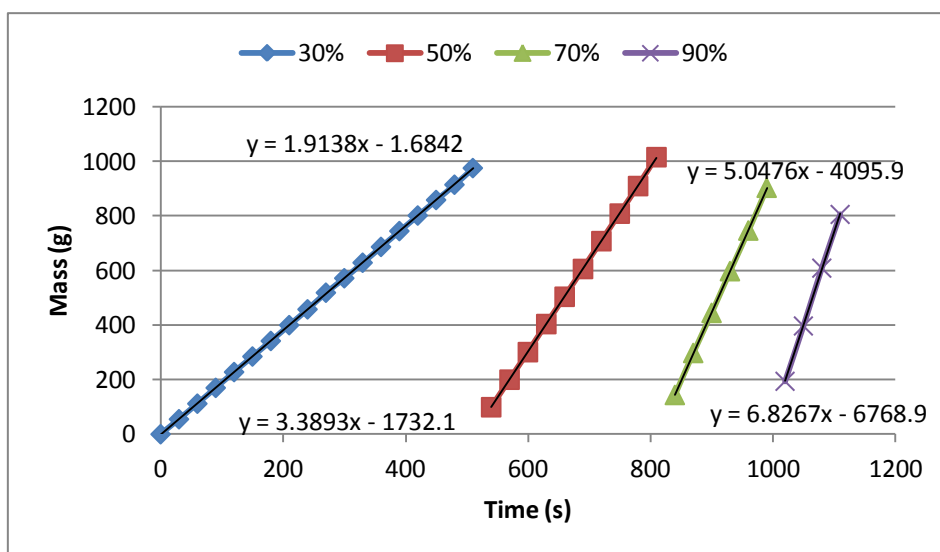


Figure 5-7: Calibration of feed system for pulverised coal at various motor speeds, with linear trend line ($R^2 > 0.999$ in each case)

Some agglomeration of coal was noticed as it emerged from the screw, as shown in Figure 5-8. Although these clumps were very easily broken apart, it was anticipated that coal adhesion may negatively impact the conversion rate by effectively reducing surface area.



Figure 5-8: Screw feeder outlet, (a) the protrusion from the pipe, (b) agglomeration of coal through the screw feeder

Some methods of separating the coal were considered, including using a distributor at the screw outlet. Two designs were trialled before selecting that in Figure 5-9. A porous disk was attached to the bottom of the screw shaft, with four pins on the outside of the pipe. As the disk rotates any coal clumps are abraded by the pins. The agglomeration effect was reduced compared with operating without the distributor.



Figure 5-9: Distributor attached to bottom of screw shaft to avoid coal agglomeration; (a) side view, (b) from below

5.1.5 Gas Flow Control and Metering

Gas flow control was also addressed prior to experimental runs taking place. The oxygen and air flows were previously directed through the same rotameter. Control was improved by purchasing separate calibrated rotameters specifically for each component for more accurate flow readings. A new rotameter calibrated for propane was also acquired to improve the flow accuracy. The existing ball valves were replaced with globe valves to allow finer adjustment to facilitate flame stability.

Each rotameter was calibrated for specific operating conditions. When used under conditions other than those specified a correction factor must be applied to maintain accuracy. Correction factors can be applied for density (K_ρ), temperature (K_T) or pressure (K_P) as follows;

$$K_\rho = \sqrt{\frac{\rho'}{\rho''}} ; K_T = \sqrt{\frac{T'}{T''}} ; K_P = \sqrt{\frac{P'}{P''}}$$

Equation 5-2: (Stoyanov and Beyazov, 2005)

Where ' refers to the nominal calibrated value and '' refers to the actual conditions of the gas stream. The scale reading is multiplied by the factor(s) to obtain a corrected flow value.

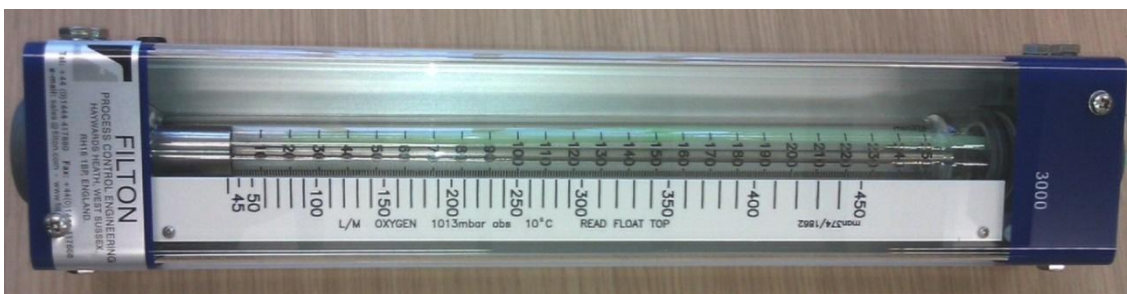


Figure 5-10: Example of new rotameters installed.

5.2 Selection of Gasification Feedstock

The feedstocks used for gasification included coal and biomass. Pulverised anthracite coal was used as the benchmark material due to its high carbon content and consistency of physical and chemical properties, as well as providing reproducible results for comparison with other works.

A biomass char was also selected, which is currently produced as a by-product in an existing combined heat and power (CHP) application in Latvia. The CHP process is based on the *Spanner Re²* process (Holz Kraft, 2016) fuelled by mixed Latvian softwood species. The feedstock is ground to size G30-G40 (<4 cm chips) and dried to a maximum moisture content of 15% before being fed to the pyrolyser/gasifier. The chips are subjected to temperatures around 900°C. This process releases the volatile gases which are cooled and filtered to remove ash and tar, before the gas is burned in an internal combustion engine (EnertecGreen, n.d.). This system provides 1 MW electrical and 2.2 MW of thermal energy, which is used for wood chip drying and to supply the district heating scheme in the town of Jekabpils, Latvia. District heating water used in the scheme is heated to 90°C before circulation and returns at <75°C.



Figure 5-11: Latvian char before sieving through 125 µm mesh for analytical testing

The solid by-product of this process is a biomass char remarkable for its high ash content due to bark, foliage and soil being processed with the wood (see Section 5.2.1.1). Currently it is produced at a rate of 40 tonnes per week with planned future expansion, but an economical use has not yet been identified. Biochar is often used for soil fertilization, however high contents of aromatic species such as naphthalene make this material unsuitable for this purpose. The material is also unsuited to typical thermal processing due to high concentrations of alkali metals giving a low ash melting point, which risks agglomeration in fluidised beds and slagging of process equipment (Chen et al., 2015; Fang and Jia, 2012). If the char can be gasified using this entrained flow system additional syngas can be produced from a material currently considered waste, which would greatly increase the fuel efficiency of the existing process.

A similar material was produced from the same process using the same wood, but without the bark and foliage. This char was similar to that described above but with a much lower ash content and higher fixed carbon. Due to the limited quantity of material obtained only a small number of tests were conducted with this material.

Another material for investigation was oak sawdust produced from the processing of spent whiskey barrels. Each time a barrel is used the inner surface is burned off to remove impurities and activate the carbon in the next layer. This allows the wood to absorb impurities from the next batch of whiskey and transfers a particular flavour from the wood to the liquid. When the barrel walls have reached a minimum thickness the barrel is recycled. Wood shavings and sawdust from spent barrel processing in Scotland was collected and tested as a material containing high levels of volatile matter.

Further information about the Latvian softwood material is presented in Appendix B. Other feedstock materials not selected for gasification tests are also described in Appendix C.

5.2.1 Description of Analytical Tests

Samples of each material were subject to analytical testing to determine their composition and heating value prior to gasification. A description of these tests is given below.

5.2.1.1 Proximate Analysis

The proximate analysis determines the amount of moisture, volatile matter, fixed carbon and ash in a given sample of combustible material. It was conducted using a *Perkins Elmer TGA 4000* Thermo Gravimetric Analyser (TGA) which heats the sample in a controlled environment while monitoring the change in mass.



Figure 5-12: Perkin Elmer TGA 4000 used for proximate analysis

The programme ran as follows;

1. Hold for 1 minute at 35°C
2. Heat from 35°C to 110°C at 40°C/min
3. Hold for 7 minutes
4. Heat from 110°C to 900°C at 40°C/min
5. Hold for 5 minute at 900°C
6. Heat from 900°C to 925°C at 20°C/min
7. Switch to O₂ atmosphere at 40ml/min
8. Hold for 7 minutes

9. Heat from 925°C to 950°C at 20°C/min
10. Hold for 1 minute

The mass/temperature data was plotted and exported for analysis, as shown in the example plots in Appendix B.

5.2.1.2 Ultimate Analysis

Ultimate analysis determines the elemental composition of a material, by incinerating a sample and measuring the concentrations of the various gas products in a gas chromatograph. In this way the percentage composition of carbon, hydrogen nitrogen and sulphur (CHNS) may be found.

The weights of the samples were input to the software sample table, together with the standard samples. The samples are then individually combusted in the internal furnace of the device, and the produced gases analysed. These concentrations are used by the software to calculate the percentage of each element contained within a sample.

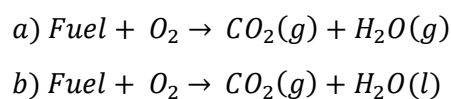
5.2.1.3 Calorific Value (CV)

A common means for comparing fuels is by heating (calorific) value. This is the parameter by which fuel sources are ranked and is reflected in their traded value. Fossil fuels have a high energy density which means they can be economically transported over long distances, unlike low energy density materials such as straw.



Figure 5-13: Parr 6200 Calorimeter used to determine gross calorific value

The difference between gross and net calorific value (also known as higher and lower heating value) is represented by the equations below;



Equation 5-3

In Equation 5-3 (a) water is produced in the gas phase in net calorific value calculations, while (b) yields liquid water for gross heating value. Considering water in the liquid phase means more heat is liberated as it includes the energy of condensation of water. In (a) the heat used to vaporise water is considered lost and is thus not considered in the lower heating value of the fuel (Schobert, 2013). Fuel heating value may be increased by reducing the amount of water present in the fuel. For this reason CV is often quoted on a dry basis for easy comparison.

For the CV test, 1 g of sample was combusted in a controlled oxygen rich environment and used to raise the temperature of a body of water using the apparatus in Figure 5-13. From the temperature change and heat capacity of the system, the energy liberated per mass of fuel was calculated from Equation 4-7.

5.2.1.4 Particle Sizing

Materials were sized following the ASTM method for pulverised coal using a nest of sieves (ASTM International, 2012). Sieves are stacked with coarsest at the top and finest at the bottom. After agitation the contents of each sieve is weighed to determine the distribution of particle sizes. The sizing results were collected using a balance sensitive to 0.1 g which deviates from the standard recommended 0.01 g accuracy.

5.2.1.5 Surface Area

The coal and char samples were subjected to Brunauer-Emmett-Teller (BET) analysis to establish specific surface area. This technique involves measuring the physical adsorption of nitrogen gas on the surface of the solid in order to determine the total surface area, including externally accessible pores, available for reaction. Solid materials which have a large surface area available for reaction tend to be more reactive than solids with a low specific surface area.

5.2.2 Results of Feedstock Analyses

Results of the analytical tests described in Section 5.2.1 are presented by analysis type.

Table 5-1: Proximate analysis and calorific value (CV) of gasification feedstock materials ('d.a.f'=dry, ash free basis)

	Coal		Softwood char		Softwood char low ash		Oak sawdust	
	%wt	%wt d.a.f	%wt	%wt d.a.f	%wt	%wt d.a.f	%wt	%wt d.a.f
Moisture	1.2		3.8		1.9		5.4	
Volatile matter	13.2	13.7	14.1	17.3	10.8	11.2	74.7	80.0
Fixed carbon	82.9	86.3	67.4	82.7	85.3	88.8	19.1	20.0
Ash	2.7		14.6		1.1		0.9	
Gross CV (MJ/kg)	32.1		22.2		29.1		17.1	

5. EXPERIMENTAL PROGRAMME

Table 5-2: Ultimate analyses of gasification feedstock materials; oxygen from balance of other elements

Sample	N	C	H	S	O (bal)
%wt					
Coal	1.44	83.34	4.08	1.23	9.91
Softwood char	0.34	76.15	1.15	0.08	22.28
Softwood char low ash	0.09	88.00	0.93	trace	10.98
Oak Sawdust	0.05	48.40	7.26	trace	44.29

Table 5-3: Sizing results of gasification feedstock materials after sieving < 600 μm . D50 = median particle size.

Sieve	Coal	Softwood char	Softwood char low ash	Oak sawdust
%wt				
μm				
>300	0.9	16.5	21.1	28.3
>250	0.7	6.6	3.2	10.3
>150	8.5	34.8	29.2	33.6
>75	30.2	32.8	33.4	20.7
>50	40.3	6.0	9.6	4.8
>45	13.6	0.4	0.5	1.1
<45	4.2	1.4	1.6	0.7
Total	98.2	98.4	98.6	99.4
D50 (μm)	69	177	167	218

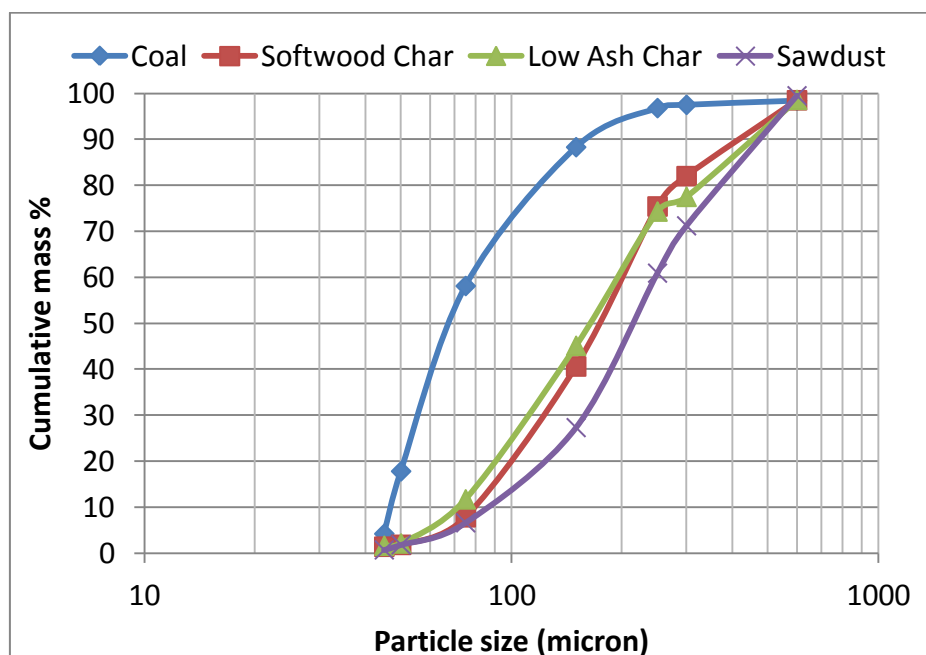


Figure 5-14: Particle size distribution of feedstock materials

The oak sawdust analyses above show good agreement with oak wood samples analysed by ECN (ECN, n.d.). The mass loss during sizing tests should be <2% to comply with ASTM standard method (ASTM, 2012b).

Figure 5-14 shows that the coal sample had a larger fraction of small particles which could have been further sieved, while the other three samples had higher fractions of material in the larger size brackets. A larger number of graduations could be achieved using additional sieves to give more complete distribution profile. The median particle size can be read from the figure and is given in Table 5-3. For all materials, particles larger than 600 micron were discarded to avoid blocking the screw feeder apparatus.

Table 5-4: Results of BET analysis for coal and char samples

	Coal	Softwood char	Softwood char low ash
Surface area (m ² /g)	47.6	292.6	357.8

5.3 Commissioning the Gasifier

This section describes the preparatory testing of the experimental rig prior to gasification experiments, including installation and testing of the components described in Section 5.1.

5.3.1 Steam Supply and Dryness

The steam line supplying the gasifier was tested using the steam generator and various line features. K-type thermocouples were located (1) after the steam separator, (2) after the globe valve controlling the steam flow rate, (3) after the steam vortex meter before the oxygen mixing point and (4) after the oxygen mixing point at the gasifier inlet. Steam vents are installed after points (2) and (3). A pressure gauge installed between the PRV and the globe valve and before vent (B). The arrangement is shown schematically in Figure 5-15 and pictured in Figure 5-16.

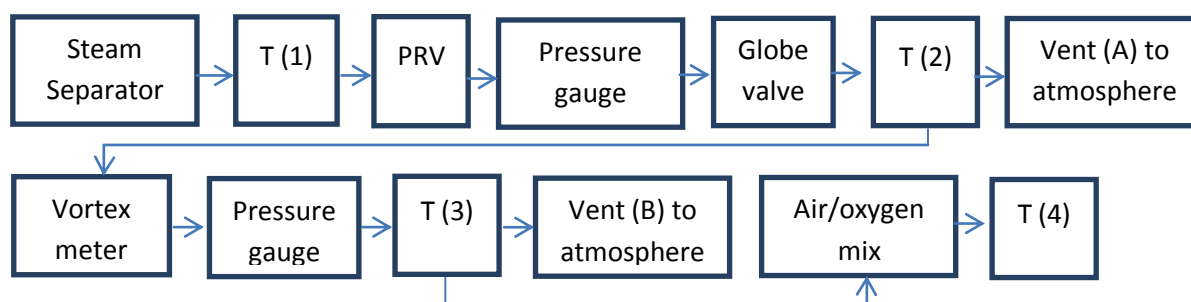


Figure 5-15: Schematic of steam supply pipe work

5. EXPERIMENTAL PROGRAMME

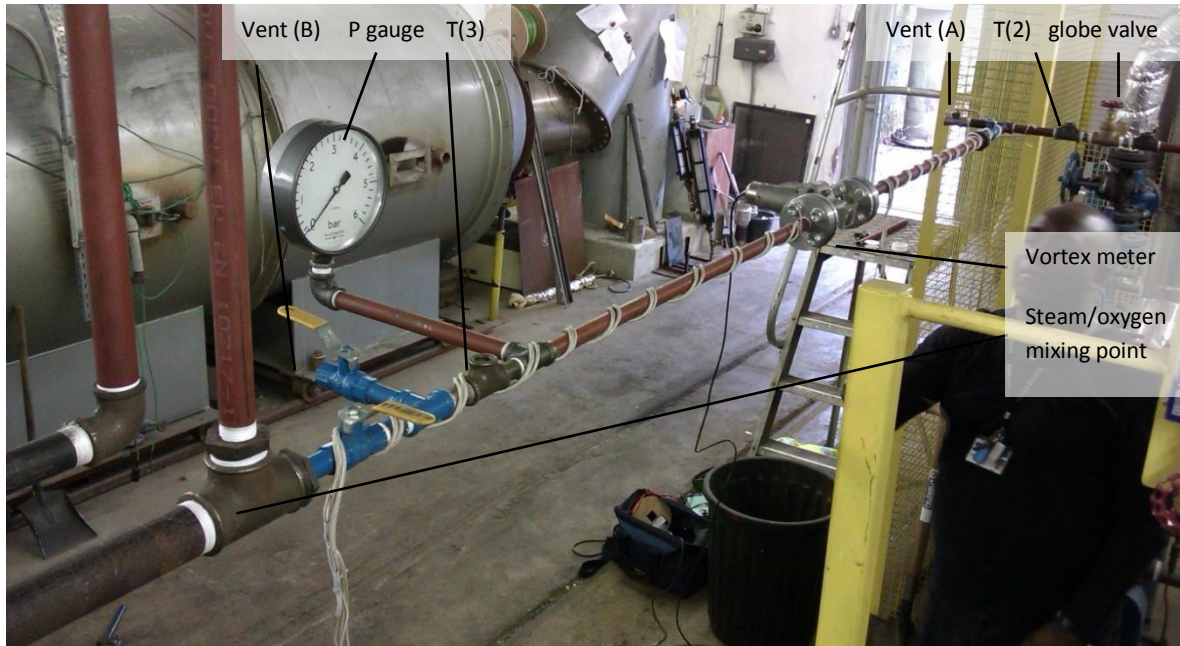


Figure 5-16: Photograph of steam supply line¹⁷.

Data was recorded at intervals of 2 seconds by a data logger and plotted to observe trends in temperature and pressure as valves were manipulated. Figure 5-17 shows data from a 20 minute steam test. Thermocouple (1) recorded a regular fluctuation of 15°C caused by the steam generator maintaining output conditions by periodic firing. The pressure reducing valve (PRV) served to dampen these fluctuations in temperature and pressure, which were not observed downstream.

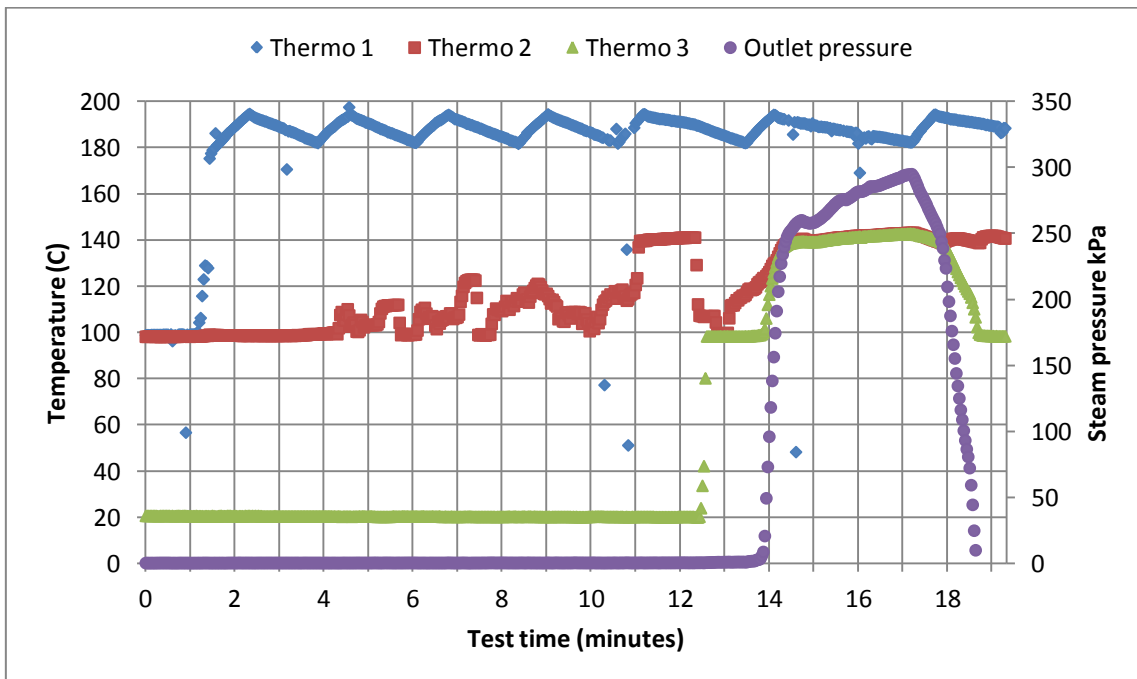


Figure 5-17: Data from steam line test, recorded by data logger

¹⁷ Image shows pressure gauge prior to replacement with U-tube and electronic pressure transducer. The rope heaters are also shown, before the pipe was lagged with insulation.

The ball valve at vent (A) was manipulated to observe the changes in pressure and temperature upstream. On partial closure of vent (A) at 7 minutes, an increase in temperature at (2) was observed, and a corresponding increase in pressure on the visual gauge. On $\frac{3}{4}$ closure of the valve, a peak temperature of 140°C was observed at (2) at 11 minutes. This confirms that higher temperature and pressure readings are observed when back pressure is provided by partial closure of the downstream valve.

After 12.5 minutes vent (A) was closed and steam flowed through to vent (B), where the temperature at (3) rises from room temperature. When steam flows unimpeded and there is no gauge pressure recorded, the temperature is equal to the saturation temperature at 0 barg, which is 100°C. As the valve is partially closed, the pressure rises to 300 kPa = 3 barg, and the temperature rises to the corresponding saturation temperature of 143°C. The transducer used has a maximum operating temperature of 150°C; as this temperature was approached the test was stopped.

5.3.1.1 Steam Dryness

The difference in temperature between points (1) and (2) demonstrates that when steam pressure is reduced there is an associated drop in temperature due to the change in enthalpy. For example from steam tables (Rogers and Mayhew, 1995), saturated steam at 10 barg and 184°C has an enthalpy of 2781 kJ/kg. Dropping the pressure to 3 barg, assuming ideal expansion with no energy losses, the temperature would decrease to 163°C to maintain the same enthalpy of 2781 kJ/kg. Figure 5-17 shows that temperature (2) is around 20°C lower than the ideal case due to friction caused by flow through the mechanical PRV in which the flow must overcome the force of a spring.

Although steam from the separator is nominally dry, it typically contains 2-3% moisture due to condensation against pipe walls. When the line pressure is reduced this remaining moisture is flashed, which absorbs energy from the bulk steam. The rope heaters were also installed to provide additional heat and avoid condensation of steam against the pipe walls. The delivered steam temperature recorded during each run was constantly monitored and was consistently above 120°C.

In summary, little heat loss was observed from the pipe work between points (2) and (3). Substantial temperature loss occurred through the PRV, which dropped the line pressure in order to dampen fluctuations in flow rate and increase the steam dryness. Reducing the pressure from 16 to 2.5 barg resulted in a temperature drop of around 70°C between points (1) and (2). When the line pressure was increased by partial or complete valve closure, the temperature was seen to increase to the saturation temperature at the given pressure; however no backpressure was permissible when supplying the gasifier as the reactor is open to the atmosphere.

5.3.2 Air/Oxygen Mixing Point

A thermocouple at point (4) monitored the temperature when oxidant was mixed with the steam line. The effect of different mixture compositions on the temperature is shown in Figure 5-18.

Steam alone registered a temperature of 100°C at point (4). After 0.5 minutes, the temperatures at (3) and (4) are equal to the saturation temperature for atmospheric steam. At 1.5 minutes air was introduced at 150 L/min, corresponding to 11 kg/hr which was the expected flow rate of oxygen in gasification tests. This caused a decrease of 10°C at point (4), though the temperature at (3) began to rise before this time. After 3.5 minutes, the air flow rate was increased to 300 L/min, which

dropped the mixture temperature by another 6°C. After 4.3 minutes the air flow was increased to 500 L/min and at 4.7 minutes the flow was again increased 600 L/min, which decreased the temperature by a further 5 and 3°C respectively.

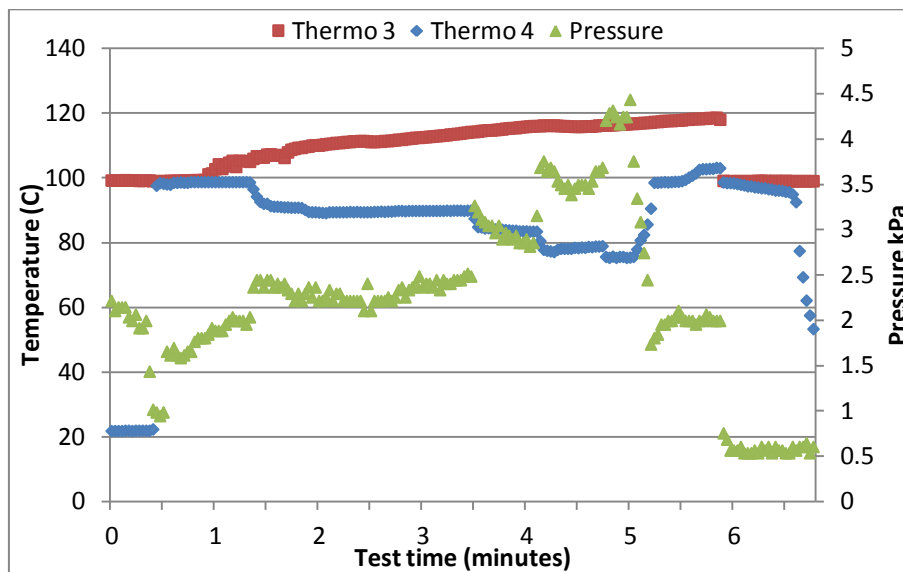


Figure 5-18: Temperature recorded at point (4) with gradual air introduction in steam test 3, recorded by data logger

The pressure at (3) was seen to increase marginally during this test as the air flow was increased. Increasing the air flow caused a small amount of backpressure in the steam line, causing the temperature at (3) to increase gradually throughout this test. The temperature profile at (3) is free from the fluctuations observed upstream when the steam flow rate is steady.

The addition of air to the steam caused a predictable drop in temperature. However dilution of steam with air or oxygen reduced the partial pressure of steam in the pipe, which reduced the effective boiling point. A volume fraction of 60% steam exerts a partial pressure of 60% of the total line pressure. From steam tables the condensation point of steam at 0.6 bar is 86°C (Rogers and Mayhew, 1995). Condensation of steam was avoided while the mixture was above this temperature.

As oxygen was supplied from a pressurised cylinder, the expansion resulted in a colder delivery temperature compared to air. The oxygen pipe was later located in a warm water bath to regulate its temperature to 30°C to reduce this effect, which required a correction factor be applied to the rotameter scale as described in Section 5.1.5.

5.3.3 Replacement of the Burner Quarl

The quarl or burner tile is the refractory cylinder into which the burner is placed for enhanced flame stability, as briefly described in Section 3.2.5. The existing quarl was found to be cracked at the start of this project. During burner removal for a routine inspection, this quarl was damaged beyond repair. A replica quarl was constructed from high temperature alumina refractory concrete using a wooden mould shown in Figure 5-19. The mould was created by taking precise measurements of the original to produce an exact reconstruction; using more resistant cast refractory.



Figure 5-19: (a) wooden mould used for quarl construction, (b) the completed replica quarl

5.4 Gasifier Operating Procedures

This section presents the operating procedures for the gasification system, including safe start up and shut down procedures for each component. For safe start up two operators were required.

5.4.1 System Start Up

The steam generator and the gas chromatograph require long preheating times before use.

5.4.1.1 ABB Gas Chromatograph Start Up

The gas chromatograph (Figure 5-20) should be started first according to the instructions below, and should be calibrated regularly using a calibration gas similar to the expected sample composition.

1. Set carrier gases to the following pressures: N₂: 50 psi, He: 48 psi, He: 91 psi, H₂: 58 psi.
2. Open compressed air valve to 40 psi.
3. Switch on system power and allow to heat up for circa 2 hours until chrome board 1 baseline detector reading does not change within 30 seconds.

The operating principle of the chromatograph is briefly explained in Section 3.5.2.

5.4.1.2 Steam Generator Start Up

The following instructions refer to components and valves marked on Figure 5-1.

1. Drain steam pressure relief line of any collected water using SV1.
2. Open SV2 to allow mains water to flow into the water drum. The water level should be between the indicated Max and Min levels, maintained by a level controller.
3. Switch on isolator switch on steam generator control panel. This should display 'Control Supply-On' and 'Immersion Heater – On'. The water requires approximately 2 hours to reach 80°C depending on fill level.



Figure 5-20: The ABB PGC2000 gas chromatograph and carrier gas cylinders

4. Prepare boiler feed water treatment agent to a concentration of 10% agent in water. Switch dosing pump to 100% - this operates automatically when the boiler pump is switched on.
5. Ensure the valve to the steam separator (SV5) is closed and the steam drain valve (SV6) is open before starting the boiler pump.
6. When the water drum has reached 80°C, switch the boiler to 'Pump Only' to feed water from the drum through the generator until temperature gauge reads 80°C.
7. Begin flow of fuel oil to the boiler by opening fuel oil valve (SV7).
8. Switch boiler to 'Pump and Burner' to ignite the burner. This will increase the temperature and pressure readings and begin producing steam in the blow down pit.
9. When the boiler temperature reads >100°C ensure the valve to the rig (SV9) is closed before opening the valve to the steam separator (SV5). Close the steam drain valve (SV6).
10. The boiler will fire until the set pressure is achieved, at which point the steam is ready to use. Switch dosing pump to 50% during normal operation.
11. Use rope heaters to preheat the pipes around the vortex meter. Introduce steam gradually through the pipe sections towards the rig, to reduce the impact on the vortex meter.

5.4.1.3 Feedstock Start Up

Powdered feedstock should be charged into the hopper before beginning experiments to avoid backdraft. Ensure the lid is securely sealed.

Compressed air is provided at 8 barg. Oxygen and fuel gas are supplied via gas cylinders. The gas supply should only be switched on after the pilot burner is lit to prevent accumulation of fuel in the gasifier.

5.4.1.4 Pilot Burner and Gasifier Start Up

1. Before operation ensure all valves leading to the gasifier are closed, including SV9, OV1, OV2, AV1, AV2, GV1, GV2, GV4.
2. Open air valve AV2 to blow through the gasifier and clear any accumulated material. Close the catch pot bung and reduce the air flow to around 150 L/min before lighting the pilot.
3. Ignite the pilot burner by opening valve GV1 and pilot air supply and use the electric starter.
4. Using GV4 set the fuel gas flow to the appropriate level for the experiment. Adjust AV2 to set the fuel/air flow to a fuel lean flame at the required gas flow rate. The pilot burner can be switched off when the main flame is established.

At this stage the gasifier body can be pre-heated using a fuel-air flame until the desired reactor temperature is achieved by monitoring wall temperature T10 (Figure 5-2). For gasification experiments, follow steps 1-4 to establish a flame then continue with step 5.

5. Using OV1, gradually introduce oxygen into the flame then add a small steam flow. Gradually increase oxygen and steam and reduce air flow with AV2 until a fuel-oxygen-steam flame is achieved. Adjust flows to desired ratios.
6. When a stable steam flame is established, the solid feedstock can be introduced via the screw feeder control panel.
7. At end of test shut off gas flows in reverse order and purge with air.

5.4.2 System Shut Down

The system should be shut down in the opposite order to the start-up procedure in Section 5.4.1.

5.4.2.1 Gasifier Shutdown

1. Switch off reactant supply and valves GV4 and OV1 to extinguish the flame. Switch off steam supply and purge gasifier with air.
2. Divert steam to vent (B) and switch off rope heaters, to allow pipes to cool.
3. Loosen the catch pot bung to prevent seizure as it cools. Open lid of solids hopper to prevent accumulation of condensation.
4. Close the remaining valves GV2, AV2, OV2 and the air valve from the compressor. Close gas cylinder valves.

5.4.2.2 Steam Generator Shutdown

1. Switch boiler power off. Vent steam through vents (A) and (B) to cool heated pipes. Close SV7 and SV9 valve to the rig.
2. When the temperature and pressure to reduce below 100°C and 1 bar, open SV6 and close SV5. Switch boiler to Pump Only, with dosing pump on 100% for 7 minutes.
3. Switch off the boiler after this time, and switch off the isolator. Close the drain valve SV6. Switch off the mains water supply SV2.

5.4.2.3 Gas Chromatograph Shut Down

1. After analysis is finished, close sample supply valve.
2. Unplug unit from mains supply. Open oven and allow to cool.
3. Turn off compressed air flow after 2 minutes. Leave carrier gases running for 30-60 minutes.

5.5 Experimental Procedure

Section 5.4 describes the start-up and shut down procedures for the apparatus used in this experimental programme. This section describes the experimental procedure used to conduct gasification experiments to compare the effects of operating conditions such as reactant flow rates, gasifier temperature and different feedstocks.

5.5.1 Mass Flow Calculation

The equivalent mass flow rate for gas components was calculated from volumetric flow measurements based on the densities calculated at a representative temperature for the component as recorded during the test. The steam conditions were recorded upstream of the oxygen mixing point by a data logger at 2 second intervals. The mean temperature and pressure values were used to find the mean density of steam during the gas analysis sample collection interval, when all gas flows and temperatures were most stable. The mass of propane and methane was based on the density at 10°C while the oxygen density was calculated at 33°C, based on temperatures observed during the experiment. The coal mass flow rate was based on the feeder calibration described in Section 5.1.4.

5.5.2 Mass Balance

The calculation of a mass balance around the gasifier required some additional data collection. During periodic inspection of the gasifier no accumulation of material was observed, so the assumption that mass flow in equalled mass flow out is valid. The residual solid material from the catch pot was weighed and subtracted from this value to give the mass of gas out.

The moisture content of the outlet stream was extrapolated from the gas samples drawn for analysis. During experiments gas was drawn from the flue line using a diaphragm pump through a cold finger for cooling and moisture removal before analysis by the gas chromatograph. The volume flow rate and temperature at the pump outlet were measured using a rotameter and K-type thermocouple. From the mixture composition and temperature, the gas density was calculated and used with the volume flow to find the mass flow rate of dry gas. The moisture collected by the cold finger was also measured to obtain the moisture mass fraction of the sample.

Assuming the sample is representative of the total gas flow, the moisture fraction was used to calculate the mass of dry product gas exiting the gasifier. This was used in completing mass and energy balances for each experiment.

5.5.3 Temperature Monitoring

Two types of thermocouple were used in this experimental work. R-type thermocouples have a sensitivity range from -50 to 1700°C for short term operation with an error of ± 1.5 below 600°C and $\pm 0.0025*[T]$ °C above 600°C where T represents measured temperature. K-type thermocouples are sensitive from -180 to 1300°C for short term operation with an error of ± 1.5 below 375°C and $\pm 0.004*[T]$ °C above this (Peak Sensors, 2016).

5. EXPERIMENTAL PROGRAMME

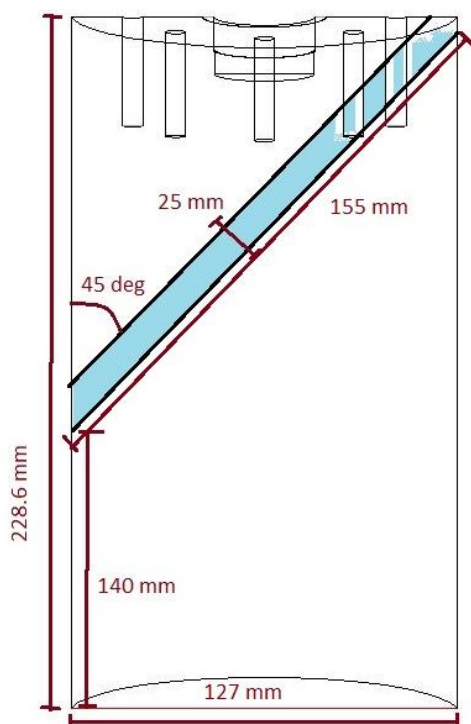


Figure 5-21: Sketch of field of view from burner viewport

Temperatures were monitored inside the gasifier at several points. View ports located in the roof of the burner offered limited access into the quarl space and are used to accommodate the pilot burner and glass viewports. Due to the channel extending around 30 mm through the refractory and burner body, the field of view is straight and narrow as shown in Figure 5-21.

The ports are inclined at a 45° angle from vertical towards the centre of the quarl. A platinum R-type thermocouple was inserted into the centre of the flame zone, within a removable ceramic probe for flame temperature monitoring.

A K-type thermocouple was inserted through the gasifier wall into the reactor below the burner quarl to monitor gas temperature in the gasifier. The outlet gas temperature at the gasifier exit was also recorded using another K-type thermocouple as pictured in Figure 5-2.

The gasifier wall temperature was monitored using a K type thermocouple inserted 32 mm into the 50 mm thick refractory wall, 600 mm from the bottom of the reactor. This was used to provide an estimate of heat transfer through the walls of the gasifier.

5.5.3.1 Suction Pyrometry

Suction pyrometry is a technique often used for furnace analysis where optical and physical access is limited. The technique involves introducing a probe to extract samples from regions of interest in a reactor or furnace using a vacuum pump. Localised regions can be analysed for gas composition or particles removed for analysis. Gas samples can be drawn past a shielded thermocouple to reduce radiative heat loss and give a closer representation of the gas temperature, as described in the Theory chapter Section 3.5.3.

5. EXPERIMENTAL PROGRAMME

A pyrometer probe was designed to fit the existing ports in the burner. The probe shaft was constructed from recrystallized alumina for high temperature resistance, with an outer diameter of 20 mm and an inner diameter of 15 mm. This was wide enough to accept a high temperature R-type thermocouple within a ceramic sheath while allowing gas to flow unimpeded through the probe out of a 90° junction as shown in Figure 5-22 and Figure 5-23.

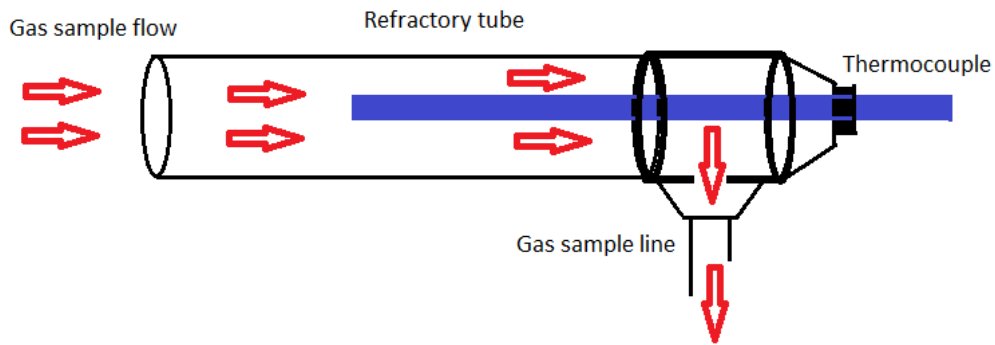


Figure 5-22: Schematic of suction pyrometer probe, incorporating a high temperature thermocouple within a refractory tube for gas extraction.

The probe was constructed and used to measure gas temperature in the centre of the burner zone. The extracted gas was found to contain high concentrations of fuel gas and partial combustion products, as reported in the computational model validation experiment Table 4-16. This would disturb the normal flow pattern and composition within the burner, such that the measurement process caused a deviation from normal burner behaviour. For this reason suction pyrometry experiments were conducted separately from gasification experiments in which the product gas was analysed. During gasification experiments a less intrusive temperature reading was taken using the thermocouple mount pictured in the lower part of Figure 5-23.

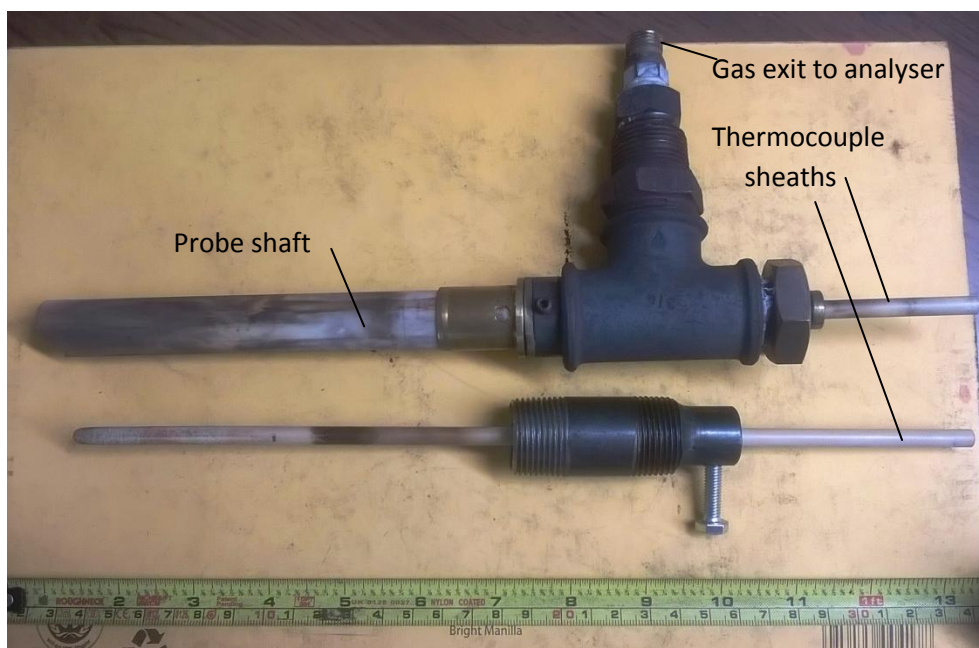


Figure 5-23: (top) Suction pyrometer probe and (bottom) simple thermocouple mount for burner

The probe design also allowed for the thermocouple to be removed and replaced with another instrument, for example a spectrometer to analyse emissions for identification of flame species.

5.6 Experimental Uncertainty

Consideration was given to the possible sources of uncertainty and error in the present experimental work.

The gaseous reactant flows were recorded using rotameters described in Section 5.1.5. These were purchased and calibrated specifically for the present work and were issued with calibration certificates from the manufacturer. The uncertainties were for a confidence probability of not less than 95% for the oxygen, propane and air meters. The use of these meters under conditions that deviate from the calibrated conditions introduces some additional uncertainty but this was small provided the conditions were held constant.

The vortex meter for steam was also ordered specifically for this application and issued with a calibration certificate by the manufacturer. The meter was calibrated using water up to the maximum rated flow velocity, with the deviation in K factor being less than $\pm 0.4\%$ across the range. Possible error in the steam measurement arose due to the fluctuation in steam generator output as described in Section 5.1.3. The fluctuation was minimised using the PRV and fine control of the generator such that the standard deviation in steam flow was kept within $\pm 5\%$ of the mean volume flow during experimental tests.

The gas compositions were recorded by the online chromatograph. The uncertainty in this measurement was minimised by regular calibration of the device against a standard sample of gas which was performed before every experimental set. Regular control runs were also performed between experiments, where analyses of flue gas were performed to flush the chromatograph columns and monitor expected gas readings.

A comparison between the standard composition and the measured composition can be used to quantify the expected uncertainty in the chromatograph. The standard gas was supplied by Air Products, certified and traceable to National Standards.

Table 5-5: Indicated composition of gas standard against measured composition, in %mol. Std. Dev.= standard deviation

	H ₂	O ₂	N ₂	CH ₄	CO	CO ₂	TOTAL
Standard	40	0	1	1	23	35	100
Calib.1	40.2	0	1.11	1.01	24.1	35.6	102.02
Calib.2	40.5	0	1.11	1.08	23.9	35.0	101.59
Calib.3	40.5	0	1.12	1.14	24.0	35.2	101.96
Calib.4	40.7	0	1.11	1.14	24.0	35.3	102.25
Calib.5	39.5	0	1.17	1.19	24.8	35.5	102.16
Mean	40.28	0	1.12	1.11	24.16	35.32	102.00
Std. Dev.	0.421	0	0.023	0.062	0.326	0.214	0.227

5. EXPERIMENTAL PROGRAMME

Comparing the measured compositions to the standard in Table 5-5, there is close agreement in all calibration tests. These were conducted over a period of months which shows that the chromatograph was consistent and reproducible. The standard composition is reported to the nearest 1%mol and the hydrogen concentration was within $\pm 1\%$ mol of the standard in all calibration tests. The CO concentration results were within +2% and the CO₂ results within +1%mol. The mean readings for these tests are all within 1%mol of the standard except CO which showed an offset of +1%. The low standard deviation indicates that this was a systematic error as opposed to random scatter. This should be taken into account when analysing experimental results.

Owing to the small concentrations of N₂ and CH₄ in the standard, these results were within +0.2%mol in each case. Oxygen was not present in the calibration standard as it would react with the other constituent species. The operating manual states that this model of GC is not reliable for oxygen analysis, and that a separate analyser should be used for best accuracy. However the GC was also tested by analysing air and found to give sufficiently accurate readings of both oxygen and nitrogen for this work, as both were expected only in minor concentrations during gasification runs.

6 EXPERIMENTAL RESULTS AND DISCUSSION

This chapter describes the results obtained following the experimental programme described in Chapter 5. This includes initial experimental work to compare with some of the sensitivity simulations performed using Aspen and FLUENT in Chapter 4. This was conducted using propane to fuel the burner. Later experimental work compared the yields obtained from different feedstocks described in Chapter 2, which used methane as a fuel for reasons explained in Section 6.2.

The objectives of this experimental programme included replicating the findings of the previous work to confirm that the gasifier operated as expected after the rig modifications described in Chapter 5. Once this was established, some manipulation of process variables was made to observe the sensitivity of the product yield to these parameters. Finally, a comparison was made between the product yields achieved using coal and biomass char as a gasification feedstock. Mass and energy balances and conversion analysis are presented for these experiments.

In total the experimental programme was conducted over a period of two years with continual improvements made during this time. During early experimental work a range of conditions were tested relatively quickly and a limited amount of data was collected, as presented in Sections 6.1 and 6.2. As the experimental technique was refined and controllability was improved, a greater number of runs were conducted to demonstrate consistency and collect viable data, presented in Section 6.3. The data in this chapter are supplemented by additional raw data presented in Appendix C. Over 140 experimental gasification runs were recorded, not including additional studies such as the spectroscopy work described in Appendix C.

6.1 Tuning Gasification Parameters

A series of experimental runs was performed using the gasification system based on the parameters set out in Simulation 1B, in Section 4.3. A summary of these runs is given in Table 6-1 including the reactant flow rates used and the product gas composition as reported by the on-line gas chromatograph pictured in Section 5.4. These runs are then discussed in Sections 6.1.1 to 6.1.3. Due to initial difficulties in setting and maintaining constant reactant feeds, Table 6-1 present data from single run repeats, though other similar supplementary runs are also presented in Table 12-3.

Table 6-1: Summary of reactant flow rates and gas yields from model validation tests¹⁸

Run	C ₃ H ₈	O ₂	Steam	Coal	ER	Gas Yields					
						H ₂	O ₂	N ₂	CH ₄	CO	CO ₂
kg/hr					%mol						
I	3.0	11.3	20.4	12.2	1.02	33.5	0.28	4.40	3.03	21.2	37.7
II	3.0	11.1	17.2	-	1.01	27.9	0.30	1.66	3.92	16.0	50.2
III	2.8	13.3	19.4	-	1.30	8.57	0.46	1.51	0.20	4.90	84.4
IV	1.9	10.2	15.0	-	1.50	6.20	0.98	1.91	0.23	3.99	86.7
V-1	3.3	15.0	14.7	6.9	1.26	22.2	0.31	1.61	0.52	17.0	58.4
V-2	3.3	15.0	14.7	-	1.26	5.41	0.46	1.84	trace	3.44	88.9
VI	2.5	13.3	13.6	6.9	1.48	17.6	0.92	1.84	1.29	14.7	63.7

For many of these tests the CO₂ reading was outside of the calibrated range (>50%mol) so was calculated from the balance of other species. Calibration was adjusted for later tests to account for this. The oxygen and steam supplied to form the synthetic air in each run are shown in Table 6-2.

Table 6-2: Synthetic air mixture compositions for Runs I-VI

Run	Oxygen supply at 1°C		Volume at 100°C	Steam supply at 100°C		O ₂ in synthair
	L/min	kg/hr	m ³ /hr	kg/hr	m ³ /hr	%vol
I	132	11.3	10.3	20.4	34.1	23.2
II	130	11.1	10.1	17.2	28.7	26.1
III	155	13.3	12.1	19.4	32.3	27.2
IV	119	10.2	9.3	15.0	25.0	27.0
V-1	175	15.0	13.6	14.7	24.6	35.7
V-2	175	15.0	13.6	14.7	24.5	35.8
VI	155	13.3	12.1	13.6	22.7	34.7

The findings of these experimental runs are discussed in the following sections.

6.1.1 Runs I and II: Replicating Previous Work

Run I was conducted to replicate run P1-A of the previous work (Shabangu, 2005) and to compare with Simulation 1B conducted using Aspen Plus, as described in Section 4.3.4. A coal flow above the 9 kg/hr graphite used in the model was used to compensate for the non-ideal nature of the experimental system and because the coal was only 83% carbon. A comparison of reactant flow rates and product gas yields is shown in Table 6-3.

¹⁸ ER = equivalence ratio. Gas compositions on dry basis as recorded by the GC, except CO₂ fractions calculated from balance for Runs II-VI.

6. EXPERIMENTAL RESULTS AND DISCUSSION

Table 6-3: Reactant flow rates and dry product yields from Run I, Simulation 1B and from previous work (Shabangu, 2005)

Reactant (g/s)	Experimental Run I	Simulation 1B	Previous work Run P1-A
Propane	0.84	0.833	0.691
Oxygen	3.1	3.03	2.50
Steam	5.7	5.22	5.22
Coal	3.4	2.50	5.89
Product Species (%mol, d.b.)			
H ₂	33.5	47.97	37.4
O ₂	0.28	Trace	-
N ₂	4.40	0.32	2.0
CH ₄	3.03	0.96	1.1
CO	21.2	32.99	22.7
CO ₂	37.7	17.76	32.6

Comparing Run I with Simulation 1B, significant differences in product composition were observed despite the similarity of the reactant flow rates. The experimental yields of syngas species H₂ and CO were lower than predicted by the model, while yields of CH₄ and CO₂ were higher. There are several possible reasons for this already listed in the modelling chapter Section 4.3.6. Briefly these included the simplified nature of the equilibrium model which did not take into account reactor geometry, residence time or reaction kinetics and the assumption of zero heat loss from the model reactor. The latter was found to be substantial, as is discussed in the energy balance Section 6.3.4. Additionally, the nitrogen gas observed in the experimental sample was likely residual air from gasifier start-up or from some small air leak in the sampling system.

The Run I yield showed a very close resemblance to Run P1-A of the previous work, in spite of the coal feed rate being over 40% lower in Run I. This supports the conclusion from the Aspen simulation that there was an excess of coal fed to the reactor in the previous work. Furthermore, at the end of Run I the catch pot was found to contain a large amount of partially reacted coal. In total 46% of the mass of coal charged during the test was collected. This is consistent with the lower syngas yield compared with the simulation.

The gasifier internals were checked for material accumulation prior to performing further tests. The inside surface was found to have some traces of dry ash which were easily swept off, as shown in Figure 6-1. No accumulation of coal was observed in the reactor or catch pot which could have influenced the experiment.

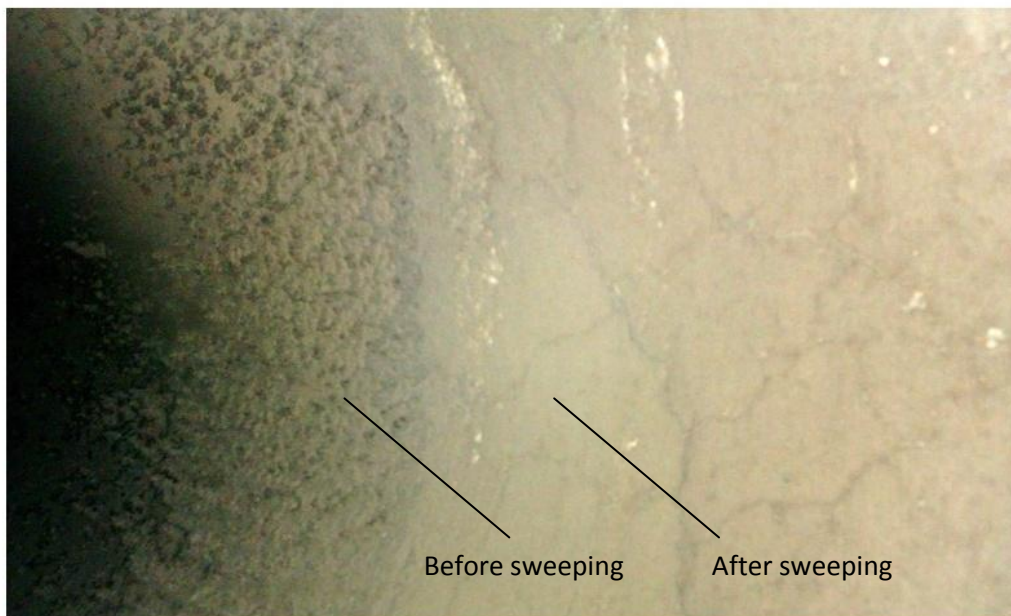


Figure 6-1: Photograph of gasifier inside surface with ash deposits before and after sweeping with a brush

In Run II a control run was conducted without coal addition. The coal hopper was emptied to ensure no particles were drawn by the gas flow. From Table 6-1 the gas yield showed a similar result to Run I, with significant concentrations of H_2 and CO. This test ran continuously for approximately one hour and several repeat measurements made with the same result. It was concluded that additional reactions to produce H_2 and CO in the absence of coal were occurring under the experimental conditions in the gasifier.

Oxygen and propane were supplied in a stoichiometric ratio following the method in the previous work. It was found that the stoichiometric oxygen supplied to the burner was not sufficient to fully combust the propane in a practical system; most commercial combustion systems utilise some degree of excess air to ensure complete combustion. This may have led to incomplete propane combustion however no trace of propane in the product gas was recorded by the GC, suggesting that the propane was involved in some alternative reaction. The propane-steam reforming reaction (Equation 3-25) would account for the absence of propane and the presence of H_2 and CO in the product gas. It is also consistent with the syngas exit temperatures being lower than predicted by the model, in addition to the energy losses discussed in Section 6.3.4.

The simulation assumed that the combustion in the burner was complete, which it appeared was not the case in practice. The reforming reaction has a high positive standard enthalpy similar to the reverse of the Methanation reaction (Equation 3-8), indicating that it is highly endothermic and would be favoured under high temperature conditions with high concentrations of propane and steam, such as in the steam flame produced in Run II.

It was hypothesised that fuel gas reacting with high temperature steam served to reduce the temperature and the quantity of steam available for reaction with the intended feedstock, which led to reduced conversion of the coal in Run I and other coal tests. It would also affect the syngas yield, as the products of the fuel gas reformation include hydrogen and carbon monoxide which

would be mistaken for the products of coal gasification. This finding casts doubt on the results from Run I and by extension those of the previous work where fuel gas reformation was not considered. This is discussed further in Chapter 7.

Based on this finding the ER was increased in subsequent runs, to attempt to reduce the effect of propane reforming. Steam reforming of propane is undesirable only inasmuch as the reforming of hydrocarbon gases is not the objective. Steam reforming of natural gas is currently conducted on an industrial scale for hydrogen production. The intention when running steam flame gasification on an industrial scale would be to recycle some of the product gas to the burner for flame production, removing propane from the process altogether. This requires an understanding of the gasification system operation without the influence of propane reforming, which is both expensive and distracting from the core process.

6.1.2 Runs III and IV: Increasing the Equivalence Ratio

Following the first two runs, Runs III and IV used an increased oxygen flow rate to test whether the effects of steam-propane reforming would be reduced with additional excess oxygen. Practical combustion systems such as internal combustion engines use excess air to improve fuel efficiency. The burner was run using an ER of 1.3 to 1.5, representing 30-50% excess oxygen, without coal addition to compare with Run II.

Table 6-1 shows that with an ER of 1.3 the H₂ and CO levels were much reduced compared to Run II but remained above zero, suggesting that some fraction of the propane continued to react with steam as per the reforming reaction, Equation 3-25. To achieve an ER of 1.5 the propane flow was reduced. The steam flow was also reduced accordingly. Table 6-1 shows that the associated H₂ and CO reductions were minor in this case. Propane reforming continued to occur with 50% excess oxygen, suggesting that the ER is not the sole factor determining the amount of propane combusted or reformed.

An additional factor investigated was the ratio of oxygen to steam, which was maintained at around 25%vol oxygen in the synthetic air during Runs I to IV, as shown in Table 6-2. The higher concentration of steam in the mixture may have contributed to the persistence of propane reforming. The oxygen content in the synthetic air was increased in the next tests.

6.1.3 Runs V and VI: The Effect of Temperature

In Run V the ratio of oxygen to steam was increased to 35%vol oxygen by increasing oxygen flow and reducing steam flow. Based on the limited impact of increasing the ER beyond 1.3 observed in Run IV, the ER was reduced to 1.26 by increasing the propane flow rate. Run V used higher propane and oxygen flow rates to increase the flame temperature, which would favour the endothermic gasification chemistry when coal was added. A lower coal feed rate was used reflecting the large amount of residual coal collected in Run I.

Run V-1 was seen to yield 22.2% hydrogen and 17.0% carbon monoxide with a coal flow rate of only 6.9 kg/hr. Although this yield is lower than from Run I, it is significant when considering Run V-2 conducted immediately following Run V-1 but without coal feed. This ensured identical reactant gas flows to highlight the effect of feedstock addition on product composition. The yield of only 5.41% H₂ and 3.44% CO without coal feed demonstrates that the gasification of coal produced the majority

of the syngas in Run V-1, with only a minor contribution from propane reforming under these conditions.

In Run VI the feed rate of propane was reduced to give a lower reactor temperature, with other conditions remaining comparable to Run V. The gas temperature recorded in the reactor was around 150°C lower than in Run V-1 and the product gas was seen to contain less H₂ and CO than in Run V-1 for an equivalent coal feed. This validates the Aspen temperature sensitivity analysis in Section 4.3.2 where increasing temperature was seen to reduce the CO₂ and CH₄ yields and increase the CO yield. The H₂ yield was also reduced in the simulation at low temperatures.

Run VI confirms the importance of high temperature and ER around 1.3 for best coal gasification results using propane.

6.2 Effect of Fuel Gas

A comparison was made using methane instead of propane to fuel the burner. Propane was observed to produce large amounts of soot in the burner indicating incomplete combustion. Because the laboratory did not have access to a mains natural gas supply, laboratory grade methane was provided from a cylinder. The flow rate of methane was configured for the same rate of energy input as 3 kg/hr propane flow. Example control runs are shown in Table 6-4.

Table 6-4: Reactant flow rates (kg/hr) and gas yields (%mol) for methane control runs. ER = equivalence ratio. %O₂ represents %vol of oxygen in synthair mixture.

CH ₄	O ₂	Steam	ER	% O ₂	H ₂	O ₂	N ₂	CH ₄	CO	CO ₂	Total
2.8	12.0	11.5	1.06	51	0.82	6.71	1.61	0.4	0	87.4	96.9
2.8	11.3	6.5	1.00	63	0	3.37	1.96	0.21	0	90.2	95.7
2.8	11.3	6.2	1.00	65	0.46	3.2	1.96	0.31	0	93.7	99.6
2.8	11.1	9.5	0.98	54	1.83	5.04	2.43	0.05	1.57	85.5	96.4

It was found that methane produced less H₂ and CO in control tests and was found to produce much less soot in the burner compared to propane runs. Furthermore, it was found that a lower excess of oxygen was required to avoid signs of fuel gas reforming, with an ER between 0.98-1.06 producing only trace amounts of these product gases.

By burning methane instead of propane for production of the steam flame, lower traces of H₂ and CO were observed in control tests and a lower excess of oxygen was required. The dry product gas before feedstock addition was a high purity CO₂, which reduced the background reading allowing clear determination of the conversion of feedstock into syngas products H₂ and CO.

As mentioned in Section 3.3.5, the presence of CO₂ from the USS production stage will have an impact on the downstream chemistry. The CO₂ in the USS will dilute the product gas, as well as move the equilibrium in equations Equation 3-3, Equation 3-5 and Equation 3-7. This is expected to reduce the yields of hydrogen and potentially increase the expected yields of CO. Using a carbon-free fuel gas was not attempted in the present work, though in a previous work experimental runs using hydrogen to fuel the burner yielded up to around 60%mol hydrogen in the product stream (Shabangu, 2005).

6.3 Gasification Feedstock Experiments

The experimental work in Section 6.1 demonstrated the importance of high gas temperature for best product yields. It also highlighted that inadequate combustion of the fuel gas can result in misleading yields as a result of fuel gas reforming. Section 6.2 showed that using methane instead of propane to fuel the burner allowed more complete combustion with much lower excess oxygen requirements.

Having established appropriate reactant flow rates for stable operation, an investigation into the effect of feedstock type was conducted. For this study the gas flow rates were maintained at a constant level with the only variable being the powdered solid feedstock. 18 m³/hr was chosen as the set point for steam to balance flame stability with gasification yield. The anthracite and high ash softwood char materials described in Section 5.2 were compared at different feed rates as shown in Table 6-5.

The sawdust material analysed was not compared in this study as problems were encountered during feeding. During calibration tests the sawdust travelled freely from the hopper along the screw shaft, however when the gasifier was operating the high temperatures caused the sawdust particles to block the feeding mechanism as described in Section 7.4. As a result it was not possible to complete gasification runs with this material. The low ash char was not available in sufficient quantities to complete a full investigation, but a limited analysis was performed as described in Section 6.3.6.1.

Table 6-5: Powdered feedstock experiment conditions; A= anthracite tests, C= softwood char tests

	A1	A2	A3	C1	C2	C3
Solid feed rate (kg/hr)	3.7	5.2	6.2	3.7	4.3	5.1
S/C ratio (molar)	3.3	2.4	2.0	3.9	3.1	2.8

Using the coal and softwood char materials, a range of steam to carbon (S/C) molar ratios was achieved by varying the solid feed rate. The S/C ratio takes into account H₂O from methane combustion as well as steam in the oxidant. Two runs were conducted for each condition. The differences in S/C ratio between the coal and char conditions are a result of the differences in carbon content (see Section 5.2.2) and volume density of the two materials. It was not possible to achieve identical carbon feeding rates due to the limited operating range of the feeding mechanism, but a close range was used.

After preheating the reactor, each test duration was approximately five minutes from establishing a stable steam flame. As described in the experimental procedure in Section 5.5, gas samples were extracted through a cold finger to condense and collect moisture before being analysed by an online GC. The results of these experimental runs are described in the following sub sections.

6.3.1 Gasifier Temperature Distribution

A steep temperature gradient was apparent in the gasifier, due to the high peak temperatures within the flame zone, the narrow reactor geometry and relatively thin walls leading to significant heat transfer through the reactor walls. As described in Section 5.5.3.1, suction pyrometry was

6. EXPERIMENTAL RESULTS AND DISCUSSION

conducted during a run prior to feedstock addition and recorded an average temperature of 1350°C in the burner zone. The same thermocouple without suction recorded temperatures approximately 150°C lower. With feedstock addition the average temperatures ranged between 1100-1150°C in the burner.

The gas temperature in the reactor below the quarl was recorded between 900-1000°C during the experimental runs, representing a reduction of around 200°C as the gases left the narrow burner quarl and entered the wider gasification chamber. Heat was absorbed during endothermic gasification reactions as well as being lost to the cooler reactor walls. The impact of the cool walls was demonstrated by repeating run A1 across a range of wall temperatures as recorded by the K-type thermocouple in the refractory layer. The results of this test are shown in Figure 6-2.

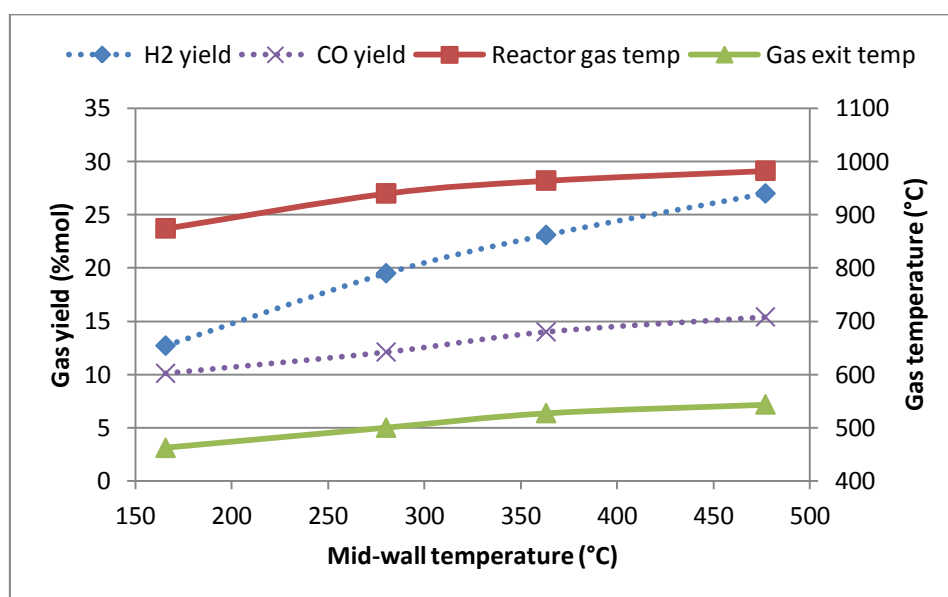


Figure 6-2: Run A1 gas temperature and yield against wall temperature

The gas temperatures in Figure 6-2 are seen to increase slightly with increasing wall temperature, while the concentrations of H₂ and CO increase more sharply. It was considered that increasing wall temperature reduced the rate of heat loss from the gas, which increased the average gas temperatures. However the increased syngas yield suggests that the wall temperature had a greater effect on feedstock particles than on the gas phase. Radiation from furnace walls is a major contributor to particle heating, proportional to temperature to the fourth power and particle emissivity as discussed in Section 3.4.1. With increasing wall temperature, the results suggest that increased radiative heating of particles by the wall may have contributed to greater particle temperatures and hence greater feedstock conversion than in cold wall runs. This is in addition to additional conversion expected from the increase in system temperature explained in the Theory chapter Section 3.1.1.3.

This important result was taken into account for the subsequent investigation into feedstock performance, with the wall temperature maintained as stable as possible across tests for fair comparison.

6.3.1.1 Burner Temperature Distribution

Due to the peak flame temperatures, a steep temperature gradient was observed across small radial lengths approaching the flame front. This was confirmed by conducting an investigation without feedstock addition under the same gas flow conditions described, in which the thermocouples were inserted to increasing depths into the burner zone. The R-type thermocouple was inserted without suction as described in Section 6.3.1 and recorded a maximum temperature of $1227\pm 3^\circ\text{C}$ when inserted below the synthair jet as shown in Figure 6-3, located approximately 110 mm from the burner roof.

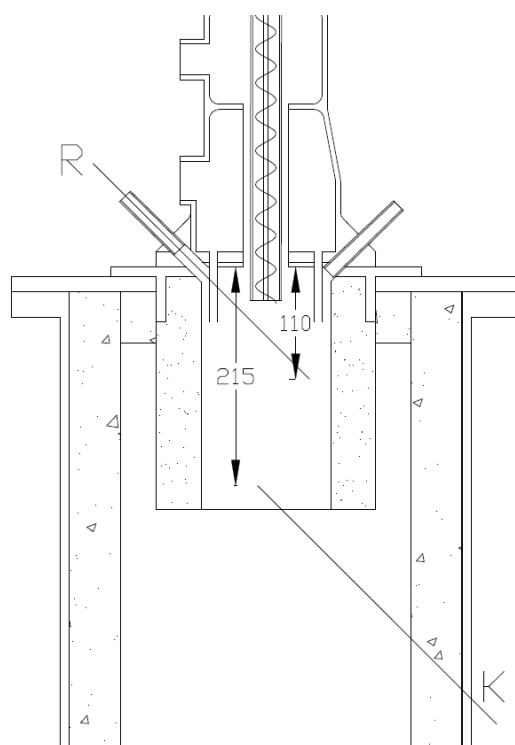


Figure 6-3: Diagram of R-type and K-type thermocouple positions, dimensions in mm

Similarly, the K-type thermocouple beneath the burner was inserted at depths between 150 and 350 mm. A maximum temperature of 1260°C was recorded at a point approximately 215 mm from the burner roof, as shown in Figure 6-3. This temperature is approaching the upper bound of the sensitivity range for this type of thermocouple, giving an uncertainty of $\pm 5^\circ\text{C}$ according to Section 5.5.3. Owing to the restricted access afforded by the burner construction, it was not possible to reach all parts of the burner volume. However the results indicate that the peak temperature zone was located near the quarl outlet, along the central axis of the burner.

6.3.2 Results of Varying S/C Ratio

The range of steam to carbon (S/C) ratios calculated from varying the rate of feedstock addition is listed in Table 6-5. These target values were used for the experimental runs, with the achieved S/C ratios and resulting product compositions shown in Table 6-6. Traces of oxygen, nitrogen and methane resulted either from residual air in the gasification chamber and sampling line or as small amounts of unburned reactants. The exact reactant flows used are shown in the mass balance in Table 6-7.

6. EXPERIMENTAL RESULTS AND DISCUSSION

Table 6-6: Results of experimental runs A1-3 and C1-3 on a dry molar basis¹⁹.

Run	S/C	H ₂	O ₂	N ₂	CH ₄	CO	CO ₂	T _g	T5	T6	T _w
%mol								°C			
A1	3.34	27.4	0.26	2.56	0.88	16.4	52.9	135.9	992.9	549.2	467.7
A1	3.28	26.6	0.28	2.94	0.42	15.7	51.1	132.5	973.1	528.9	487.4
Mean	3.31	27.0	0.27	2.75	0.65	16.05	52.0	134.2	983.0	539.1	477.6
Std Dev	0.04	0.57	0.01	0.27	0.33	0.49	1.27	2.45	14.01	14.33	13.89
A2	2.48	27.2	0.24	2.79	3.13	17.0	50.4	136.3	924.3	530.6	496.1
A2	2.40	29.5	0.23	2.51	4.06	17.8	45.9	135.0	909.6	498.8	502.2
Mean	2.44	28.4	0.24	2.65	3.60	17.40	48.15	135.6	916.9	514.7	499.1
Std Dev	0.06	1.63	0.01	0.20	0.66	0.57	3.18	0.91	10.38	22.49	4.30
A3	2.10	29.9	0.21	2.30	1.88	17.0	44.9	136.4	962.3	530.9	497.2
A3	1.96	33.1	0.20	1.84	0.50	18.7	43.4	142.1	989.2	541.4	511.2
Mean	2.03	31.50	0.21	2.07	1.19	17.85	44.15	139.2	975.7	536.2	504.2
Std Dev	0.09	2.26	0.01	0.33	0.98	1.20	1.06	4.01	18.97	7.41	9.89
C1	3.80	34.0	0.15	1.61	1.75	23.0	38.6	143.3	929.2	555.9	456.7
C1	4.01	32.6	0.16	1.86	1.50	22.6	38.6	145.0	899.7	564.0	473.9
Mean	3.90	33.3	0.16	1.74	1.63	22.80	38.60	144.1	914.4	560.0	465.3
Std Dev	0.14	0.99	0.01	0.18	0.18	0.28	0.00	1.18	20.85	5.79	12.17
C2	3.12	32.4	0.15	1.59	3.04	24.4	37.1	136.0	909.8	530.6	454.1
C2	3.17	32.8	0.15	1.74	2.90	24.3	36.2	135.5	909.9	543.9	465.1
Mean	3.14	32.6	0.15	1.67	2.97	24.35	36.65	135.8	909.8	537.3	459.6
Std Dev	0.04	0.28	0.00	0.11	0.10	0.07	0.64	0.35	0.04	9.45	7.81
C3	2.80	33.5	0.14	1.85	2.73	25.1	35.5	140.5	872.8	551.2	477.4
C3	2.77	34.9	0.14	1.71	2.96	24.9	33.2	138.9	915.7	558.2	487.0
Mean	2.79	34.2	0.14	1.78	2.85	25.0	34.35	894.2	894.2	554.7	482.2
Std Dev	0.02	0.99	0.00	0.10	0.16	0.14	1.63	1.07	30.33	4.97	6.83

The yields of species of interest are plotted against S/C in Figure 6-4, with softwood char results shown as dashed lines. Each run was found to yield a high concentration of CO₂, which was the majority constituent of the dry product gas in each case. This was also observed during the previous experimental set in Table 6-1, and was found to result primarily from fuel gas combustion used to produce the flame. The supporting calculation is described in the mass balance (Section 6.3.3). The CO₂ content could be reduced by using an alternative fuel such as recycled syngas to produce the steam flame, or by reducing the heating demand to reduce the quantity of fuel required.

It was observed from Figure 6-4 that increasing the feedstock loading to reduce the S/C ratio had only a minor effect on the gas composition under the conditions tested. This was due to the small scale of the gasifier which restricted the residence time for particle reaction and limited feedstock conversion. This was evidenced by the increasing amount of residual unreacted feedstock collected after each test, as detailed in Table 6-7. Residual solid material was collected in every test including those with the lowest solid loading, which demonstrates that the quantity of feedstock introduced

¹⁹ Two repeats shown for each case, with mean and sample standard deviation. T_g = average temperature of steam before mixing with oxygen. T5 = gas temperatures below the burner. T6 = gas temperature at the gasifier outlet. T_w = mid wall temperature in the refractory layer.

was not limiting the extent of gasification achieved over the range tested. The small increases in H_2 and CO yields observed with increasing solid feed were either from devolatilisation of the additional feedstock, which is a rapid process compared with char conversion, or a result of the small increase in T_w observed from Table 6-6.

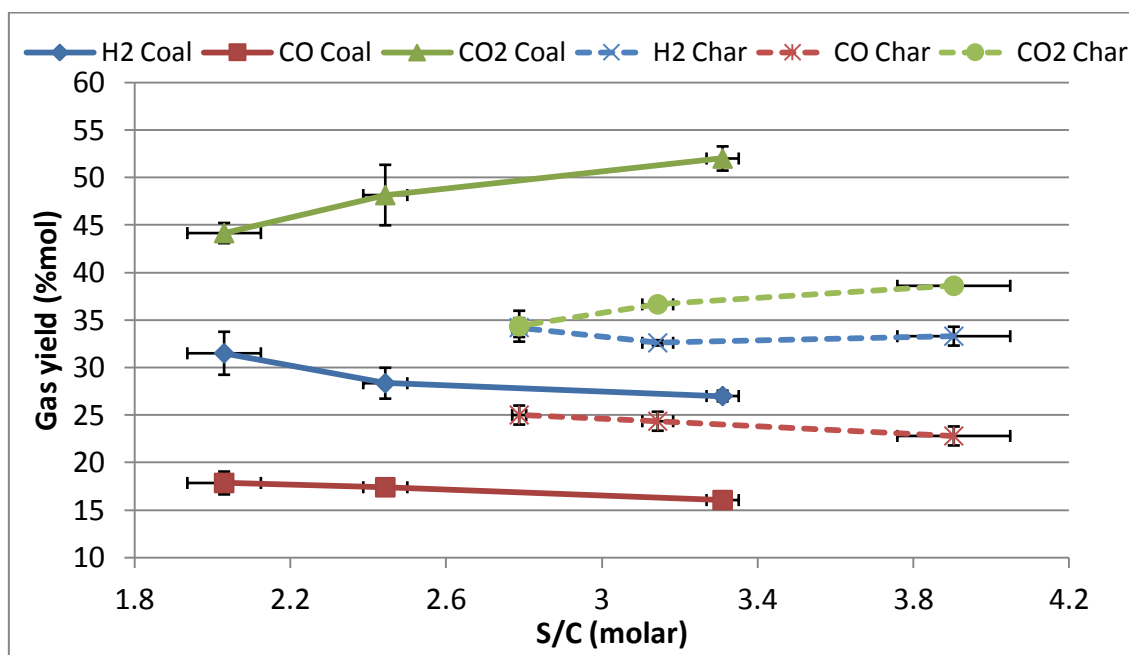


Figure 6-4: Dry product gas composition against S/C. Solid lines represent coal runs A1-3, dashed lines represent char runs C1-3. Mean of two runs shown with bars representing \pm one standard deviation.

In comparing the coal and biochar feedstocks, Figure 6-4 shows that the softwood char consistently yielded higher H_2 and CO fractions compared to the coal feedstock, even with a lower carbon feed rate. Comparing runs A1 and C2 which had a close match in S/C ratio, the char yielded a 20% higher hydrogen concentration and a 50% higher CO concentration in the product stream than in the coal run. In particular, the lower yields of CO_2 and residual solid carbon from biochar tests suggest that the Boudouard reaction (Eq. 3-3) progressed to a greater extent with char than in coal tests, giving a greater yield of CO in the product. The increase in combustible gas yield and reduction in CO_2 gave a higher product heating value from char tests, as discussed in the energy balance in Section 6.3.4. Differences between the coal and biochar materials are further discussed in Section 6.3.6.

6.3.3 Mass Balance Results

The mass flows of reactants and products for each test are shown in Table 6-7. Based on the conservation of mass, the sum of the mass inflows was set as the total mass outflow and the mass of residual solids subtracted to find the mass flow of wet gas out. The moisture fraction of the gas sample was used to calculate the flows of moisture and dry gas as described in Section 5.5.2. The H_2O outflow exceeded the steam supplied to the gasifier in many cases due to moisture from fuel gas combustion. From 2.4 kg/hr of methane up to 5.4 kg/hr water is obtained assuming complete combustion to H_2O and CO_2 .

6. EXPERIMENTAL RESULTS AND DISCUSSION

This assumption can also give an estimate of the expected CO₂ flow in each test. Comparing the mass of CO₂ expected from methane combustion with that calculated from the mole fraction and flow rate of dry product gas, it was estimated that 58-64% of the CO₂ mass flow in the product was produced from methane combustion. The high CO₂ content in the product is detrimental to its heating value and represents carbon emissions which increase the environmental impact of gasifier operation. It also inhibits the water gas shift reaction from producing the expected hydrogen yields. It was intended that on a commercial system this could be reduced by recycling a part of the syngas product back to the burner to provide heat to the flame. Also reducing heat losses from the gasifier would reduce the heating demand and hence the fuel requirement (see Figure 6-5).

Table 6-7: Mass balances for coal tests (A1-3) and char tests (C1-3). Data is mean of two repeats.

Mass in (kg/hr)	A1	A2	A3	C1	C2	C3
CH ₄	2.4	2.4	2.4	2.4	2.4	2.4
O ₂	10.5	10.5	10.5	10.5	10.4	10.4
Steam	10.0	10.5	10.3	10.8	10.1	10.7
Coal/char	3.7	5.2	6.2	3.7	4.3	5.1
Total	26.6	28.5	29.5	27.4	27.2	28.5
Mass out (kg/hr)						
Dry gas	13.0	14.1	14.7	16.6	16.1	17.8
Moisture	11.6	12.0	11.3	10.2	10.1	9.6
Residual solids	2.0	2.5	3.4	0.6	1.0	1.1
Total	26.6	28.5	29.5	27.4	27.2	28.5

6.3.4 Energy Balance Calculation

An energy balance was conducted using the mass flows from Table 6-7. From the dry product gas composition, a weighted average of the heating values of hydrogen, carbon monoxide and methane was used to calculate the heating value of the dry product gas mixture.

Table 6-8: Heating value of product gas for each run on a dry basis. Data is mean of two repeats.

CV	A1	A2	A3	C1	C2	C3
kJ/kg	%wt (d.b.)					
H ₂	141790	1.9	2.0	2.4	2.6	2.7
CH ₄	55530	0.4	2.1	0.7	1.1	1.9
CO	10087	15.6	17.4	19.3	25.8	27.7
Product gas CV (kJ/kg)	4422	5764	5806	6912	7631	8105

From the dry gas densities it was calculated that the calorific value of the syngas produced from coal ranged between 5.3-6.6 MJ/Nm³ on a dry basis. The syngas produced from the softwood char had a calorific value range of 7.2-8.1 MJ/Nm³. The total energy flows for each run are shown in Table 6-9. These were calculated from the mass flow and CV for fuels such as methane, solid feedstock and product gas out. The total energy out was set equal to the sum of the energy inflows based on the conservation of energy. The difference between the total energy out and the individual outflow components was attributed to energy losses, as discussed below.

6. EXPERIMENTAL RESULTS AND DISCUSSION

The methane and feedstock inflows entered the system at room temperature so were assumed to have no sensible heat associated with them. Oxygen was moderated to between 30-35°C to compensate for the cooling effect of the pressure drop on leaving the gas cylinder. The heat capacity of oxygen at this temperature was calculated to be 29.4 kJ/kg [using data from Cox, Wagman, et al., 1984; Chase, 1998 as cited in (NIST, 2016)]. Steam enthalpy was calculated using thermodynamic tables for the average delivery temperatures in Table 6-6, ranging between 130-145°C (Rogers and Mayhew, 1995). Similarly the outlet temperature T6 was used to find the outlet steam enthalpy.

The sensible heat in the product gas was found from a weighted average of the heat capacities of the constituent species, calculated at 298 K and at T6 from Table 6-6 and the average of these two values used. This was also estimated for residual solids using heat capacity data from literature. For softwood char the heat capacity was estimated using the following expression valid between 313 < T < 686 Kelvin;

$$c_p = -0.0038 T^2 + 5.98 T - 795.28$$

Equation 6-1 (Gupta et al., 2003)

Equation 6-1 gave values of 768 J/kgK at 313 K and 1518 J/kgK at 686 K. The upper bound temperature for this expression is below the gasifier outlet temperatures observed in Table 6-6. However the heat capacity has been reported to rise more slowly at elevated temperature, according to Grønli (1996) Fredlund (1998) and Gupta (2003) as cited in (Hankalin et al., 2009). Further, the temperature of the solids exiting the gasifier is not known precisely, but is assumed equal to the gas temperature. The composition of the char will change as it is gradually reacted which will also have an effect on the heat capacity. Due to the relatively small energy contribution from this source the accuracy of the heat capacity has a minimal effect on the overall results. In the absence of higher temperature and compositional data the average of 768 and 1518 J/kgK was used giving a heat capacity of 1.14 kJ/kgK for all char runs.

Table 6-9: Total energy flows in and out of gasifier for each run. Data is mean of two repeats. See text for details.

Energy In	A1	A2	A3	C1	C2	C3
	MJ/hr					
CH ₄	131.7	131.7	131.7	131.7	131.7	131.7
O ₂	0.3	0.3	0.3	0.3	0.3	0.3
Steam enthalpy	27.4	28.7	28.4	29.9	27.8	29.4
Coal / Char	119.0	166.4	199.9	82.4	96.0	112.8
Total	278.4	327.1	360.3	244.3	255.9	274.2
Energy Out						
Gas HHV	57.5	81.2	81.8	114.5	122.8	130.4
Sensible heat	10.1	10.6	11.8	12.9	11.9	12.3
Steam enthalpy	41.4	42.1	40.4	37.0	36.1	34.6
Residual solids	51.3	63.5	87.8	8.2	11.8	13.6
Losses	118.0	129.6	138.5	71.7	73.2	83.4
Total	278.4	327.1	360.3	244.3	255.9	274.2

6. EXPERIMENTAL RESULTS AND DISCUSSION

Similarly for coal, a polynomial expression from literature was used to find the heat capacity of anthracite (Tomeczek and Palugniok, 1996). This was found to be approximately 1 kJ/kgK at room temperature and peaking at around 2 kJ/kgK at a temperature of 520°C. The average of these values was used to estimate the sensible heat in the residual coal material.

The various energy flows are represented as a percentage of the total input energy in Figure 6-5. For each run there is a bar for energy flows into the system and a second bar showing the distribution of energy out. The graphic highlights that around half of the energy input in each run was provided by methane and around half from the feedstock; the input contribution from steam enthalpy was smaller and that from sensible heat of oxygen was less than 1%. It is evident from Table 6-9 that the difference in heating values between coal feedstock (32 MJ/kg) and softwood char (22 MJ/kg) as well as the different mass flows resulted in substantially different total energy inputs between coal and char runs.

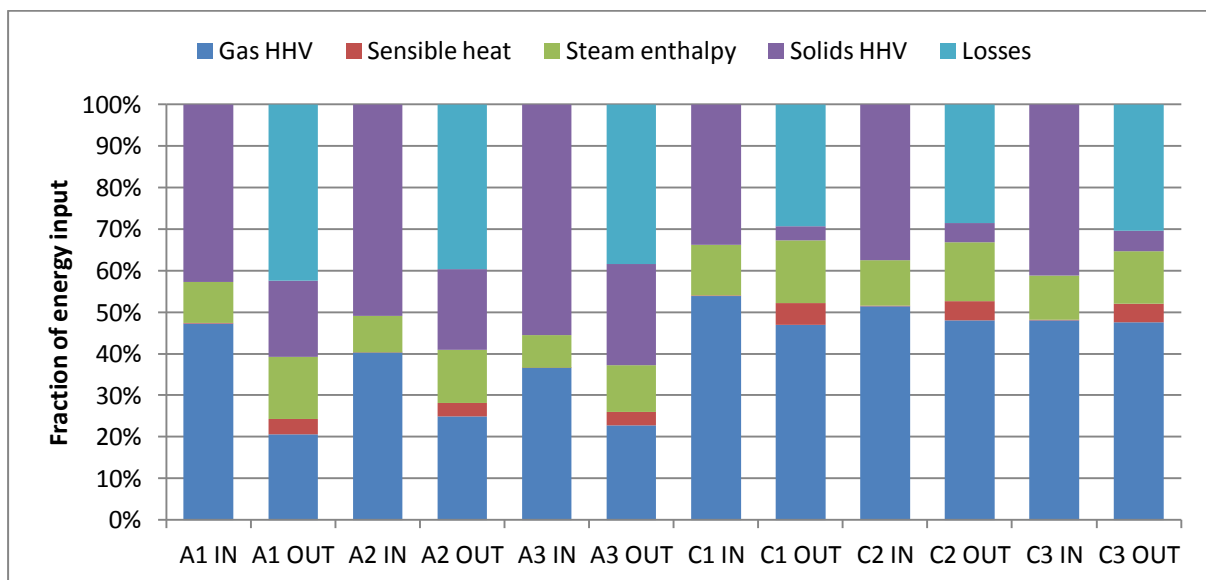


Figure 6-5: Energy in and out of gasifier as a percentage of total energy input, from Table 6-9²⁰.

Figure 6-5 highlights energy losses of around 40% of the energy input for coal runs and around 30% for char runs which were not accounted for in the heating value or sensible heat of the recorded output products. These were primarily associated to heat losses from the gasifier wall. An estimate of this heat transfer can be made using Fourier's law of conduction through the wall of a hollow cylinder (Eq. 3-27) which shows that the rate of heat transfer is a function of thermal conductivity, temperature difference and wall thickness.

The rate of heat transfer Q was estimated using the mid-wall and outside surface temperature measurements. An average mid wall temperature T_w for all runs was taken as 480°C from Table 6-6 and the outside surface temperature was recorded at up to 360°C under the insulating blanket using a digital infrared thermometer. This reading was indicative only due to limitations in the accuracy of the device and the surface condition of the gasifier outside wall. However an estimate of the rate of

²⁰ "Gas HHV" = higher heating value of methane for inflow or syngas for outflow. "Solids HHV" = higher heating value of feedstock or residual solids from catch pot. "Sensible heat" includes the product gas and residual solids. "Losses" include heat transfer through reactor wall and any solids lost by entrainment.

heat transfer was calculated using Equation 3-27. Taking the thermal conductivity of refractory as 2.5 W/mK (Shabangu, 2005), the total heat transfer through the refractory wall was approximately 19 kW. This represents 19-25% of the energy supplied during the coal runs and 25-28% of that supplied in the char tests. This equation also allowed the inside wall surface temperature to be estimated as 643°C at the point adjacent to the T_w thermocouple, 600 mm from the gasifier outlet.

The high rate of energy transfer through the gasifier wall is partly a result of the high temperature difference between the flame zone and the outside wall surface. The small volume of the gasifier also gives it a higher surface area to volume ratio than for a larger reactor, which gives a large surface available for heat transfer. This system relies on high flame temperatures, but the feedstock loading is limited by the reactor size, giving a high fuel requirement for a low throughput. Some optimisation is required to find the most economical feedstock loading to fuel requirement. Increasing the thickness of the refractory wall would reduce the heat loss.

This level of heat transfer corresponds well to the expected energy loss reported in the char tests, but accounts for only half of the expected losses reported in the coal runs. The additional source of energy loss in the coal runs was considered to result from unreacted coal particles being entrained by the flue gas, and hence not accounted for in the residual solids' HHV. Because the conversion of coal was low in the gasifier, the heating value of entrained coal particles would be high, giving a significant loss of energy from the system. Also the smaller particle size of the pulverised coal would lead to a greater amount of entrainment expected than for the larger char particles.

This demonstrates a compromise is required in selecting an optimum particle size for this system. Smaller particles with larger total surface area provide increased reaction rate, however they stand a higher risk of being entrained and so cannot be recycled back into the system. A more comprehensive dust capture system would alleviate this problem, provided that the pressure drop imposed by a cyclone or similar did not interfere with the gasifier flow. On the experimental system restricting the outlet was found to cause flame instability. This feature requires further development for a larger, commercial system to allow recycling of partially converted feedstock and improve system efficiency (Section 6.3.7).

6.3.5 Gas Residence Time

From the mass balance the total gas outflow was calculated to be around 26 kg/hr in the experimental runs. Taking run C2 as an example, the gas residence time was estimated as follows. The moisture fraction of outlet gas was found to be 38.6% on a mass basis. The dry molar gas composition for the two runs was averaged and used to find the mass composition. This was combined with the moisture fraction to find the total stream composition on a wet basis. The CO, CO₂ and H₂O alone were found to comprise over 95% of the stream mass. Gas densities for these species at the mean syngas exit temperature of 537°C were used to calculate a weighted average density representative of the stream at this temperature.

Table 6-10: Gas yields from C2 runs, on dry molar basis as recorded by the online GC; dry mass basis and wet mass basis

Run	H ₂	O ₂	N ₂	CH ₄	CO	CO ₂	Total
C2 #1	32.4	0.15	1.59	3.04	24.4	37.1	98.68
C2 #2	32.8	0.15	1.74	2.90	24.3	36.2	98.09
C2 mean (%mol, d.b)	32.6	0.15	1.7	3.0	24.4	36.7	98.4
C2 mean (%wt, d.b)	2.7	0.2	1.9	1.9	27.7	65.6	100.0
C2 mean (%wt, w.b)	1.6	0.1	1.2	1.2	17.0	40.3	61.4

The representative gas density was calculated to be 0.437 kg/m³. For the gas flow of 26.2 kg/hr this approximates to 60 m³/hr. The volume of the gasifier was taken from the FLUENT geometry (Section 4.4.5) to be 0.0666 m³. Dividing gives the estimated gas residence time to be 4 seconds for this run. This is consistent with the design calculations for the gasification chamber which were based on a one second residence time, using approximately four times the gas flows used in the present work (Shabangu, 2005).

6.3.6 Feedstock conversion

The coal feedstock was found to undergo incomplete conversion in the gasifier. The mass balance in Table 6-7 shows that around 50% of the solid feed was collected from the catch pot in each coal test, not including any material which was entrained by the gas flow. The residual coal collected from run A1 had a heat value of around 25.5 MJ/kg which is 79% of that of the unreacted feedstock. The fixed carbon (FC) content increased from 83% to 87%, indicating that the moisture and volatile components had reacted preferentially during the short residence time in the reactor.

Table 6-11: Results of residual solids analyses for available samples. Data is mean of two repeats.

	A1	A3	C1	C3
	%wt			
Moisture	0.4	0.3	2.7	2.7
Volatile matter	6.1	7.2	15.0	17.3
Fixed carbon	87.0	85.6	48.3	41.3
Ash	6.2	6.9	34.0	38.7
Gross CV (MJ/kg)	25.5	25.7	13.2	11.6

The softwood char feedstock experienced greater conversion than coal, with only around 20% of the feed collected in the catch pot. Run C3 yielded the highest feedstock conversion; the heating value of the residual char decreased by 48% to 11.6 MJ/kg in a single pass. The fixed carbon content decreased from 67% to 41% while the ash fraction increased from 15% to 39% of the material mass, indicating that much of the carbon content was reacted. The gas yield from char was also richer in H₂ and CO than from coal tests. These results indicate that the softwood char was more reactive than coal.

The greater reactivity of biomass char compared to coal is a recognised characteristic discussed in Section 3.1.3.3 of the Theory chapter and is a culmination of several factors including the material

structure, surface area and the effect of mineral content. The porous nature of biomass char can give a substantial internal surface area available for reaction, as highlighted in Table 5-4; considering high temperature gasification is predominantly a diffusion controlled process this may contribute to the greater gas yield from char.

The high mineral content of the softwood char is also likely to have contributed to its higher reactivity. The catalytic effect of inorganic elements such as potassium has been documented in literature as also described in Section 3.1.3.3.

To quantitatively compare the effects of these two factors, additional analyses are required which are beyond the scope of this work. A preliminary investigation was undertaken with the resources available including Brunauer-Emmett-Teller (BET) analysis, described in Section 5.2. This technique revealed the specific surface area of the softwood char to be 292.6 m²/g as received while that of the coal was 47.6 m²/g before being gasified. A sample of similar anthracite coal in the 74-125 µm size range was reported to have a specific surface area of only 0.24 m²/g, rising to 44.78 m²/g after heating slowly up to 800°C (Xia and Xie, 2015). For lower rank coals the surface area has been reported to be higher [Hodge, 2009 as cited in (Hla et al., 2015; Vascellari et al., 2015)]. This analysis suggests a significant difference in surface area between coal and biochar, and presents an opportunity for further investigation.

The difference in mineral contents of the two materials can be inferred from the ash contents determined by proximate analysis in Section 5.2.2. This analysis reported a 2.7%wt ash content for coal and a 14.6%wt ash content for the softwood char. In order to obtain some information as to the composition of the ash from the softwood char, an analysis was conducted by an external laboratory (see Appendix B). This revealed a potassium content in excess of 25 g/kg of the dry biochar, and over 7.7 g/kg of magnesium content. As potassium is recognised to be a particularly active material in the catalysis of char devolatilisation and burnout, it is considered highly likely that this was a contributing factor to the high biochar reactivity. Alkali and alkaline earth metals have also reportedly been added to coal gasifiers owing to their strong catalytic effect and relatively low cost (Rizkiana et al., 2014). To identify whether the surface area or the mineral content are most significant in distinguishing the reactivity of these two materials, a preliminary gasification experiment was conducted using low ash softwood char with a similar surface area.

6.3.6.1 Comparison of Low Ash Char

In order to assess the effect of ash on the gasification performance of the softwood char, a similar material was obtained with a reduced mineral content. This material was produced from the same mixed softwood feedstock using the same industrial process, but excluding the bark and foliage which contributed the majority of the ash content.

Because only a limited quantity of this material was available it was not possible to conduct a full comparison over the range of S/C ratios. However a successful run was conducted under similar experimental conditions to compare with the yields produced from high ash char and coal. The result is shown in Table 6-12. The temperature T5 in this run is higher as the thermocouple was located at the point of maximum temperature observed in Section 6.3.1.1, which is not directly comparable to the temperatures in Table 6-6.

Table 6-12: Results of experimental run using low ash softwood char on a dry basis²¹.

Run	S/C	H ₂	O ₂	N ₂	CH ₄	CO	CO ₂	T5	T6	T _w
		%mol						°C		
Low ash	2.54	28.7	0.16	1.34	5.74	21.6	43.5	1139.9	526.2	518.1

The low ash test was conducted with a relatively high rate of feedstock addition, comparable to Runs A2 and C3 in terms of S/C ratio. Comparing the gas yields from these runs it is seen that the low ash char gave a similar H₂ yield but a higher CO yield than the coal run A2. Both H₂ and CO yields were lower than from run C3. The mass of material collected in the low ash test represented 29.9% of that fed, again lying between the coal and the high ash char tests. These results suggest that the high ash content in the char had a positive effect on char reactivity, increasing the syngas yield and char conversion.

Furthermore, the BET analysis of the low ash char recorded a surface area of 357.8 m²/g; around 20% higher than the high ash material. This means the low ash material produced a lower gas yield and lower conversion in spite of having a higher specific surface area than the high ash material. This result supports the proposition that the ash content has a greater effect than the surface area on the material reactivity.

It should be remembered that these remarks are based on only one gas result owing to the limited supply of feedstock. Only limited confidence can be placed in a result obtained from a single successful run; as such these tentative conclusions show the potential for further investigation into the effects of mineral matter and specific surface area on gasification feedstock reactivity.

6.3.6.2 Biochar Reactivity

The low ash char test revealed that a material with low mineral content but higher surface area exhibited lower conversion than the equivalent high ash softwood char in the present system. This indicated that minerals in the ash contributed to the reactivity of the feedstock material in a positive way. This is in agreement with a study in which char samples were demineralised resulting in higher surface area than the parent samples yet exhibited much reduced reactivity (Várhegyi et al., 2006).

The study of feedstock surface area in a gasification environment is more complex than the BET analysis as the area will change during the gasification process. As mentioned in Section 3.1.3.3 the reactivity of biochars tends to increase with conversion but decrease for coals due to the sintering of pores (Duman et al., 2014; Mahinpey and Gomez, 2016)

At this stage it is not known which mechanism was responsible for this effect or which minerals were most active. This presents an opportunity for future investigation, following an extension of the experimental set using the low ash material; a detailed ash analysis of the feedstocks in question with the ability to selectively add and remove different ash species would allow the identification of particularly active minerals which assist the gasification process. This could be achieved using acid leaching of minerals and atomic spectroscopy for their identification, before adding selected minerals to a demineralised sample consecutively for gasification testing. A recent study found that

²¹ T5 represents average temperature recorded in the gasifier below the burner. T6 represents gas temperature at the outlet. T_w represents mid wall temperature in the refractory layer.

biomass ash with a high content of alkali and alkaline earth metals had a stronger catalytic effect on coal gasification compared to silica based ashes (Rizkiana et al., 2014).

Gasification chemistry may be replicated on a smaller scale in a TGA analyser in order to closely monitor the mass loss with temperature under different gas environments. Such studies can be used to gain understanding of the kinetics of gasification reactions using steam or CO₂ reactants, which could be used to extend the simulation work and identify key factors in feedstock conversion. The findings of such a laboratory study are somewhat restricted by limited mass transfer by diffusion in a controlled environment (Mahinpey and Gomez, 2016). Differences are expected between laboratory and gasifier kinetics, though a detailed analysis of conversion with temperature under gasification atmosphere could be used to enhance the existing particle tracks by incorporating expected mass loss with temperature and time in the reactor.

Comparison of selected mineral species as described above, as well as other factors which allow a high yield of hydrogen to be produced can be identified for the chosen feedstocks. Additional feedstock materials beyond those described in this work can also be compared in this way.

6.3.7 Gasifier Efficiency

The cold gas efficiency (CGE, Equation 3-12) is a ratio of the heating value of the product gas to that of the feedstock. As described in Section 3.1.2 this measure of efficiency is commonly used for gasification applications but favours those in which methane is produced, due to the high CV of methane compared to other gasification products such as hydrogen and carbon monoxide. Multiplying the heating value from Table 6-8 by the mass flows from Table 6-9 gives the heat flows used for the CGE listed in Table 6-13.

Table 6-13: Cold gas efficiencies (CGE) and gross cold gas efficiency (G-CGE) for runs A1-C3. G-CGE includes energy in fuel gas and supplied steam as well as in the feedstock, as shown in Equation 6-2.

	A1	A2	A3	C1	C2	C3
CGE	48.3%	48.8%	40.9%	138.9%	127.9%	115.6%
G-CGE	20.7%	24.9%	22.7%	46.9%	48.0%	47.6%

It can be seen that the CGE calculated in this way yields a value greater than 100% for the char tests. This is because the steam and the burner fuel gas contribute substantial energy inputs in this gasification system. The CGE is not a representative measure of the gasifier performance in this case.

Another method of calculating the CGE, sometimes known as the gross or modified CGE, uses the ratio of heating value in the product gas to the total energy input to the gasifier (Probstein and Hicks, 2006; Umeki et al., 2010);

$$\text{Gross CGE} = \frac{\text{Chemical energy of product gas}}{\text{Total input energy to gasifier}}$$

Equation 6-2 (Umeki et al., 2010)

In this case the chemical energy in the methane and the sensible heat of steam are taken into account to give a more representative indication of the gasifier efficiency. These values are shown as

G-CGE in Table 6-13. The coal runs A1-3 score less than 25%, which means that only one quarter of the energy supplied in each run is converted into product gas heating value. The char runs C1-3 score much better with almost half of the energy being converted into this product, which indicates that operation with char is more economical and efficient.

This score could be improved by reducing heat losses from the gasifier which would reduce the heating demand. These include heat transferred through the gasifier walls and any solids entrained by the gas flow as described. Recycling the unreacted steam and unreacted solids would also improve the CGE as these represent large fractions of energy output in Figure 6-5.

6.3.8 Ash Deposition

The effect of mineral ash content is considered to be potentially beneficial to gasification chemistry in Section 6.3.6. However the practical implications of using a high ash material in an industrial process often outweigh any potential catalytic advantages, due to the deposition of ash onto heat transfer surfaces and downstream process equipment. Existing gasification systems distinguish between slagging and non-slagging systems according to their ash treatment method as described in Chapter 2.

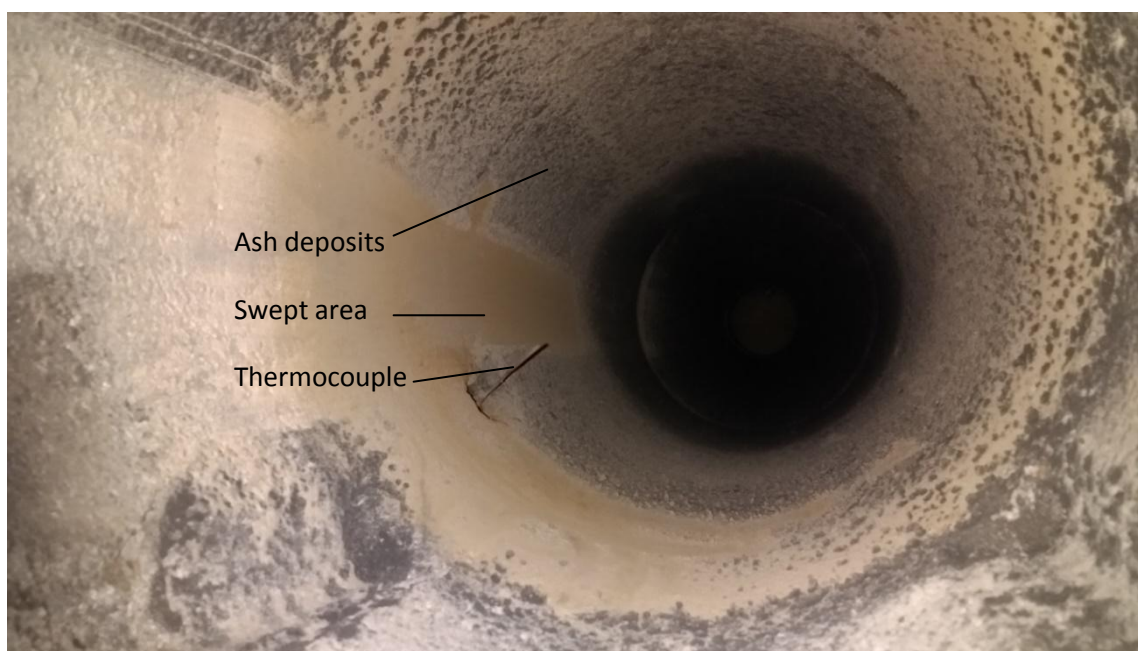


Figure 6-6: View of gasifier inside wall from above, showing ash deposits. After passing a brush across the surface these deposits were easily removed as shown.

During experimental operation, substantial ash deposition was observed on the burner jets and gasifier inside surfaces, particularly during biochar runs. This was expected due to the high ash concentration in the feedstock material. However the deposits observed were dry and non-sticky, in contrast to the melted ashes observed in other high temperature processes (Li et al., 2013; McKendry, 2002; Molcan et al., 2009). The ash on the gasifier walls and the burner surface was easily removed by brushing or compressed air, as pictured in Figure 6-6. It was not found to be detrimental to gasifier operation during the experimental runs; however it is noted that the experiment duration was only for a few minutes. If the gasifier was operated continuously over a period of hours, the

temperatures achieved may affect the structure of these deposits. Further work is required to confirm whether long term, high temperature operation results in a change in the ash behaviour. Analysis of the ash composition and structure would allow comparison with other similar ash deposits to identify any differences and explain its dry nature.

6.4 Summary of Experimental Results

The first objective of this chapter was to replicate the experimental results from the previous work, which was achieved in Run I. The product composition was found to show a close similarity to the yield obtained in that work, indicating a high level of reproducibility with this experimental set up. In Run II the gasifier was run without feedstock addition and found to yield a similar product composition, indicating that the coal feedstock was not the major contributor of syngas produced in the current arrangement. The reaction between propane and steam was considered a likely source for the H₂ and CO yields. In subsequent tests the reactant mixture was adjusted to reduce the evidence of this reaction, such that the performance of other parameters such as temperature and feedstock could be compared from a baseline. Increasing the ER reduced the yields of H₂ and CO from propane reforming substantially.

Increasing the gasifier temperature by increasing the flow of propane was found to improve the H₂ and CO yields from coal, which was confirmed through Run V-2 under equivalent conditions without coal addition. The effect of temperature was as predicted by the Aspen sensitivity analyses.

It was found that swapping the fuel gas from propane to methane provided more complete combustion with a lower excess oxygen requirement, giving a near pure CO₂ dry product yield. This baseline was used to compare the effects of gasifier wall temperature and feedstock type.

The reactor wall temperature was found to have a substantial effect on the product gas yield, though a much smaller impact was observed on gas temperatures inside the reactor. It was considered that radiation from the wall increased the temperature of the feedstock particles and contributed to increased conversion, owing to the high emissivity of black solid particles. The gases inside the reactor had low emissivity and were less affected by the radiation.

The variation in S/C from varying the quantity of feedstock added had almost no effect on the product yield, as in each case the feedstock conversion was incomplete. Because the quantity of feedstock was not found to be a limiting factor in the range of S/C tested, increasing the rate of addition only increased the amount of partially reacted material collected by the catch pot.

The softwood char was found to yield higher fractions of H₂ and CO than coal and proportionally less unreacted material was collected from the catch pot in char tests compared to coal. This indicated that a greater conversion of softwood char was achieved in equivalent gasification runs. This was attributed to the greater reactivity of biomass chars than coals, which is already widely documented. The differences in surface areas and mineral contents of these two materials are discussed as possible causes for reactivity differences. A preliminary comparison made using a low ash, high surface area material indicated that mineral content had a greater impact on feedstock reactivity than surface area in this case. Further investigation is required to confirm this finding.

7 DISCUSSION AND EVALUATION

This chapter presents an overall discussion of the work presented in the previous three chapters. In particular, elements of the experimental results outlined in Chapter 6 are discussed together with the findings of the modelling work in Chapter 4 and against similar published works. An evaluation of the experimental system is done from an economical viewpoint, and the opportunities for further study and any industrial applications of the system are explored.

7.1 Equilibrium Model Discussion

Chapter 4 presented the model of the gasification system created using Aspen Plus. This consisted of an equilibrium reactor to represent the gasifier, into which the reactant gases were added at temperatures and pressures representative of the experimental system. The reactant flow rates used were taken from an experiment conducted in a previous work (Shabangu, 2005) in advance of the present experimental programme. An estimate of the ideal product yield was achieved quickly and simply by assuming instantaneous chemistry.

The yield from the equilibrium model was compared with an early experimental result using similar reactant flows in Table 6-3. The experimental Run I was found to contain higher concentrations of CO₂ and CH₄ as well as substantial residual solid feedstock compared to the simulation, while concentrations of hydrogen and CO were lower than predicted by the ideal model.

The high CO₂, high residual carbon and lower yield of CO indicate that the progress of the Boudouard reaction (Equation 3-3) was lower than predicted by the model. This could be a result of the restricted residence time in the experiment, as the model did not take reactor volume into account. The Boudouard reaction is also noted to be highly endothermic from Table 3-1, making it sensitive to the amount of heat available in the reactor. Any heat losses or inefficiencies in the experimental system that reduced the available energy would be expected to result in a decreased yield from this reaction. The adiabatic simulation shows that minimising heat loss offers opportunities to improve yield.

7.1.1 Coal Conversion

The simulation was also based on flowrates taken from the previous work in which the gasifier was designed and sized. The reported coal loading in the previous experimental work was found to be more than could be consumed in the present equilibrium model. Reducing the coal charge in the model by around 40% was found to have a negligible effect on the gas yield and reduced the amount of residual solid exiting the reactor to zero. Run I was conducted with the revised coal charge but, a large amount of unreacted coal was observed in spite of this reduction. In the previous work the quantity of residual material collected was not reported, though a low conversion for solid feedstocks was discussed which suggests that much of the feedstock was not fully gasified. It was hypothesised therein that the residence time was not the primary limiting factor, but that inadequate enthalpies were reached in the reactor to achieve full conversion (Shabangu, 2005).

However, considering the rate equation in Section 3.1.3, rate of reaction and time required for a given conversion are proportional to reactor temperature. This shows that for an endothermic reaction, conversion could in theory be improved by increasing either the available heat energy or the reaction time.

Following the experimental programme in the present work, it is thought that the high coal charge in the previous work was a compensation for the low conversion achieved in gasification experiments. The reaction mechanism of solid fuels includes devolatilisation and char reaction steps; devolatilisation is known to occur quickly while char conversion is relatively slow. Under limited residence time, the char reaction rates may be too slow for any significant conversion to occur. The introduction of additional feedstock would allow rapid devolatilisation of the extra coal to yield additional product species at lower temperatures and residence times, producing a richer syngas at the cost of high coal throughput and limited conversion. This is evidenced by the composition of the residual coal in that work being similar to those recorded in Table 6-11, suggesting a similar degree of coal conversion using lower S/C ratios.

7.1.2 Chemical Kinetics

Some chemical kinetic data was incorporated into the process model, together with a temperature profile to limit the extent of equilibrium achieved. This gave a much closer agreement with the experimental gas yield than the equilibrium model, with potential for further development (see Section 7.3.1).

Incorporating additional reactions into the PFR model, such as propane steam reforming, could investigate the tendency of propane to react with steam over oxygen in the reactor. This was observed to occur over a range of fuel-oxygen ratios tested experimentally and will account for some of the differences in product yield.

The combustion of H₂ and CO with free oxygen could also be included since oxygen was predicted in the simulation product stream. This would ascertain whether limiting the charge of oxygen, which would reduce the temperature, would improve the yields of hydrogen and CO (see Section 7.2.2). It would also reveal whether any additional H₂ or CO yield arises from propane reformation or feedstock gasification, and hence whether limited oxygen was of benefit or detriment to feedstock conversion.

7.2 Similar Superheated Steam Models

Since the technique for producing Ultra Superheated Steam (USS) was patented (Lewis, 2007), other works involving steam flame gasification have been conducted to simulate fluidised bed systems. Data produced using Aspen Plus by T. B. Karim was cited for a model in which steam temperatures over 2200°C were achieved by supplying superheated steam to a burner together with methane and oxygen, with the resulting mixture fed via a distributor to a fluid bed. Using high rank coal as a feedstock the simulated gasification products comprised up to 40%vol H₂, 20%vol CO and 12-15%vol CO₂ on a wet basis (Pei and Kulkarni, 2008). Details of the nature of the Aspen Plus model are not given; it is assumed that the model was also of an equilibrium nature owing to the similarity of the gas yield to that from Simulation 1B shown on a dry basis in Table 4-6. Also, while the assumption of

7. DISCUSSION AND EVALUATION

adiabatic operation was not stated, the flame temperatures resemble those of a similar adiabatic, equilibrium combustion model to predict the composition of the steam flame (Xin, 2013).

A recent PhD Thesis aimed to construct a comprehensive kinetic model for USS gasification in a fluidised bed. This work considered four heterogeneous reactions and two homogeneous reactions, after the author considered several published kinetic approaches which had “no essential discrimination among them” (Xin, 2013). An equilibrium model was used to calculate the composition and temperature of the USS mixture prior to gasification, produced by combustion of methane in a mixture of steam and oxygen as used in the present work. The combustion was under lean oxygen conditions to ensure O₂ was fully consumed in the burner and avoid combustion of the feedstock. In the four conditions tested, the equivalence ratio (ER as defined in Section 3.1.1.4) ranged from 0.45 to 0.71, representing 45 to 71% of the stoichiometric oxygen requirement. This was reflected in the repressed adiabatic flame temperatures at low oxygen flows, though as oxygen was increased the steam flow was proportionally decreased such that the predicted flame temperature at ER=0.71 was around 2427°C. The condition closest to that used in the present work was Test E2 which used similar mass flows of steam and oxygen, with O₂ comprising 37%mol of the synthetic air mixture. This condition gave an adiabatic flame temperature of around 1850°C, still lower than those in Table 7-1 due to the ER of 0.56 limiting the extent of combustion.

A comparison of the temperatures achieved in various similar Ultra-Superheated Steam simulations and measurements is presented in Table 7-1. In early experiments at Sheffield with a trial burner the USS flame was observed to melt a platinum thermocouple, indicating actual temperatures over 1760°C.

Table 7-1: Comparison of Ultra Superheated Steam temperatures calculated, simulated or measured across different works

Temperature description	Value °C	Source
Adiabatic flame temperature	2277	Present work
Peak burner temperature from FLUENT	1977	Present work
Peak flame temperature measured using suction pyrometry with R-type thermocouple	1420	Present work
Equilibrium flame temperature, FLUENT	2130	(Ryu et al., 2004)
Peak temperature, Aspen Plus	2048	Karim, cited by (Pei and Kulkarni, 2008)
Adiabatic flame temperature	1363-2427	(Xin, 2013)
Maximum measured USS temperature	1260	(Hlebak, 2011)

The assumption of adiabatic operation resulted in increasing discrepancy between simulation and experimental measurements with increasing temperature. In test E2 at comparable temperatures to the present work, the model temperature was around 320°C higher than experimental measurement; a very similar discrepancy to that observed in Section 4.5.3.

Further, the author stated that it was not recommended to use a kinetic model to simulate combustion in the burner as published literature had shown these to be “highly complex and variable” (Xin, 2013). For this reason the USS composition was found using an equilibrium model before the kinetic model was used for the gasification stage. In the present work, the combination of

the combustion zone with the gasification zone was integral to the concept, making use of the peak flame temperatures and combustion radicals to accelerate gasification reactions. The complexity of constructing a kinetic model that could accommodate oxygen-enriched combustion and solids gasification resulted in the decision to use the simpler equilibrium approach in the present work.

7.2.1 Ultra-Superheated Steam Composition

The thesis described above also highlighted the effect of sub-stoichiometric combustion on steam flame composition. The composition of the USS mixture calculated by the equilibrium model showed evidence of substantial methane reforming, with hydrogen comprising 15-30%mol and CO around 12%mol of the mixture fed to the gasifier (Xin, 2013). An absence of experimental validation of predicted USS composition was observed in all the works described in this Section (Hlebak, 2011; Pei and Kulkarni, 2008; Ryu et al., 2004; Shabangu, 2005; Xin, 2013). This introduces substantial uncertainty into any reported gasification yields, as differing methods and flow rates in the production of the USS mixture can result in a range of gas compositions being fed to the gasifier, before reaction with feedstock.

Gasification tests were conducted using graphite feedstock. In test E2 the model predicted almost 50%mol H₂ in the product gas which was also recorded in the validation test despite the discrepancy in bed temperature, showing very good agreement. The CO yield was predicted to reach almost 50%mol and reached 41%mol (Xin, 2013). These yields are substantially higher than were achieved in the present experimental system, though around 25%mol H₂ and 15% CO were recorded in the USS mixture before gasification of graphite occurred. This can be misleading if comparing against gas yields solely from solid feedstock.

It is expected that reformation of the fuel gas also contributed to some extent to the yields reported in the work on which this project was based, given the stoichiometric oxygen supply. Because the composition of the USS mixture was not experimentally measured it is not known how much of an effect this had. However it was noted that the gasification product gas yields in the previous work were generally slightly lower in hydrogen when methane was used to fuel the burner instead of propane, in spite of a higher fuel flow rate (Shabangu, 2005). The greater fuel flow was expected to increase the yield of H₂ and CO by raising the reactor temperature but this was not the case. Higher syngas exit temperatures were achieved using propane.

Methane was also found to exhibit less reformation in the present work, with almost no traces of H₂ and CO recorded in Table 6-4. This could be due to the difference in enthalpies of the reformation of methane and propane; while both are highly endothermic reactions as described in Sections 3.3.6 and 6.1.1, methane reforming has less than half the standard enthalpy of propane reformation. This suggests that the propane reaction would be favoured to a greater extent under similar high temperature conditions. Alternatively it may be a result of the burner geometry, which was designed for natural gas operation so may offer improved mixing and contact using low density methane over propane.

7.2.2 Operation with Sub-Stoichiometric Oxygen

Experiments in Sections 6.1 and 6.2 showed that under comparable conditions methane produced much lower yields of H₂ and CO, using a stoichiometric oxygen supply. Efforts were taken in the

present work to reduce the evidence of the gas phase hydrocarbon reforming reactions in order to provide a clear basis for comparison between experiments and with other works. However as a result the yields of desirable syngas species are lower than could have been achieved by using sub-stoichiometric oxygen, as in some other works described above. Reducing the oxygen flow would result in higher yields and increase the heating value of the product gas. Introducing less oxygen to the burner also has the advantage of reducing the likelihood of combusting the feedstock or product gases.

The heating of a feedstock in an oxygen deprived atmosphere is the fundamental principle of pyrolysis and gasification. Clarity is required when the two processes of combustion and gasification are distinct but connected, as in the examples of fluid bed USS gasification described where combustion of a fuel gas occurs first in a burner, separated from the gasification chamber. In combustion an excess of oxygen is usually employed for maximum fuel efficiency, though in the described works the priority was to avoid any excess oxygen from being entrained into the gasification zone, where steam and CO₂ were the intended reagents.

Difficulty was experienced in the present work in distinguishing the combustion and gasification zones as they were deliberately simultaneous. This meant that efforts to minimise oxygen for the benefit of the gasification chemistry were to the detriment of the combustion reaction and vice versa. While the priority in this work was to explain the process by which this particular gasifier operated, it was of benefit to have no background yield of syngas from other sources. Further investigation could build on the present work in order to maximise the gas yields through investigation of the optimum ER, or introducing the feedstock at a later stage.

7.3 Fluid Model Discussion

The fluid model was used to investigate the effects that the reactor size and shape had on the gas flow pattern and the distribution of feedstock particles. This model looked at the mixing between reactants in the burner zone and the turbulence created by the high velocity inlet jets. In contrast to the Aspen model, the FLUENT simulations were done with limited chemistry. The Non-Premixed Combustion (NPC) model used a similar equilibrium approach to the Aspen model, but applied only to the gas phase reactants. The model calculated a local equilibrium composition in each volume from the gas composition and temperature conditions of the neighbouring cells. This method allowed the distribution of gas species within the reaction zone to be simulated and the associated temperature distribution mapped without the need to specify a reaction set or kinetic data. This approach was relatively computationally inexpensive allowing rapid manipulation of variables and short computation times at the cost of the detail and accuracy available from specific chemical kinetic models, which are often based on empirical data for specific feedstocks and reaction systems.

Disadvantages of the NPC model are that it is based on equilibrium chemistry which gives an idealised representation of the expected product yields. Without kinetic data the conversion of reactants to products tends to occur more quickly than would be expected in practice. For combustion reactions this results in a greater rate of heat release in a smaller volume which leads to over prediction of expected temperatures, as described in Section 4.4.5. This resulted in slightly higher peak temperatures in the model than in the experimental validation experiments in Section 4.5.3. The location of the onset of ignition is also likely to be over anticipated using this model, which

means that the combustion heat is likely to be distributed further along the reactor length in practice.

The incorporation of solid feedstock particles was made using the Discrete Phase Model (DPM). This model allowed injection of particles separately from the continuous phase and for the physical interaction between the phases to be simulated. This method is suitable when the discrete phase is dilute compared with the continuous phase and is less computationally demanding than a full multiphase model. This allowed efficient comparison of the trajectories of different types of particle in the reactor, to observe the differences in residence time for particles of different size and density. Trajectories were determined using the stochastic tracking model, which calculates a statistically likely path for each particle. Increasing the number of repeat calculations increases the statistical significance of the determined trajectories, as explained in Section 4.4.6.

The model successfully revealed additional information regarding the particle temperatures and heating rate which could be mapped against location in the reactor giving an additional approach to understanding particle behaviour in the gasifier.

Additionally, the particle temperature data from the DPM can be used in conjunction with particle data obtained from thermogravimetric analysis (TGA) to estimate the location of the onset of particle devolatilisation in the gasifier. Devolatilisation depends on temperature and rate of heating as described in the Theory chapter. From the TGA it was found that devolatilisation of both coal and biomass fuels occurred between 200-800°C, with a maximum rate observed usually around 400-500°C. Given that the fluid model predicted that the particle temperature reached up to 1800 K in around 0.25 seconds, devolatilisation is expected to occur immediately owing to the very high flame temperatures experienced on entry to the flame zone. This indicates that devolatilisation and gasification would occur simultaneously in a short timeframe.

It has been suggested in a combustion study that devolatilisation causes a particle to be enveloped in a volatile flame during this stage, shielding it from other reactant gases until this stage is complete. This is contrary to many CFD models which assume turbulent mixing (Jones et al., 2007). The implication is that during the initial devolatilisation stage, gasification of the solid char would be inhibited by the surrounding volatiles, delaying any heterogeneous reactions. Further, because devolatilisation is an endothermic process, particle heating rates and final temperatures are expected to be lower than predicted for the inert particles used in the present DPM study.

7.3.1 Detailed Modelling Approaches

Much literature is available on simulation of coal and biomass gasification, reflecting the efforts of many researchers in this field. A number of modelling approaches are taken; some of the options and variations are described here.

To incorporate the effects of some of the physical and chemical transformation of a feedstock in a gasifier, many simulations include sub-models, split into particle drying, devolatilisation, and gasification. Because drying and devolatilisation are much more rapid they are sometimes taken to be instantaneous while the rate of gasification of the remaining char governs the process (Basu, 2010). For coal combustion, a proper pyrolysis description plays a key role and can be modelled using a single kinetic rate model, two competing rates model or more complex network models (Yin, 2016).

For coal gasification, the two competing rates Kobayashi model has also been adopted (Roy et al., 2011; Shi et al., 2006; Vascellari et al., 2015).

The approach by Shi *et al* included two equations for char gasification and one for char combustion, with the rate modelled as a kinetic/diffusion controlled process using empirical formulations for various coefficients and constants in each equation (Shi et al., 2006). For every additional reaction considered in the model, additional empirical data is required.

Particles also drop in mass and diameter as they are consumed by devolatilisation and gasification, which means simulating the trajectory of an inert particle of constant mass is of limited application, particularly in high temperature environments. This means that the simulation of large particles may be valid during the initial time steps, while that of smaller particles may be more applicable in the latter phases.

The reactions of solid carbon with CO₂ and H₂O are considered in detail by Di Blasi who summarises the expressions used for lignocellulosic char conversion rates by many other researchers, pointing out the range in activation energies reported for these two reactions. The kinetic parameters were found to depend on pyrolysis conditions and ash composition of the feedstock as well as the composition of the gaseous mixture. It was concluded that while there is agreement amongst researchers as to the qualitative effect of factors such as pyrolysis conditions on reactivity, there is still substantial quantitative variation observed, with predicted gasification reactivities varying by four orders of magnitude (Di Blasi, 2009).

There is a wealth of literature available on CFD modelling of coal gasification and increasingly on biomass fuelled processes as well. From consideration of some of the literature it was observed that substantial variation was prevalent in the empirical kinetic data used in the various approaches, owing to differences in feedstock composition and preparation, reactor conditions and measurement methods. The data was often only applicable in modelling specific systems rather than for general use, so while good agreement has often been reported between simulation results and experimental validation tests, the models described are often limited in their wider applicability (Di Blasi, 2009; Hla et al., 2006; Lu and Wang, 2013; Roy et al., 2011; Vascellari et al., 2015).

Considering the unique nature of the char feedstock used in the present work, a simple approach excluding gasification chemistry was taken in the CFD simulations of this work. The simulation was intended to extend the understanding of the existing experimental system. While a detailed fluid model was highly desirable, it was not possible to conduct the necessary supporting work to collect sufficient detailed kinetic data specific to the current system to produce a detailed model of any significant accuracy or reliability. Future efforts may be directed towards the construction of a more rigorous model with the help of some of the experimental findings of this work. The aims of the present modelling work were satisfactorily met with the approach chosen.

7.3.1 Opportunities for Model Development

The model presented in this work was successful in meeting the aims of investigating the gas and particle flows. Following the method used in some similar works it was considered that the model constructed for the present work could be developed in a number of ways. The first of these would be to incorporate solid phase chemistry with the particles injected via the DPM. Presently inert

particles were used for simplicity; this allowed trajectories and distributions to be predicted but was limited by the absence of any physical change to the particles in the reactor. A real feedstock would undergo rapid mass loss during heating, potentially causing the particle to fracture and break apart. Altering the size, shape and density of the particle will have a large effect on the predicted trajectory, as demonstrated in Section 4.4.6.

Following the method of (Xin, 2013) a combination of equilibrium and kinetic modelling could be employed to improve the scope of the existing model. An equilibrium model for the combustion stage in producing the USS mixture avoided the inherent complexities of kinetic combustion modelling, allowing further computational effort to be directed towards gasification reactions, particularly the homogeneous reactions which play an important role in defining the final gas composition. The relative reaction rates will determine which reactions are most influential in a reactor of limited residence time.

Such a division would require a redesign of the fluid model used in the present work, in order to physically separate the combustion from the gasification stages. While it would be possible to determine an equilibrium composition of USS *a priori* and inject this directly via the current reactor inlets, this would radically change the distribution of gases in the burner, the circulation patterns and heat release pattern which were determined using the present model.

An emerging modelling approach called Reduced Order Modelling (ROM) identifies the need for accurate simulation to promote commercialisation of gasification and the impracticality of including many detailed sub-models which increase complexity and computational demand. The list of necessary sub-models identified includes devolatilisation, char conversion, particle and feedstock properties, chemical reactions as well as mixing and recirculation, slag behaviour, heat loss through walls and pollutant formation (Monaghan and Ghoniem, 2012a). A technique known as a Reactor Network Model (RNM) can be used to represent the complex circulation zones in a real reactor with a series of idealised reactor models, such as a well stirred or plug flow reactor. The approach was first developed by Pedersen *et al* and involves first creating a CFD model to identify the locations of the major flow regions and the boundaries between the zones. A suitable RNM can then be matched to the findings and validated against the CFD model and experimental data. Such an approach has been shown to be much less computationally expensive and also more versatile, with the flexibility to be applied to a variety of gasifier configurations (Hla *et al.*, 2015; Monaghan and Ghoniem, 2012b). This could be a step towards a general gasification model that can be adapted for use with a range of systems with improved accuracy and reduced computational time and resources over current approaches.

7.4 Sawdust Feeding Issues

Some difficulties were experienced when attempting to feed the sawdust to the gasifier. The raw material was composed of wood shavings, small chips and sawdust from the processing of waste whiskey barrels. During calibration of the feeder, it was found that only the smallest particles could be reliably conveyed through the screw shaft. This required thorough sieving to remove all shavings which would become wound around the screw shaft.

The sieved sawdust passed through the screw without problems when cold. When operating at temperature the residual material in the catch pot was found to have agglomerated into large clumps. This vastly reduced the available surface area for reaction with the gas phase and contributed to poor conversion.

After some minutes of operation the screw feeder became blocked as similar clumps of material formed inside the screw shaft. Volatile matter was liberated under the high temperature conditions, causing the dust to stick together. This made it impossible to collect any useable data for sawdust operation, so the material was excluded from the comparison in Chapter 6.

In order to increase system versatility towards additional feedstock materials, an alternative feeding mechanism is required such as compressed inert gas such as nitrogen. A novel pressurised feeding system developed at the University of Sheffield has been shown to efficiently pressurise solid feeds using a lock hopper system based on the incompressibility of water (Craven et al., 2014).

7.5 Comparing Experimental Results

The experimental programme was based around a gasification system designed and constructed in a previous project. Some modifications were made to the system to facilitate stable, continuous operation with biomass based feedstocks. Following some initial work to establish a suitable operating point, experiments were conducted to observe the effects of reactor temperature, steam to biomass ratio and feedstock type on the gas yield produced. The work is compared here with some similar works in terms of the nature of feedstock, model approaches and experimental results.

7.5.1 Char Gasification Using Present System

The experimental system described was used in some previous work to compare coal and gas oil feedstocks (Shabangu, 2005). In a related work, a fluid model of the gasifier was constructed using FLUENT using both the mixture fraction model described in the present work, and a species transport model. The mixture fraction approach is better suited to turbulent diffusion flames such as the steam flame used here, but has limited scope for inclusion of discrete phase chemistry. The species transport approach requires conservation equations for each species considered in the simulation, and requires each reaction to be specified with appropriate kinetic data. However it allows greater flexibility for a wide range of systems and inclusion of the solid phase chemistry.

The results of a report commissioned by Onyx Environmental Trust showed that the peak temperatures predicted using the species transport model were 350°C higher than in the mixture fraction approach, as by specifying the reaction set thermal dissociation and intermediate combustion species were omitted. The species distribution also suggested that the combustion reactions occurred more quickly in the species transport model, which may have led to higher temperature peaks (Ryu et al., 2005). Generally the flow patterns and temperature distributions were very similar to those obtained in the present work, showing close agreement despite the reduction in reactant flow rates in the present work. The temperature peak in the burner was higher as the quartz wall section was considered adiabatic, while in the present work heat loss through this section was included.

7. DISCUSSION AND EVALUATION

In the experimental phase, a sample of pine wood was pyrolysed to give a char comprised of 22% volatile matter, 78% fixed carbon and 1.4% ash. This material was pulverised to a fine dust before being gasified using the USS gasification system. The volume averaged particle diameter was 50 μm and 28 μm , much smaller than the range in the present work. Gasification tests were conducted with stoichiometric combustion of propane in the mixture of steam and oxygen. The resulting product composition was in very close agreement with the present work, as shown in Table 7-2.

Table 7-2: Product gas composition using wood char (Ryu et al., 2004), ²²

	Gas composition %mol				Residue
	H ₂	CH ₄	CO	CO ₂	% mass fed
1a	32.2	0.2	25.6	39.7	3.8
2a	32.3	2.0	25.4	40.0	3.5
2b	37.0	1.9	23.6	37.3	
C2	32.6	3.0	24.4	36.7	23.3

It can be seen from the reported gas compositions that the yields of all gas species were very similar in the compared works, in spite of the char flow being around 57% lower in the present work. The gas flows quoted were very high, around three times higher than in the present work.

The major difference between these two works was in the reported conversion of feedstock. Table 7-2 shows that less than 4% of the mass of char fed was collected in the catch pot in the work described; this is in contrast to the 23% collected in the present work which used a lower feed rate. Analysis of the residue found it to be comprised primarily of larger (>100 μm) particles with an ash content of 4-6% (Ryu et al., 2004); only a small increase from the 1.4% in the raw char, indicating low conversion. This may suggest that all smaller particles were fully gasified, with only the larger particles showing limited conversion and appearing in the catch pot. However the ash content in the char in the present work was found to increase from 14.1% to around 36%wt, implying that the residual material was more fully consumed at higher particle size.

It is considered that owing to the high gas flow rate and small particle size used in the study, that a part of the unreacted solids was entrained with the gas flow and not collected by the catch pot. The catch pot was originally designed to catch any molten slag produced in the gasifier and was found to be ineffective in separating fine solids from the gas flow. The implication is that using lower flow rates allowed for more solids collection in the present work, which facilitated the mass balance calculation and allowed for feedstock recycling if desired.

The study also reported lower conversion efficiency in cases using less O₂ in the steam mixture, however higher H₂ fractions were also reported under these conditions. This was associated with lower adiabatic flame temperatures and reduced concentrations of CO₂ in the steam flame, which favoured the conversion of H₂O and CO to H₂ and CO₂ via the WGS reaction (Ryu et al., 2004). It would also correspond with the argument in Section 7.2.2 that limiting the oxygen would promote formation of H₂ and CO within the steam mixture prior to reaction with the feedstock, thus leading to higher H₂ concentrations and lower feedstock conversion compared to the high O₂ case.

²² Test number 1 = 50 μm average particle size, 2 = 28 μm average particle size, a = 40%wt O₂ in synthair, b = 30%wt O₂ in synthair. Test C2 from present work is included for comparison

Their study was not able to conclude that the char showed better conversion than coal owing to the very small particle size being an additional variable (Ryu et al., 2004). The present work was able to show that biochar exhibited significantly greater conversion than coal in spite of higher average particle size. The specific surface area of the softwood char was found to be around six times higher than the coal tested, indicating that particle diameter is not the significant factor distinguishing the conversion of these two materials.

7.5.2 Large Scale Updraft Gasifier

The experimental results were compared with a large pilot scale updraft gasifier study (Umeki et al., 2010) described in Section 2.4.4.

The feedstock in this study was wood chips from crushed pallets, having higher moisture and volatile contents than wood char. A similarly steep temperature gradient was observed in both works between the high temperature steam inlet and the reactor outlet, as shown in Figure 7-1. Steam was recorded in six experiments between 1209 and 1334 K at the reactor inlet; decreasing by around 400 degrees over 500 mm reactor length even in the blank run without feedstock addition. This was attributed to heat loss from the reactor; a similar finding to the present work.

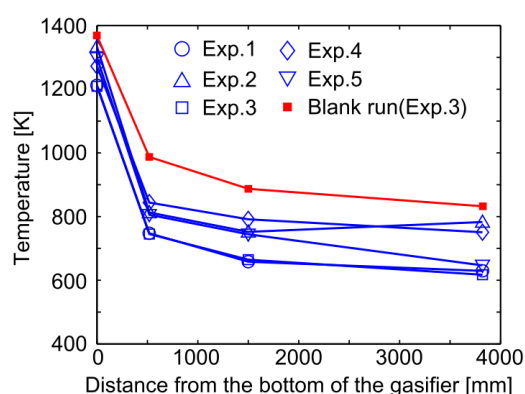


Figure 7-1: Temperature distribution in pilot scale updraft gasifier. Reproduced from (Umeki et al., 2010) with permission from Elsevier.

The gas yield was found to be much richer in hydrogen in the study, peaking at around 50%vol at an S/C ratio of 4.3, as discussed in Chapter 2 and shown in Figure 2-15. In comparison, the highest hydrogen yield observed in the present work was around 33%mol at an S/C of 2.8. The difference in S/C ranges is due to the difference in carbon contents between the feedstocks used, as was observed in comparing coal to char in the present work. The wood chips used in the study had a fixed carbon content much lower than the 85%wt in the present softwood char samples, meaning that a lower amount of carbon was charged to the reactor for a given mass of feedstock, giving a higher S/C range than for carbon-rich materials.

The compromise between increasing reactor temperature and reaction rate and decreasing residence with increasing steam flow was described to explain the peak in hydrogen yield. The water gas shift reaction was considered to be most influential in determining the gas composition under these experimental conditions.

A numerical analysis in the same study predicted an increase in hydrogen and a decrease in CO concentrations with increasing distance along the reactor, as was also shown in Figure 2-15. Reading from this figure, good agreement is predicted at 1.3 metres from the inlet with the experimental yields of H₂ and CO in the present work. This analysis indicates that the water gas shift (WGS) reaction is active under these conditions, and that a greater concentration of hydrogen could be expected if the reactor were longer. This is consistent with the conclusion of the present experimental work, in which the lower feedstock conversion in the experimental reactor than in the equilibrium model was considered to be due to limited residence time at peak temperatures.

On the other hand the CO₂ yield was higher in the present work than predicted in the figure, owing to the combustion of methane within the gasifier as described in Section 6.3.3 which did not feature in the numerical study. The higher concentration of CO₂ would be expected to impede the WGS reaction by shifting the equilibrium towards the reactants, which may alter the expected result. The addition of CO₂ in the USS was expected to result in lower yields of hydrogen and higher yields of CO and CO₂ compared to a steam-only system as modelled in the figure. Some method of removing CO₂ within the gasifier itself may be used to alter this equilibrium in favour of producing more hydrogen, such as the CO₂ sorption techniques described in Section 2.4.3. The USS system will yield a baseline CO₂ content in the product when using carbon based fuels to produce the USS mixture. The numerical model could be extended to investigate this effect in more detail.

The high H₂ yield in the Aspen simulation is consistent with the analysis in Figure 2-15, as for an ideal infinitely long reactor the predicted hydrogen yield was greater than observed experimentally. However the CO and CO₂ predictions showed opposite trends between the equilibrium model and the numerical analysis in Figure 2-23. This was expected given that the Aspen model was adiabatic, maintaining higher temperatures which strongly favour the Boudouard reaction ($dH = 173 \text{ kJ/mol}$) leading to consumption of CO₂ and production of CO. Conversely in Figure 2-23 the temperatures were lower, which favoured the WGS reaction ($dH = -41 \text{ kJ/mol}$) for production of H₂ and CO₂. Lower temperatures towards the reactor outlet were observed by experimental measurement compared with the Aspen simulation, and the experimental gas composition correlated more closely with Figure 2-15 than with the Aspen prediction, indicating that the numerical analysis based on a hybrid model of equilibrium and kinetics was more accurate than the basic equilibrium model. Such an approach could be adapted for the increased CO₂ concentration and higher temperature at the inlet to observe the effect on the predicted gas yield.

7.6 Economic Analysis

This section addresses the economics of the gasification system. The amount of energy flowing in and out of the system was calculated in the mass and energy balances in Sections 6.3.3 and 6.3.4. This section will look at the value of the product species, their applicability and potential value as useable or saleable products as compared to the feedstock materials. Methods for improving the economic performance are suggested.

7.6.1 Value of Products

The gross calorific values of the feedstocks were found to be 32 MJ/kg for coal and 22 MJ/kg for the softwood char. As described in the energy balance, the heating value of the dry syngas product was

calculated to be up to 5.8 MJ/kg from coal and up to 8.1 MJ/kg from char. This represents a large decrease in the heating value of the fuel. A significant portion of this energy is contained within the product gas as sensible heat, as it exits the process at high temperature. There is also steam contained within the gas from an excess of supplied steam and from methane combustion. The energy contained within this steam is not accounted for in the heating value of the syngas. If the sensible heat in the gas stream and the enthalpy of the steam can be usefully recovered, this will improve the efficiency of the process. Extracting the sensible heat from this stream would also cause the steam to condense, allowing it to be easily removed from the syngas.

In the current system methane is used to fuel the burner to generate high temperature steam for gasification. On a commercial system a part of the syngas produced could be recycled for this purpose, eliminating fossil fuels from the process and making it more sustainable. The energy supplied by methane is given in Table 6-9 as 131.7 MJ/hr. For this to be supplied by the dry syngas with the highest CV obtained of 8.1 MJ/kg, the required flow rate would be $131.7 / 8.1 = 16.3$ kg/hr of syngas, representing almost all of the dry gas yield from Run C3. This would not be economical under the current arrangement and would require improvements in gas yield quality and/or quantity to be feasible. The recycling of CO₂ and other inert products would also further dilute the syngas so gas cleaning or separation would be required before the syngas could be recirculated as process fuel. Ideally, pure hydrogen gas could be used for steam flame generation as its combustion produces no CO₂. This would be expected to reduce the levels of CO₂ in the syngas by around half (analysis in Chapter 4) and increase the heating value of the product gas.

7.6.1.1 Solid versus Gas Fuel

As described in Chapter 1, there are a number of advantages to using a fuel gas compared to solid fuel. Gases can be compressed, which means they can be economically transported via pipelines across large distances. Fuel gases can be combusted in gas turbines to produce electricity with a higher efficiency than solid fuelled systems with steam generation. A modern combined cycle gas fired power station can produce electricity with efficiencies approaching 60%, while coal fired stations operate at a European average of 36% (RWE, n.d.). This is because a Combined Cycle Gas Turbine makes use of a gas turbine as well as a heat recovery steam turbine for electricity production, which allows for greater electrical yields for the same amount of fuel combusted.

Comparing the useful energy obtained through combusting coal with a CV of 33 MJ/kg with 36% efficiency yields 11.9 MJ/kg of useful electrical output. For syngas with a CV of 8.1 MJ/kg combusted at 60% efficiency, the useful electrical yield is 4.9 MJ/kg. Thus the reduction in CV between coal and syngas is largely but not entirely offset by the increased efficiency of generation.

Fuel gas also tends to produce fewer polluting species than solids such as coal, as many of the nitrogen, sulphur and ash compounds are removed in the gasification and gas clean up stage. This means there are fewer such pollutants present during the combustion stage, which makes the flue gas clean-up simpler. Gas engines also benefit from rapid start-up and shutdown relative to solid fuel systems, and can be economical at smaller scale allowing for use of modular units in a decentralised network.

7.6.1.2 Use of Gas Engine for Electricity Production at Pilot Scale

Using the results presented in the previous sections, an estimate of the amount of electricity which could be produced on a small scale using a gasifier of this scale can be made. The use of syngas in

internal combustion engines has received relatively little research attention in spite of the potential advantages. Internal combustion engines are more tolerant to contaminants than gas turbines and have the advantage of being compact, low cost and modular. Disadvantages of using syngas in such an engine arise from the high volume of a hydrogen rich gas. The increased volume means less fuel can be charged into the combustion chamber per cycle, reducing the power output. Also there are increased pumping and heat losses in certain engine types (Hagos et al., 2014).

In this study a commercially available gas engine specifically adapted for syngas use was chosen. Because hydrogen gas burns faster than a typical gas engine fuel such as methane, modifications must be made to prevent pre-ignition and backfiring in the engine. A purpose designed syngas engine has a representative electrical efficiency of 37% (Clarke Energy, n.d.). Based on this figure and Run C3, the CV of the syngas produced being 8.1 MJ/kg and the dry gas flow rate of 17.8 kg/hr an electricity output of 53.3 MJ/hr could be achieved, equating to 14.8 kWe. This is far below the optimum output range defined for this engine, but may allow for blending with a supplementary fuel to give a suitable output.

7.6.2 Preliminary Costing of USS Gasification Process

A preliminary costing of the gasification process was performed to obtain a rough estimate of the cost of operation. The estimate was made for the current scale operation based on producing steam on site on demand, using anthracite coal as a feedstock and natural gas for flame generation. The capital cost of the gasifier was estimated in a University of Sheffield report at £70,000 for the experimental scale model (Swithenbank and Sharifi, 2013). The operating costs estimated here were based on operating 8 hours per day for 350 days per year, to allow for maintenance and other downtime.

Table 7-3: Estimate of annual operating costs for gasification system in current format²³.

Operating Costs	£/year	
Maintenance	£2,100.00	Based on 3% of capital cost.
Electrical supply	£213.64	Based on 1kW, 2800hrs/year. Average electricity price 7.63p/kWh
<u>Steam supply</u>		
Cold water	£37	Based on 10.5 kg/hr, cost average £1.26/m ³
Immersion heater	£186.94	Enthalpy change from 8-80°C = 300 kJ/kg. For 10.5 kg/hr gives 0.9 kWh/hr
Gas oil	£734.89	Water from 80°C to sat.vap at 8 bar =2434 kJ/kg. Assumed 85% efficient. Gas oil: 48 MJ/kg, £419/tonne
<u>Feedstock</u>		
Coal	£1,141.50	Heating value = 32 MJ/kg, 5.2 kg/hr. Cost £2.45/GJ
Methane	£1,702.15	2.4 kg/hr, 1.643 p/kWh
Oxygen	£8,842.34	£4.49 per 11.09 m ³ cylinder, exc. delivery
Subtotal	£14,958.46	per annum

²³ Based on Run A2. Data from (Anglian Water, 2016; DECC, 2016c, 2016d; Southern Water, 2016; Swithenbank and Sharifi, 2013)

This estimate does not include the cost of ash disposal, which at 2.7%wt of the coal would be produced at a rate of approximately 400 kg per year. It also does not account for labour costs of operatives which, taken on a full time basic wage basis would be the single largest operating expense. The cost of gas cleaning is also not considered as this is not in place on the current pilot system, so there is no data from which to estimate costs.

Table 7-3 presents the estimated costs for continuous annual operation using the existing system with coal as in Run A2. It shows that the sum of the operating costs is £15,000 per year, which means that, based on producing 14.1 kg/hr of dry syngas per hour, the sale price of syngas would need to be £0.38 per kg in order to break even. Factoring in the capital outlay, it would require an additional £0.36 per kg of raw syngas in order to payback the £70,000 within 5 years, meaning that the raw syngas must be sold at £0.74 per kg. Based on a CV of 5.8 MJ/kg, this would equate to around £0.46 per kWh, which is currently around thirty times the average industry price of buying natural gas from the grid (DECC, 2016c). Clearly in this format the system is not economically competitive as a method of fuel production, and using coal would not be eligible for any government backing for renewable fuels.

7.6.3 Alternative Scenarios to Improve Competitiveness

The following section addresses some alternatives which could be employed to reduce the operating costs presented in Table 7-3. The highest individual costs include the feedstock and gas flows, particularly oxygen, which comprises over half of the operating expense in the current scenario. The cost of maintenance was taken as 3% of the capital expense per year, though for a simple arrangement such as the experimental gasifier, there are few moving parts and access can be gained by removing the burner to all parts of the unit. During experimental operation, a period of several hours was required for start up to allow the thermal mass of the gasifier body to reach operating temperature, as described in Section 6.3.1. This heating period can be avoided by continuous operation. The above costing assumed 8 hours of operation per day, that would allow the gasifier to cool between shifts and would require preheating before operation each day. This would increase the fuel requirement and potentially limit the availability. However adaptations made to the experimental system in the present work allowed for increased automation once stable operation was reached, which reduced operating staff requirements.

7.6.3.1 Alternative Oxygen Source

It can be seen from this estimate that, excluding the cost of labour, the greatest single operating expense is the oxygen used in the burner. Oxygen is used in place of air to avoid nitrogen dilution of the product gas. The cost of purchasing oxygen in gas cylinders, even with a university discount, is very high due to the high flow rates required. A single cylinder was found to supply approximately 80 minutes of experimental operation. In order to meet this demand, oxygen could be produced on site using an air separation unit (ASU). This would impose a significant additional capital expense for an ASU, higher than that of the gasifier itself, which makes this solution unfeasible unless shared between another process or plant. Ideally the gasification system could be located on a site which already has access to an ASU, as the oxygen demand of the gasification is small compared to the rated output of a commercial ASU. Alternatively, a pressure swing absorption oxygen generator could be sized for the process and fed by compressed air to give a continuous oxygen feed (Atlas Copco, 2015).

The electrical cost of producing oxygen using an ASU was estimated to be 0.216 kWh/kg pure O₂ (Pei and Kulkarni, 2008). From the electricity cost assumed in Section 7.6.2 of 7.63 p/kWh, the annual cost of oxygen would be £485. This is a dramatic saving from the £8,840 for delivery of individual bottles, and more appropriate to the scale of the operation. The cost should be balanced against the capital and maintenance costs of an ASU.

7.6.3.2 Fuel Gas Cost

In this work methane was used as the burner fuel gas to power the gasification system. The laboratory location meant that a mains supply of natural gas was not available, which required the purchase of fuel gas cylinders. Typically in off grid locations, cylinders of propane or butane are used as these fuels can be liquefied at low pressures allowing for a greater quantity to be compressed into a single cylinder for economical transportation. However as explained in the experimental programme, propane was found to produce sooty deposits and react in side reactions with steam, while methane did not. Natural gas is not available in cylinders because of its low density and low value, making it uneconomical to distribute. Instead laboratory grade methane was used for the experimental programme described, which has a much higher methane purity than natural gas but is also much more expensive.

The cost of natural gas is most affordable when supplied via domestic gas pipes as opposed to requiring gas cylinder rental and delivery costs. The average cost of gas to the manufacturing industry in the UK in the first quarter of 2016 was 1.643 pence/kWh, down from 2.474 p/kWh two years earlier (DECC, 2016d). This method of supply was used in the costing in Table 7-3, as it is also the most convenient for the majority of locations that have access to a mains supply.

7.6.3.3 Cost of Gasification Feedstock

The next largest expense in Table 7-3 is the coal feedstock. The coal chosen had a high calorific value owing to its high fixed carbon and low ash. The cost of coal has also reduced over recent years to 0.883 p/kWh on average to UK industry, down from 1.086 p/kWh in early 2014 (DECC, 2016c). The costing was based on the coal flow used in Run A2, though the low coal conversion indicated that unreacted coal could be recycled in the process to improve conversion and economics.

The entrainment of coal particles has also been mentioned; an efficient dust capture system would be required on a commercial system, which would also assist in increasing feedstock recycle rates.

The Latvian softwood char was found to yield higher concentrations of H₂ and CO in the product, giving a more valuable product from a lower value feedstock. This char is produced as a by-product of an existing power process and has a much lower specification making it very low cost. If incorporated into the existing process it would constitute essentially free feedstock. It can also fall into the category of energy from waste as at time of writing there is no use for this by-product, which improves the green credentials of the gasification process.

The economics of using the softwood char in place of coal would depend on the cost and availability of the char. If the present gasification system were located at the char production site it could be assumed that there is no cost associated with this feedstock. The product gas was also found to have a higher CV than in the coal cases; in Run C3 the CV was calculated to be 8.1 MJ/kg with gas produced at a rate of 17.8 kg/hr. Removing the cost of coal from Table 7-3 and increasing the dry gas output reduces the break-even price from £0.38 to £0.28 per kg, or £0.57 per kg including the capital

expense. The increase in CV of the product gas decreases the required price from 46 to 33p/kWh, which while improved from the coal scenario is still twenty times the cost of natural gas. There is also significantly more ash produced which will have an associated cost of disposal.

7.6.3.4 Cost of Alternative Steam Source

The current cost estimate is based on producing low pressure steam on site exclusively for use by the gasifier. This is not an economical system; industrial plants typically have large boilers that supply entire plants, or at least several large processes. Depending on the steam conditions required, it is most often produced at high temperatures and pressures to provide high temperature heat and/or for expansion through a turbine to produce electricity.

The current cost for steam generation from Table 7-3 totals almost £1,000 per year not including the capital cost of the generator. This is based on use of 10.5 kg/hr steam produced saturated at 8 bar, and equates to £32.6 /tonne. To meet the demand, the current generator operates intermittently at very low throughput. More economical operation can be achieved by sizing the steam generator appropriately for the process, or by using a centralised boiler shared between other processes. Because the steam requirement for the gasifier is low pressure and temperature compared to most industrial applications, it could easily make use of waste heat or steam which would otherwise be vented or condensed in other industries. If the gasifier could be installed near to a source of low pressure waste steam this could be purchased 'over-the-fence' at a much lower cost than the cost of producing it on site in low quantities.

The price of steam is not universal; it varies strongly from site to site depending on conditions and quantities consumed. Economies of scale dictate that large users can generate at a cheaper cost per tonne, and the choice of fuel also affect the cost of production (Sinnott and Towler, 2009).

7.6.4 Summary of Economic Analysis

The costing presented highlighted the major operating expenses for the gasification system at the current scale. The scale defines some expenses such as the reactant gas flows currently supplied from cylinders. While this is an appropriate arrangement for experimental use, for continuous or commercial operation a more cost effective source of gases is required. Fuel gas can conveniently be supplied from the gas main provided this is accessible; small variations in the energy content of natural gas versus pure methane can be compensated by a small increase in flow rate if required. Alternative sources of oxygen are discussed though this will continue to present a major expense at most scales of operation.

The value of the product gas was compared with natural gas on a £/kWh basis which, as stated in the Theory chapter, favours fuels with a high CV. While the gasification system is not competitive for production of fuel gas, the value of syngas is in its versatility for use in other industries such as chemicals manufacture, upgrading into liquid fuels or used to power fuel cells etc. as discussed in Section 7.6.1.

The capital expense would be proportionally lower for a large plant, following the 0.6 power law with scale up. Further development to the design was suggested in the energy balance to reduce the heat losses from the unit. However this negates one advantage of this system which is its relatively

compact size and mobility. A scaled-up system would require a different steam supply than the one used on the experimental system.

The concept of a mobile gasification system was considered for use in remote areas for gas production to power an electrical generator or motor. This system however still relies on high temperatures for worthy gas yields, and would need a suitable source of steam which appears impracticable in such a scenario. A pyrolysis system yielding volatile gases from woody biomass would likely be more suited to such an application, though the production of tars would hinder the use of product gas in an engine.

Based on the current analysis, this system would operate most economically if located on or near to an existing site with feedstock production, such as the Latvian power station site. This would allow access to shared facilities such as a steam source and ideally an oxygen generator. The production of feedstock on site would reduce or eliminates feedstock purchase and transportation costs. This would mutually benefit the existing process by consuming a low value by-product and upgrading this to a higher value fuel gas, which could be blended with the existing fuel gas system and used to augment the plant power output.

This section shows the importance of considering the economic aspects of a system early during the design phase. It was highlighted that use of a high value feedstock does not necessarily lead to a high value product; the most economical solution would be to adapt the system to fit with an existing arrangement with available facilities. The value of syngas produced in the arrangement described is currently not able to compete with natural gas as a fuel, however if gas clean-up could achieve a high purity of hydrogen this may provide an additional market for the product in the gasifier.

Continued development of the process will also aim to improve the economic potential by improving the syngas quality and yield, reducing losses to reduce fuel demand and recycling unused solids and steam. Section 7.2.1 considers the steam flame composition in other similar works, noting that substoichiometric oxygen is often used in the burner environment to produce the high temperature steam. Reducing the oxygen flow can improve the process economics by increasing the concentrations of H₂ and CO in the product and reducing the CO₂ concentration, thereby increasing the heating value and financial value of the product. This method has the added advantage of reducing the operational cost of oxygen supplied. Further development is required to identify the optimum amount of oxygen to maximise product yield without compromising reactor temperature.

7.7 Considerations for System Scale Up

It has been shown that the economics of the USS gasification system presented in this work could be improved at a larger scale. Several benefits are expected with economy of scale, described briefly in this section.

The current scale of the system was designed for a large laboratory or for semi-permanent installation off-grid to produce fuel for a modified gas engine. This application is described in detail elsewhere (Swithenbank and Sharifi, 2013) but did not progress beyond the concept and initial laboratory tests. With increasing scale, the throughput of the unit can be increased as appropriate to the application. Many existing power plant facilities are built on very large scale to minimise capital expense per unit of output and produce electricity as cheaply as possible. Economic analysis of the

7. DISCUSSION AND EVALUATION

present system has indicated that operation alongside other industries which can produce feedstock as a by-product would be most appropriate. The existing material supplier, described in Section 5.2 produces sufficient volumes of feedstock likely to support a small to medium scale commercial unit depending on the frequency of operation. Continuous operation is favoured where possible to allow the unit to reach a stable operating temperature for consistent production.

Increasing the reactor width is expected to reduce heat losses from the gasifier by reducing the surface area to volume ratio. In the present work the walls of the burner quartz were observed to glow red during operation, suggesting a large amount of heat was absorbed by the refractory walls. It was postulated in Section 6.3.1 that this had the beneficial effect of increasing the radiation incident on particles passing through this space. However it is expected that any reduction in radiation from the quartz could be compensated for through the increased gas temperatures achieved by reducing the heat lost through the refractory wall. The existing simulation work could be extended to identify the optimum reactor width for a given rated capacity in order to optimise the scaled reactor design.

A longer reactor would increase residence time of gases and particles, as described in the literature and theory chapters as well as the simulation and experimental analysis. The existing reactor has a length of 1300 mm which could be extended using additional modules of the same length, since the reactor was constructed from a standard mild steel pipe outer shell. However an appropriate length to diameter ratio should be maintained to ensure suitable flow characteristics, which would require an increase in both length and diameter.

As the chamber size is increased the gas flow pattern will be affected owing to the distribution of inlets, outlets and dead zones. The current burner is a commercially available dual fuel model modified to accommodate granulated feed into the centre of the flame. This is located within a quartz for flame stability. At larger scale a larger burner could be used, or it may be appropriate to use more than one; diametrically opposed burners are used in several existing gasification systems described in Section 2.2.3. A swirl burner could be considered in order to increase the contact between gas and particles, facilitate ignition and maintain flame stability. Any such modifications would benefit from additional CFD modelling to optimise the geometry and the reactant ratios such as the equivalence ratio (ER).

An appropriate development pathway for this gasification system would be to design a system at a scale appropriate to the rate of production of waste char. The existing CHP system which provided the char for the present work is at the 1 MW scale, composed of around 20 smaller modules of 45 kW each using 45 kg/hr of wood chips. The plant currently produces around 40 tonnes of char per week. Assuming 24 operation, this equates to 238 kg/hr of char. The present experimental system was able to process up to 5 kg/hr which is expected to increase if continuous operation was employed. The scale of mass flow would need to be around fifty times greater to accept all of this material, which would require substantial increase in reactor volume.

As with the parent CHP plant, a modular design may be appropriate. This has the added advantage that individual modules can be taken offline for maintenance without interrupting the supply. A modular design would allow the system to be adapted for use at varying scales more easily, in order to match with the needs of the application. Due to the variable quality of waste biomass feeds the rates of heat input will vary considerably across applications, industries and producers. The ability to

adapt to the nature of the feedstock is integral to the success of this enterprise. Different configurations of reactors could be simulated to find the most cost effective approach, before validating the model findings using a larger pilot scale plant.

Continuous operation is a major milestone which can be attempted first with the laboratory scale system. Key outcomes will include what stable working temperature is achieved in the reactor walls and how this affects the maximum throughput of the system. Current experimental tests were below the maximum throughput of the system in order to conserve materials and allow multiple tests in a short time frame. Increasing the throughput and establishing a natural, stable operating point are the next objectives for the process development. This would be done in parallel with the simulation work to continue to compare the experimental performance with the predicted yields. The amount of heat loss during continuous operation can also be monitored with measures taken to limit this where possible. The condition of any ash deposition should also be closely monitored to verify that this does not become an operational obstacle under prolonged elevated temperatures.

Several existing gasification systems operate at elevated pressure. The primary advantage, other than to the process chemistry for tailoring the product yield, is that the product gases exit the process at elevated pressure which reduces the subsequent compressions costs. This is particularly important for processes which intent to feed gases into a pipeline or the gas grid, for example. Higher temperatures can also be achieved.

Pressurised operation requires the reactants to be fed accordingly. If steam is drawn from a neighbouring process this must be matched to the gasifier pressure. Solids feeding presents a challenge for pressurised operation; some existing coal gasifiers use slurry as this can more easily be pumped to meet the process requirements. The present screw feed mechanism would not be suitable for larger scale or pressurised operation and would need to be redesigned. During the experimental programme, any attempt to restrict the gas outlet in order to produce back pressure caused instabilities to develop in the burner. This would require further research to avoid operational issues if pressurised operation were to be pursued.

7.7.1 Competing Technologies

Any potential commercial enterprise should consider other similar technologies available. This system is intended to produce hydrogen gas from sustainable sources, where possible making use of by-product or waste feed sources. Presently, the primary source of global hydrogen is from steam methane reforming as this is the most economical production method. It benefits from being a reliable established and proven technology, with abundant and affordable feedstock. However as a fossil fuel based technology it is susceptible to volatile market conditions and is not sustainable in the long term. As discussed in Section 1.7 such proven technologies may be used to establish and extend hydrogen markets, such as for the Leeds Gateway H21 project and hydrogen vehicle fuel networks. These are considered likely to create additional demand for sustainable hydrogen in the future which can be exploited by developing technologies.

Other hydrogen producing technologies include electrolysis, digestion and various gasification technologies as described in Section 2.4. Many of these can benefit from a variety of feedstocks including sustainable materials. Electrolysis must be powered by renewable electricity in order for the hydrogen product to be considered renewable. Wind turbines which produce excess electricity

can be used to power electrolysis of water in order to produce hydrogen as a storable, on-demand fuel. Electrolysis releases oxygen as a by-product, which is currently not exploited but could potentially be collected and marketed. There is potential for some synergy with a gasification system which could make use of this by-product oxygen to reduce costs.

Technologies which can be used to dispose of waste materials include direct incineration, staged combustion, digestion and gasification. Direct incineration is simplest and widely used for disposal of municipal waste. It is widely used in other European countries but encounters public resistance in the UK due to the perceived risks of pollution (see Section 1.3.4). Facilities using more sophisticated technologies such as gasification may be more acceptable. Digestion is suited to high moisture materials and lends itself to production of fuel gases such as methane. Digestion is being used for waste food disposal but the rate of energy recovery is much lower than for thermal technologies. There are relatively few technologies which are suited to treating high ash or hazardous materials, which indicates a market sector which can be exploited by the present USS gasification technology.

7.7.2 Process Safety

An important consideration for any system is the safety of the users and the surrounding environment. A commercial or industrial scale system will be subject to industry certification and is unlikely to be built unless the appropriate standards are satisfied. Potential hazards identified in the present system include the USS flame which can reach temperatures up to 2760°C (Lewis, 2007) with a colourless flame which can be more difficult to detect. Gasification processes produce varying quantities of carbon monoxide as a product which is a known asphyxiant and should be monitored for leaks. The feedstocks and any residual solids can contain traces of heavy metals, PAHs and other toxic species which should be contained to avoid unnecessary distribution or leakage. To promote inherent safety, stockpiles of harmful substances should be kept to a minimum which removes the possibility of any uncontrolled releases.

The USS system relies on a supply of oxygen to produce the high temperatures required. As discussed in the economic analysis, this presents one of the major operating expenses at all conceived scales. Oxygen presents a potential hazard as it can exacerbate a fire, so should be kept isolated from any sources of ignition or fuel. At large scales, oxygen is likely to be produced by an air separator which will produce oxygen on demand and avoid the need to store large quantities on site.

Processing of biomass and chars, as well as residual ashes will produce dust which should be contained as much as possible to minimise respiratory problems for surrounding populations. Dust deposition in the surrounding environment can cause damage to leaves and waterways. Effective dust capture systems should be employed to prevent entrained particulates from the gasifier from entering the atmosphere. For hot gases, ceramic candle filters are often used to avoid the need to cool the gases which can reduce process efficiency. Collected unburned dusts can be recycled to the process; ashes should be disposed of in a responsible manner which will depend on their composition. Use of ashes for catalysis of less reactive gasification feedstocks was discussed above.

Maintenance of the scaled up systems should be considered at the design stage. If burners are likely to require maintenance or cleaning, accessibility to maintenance personnel should be considered to avoid potentially hazardous conditions for operatives wherever possible. This can include ladders and platforms where appropriate, and sufficient insulation from high temperature regions. Modular

design of reactors using standard pipe sizes and components will facilitate maintenance and replacement, which will assist in prolonging the service lifetime of the unit.

Operation at elevated pressure presents an additional hazard for potential leaks. The reactor and pipe work should be rated to the appropriate pressures and pressure relief should be incorporated into the design such that the rated pressures are not exceeded in sensitive areas. Adequate ventilation should be provided and excess flammable gases should be flared if they cannot be safely contained to prevent accumulation. Entrained flow systems benefit from having relatively low loadings in the reactor at any one time which gives high controllability. In the event of a problem, reactant supply can be ceased quickly to mitigate problems downstream.

The production of highly flammable product gases rich in hydrogen presents an explosion risk. The volumes of flammable gases stored on site should be kept to a minimum and ideally consumed or exported as soon after production as possible. The reactor should be flushed to prevent build up of flammable gases after operation and good housekeeping upheld to prevent dust accumulation which can cause dust explosions. It is expected that the operation of such a gasification unit should be no more hazardous than existing large scale gasification or reforming plants. Appropriate containment and hazard management facilities should be put in place to mitigate the effects of any incidents that can occur. These can be more fully identified using typical safety tools such as a HAZOP, to identify potential hazards before they occur. These will be particular to individual sites.

7.8 Industrial Applications

Some wider implications are evident from this work, beyond purely academic interest. The greater reactivity of biochar over coal chars has been documented, which has implications for the reaction time and the size of equipment required for processing. The factors affecting this reactivity include material structure and porosity, which are related to the char preparation prior to use. Temperature and heating rate in char formation determine char structure as well as the distribution of solid, liquid and gas products as described in Section 2.2.2.

The present work demonstrated the recovery of energy in the form of a versatile syngas from a material considered of low value. This material was considered unsuitable for use in many typical processes such as fixed or fluid bed arrangements due to the high ash content, which was found not to impede the operation of the experimental entrained flow configuration. The mineral content of the feedstock material has been shown to have a catalytic effect on devolatilisation and char burn out. Alkali metals such as potassium in particular have been shown to be particularly active in this role (Jones et al., 2007; Nowakowski et al., 2007). Further investigation is invited to determine whether the softwood ash has any potential as an additive catalyst to improve conversion of less reactive feedstocks such as coal.

Production of syngas from solid feedstocks can extend their versatility. Fuel gas can be used for power generation in typical installations or in gas engines for small scale applications, or upgraded to liquid fuels or other chemicals. Gas engines or combined cycle gas turbines have a much higher efficiency of generation compared to a typical solid fuel combustion system.

Hydrogen gas has several advantages as an urban fuel. Its use for vehicles is under continued development, while domestic and commercial buildings' electrical and heating requirements could

7. DISCUSSION AND EVALUATION

be met and via fuel cells or gas engines for increased fuel efficiency. Carbon emissions and particulate emissions are avoided at the point-of-use. This has the potential to vastly improve air quality in densely populated urban areas, and reducing fuel use overall by encouraging combined heat and power generation close to the point of use.

The present work demonstrates that conversion of biochar in a small scale gasifier can achieve energy recovery from low value waste materials. The economic analysis presented in Section 7.6 shows that the system would be most suitable on an existing industrial site to make use of low pressure steam and industrial by-products at low cost. The produced syngas can be used to offset existing fuel requirements or used for local combined heat and power needs to reduce carbon emissions while utilising by-products or waste materials.

On a commercial system the economics of the process could be improved by optimising the gasifier scale to reduce heat loss and using recycled syngas to fuel the flame, in order to make the system self-sufficient and remove fossil fuels from the process.

8 CONCLUSION

This chapter summarises the findings presented in this thesis. The main objectives were to apply the USS gasification system to a renewable biomass feedstock and compare the conversion and product yields, and to develop a process model for optimisation of the system. The objectives were successfully achieved as detailed below.

Literature Review

- Existing coal gasification processes often employ partial oxidation of coal to provide heat for the gasification chemistry. High temperature operation tends to increase gas yields. Entrained flow processes compensate for the reduced feedstock residence time with high heating rates, which allow carbon conversion generally above 97%.
- Currently there is much research into the gasification of biomass and waste materials. Allothermic systems provide heat from an external source as opposed to from combustion of the feedstock, which eliminates the need for oxygen supply to the gasifier. Steam only gasification systems showed greater hydrogen yields than air/oxygen blown systems.

Experimental Conclusions

- An experimental programme was successfully undertaken using the steam gasification system. Modifications to increase controllability and reduce fluctuation resulted in increased operational stability, allowing for autonomous continuous operation of the gasifier subject to the capacity of the feedstock hopper.
- Stoichiometric propane combustion was found to yield substantial CO and H₂ in the steam mixture before feedstock addition, attributed to steam propane reformation. Yields quoted in other similar works can contain significant contributions of these gases from fuel gas reformation as well as from feedstock gasification.
- In the present work fuel gas reformation was avoided in order to provide a basis for comparison of gasification yields. Methane was found to yield much lower traces of H₂ and CO from reformation, allowing for lean efficient operation.
- Coal and biochar were successfully gasified in the entrained flow system. Up to 34.9%mol H₂ and 25.1%mol CO were observed in product yields from the softwood char. Biochar demonstrated higher conversion and yielded richer H₂ and CO concentrations owing to greater reactivity than coal. This was in agreement with other studies in the literature.

8. CONCLUSION

- Limited comparison with a low ash softwood char indicated that the mineral content played a greater role than the material surface area in defining the greater reactivity of biochar over coal. This was supported by other literature studies.
- The reactor wall temperature was found to have a strong influence on feedstock conversion, considered to be due to the higher equilibrium temperatures and radiative interaction between walls and solid particles as demonstrated with the CFD model. This had a greater impact on product composition than the S/C ratio within the range observed.

Modelling Work

- An equilibrium model of the system confirmed that high yields of CO are expected at high reactor temperatures. It also allowed optimisation of the reactant flows; very similar experimental gas yields were achieved to previous results, despite a circa 40% reduction in coal feed.
- An investigation into the gas flow pattern, temperature distribution and particle trajectories was conducted using ANSYS FLUENT. The predicted temperature was found to be in good agreement with validation measurements, in similar agreement to other published works.
- Simulated particle residence times were found to be inversely proportional to particle size and density. Smaller particles could expect greater conversion and were also more likely to be entrained by the flue gas at the reactor exit. A comprehensive dust capture system was recommended to improve efficiency.

Wider Implications

- Promising gas yields were achieved using the experimental system. A longer reactor would allow the water gas shift to play a more significant role. With increased equipment size and insulation, this technology has the potential to produce syngas on a commercial scale.
- The high ash biochar exhibited higher conversion and richer gas yields than coal or low ash char, indicating that the ash was beneficial to feedstock conversion. Despite this high ash content, no detrimental effect on equipment was observed from ash deposition.

8.1 Recommendations for Future Work

Suggestions and opportunities for further development and investigation are given, following from the conclusions described.

- Potential exists to improve the H₂ and CO yields by increasing the gasifier size, reducing heat losses and limiting the oxygen supply. Limiting oxygen avoids combustion of feedstock and product gases and can result in reformation of the fuel gas, to enhance the syngas content.

8. CONCLUSION

- Continuous operation of the gasifier would allow higher wall temperatures to improve feedstock conversion and gas yields. Electrical heating could allow for preheating of the experimental unit.
- This work indicated that the ash content was significant to the reactivity of biochar. Further analysis is required to confirm this finding and a deeper investigation into which components within the ash contribute to this effect could also be conducted. The catalytic properties of the ash may be beneficial to unreactive feedstocks to improve conversion, as has been researched in some similar works. This would create a potential application for the high ash char which is currently a waste product.
- The residual high ash char can be analysed for levels of PAH etc. following USS gasification. High temperature treatment may break down these species to reduce their environmental impact. If the residual solids remaining after USS gasification are more benign this would facilitate their disposal compared to the existing material.
- The effects of steam addition on flame structure, radicals' concentration and reactivity could be investigated using spectrometry or other means, to determine the optimum steam mixture content for fuel efficiency.
- The FLUENT model could be developed with a user defined model to specify heterogeneous reactions. Other factors such as pore diffusion, devolatilisation and particle breakup can be included.
- With further optimisation, product gas could be recirculated to fuel the burner and avoid the need for supplementary fuel gas. This can be simulated to calculate the necessary recycle rate and purging requirements to avoid build-up of unwanted species.

9 REFERENCES

- Acharya, C.K., Jiang, F., Liao, C., Fitzgerald, P., Vecchio, K.S., Cattolica, R.J., 2013. Tar and CO₂ removal from simulated producer gas with activated carbon and charcoal. *Fuel Process. Technol.* 106, 201–208. doi:10.1016/j.fuproc.2012.07.026
- ADE, 2016. More about District Heating [WWW Document]. Assoc. Decent. Energy. URL http://www.theade.co.uk/more-about-district-heating_3592.html (accessed 6.5.14).
- Agency for Toxic Substances and Disease Registry, 1996. Polycyclic Aromatic Hydrocarbons (PAHs) [WWW Document]. ToxFAQs. URL <http://www.atsdr.cdc.gov/tfacts69.pdf> (accessed 3.24.14).
- Air Products and Chemicals Inc, 2016a. Air Products Tees Valley Renewable Energy Facility [WWW Document]. URL http://www.airproducts.co.uk/teesvalley/industrial_gas_facility.htm
- Air Products and Chemicals Inc, 2016b. Air Products Will Exit Energy-from-Waste Business [WWW Document]. URL http://www.airproducts.com/Company/news-center/2016/04/0404-air-products-will-exit-energy-from-waste-business.aspx?_ga=1.195949164.1932402347.1457719687 (accessed 4.21.16).
- Anglian Water, 2016. Anglian Water- business standard tariffs [WWW Document]. URL http://www.anglianwater.co.uk/_assets/media/Business_tariffs_2015-16.pdf (accessed 5.2.14).
- ANSYS Inc, 2010a. ANSYS FLUENT User's Guide, Release 13. ed. SAS IP, Inc.
- ANSYS Inc, 2010b. ANSYS FLUENT Theory Guide, ANSYS Inc. Canonsburg, PA.
- ASTM, 2012a. Designation: D388 – 12: Standard Classification of Coals by Rank. doi:10.1520/D0388-12.2
- ASTM, 2012b. Standard Test Method for Sampling and Fineness Test of Pulverized Coal. Des. D197 – 87 (Reapproved 2012) Stand. 1–7. doi:10.1520/D0197-87R12.2
- ASTM, 1992. Manual on Drilling, Sampling, and Analysis of Coal. ASTM International, Philadelphia.
- ASTM International, 2012. Designation: D197 – 87 (Reapproved 2012): Standard Test Method for Sampling and Fineness Test of Pulverized Coal. D197-87 1–7. doi:10.1520/D0197-87R12.2
- Atlas Copco, 2015. Atlas Copco PSA Oxygen Generators.
- Balat, H., Kirtay, E., 2010. Hydrogen from biomass – Present scenario and future prospects. *Int. J. Hydrogen Energy* 35, 7416–7426. doi:10.1016/j.ijhydene.2010.04.137
- Basu, P., 2013. Biomass Gasification, Pyrolysis and Torrefaction: Practical Design and Theory. Academic Press.
- Basu, P., 2010. Biomass Gasification and Pyrolysis: Practical Design and Theory. Academic Press.
- Basu, P., Butler, J., Leon, M.A., 2011. Biomass co-firing options on the emission reduction and electricity generation costs in coal-fired power plants. *Renew. Energy* 36, 282–288.

9. REFERENCES

doi:10.1016/j.renene.2010.06.039

- Baukal, C.E., 2003. *Industrial Burners Handbook*. CRC Press.
- Baukal, C.E., Gershtein, V.Y., Li, X., 2001. *Computational Fluid Dynamics in Industrial Combustion*. CRC Press.
- Baxter, L., 2005. Biomass-coal co-combustion: opportunity for affordable renewable energy. *Fuel* 84, 1295–1302.
- Bayarsaikhan, B., Sonoyama, N., Hosokai, S., Shimada, T., Hayashi, J., Li, C.-Z., Chiba, T., 2006. Inhibition of steam gasification of char by volatiles in a fluidized bed under continuous feeding of a brown coal. *Fuel* 85, 340–349.
- BBC News, 2016. Hinkley Point: Pressure grows at EDF - BBC News. BBC Bus. News.
- Bell, D.A., Towler, B.F., Fan, M., 2011. *Coal Gasification and Its Applications*. William Andrew.
- Bergman, T.L., Incropera, F.P., DeWitt, D.P., Lavine, A.S., 2011. *Fundamentals of Heat and Mass Transfer*. John Wiley & Sons.
- Bhuiyan, A.A., Naser, J., 2016. Thermal characterization of coal/straw combustion under air/oxy-fuel conditions in a swirl-stabilized furnace: A CFD modelling. *Appl. Therm. Eng.* 93, 639–651. doi:10.1016/j.applthermaleng.2015.10.024
- Bhutto, A.W., Bazmi, A.A., Zahedi, G., 2013. Underground coal gasification: From fundamentals to applications. *Prog. Energy Combust. Sci.* 39, 189–214. doi:10.1016/j.pecs.2012.09.004
- Bibrzycki, J., Mancini, M., Szlęk, A., Weber, R., 2016. A char combustion sub-model for CFD-predictions of fluidized bed combustion - experiments and mathematical modeling. *Combust. Flame* 163, 188–201. doi:10.1016/j.combustflame.2015.09.024
- Bilitewski, B., Härdtle, G., Marek, K., 1997. *Waste Management*. Springer.
- Biomass Energy Centre, 2011. Sources of biomass [WWW Document]. URL http://www.biomassenergycentre.org.uk/portal/page?_pageid=75,15174&_dad=portal&_schema=PORTAL (accessed 7.14.14).
- Biswas, P., 2009. Water Use and Re-Use in Energy Technologies in a Carbon Constrained World, in: Yang, J. (Ed.), *Proceedings of the First National Expert and Stakeholder Workshop on Water Infrastructure Sustainability and Adaptation to Climate Change*. DIANE Publishing, pp. 56–57.
- Borghini, R., Destriau, M., Soete, G. De, 1998. *Combustion and Flames*. Editions Technip, Paris.
- Bowen, B.H., Irwin, M.W., 2008. COAL CHARACTERISTICS - CCTR Basic Facts File # 8 [WWW Document]. URL <http://www.purdue.edu/discoverypark/energy/assets/pdfs/cctr/outreach/Basics8-CoalCharacteristics-Oct08.pdf> (accessed 2.19.14).
- BP, 2016. *BP Energy Outlook 2016*.
- Bratek, K., Bratek, W., Gerus-Piasecka, I., Jasieńko, S., Wilk, P., 2002. Properties and structure of different rank anthracites. *Fuel* 81, 97–108. doi:10.1016/S0016-2361(01)00120-X
- Bridgwater, A.V., 2012. Review of fast pyrolysis of biomass and product upgrading. *Biomass and Bioenergy* 38, 68–94.

9. REFERENCES

- BTG-BTL, 2016. BTG-BTL Pyrolysis process [WWW Document]. URL <http://www.btg-btl.com/en/technology> (accessed 4.28.16).
- Bulutoglu, P.S., Koc, S., Avci, A.K., 2016. Simulation of exhaust gas reforming of natural gas in a microchannel reactor. *Int. J. Hydrogen Energy* 41, 8184–8192. doi:10.1016/j.ijhydene.2015.10.126
- Casper, J.K., 2010. *Greenhouse Gases: Worldwide Impacts*. Infobase Publishing.
- Cempa-Balewicz, M., Łączny, M.J., Smoliński, A., Iwaszenko, S., 2013. EQUILIBRIUM MODEL OF STEAM GASIFICATION OF COAL, x. *J. Sustain. Min.* 12, 21–28.
- CEWEP, 2012. Municipal waste treatment in 2012 [WWW Document]. Confed. Eur. Waste to Energy Plants - Graph Eur. Waste Manag. URL http://www.cewep.eu/information/data/graphs/m_1217 (accessed 5.4.16).
- Chalmers, H., Gibbins, J., 2007. Initial evaluation of the impact of post-combustion capture of carbon dioxide on supercritical pulverised coal power plant part load performance. *Fuel* 86, 2109–2123. doi:10.1016/j.fuel.2007.01.028
- Chang, A.C.C., Chang, H.-F., Lin, F.-J., Lin, K.-H., Chen, C.-H., 2011. Biomass gasification for hydrogen production. *Int. J. Hydrogen Energy* 36, 14252–14260.
- Chen, S.G., Yang, R.T., 1997. Unified Mechanism of Alkali and Alkaline Earth Catalyzed Gasification Reactions of Carbon by CO₂ and H₂O. *Energy & Fuels* 11, 421–427. doi:10.1021/ef960099o
- Chen, X., Tang, J., Tian, X., Wang, L., 2015. Influence of biomass addition on Jincheng coal ash fusion temperatures. *Fuel* 160, 614–620. doi:10.1016/j.fuel.2015.08.024
- Chen, Y., Guo, L., Cao, W., Jin, H., Guo, S., Zhang, X., 2013. Hydrogen production by sewage sludge gasification in supercritical water with a fluidized bed reactor. *Int. J. Hydrogen Energy* 38, 12991–12999.
- Cheng, X., Ng, H.K., Gan, S., Ho, J.H., Pang, K.M., 2015. Development and validation of a generic reduced chemical kinetic mechanism for CFD spray combustion modelling of biodiesel fuels. *Combust. Flame* 162, 2354–2370. doi:10.1016/j.combustflame.2015.02.003
- Chigier, N., 1991. *Combustion Measurements*. CRC Press.
- Clarke Energy, n.d. Synthesis gas, (syngas), producer gas use in gas engines [WWW Document]. URL <http://www.clarke-energy.com/gas-type/synthesis-gas-syngas/> (accessed 5.16.14).
- Clean Energy Council (Australia), 2013. Renewable Energy Target [WWW Document]. URL <http://www.cleanenergycouncil.org.au/policyadvocacy/Renewable-Energy-Target.html> (accessed 10.10.13).
- COP21, n.d. COP21 | More details about the agreement [WWW Document]. URL <http://www.cop21.gouv.fr/en/more-details-about-the-agreement/> (accessed 4.5.16).
- Cortés, C.G., Tzimas, E., Peteves, S.D., 2009. *Technologies for Coal based Hydrogen and Electricity Co-production Power Plants with CO₂ Capture*. Luxembourg.
- Cotton, A., Patchigolla, K., Oakey, J.E., 2013. Overview of, and Experimental Methodology for, Sorption Enhanced Hydrogen Production. *Energy Procedia* 37, 2232–2244. doi:10.1016/j.egypro.2013.06.104

9. REFERENCES

- Craven, J.M., Swithenbank, J., Sharifi, V.N., Peralta-Solorio, D., Kelsall, G., Sage, P., 2014. Development of a novel solids feed system for high pressure gasification. *Fuel Process. Technol.* 119, 32–40. doi:10.1016/j.fuproc.2013.10.016
- Cuoci, A., Frassoldati, A., Faravelli, T., Ranzi, E., Candusso, C., Tolazzi, D., 2010. CFD simulation of a turbulent oxy-fuel flame, in: *Processes and Technologies for a Sustainable Energy2*. Ischia. doi:10.4405/ptse2010.VII4
- Danish Board of District Heating (DBDH), n.d. District heating – Danish and Chinese experience. Frederiksberg.
- Danish Energy Authority, 2005. Heat Supply in Denmark Who What Where and - Why. The Danish Energy Authority, Copenhagen.
- Dawson, B., Spannagle, M., 2008. *The Complete Guide to Climate Change*. Routledge.
- Dayton, D., 2002. A Review of the Literature on Catalytic Biomass Tar Destruction: Milestone Completion Report NREL/TP-510-32815. Golden, CO.
- DECC, 2016a. Energy Trends: electricity, Energy Trends. London.
- DECC, 2016b. What the Government is doing to secure investment in clean, secure and affordable energy - News stories - GOV.UK [WWW Document]. UK Energy Secur. URL <https://www.gov.uk/government/news/what-the-government-is-doing-to-secure-investment-in-clean-secure-and-affordable-energy> (accessed 4.7.16).
- DECC, 2016c. QUARTERLY ENERGY PRICES - 30 June 2016. London.
- DECC, 2016d. Prices of fuels purchased by manufacturing industry - Statistical data sets - GOV.UK [WWW Document]. Ind. energy price Stat. URL <https://www.gov.uk/government/statistical-data-sets/prices-of-fuels-purchased-by-manufacturing-industry> (accessed 9.6.16).
- DECC, 2015. Large Combustion Plant Directive (LCPD): Running hours during winter 2014/15 and capacity for 2015/16 [WWW Document]. Energy Trends Spec. Featur. – Large Combust. Plant Dir. URL https://www.gov.uk/government/uploads/system/uploads/attachment_data/file/462364/LCPD.pdf
- DECC, 2013a. Calorific values - GOV.UK [WWW Document]. Estim. Aver. calorific values fuels. URL <https://www.gov.uk/government/collections/calorific-values> (accessed 7.14.14).
- DECC, 2013b. Running hours during winter 2012/13 for plants opted-out of the Large Combustion Plant Directive (LCPD) [WWW Document]. Energy Trends Spec. Featur. – Large Combust. Plant Dir. URL https://www.gov.uk/government/uploads/system/uploads/attachment_data/file/249685/3_lcpd_running_hours_2012_13.pdf (accessed 10.1.16).
- DECC, 2013c. The Renewables Obligation (RO) [WWW Document]. Increasing use low-carbon Technol. URL <https://www.gov.uk/government/policies/increasing-the-use-of-low-carbon-technologies/supporting-pages/the-renewables-obligation-ro>
- DECC, 2013d. UK Renewable Energy Roadmap Update 2013. London.
- DECC, 2011. UK Renewable Energy Roadmap URN 11D/698. London.
- DECC, CCC, DEFRA, DFT, 2013. Reducing the UK's greenhouse gas emissions by 80% by 2050 - Policy -

9. REFERENCES

- GOV.UK [WWW Document]. URL <https://www.gov.uk/government/policies/reducing-the-uk-s-greenhouse-gas-emissions-by-80-by-2050>
- DEFRA, 2013. Reducing and managing waste - Policy - GOV.UK [WWW Document]. URL <https://www.gov.uk/government/policies/reducing-and-managing-waste>
- Demirbaş, A., 2003. Sustainable cofiring of biomass with coal. *Energy Convers. Manag.* 44, 1465–1479.
- Department for Business Energy & Industrial Strategy, 2016. Renewable sources of energy: Chapter 6, Digest of United Kingdom Energy Statistics (DUKES) - Publications - GOV.UK [WWW Document]. URL <https://www.gov.uk/government/statistics/renewable-sources-of-energy-chapter-6-digest-of-united-kingdom-energy-statistics-dukes> (accessed 9.30.16).
- DeSá, D.O.J., 2001. Instrumentation Fundamentals for Process Control. Taylor & Francis, London.
- Di Blasi, C., 2009. Combustion and gasification rates of lignocellulosic chars. *Prog. Energy Combust. Sci.* 35, 121–140. doi:10.1016/j.pecs.2008.08.001
- Di Blasi, C., 1996. Kinetic and Heat Transfer Control in the Slow and Flash Pyrolysis of Solids. *Ind. Eng. Chem. Res.* 35, 37–46. doi:10.1021/ie950243d
- Dones, R., Heck, T., Hirschberg, S., 2004. GREENHOUSE GAS EMISSIONS FROM ENERGY SYSTEMS : COMPARISON AND OVERVIEW. *Encycl. Energy* 3, 77–95. doi:10.1016/B0-12-176480-X/00397-1
- Dong, Y., Borgwardt, R.H., 1998. Biomass reactivity in gasification by the hynol process. *Energy & Fuels* 12, 479–484. doi:10.1021/ef970127i
- Döring, S., 2012. Power from Pellets: Technology and Applications. Springer, Berlin.
- Drax, 2014. Our biomass plans | Drax [WWW Document]. URL <http://www.drax.com/biomass/our-biomass-plans/> (accessed 6.9.14).
- Duman, G., Uddin, M.A., Yanik, J., 2014. The effect of char properties on gasification reactivity. *Fuel Process. Technol.* 118, 75–81. doi:10.1016/j.fuproc.2013.08.006
- ECN, 2011. Milena Technology: MILENA Biomass gasification process [WWW Document]. URL <http://www.milenatechnology.com/> (accessed 4.22.16).
- ECN, n.d. Phyllis2 - ECN Phyllis classification [WWW Document]. ECN Phyllis Classif. URL <https://www.ecn.nl/phyllis2/Browse/Standard/ECN-Phyllis> (accessed 7.18.16).
- EIA, 2016a. Average Power Plant Operating Expenses for Major U.S. Investor-Owned Electric Utilities, 2004 through 2014 [WWW Document]. *Electr. Power Annu.* URL <http://www.eia.gov/electricity/annual/> (accessed 4.7.16).
- EIA, 2016b. International Energy Statistics - EIA [WWW Document]. URL <http://eia.doe.gov/cfapps/ipdbproject/IEDIndex3.cfm?tid=1&pid=7&aid=1> (accessed 4.8.16).
- EIA, 2015. Levelized Cost and Levelized Avoided Cost of New Generation Resources.
- Emerson Process Management, 2009. Rosemount 8800 Vortex: Adaptive Digital Signal Processing [WWW Document]. Tech. Note 00840-0200-4004, Rev AA. URL http://www2.emersonprocess.com/siteadmincenter/PM_Rosemount_Documents/00840-0200-4004.pdf (accessed 4.1.14).

9. REFERENCES

- Encinar, J.M., González, J.F., Rodríguez, J.J., Ramiro, M.J., 2001. Catalysed and uncatalysed steam gasification of eucalyptus char: influence of variables and kinetic study. *Fuel* 80, 2025–2036. doi:10.1016/S0016-2361(01)00073-4
- Encyclopedia Britannica, 2014. Coal (fossil fuel):: Chemical content and properties [WWW Document]. Encycl. Br. Online. URL <http://www.britannica.com/EBchecked/topic/122863/coal/50682/Chemical-content-and-properties> (accessed 7.14.14).
- Energos, 2016. Proven advanced thermal conversion technology | ENERGOS [WWW Document]. URL <http://www.energ-group.com/energy-from-waste/the-process/> (accessed 4.28.16).
- Energy Storage Association, 2016. Liquid Air Energy Storage (LAES) | Energy Storage Association [WWW Document]. URL <http://energystorage.org/energy-storage/technologies/liquid-air-energy-storage-laes> (accessed 4.15.16).
- EnertecGreen, n.d. Green Concept: EnertecGreen [WWW Document]. URL <http://www.enertecgreen.com/en/green-concept/> (accessed 3.24.14).
- Environment Agency, 2013. Waste: incineration and energy recovery [WWW Document]. URL <http://www.environment-agency.gov.uk/business/sectors/143711.aspx> (accessed 11.18.13).
- EPA, U., 2010. Amendments to the Montreal Protocol | Ozone Layer Protection [WWW Document]. URL <http://www.epa.gov/ozone/intpol/history.html> (accessed 11.12.13).
- Erkiaga, A., Lopez, G., Amutio, M., Bilbao, J., Olazar, M., 2014. Influence of operating conditions on the steam gasification of biomass in a conical spouted bed reactor. *Chem. Eng. J.* 237, 259–267. doi:10.1016/j.cej.2013.10.018
- Erkiaga, A., Lopez, G., Amutio, M., Bilbao, J., Olazar, M., 2013. Steam gasification of biomass in a conical spouted bed reactor with olivine and γ -alumina as primary catalysts. *Fuel Process. Technol.* 116, 292–299. doi:10.1016/j.fuproc.2013.07.008
- ETI, 2016. Waste Gasification « ETI [WWW Document]. Bioenergy. URL <http://www.eti.co.uk/project/waste-gasification/> (accessed 4.28.16).
- European Commission, 2016. The Industrial Emissions Directive - Environment - European Commission [WWW Document]. URL <http://ec.europa.eu/environment/industry/stationary/ied/legislation.htm> (accessed 4.13.16).
- European Commission, 2013. EU ETS: continuing decline in emissions but growing surplus of allowances in 2012 - European Commission [WWW Document]. Clim. Action Newsroom. URL http://ec.europa.eu/clima/news/articles/news_2013051601_en.htm
- European Commission, 2012. Large Combustion Plant Directive [WWW Document]. URL <http://ec.europa.eu/environment/air/pollutants/stationary/lcp/legislation.htm> (accessed 10.8.13).
- European Environment Agency (EEA), 2009. Europe's onshore and offshore wind energy potential [WWW Document]. URL <http://www.eea.europa.eu/publications/europes-onshore-and-offshore-wind-energy-potential> (accessed 6.5.14).
- European Union, 2001. Directive 2001/80/EC of the European Parliament and of the Council of 23 October 2001 on the limitation of emissions of certain pollutants into the air from large combustion plants.

9. REFERENCES

- Fang, X., Jia, L., 2012. Experimental study on ash fusion characteristics of biomass. *Bioresour. Technol.* 104, 769–774. doi:10.1016/j.biortech.2011.11.055
- Fives North American Combustion Inc., 2013. Bulletin 6422 Burner Specification.
- Foong-Kheong, Y., Sundram, K., Basiron, Y., 2014. Palm Oil Biofuel: Its Sustainability, Direct and Indirect Land Use Effects, in: 7th Biofuels International Conference. Ghent.
- Funk, J.E., Reinstrom, R.M., 1966. Energy Requirements in Production of Hydrogen from Water. *Ind. Eng. Chem. Process Des. Dev.* 5, 336–342.
- Gao, N., Li, A., Quan, C., Gao, F., 2008. Hydrogen-rich gas production from biomass steam gasification in an updraft fixed-bed gasifier combined with a porous ceramic reformer. *Int. J. Hydrogen Energy* 33, 5430–5438.
- Gikas, P., 2014. Electrical energy production from biosolids: a comparative study between anaerobic digestion and ultra-high-temperature gasification. *Environ. Technol.* 35, 2140–2146. doi:10.1080/09593330.2014.895049
- Gil, J., Corella, J., Aznar, M.P., Caballero, M.A., 1999. Biomass gasification in atmospheric and bubbling fluidized bed: Effect of the type of gasifying agent on the product distribution. *Biomass and Bioenergy* 17, 389–403.
- Glassman, I., Yetter, R.A., 2008. *Combustion*, 4th ed. Academic Press.
- Global CCS Institute, 2013. *The Global Status of CCS 2013: Summary report*.
- Goldman, J., Xieu, D., Oko, A., Milne, R., Essenhigh, R.H., 1984. A comparison of prediction and experiment in the gasification of anthracite in air and oxygen - enriched/ steam mixtures, in: Twentieth Symposium (International) on Combustion. The Combustion Institute, pp. 1365–1372.
- Green, D.W., Perry, R.H., 2008. *Perry's Chemical Engineers' Handbook*, Eighth Edition, 8th ed. McGraw Hill Professional.
- Grimes, C.A., Varghese, O., Ranjan, S., 2008. *Light, Water, Hydrogen: The Solar Generation of Hydrogen by Water Photoelectrolysis*. Springer.
- GSTC, 2016. Gasification & Syngas Technologies Council > The Gasification Industry [WWW Document]. URL <http://www.gasification-syngas.org/resources/the-gasification-industry/> (accessed 4.29.16).
- Gupta, M., Yang, J., Roy, C., 2003. Specific heat and thermal conductivity of softwood bark and softwood char particles. *Fuel* 82, 919–927. doi:10.1016/S0016-2361(02)00398-8
- Gupta, M., Yang, J., Roy, C., 2002. Density of softwood bark and softwood char: procedural calibration and measurement by water soaking and kerosene immersion method. *Fuel* 81, 1379–1384. doi:10.1016/S0016-2361(02)00043-1
- Hagos, F.Y., Aziz, a. R. a., Sulaiman, S.A., 2014. Trends of Syngas as a Fuel in Internal Combustion Engines. *Adv. Mech. Eng.* 2014, 1–10. doi:10.1155/2014/401587
- Hankalin, V., Ahonen, T., Raiko, R., 2009. On Thermal Properties of a Pyrolysing Wood Particle, in: Finnish-Swedish Flame Days 2009. Finnish Flame Research Committee, Naantali, Finland.
- He, C., Feng, X., Chu, K.H., 2013. Process modeling and thermodynamic analysis of Lurgi fixed-bed

9. REFERENCES

- coal gasifier in an SNG plant. *Appl. Energy* 111, 742–757. doi:10.1016/j.apenergy.2013.05.045
- Hernández, J.J., Ballesteros, R., Aranda, G., 2013. Characterisation of tars from biomass gasification: Effect of the operating conditions. *Energy* 50, 333–342. doi:10.1016/j.energy.2012.12.005
- Herrmann, U., Kelly, B., Price, H., 2004. Two-tank molten salt storage for parabolic trough solar power plants. *Energy* 29, 883–893. doi:10.1016/S0360-5442(03)00193-2
- Higman, C., van der Burgt, M., 2008. *Gasification*, Second Edition. Gulf Professional Publishing.
- Higman, C., Van der Burgt, M., 2003. *Gasification*. Gulf Professional Publishing.
- Hla, S.S., Harris, D.J., Roberts, D.G., 2006. CFD Modelling for an Entrained Flow Gasification Reactor Using Measured “Intrinsic” Kinetic Data 1–7.
- Hla, S.S., Roberts, D.G., Harris, D.J., 2015. A numerical model for understanding the behaviour of coals in an entrained-flow gasifier. *Fuel Process. Technol.* 134, 424–440. doi:10.1016/j.fuproc.2014.12.053
- Hlebak, J.J., 2011. *Equilibrium Modeling, Design, Construction, and Validation Testing of a Pilot Scale, USS Gasification Reactor*. MSc Thesis. University of Ohio. doi:10.1017/CBO9781107415324.004
- Holz Kraft, 2016. *Spanner Re2 Wood cogeneration plant [WWW Document]*. URL <http://www.holz-kraft.de/en/products/wood-cogeneration-plant-hv> (accessed 1.21.16).
- Howe, W.H., Lipták, B.G., 2003. Orifices, in: Lipták, B. (Ed.), *Instrument Engineers’ Handbook, Fourth Edition, Volume One: Process Measurement and Analysis*. CRC Press, p. 1920.
- IEA, 2016. *Key World Energy Statistics 2016*.
- IEA, 2011. *WORLD ENERGY OUTLOOK*. Paris.
- IEA, 2010. *Coal information 2010: with 2009 data*. The Stationery Office.
- IEA/ETSAP, 2010. *Technology Brief E02 – Gas-Fired Power*.
- Iliuta, I., Leclerc, A., Larachi, F., 2010. Allothermal steam gasification of biomass in cyclic multi-compartment bubbling fluidized-bed gasifier/combustor – New reactor concept. *Bioresour. Technol.* 101, 3194–3208.
- Iniesta, E., Sánchez, F., García, A.N., Marcilla, A., 2001. Influence of the holding temperature of the first heating step in a two-heating step carbonisation process on the properties of chars and activated carbons from almond shells. *J. Anal. Appl. Pyrolysis* 58–59, 967–981. doi:10.1016/S0165-2370(00)00202-3
- IPCC, 2007. Contribution of Working Group I to the Fourth Assessment Report of the Intergovernmental Panel on Climate Change, in: Solomon, S., Qin, D., Manning, M., Chen, Z., Marquis, M., Averyt, K.B., Tignor, M., Miller, H.L. (Eds.), *Climate Change 2007 The Physical Science Basis*. Cambridge University Press, p. 996.
- IPCC, 1996. *Climate Change 1995, The Science of Climate Change*.
- Jachimowski, C.J., 1984. Chemical kinetic reaction mechanism for the combustion of propane. *Combust. Flame* 55, 213–224. doi:10.1016/0010-2180(84)90029-4
- Jennings, W., 2012. *Analytical Gas Chromatography*. Elsevier Science.

9. REFERENCES

- Jin, H., Lu, Y., Liao, B., Guo, L., Zhang, X., 2010. Hydrogen production by coal gasification in supercritical water with a fluidized bed reactor. *Int. J. Hydrogen Energy* 35, 7151–7160.
- Jones, J.M., Darvell, L.I., Bridgeman, T.G., Pourkashanian, M., Williams, a., 2007. An investigation of the thermal and catalytic behaviour of potassium in biomass combustion. *Proc. Combust. Inst.* 31 II, 1955–1963. doi:10.1016/j.proci.2006.07.093
- Jones, W.P., Lindstedt, R.P., 1988. Global reaction schemes for hydrocarbon combustion. *Combust. Flame* 73, 233–249.
- Kantarelis, E., Donaj, P., Yang, W., Zabaniotou, A., 2009. Sustainable valorization of plastic wastes for energy with environmental safety via High-Temperature Pyrolysis (HTP) and High-Temperature Steam Gasification (HTSG). *J. Hazard. Mater.* 167, 675–684.
- Kelly-Yong, T.L., Lee, K.T., Mohamed, A.R., Bhatia, S., 2007. Potential of hydrogen from oil palm biomass as a source of renewable energy worldwide. *Energy Policy* 35, 5692–5701. doi:10.1016/j.enpol.2007.06.017
- Klein, S., Nellis, G., 2011. *Thermodynamics*. Cambridge University Press.
- Kohse-Hoinghaus, K., Jeffries, J.B., 2002. *Applied Combustion Diagnostics*. CRC Press.
- Koroll, G.W., Mulpuru, S.R., 1986. THE EFFECT OF DILUTION WITH STEAM ON THE BURNING VELOCITY AND STRUCTURE OF PREMIXED HYDROGEN FLAMES, in: *Twenty-First Symposium (International) on Combustion/The Combustion Institute*. pp. 1811–1819.
- Krutka, H., Sjostrom, S., Bustard, C., Durham, M., Baldrey, K., Stewart, R., 2008. Summary of Post-Combustion CO₂ Capture Technologies for Existing Coal-Fired Power Plants 1–10.
- Lahti Energia, 2012. Power plant technology / Lahti Energia [WWW Document]. URL <http://www.lahtigasification.com/power-plant/power-plant-technology> (accessed 4.29.16).
- Lee, S., Speight, J.G., Loyalka, S.K., 2007. *Handbook of Alternative Fuel Technologies, Handbook of Alternative Fuel Technologies*. CRC Press.
- Leite, G.B., Abdelaziz, A.E.M., Hallenbeck, P.C., 2013. Algal biofuels: Challenges and opportunities. *Bioresour. Technol.* 145, 134–141.
- Lewis, F.M., 2007. Generation of an ultra-superheated steam composition and gasification therewith. United States Patent US007229483B2.
- Li, Q.H., Zhang, Y.G., Meng, A.H., Li, L., Li, G.X., 2013. Study on ash fusion temperature using original and simulated biomass ashes. *Fuel Process. Technol.* 107, 107–112. doi:10.1016/j.fuproc.2012.08.012
- Lienhard, J.H., 2013. *A Heat Transfer Textbook: Fourth Edition*. Courier Corporation.
- Lin, S., Harada, M., Suzuki, Y., Hatano, H., 2006. Continuous experiment regarding hydrogen production by Coal/CaO reaction with steam (II) solid formation. *Fuel* 85, 1143–1150. doi:10.1016/j.fuel.2005.05.029
- Lin, S., Harada, M., Suzuki, Y., Hatano, H., 2004. Continuous experiment regarding hydrogen production by coal/CaO reaction with steam (I) gas products. *Fuel* 83, 869–874.
- Lin, S., Harada, M., Suzuki, Y., Hatano, H., 2002. Hydrogen production from coal by separating carbon dioxide during gasification. *Fuel* 81, 2079–2085.

9. REFERENCES

- Liu, K., Song, C., Subramani, V., 2009. Hydrogen and Syngas Production and Purification Technologies. John Wiley & Sons.
- Lu, G., Yan, Y., Colechin, M., 2004. A Digital Imaging Based Multifunctional Flame Monitoring System. *IEEE Trans. Instrum. Meas.* 53, 1152–1158.
- Lu, X., Wang, T., 2013. Water–gas shift modeling in coal gasification in an entrained-flow gasifier – Part 2: Gasification application. *Fuel* 108, 620–628.
- Lucas, C., Szewczyk, D., Blasiak, W., Mochida, S., 2004. High-temperature air and steam gasification of densified biofuels. *Biomass and Bioenergy* 27, 563–575.
- MacKay, D.J., 2008. Sustainable Energy - Without the Hot Air, 1st ed. UIT, Cambridge.
- Mahinpey, N., Gomez, A., 2016. Review of gasification fundamentals and new findings: Reactors, feedstock, and kinetic studies. *Chem. Eng. Sci.* 148, 14–31. doi:10.1016/j.ces.2016.03.037
- Mahishi, M.R., Goswami, D.Y., 2007. An experimental study of hydrogen production by gasification of biomass in the presence of a CO₂ sorbent. *Int. J. Hydrogen Energy* 32, 2803–2808.
- Mallard, E., Le Chatelier, H., 1883. Thermal model for flame propagation. *Ann. des Mines.*
- Manassah, J., 1981. Alternative Energy Sources, Part 1. Elsevier.
- Mayr, B., Prieler, R., Demuth, M., Potesser, M., Hochenauer, C., 2015. CFD and experimental analysis of a 115kW natural gas fired lab-scale furnace under oxy-fuel and air–fuel conditions. *Fuel* 159, 864–875. doi:10.1016/j.fuel.2015.07.051
- McKendry, P., 2002. Energy production from biomass (Part 3): Gasification technologies. *Bioresour. Technol.* 83, 55–63. doi:10.1016/S0960-8524(01)00120-1
- Met Office, 2016. Global surface temperature [WWW Document]. URL <http://www.metoffice.gov.uk/research/monitoring/climate/surface-temperature> (accessed 10.6.13).
- Met Office, n.d. The Great Smog of 1952 [WWW Document]. URL <http://www.metoffice.gov.uk/education/teens/case-studies/great-smog> (accessed 10.7.13).
- Milne, T.A., Evans, R.J., Abatzoglou, N., 1998. NREL technical report - Biomass Gasifier “Tars”: Their Nature, Formation, and Conversion. NREL/TP-570-25357, NREL/TP-570-25357.
- Mirza, U.K., Ahmad, N., Harijan, K., Majeed, T., 2009. A vision for hydrogen economy in Pakistan. *Renew. Sustain. Energy Rev.* 13, 1111–1115. doi:10.1016/j.rser.2008.08.005
- Mohamed Ismail, H., Ng, H.K., Gan, S., Lucchini, T., Onorati, A., 2013. Development of a reduced biodiesel combustion kinetics mechanism for CFD modelling of a light-duty diesel engine. *Fuel* 106, 388–400. doi:10.1016/j.fuel.2012.10.015
- Molcan, P., Lu, G., Bris, T. Le, Yan, Y., Taupin, B., Caillat, S., 2009. Characterisation of biomass and coal co-firing on a 3MWth Combustion Test Facility using flame imaging and gas/ash sampling techniques. *Fuel* 88, 2328–2334. doi:10.1016/j.fuel.2009.06.027
- Monaghan, R.F.D., Ghoniem, A.F., 2012a. A dynamic reduced order model for simulating entrained flow gasifiers: Part I: Model development and description. *Fuel* 91, 61–80. doi:10.1016/j.fuel.2011.07.015

9. REFERENCES

- Monaghan, R.F.D., Ghoniem, A.F., 2012b. A dynamic reduced order model for simulating entrained flow gasifiers. Part II: Model validation and sensitivity analysis. *Fuel* 94, 280–297. doi:10.1016/j.fuel.2011.08.046
- Monnot, G., 1985. Principles of Turbulent Fired Heat. Editions TECHNIP, Paris.
- Müller-Dethlefs, K., Schlader, A.F., 1976. The Effect of Steam on Flame Temperature, Burning Velocity and Carbon Formation in Hydrocarbon Flames. *Combust. Flame* 27, 205–215.
- Nakamura, S., Siriwat, U., Yoshikawa, K., Kitano, S., 2015. Development of Tar Removal Technologies for Biomass Gasification using the By-products. *Energy Procedia* 75, 208–213. doi:10.1016/j.egypro.2015.07.305
- National Institute of Standards and Technology, 2000. NIST-JANAF Thermochemical Tables [WWW Document]. NIST Database. URL <http://kinetics.nist.gov/janaf/> (accessed 2.21.14).
- NETL, 2013. NETL: Gasifipedia [WWW Document]. Natl. Energy Technol. Lab. URL <http://www.netl.doe.gov/technologies/coalpower/gasification/gasifipedia/egas.html>
- Nexterra, 2014. Birmingham Bio Power Ltd. Power Plant | Nexterra - The Next Generation of Industrial Gasification Systems [WWW Document]. URL <http://www.nexterra.ca/files/BBPL-project.php> (accessed 4.28.16).
- Nikrityuk, P.A., Gräbner, M., Kestel, M., Meyer, B., 2013. Numerical study of the influence of heterogeneous kinetics on the carbon consumption by oxidation of a single coal particle. *Fuel* 114, 88–98. doi:10.1016/j.fuel.2012.10.037
- NIST, 2016. Chemistry Webbook [WWW Document]. Chem. Webb. URL <http://webbook.nist.gov/>
- Northern Gas Networks, Wales & West Utilities, Kiwa, Amec Foster Wheeler, 2016. H21 Leeds City Gate. Leeds.
- Nowakowski, D.J., Jones, J.M., Brydson, R.M.D., Ross, A.B., 2007. Potassium catalysis in the pyrolysis behaviour of short rotation willow coppice. *Fuel* 86, 2389–2402. doi:10.1016/j.fuel.2007.01.026
- OECD/IEA, 2015. World Energy Outlook 2015. Paris.
- Onwudili, J.A., Williams, P.T., 2016a. Catalytic supercritical water gasification of plastics with supported RuO₂: A potential solution to hydrocarbons-water pollution problem. *Process Saf. Environ. Prot.* 102, 140–149. doi:10.1016/j.psep.2016.02.009
- Onwudili, J.A., Williams, P.T., 2016b. Catalytic conversion of bio-oil in supercritical water: Influence of RuO₂/γ-Al₂O₃ catalysts on gasification efficiencies and bio-methane production. *Appl. Catal. B Environ.* 180, 559–568. doi:10.1016/j.apcatb.2015.06.058
- Park, S.-W., Jang, C.-H., 2012. Effects of pyrolysis temperature on changes in fuel characteristics of biomass char. *Energy* 39, 187–195.
- Patel, S., 2013. Norway Terminates Full-Scale CCS Project at Mongstad [WWW Document]. Powermag. URL <http://www.powermag.com/42579/>
- Peak Sensors, 2016. Type R and Type S Thermocouples - Peak Sensors [WWW Document]. URL <http://www.peakensors.co.uk/thermocouples/type-r-thermocouple/> (accessed 8.17.16).
- Pearse, R.W.B., Gaydon, A.G., 1965. THE IDENTIFICATION OF MOLECULAR SPECTRA - THIRD EDITION WITH SUPPLEMENT, Third. ed. Chapman and Hall Ltd, London.

9. REFERENCES

- Pei, P., Kulkarni, M., 2008. Modeling of Ultra Superheated Steam Gasification in Integrated Gasification Combined Cycle Power Plant with Carbon Dioxide Capture, in: Es2008: Proceedings of the 2nd International Conference on Energy Sustainability, Vol 2. ASME, pp. 763–773.
- Pereira, E.G., da Silva, J.N., de Oliveira, J.L., Machado, C.S., 2012. Sustainable energy: A review of gasification technologies. *Renew. Sustain. Energy Rev.* 16, 4753–4762.
- Petchers, N., 2003. *Combined Heating, Cooling, and Power Handbook*. The Fairmont Press, Inc.
- Piarpuzán, D., Quintero, J.A., Cardona, C.A., 2011. Empty fruit bunches from oil palm as a potential raw material for fuel ethanol production. *Biomass and Bioenergy* 35, 1130–1137. doi:10.1016/j.biombioe.2010.11.038
- Piatkowski, N., Steinfeld, A., 2008. Solar-Driven Coal Gasification in a Thermally Irradiated Packed-Bed Reactor. *Energy & Fuels* 22, 2043–2052. doi:10.1021/ef800027c
- Pinto, F., André, R., Costa, P., Carolino, C., Lopez, H., Gulyurtlu, I., 2010. Solid Biofuels for Energy: A Lower Greenhouse Gas Alternative: Chapter 7- Gasification Technology and its Contribution to Deal with Global Warming, in: Grammel, P. (Ed.), . Springer, p. 256.
- Poole, D.J., Sharifi, V., Swithenbank, J., Kilgallon, P., Simms, N., Oakey, J., Ardelt, D., 2007. Continuous analysis of elemental emissions from a biofuel gasifier. *J. Anal. At. Spectrom.* 22, 532. doi:10.1039/b616798e
- Potsdam Institute for Climate Impact Research and Climate Analytics, 2012. Turn Down the Heat- Why a 4C Warmer World Must be Avoided.
- Prawisudha, P., Namioka, T., Yoshikawa, K., 2012. Coal alternative fuel production from municipal solid wastes employing hydrothermal treatment. *Appl. Energy* 90, 298–304. doi:10.1016/j.apenergy.2011.03.021
- Probstein, R.F., Hicks, R.E., 2006. *Synthetic Fuels*, Dover. ed. Courier Corporation, Mineola, N.Y.
- Puig-Arnavat, M., Tora, E.A., Bruno, J.C., Coronas, A., 2013. State of the art on reactor designs for solar gasification of carbonaceous feedstock. *Sol. Energy* 97, 67–84.
- Quaak, P., Knoef, H., Stassen, H.E., 1999. *Energy from Biomass: A Review of Combustion and Gasification Technologies*, Volumes 23-422. World Bank Publications.
- Rakib, M.A., Grace, J.R., Lim, C.J., Elnashaie, S.S.E.H., Ghiasi, B., 2010. Steam reforming of propane in a fluidized bed membrane reactor for hydrogen production. *Int. J. Hydrogen Energy* 35, 6276–6290. doi:10.1016/j.ijhydene.2010.03.136
- Rane, V., Rajput, A., Karkamkar, A., Choudhary, V., 2004. Energy-efficient conversion of propane to propylene and ethylene over a V2O5/CeO2/SA5205 catalyst in the presence of limited oxygen. *Appl. Energy* 77, 375–382. doi:10.1016/S0306-2619(03)00156-9
- Rathakrishnan, E., 2005. *Fundamentals of Engineering Thermodynamics*. PHI Learning Pvt. Ltd.
- Reddy, P.J., 2013. *Clean Coal Technologies for Power Generation*. CRC Press.
- REN21, 2015. *Renewables 2015 Global Status Report*. REN21 Secretariat, Paris.
- Rezaian, J., Cheremisinoff, N.P., 2005. *Gasification Technologies: A Primer for Engineers and Scientists (Chemical Industries)*. CRC Press, Boca Raton, FL.

9. REFERENCES

- Rizkiana, J., Guan, G., Widayatno, W.B., Hao, X., Li, X., Huang, W., Abudula, A., 2014. Promoting effect of various biomass ashes on the steam gasification of low-rank coal. *Appl. Energy* 133, 282–288. doi:10.1016/j.apenergy.2014.07.091
- Robinson, J.W., Skelly Frame, E.M., Frame II, G.M., 2004. *Undergraduate Instrumental Analysis*, Sixth Edition. CRC Press.
- Rogers, G.F.C., Mayhew, Y.R., 1995. *Thermodynamic and Transport Properties of Fluids: S. I. Units*, Fifth. ed. Blackwell, Oxford.
- Roy, A., Ekkad, S. V, Vandsburger, U., 2011. Prediction and Validation of Performance of an Entrained Flow Gasifier Model, in: *Proceedings of the ASME 2011 International Mechanical Engineering Congress & Exposition*. Denver, pp. 1–9.
- Roy, M.M., Dutta, A., Corscadden, K., 2013. An experimental study of combustion and emissions of biomass pellets in a prototype pellet furnace. *Appl. Energy* 108, 298–307. doi:10.1016/j.apenergy.2013.03.044
- RSC, 2016. Carbon Dioxide Utilisation: Faraday Discussion, in: *Carbon Dioxide Utilisation: Faraday Discussion*. Sheffield.
- RWE, n.d. RWE AG - Coal and gas power plants [WWW Document]. URL <http://www.rwe.com/web/cms/en/183542/rwe/innovation/projects-technologies/power-generation/fossil-fired-power-plants/> (accessed 4.29.14).
- Ryu, C., Nasserzadeh Sharifi, V., Swithenbank, J., 2004. Gasification of Wood Char by Ultra-Superheated Steam in an Entrained Flow Reactor. *J. Energy Inst.* 77, 46–52.
- Ryu, C., Sharifi, V., Swithenbank, J., 2005. *Waste Pyrolysis and Generation of Storable Fuel*.
- Sajwan, K.S., Alva, A.K., Twardowska, I., Punshon, T., 2006. *Coal Combustion Byproducts and Environmental Issues*. Springer.
- Schilling, H.-D., Bonn, B., Krauss, U., 1981. *Coal gasification: existing processes and new developments*, Second. ed. Graham & Trotman.
- Schmidt, S., Giesa, S., Drochner, A., Vogel, H., 2011. Catalytic tar removal from bio syngas—Catalyst development and kinetic studies. *Catal. Today* 175, 442–449. doi:10.1016/j.cattod.2011.04.052
- Shabangu, S., 2005. *An innovative coal gasifier utilising steam raised to ultra-high temperatures*. PhD Thesis. University of Sheffield.
- Shen, Y., Yoshikawa, K., 2013. Recent progresses in catalytic tar elimination during biomass gasification or pyrolysis—A review. *Renew. Sustain. Energy Rev.* 21, 371–392. doi:10.1016/j.rser.2012.12.062
- Shi, S.-P., Zitney, S.E., Shahnam, M., Syamlal, M., Rogers, W.A., 2006. Modelling coal gasification with CFD and discrete phase method. *J. Energy Inst.* 79, 217–221. doi:10.1179/174602206X148865
- Sinnott, R.K., Towler, G., 2009. *Chemical Engineering Design: Chemical Engineering, Volume 6*, 5th ed. Butterworth-Heinemann.
- Sjølie, H.K., Solberg, B., 2011. Greenhouse gas emission impacts of use of Norwegian wood pellets: a sensitivity analysis. *Environ. Sci. Policy* 14, 1028–1040.
- Smith, G.P., Golden, D.M., Frenklach, M., Moriarty, N.W., Eiteneer, B., Goldenberg, M., Bowman,

9. REFERENCES

- C.T., Hanson, R.K., Song, S., William C. Gardiner, J., Lissianski, V. V., Qin, Z., 2000. GRI-Mech 3.0.
- Southern Water, 2016. Southern Water- Our charges [WWW Document]. URL <https://www.southernwater.co.uk/business-our-charges> (accessed 4.30.14).
- Spliethoff, H., 2010. Power Generation from Solid Fuels. Springer, Berlin.
- Stevens, D.J., 2001. Hot Gas Conditioning: Recent Progress With Larger-Scale Biomass Gasification Systems. NREL/SR-510-29952. Golden, CO.
- Stevens, P., 2012. The “Shale Gas Revolution”: Developments and Changes. London.
- Stoyanov, B., Beyazov, J., 2005. Determination of the Flow Rate of Different Fluids by a Rotameter. *Probl. Eng. Cybern. Robot.* 55.
- Strahle, 1993. An Introduction to Combustion. CRC Press.
- Suh, J., Atreya, A., 1995. The Effect of Water Vapor on Counterflow Diffusion Flames, in: International Conference on Fire Research and Engineering, NIST.
- Swanson, R.M., 2009. Techno-economic analysis of biomass-to-liquids production based on gasification. Iowa State University.
- Swithenbank, J., 2013. Future Energy Challenges, in: Academy of Finland - Helsinki Congress Paasitorni. Academy of Finland, Helsinki.
- Swithenbank, J., Sharifi, V., 2013. Wetland Biomass to Bioenergy: Efficient harvesting, processing and conversion of wetland biomass.
- Syngas Products, 2016. Syngas Products with steam turbine [WWW Document]. URL <http://www.syngas-products.com/technology/neat-g2s/> (accessed 4.21.16).
- Thyssen-Krupp Uhde, n.d. Gasification Technologies [WWW Document]. Brochure. URL http://www.thyssenkrupp-uhde.de/fileadmin/documents/brochures/gasification_technologies.pdf
- Tomeczek, J., Palugniok, H., 1996. Specific heat capacity and enthalpy of coal pyrolysis at elevated temperatures. *Fuel* 75, 1089–1093.
- Trinks, W., Mawhinney, M.H., Shannon, R.A., Reed, R.J., Garvey, J.R., 2004. Industrial Furnaces, Volume 1, 6th ed. John Wiley & Sons, Hoboken, NJ.
- Tuomi, S., Kaisalo, N., Simell, P., Kurkela, E., 2015. Effect of pressure on tar decomposition activity of different bed materials in biomass gasification conditions. *Fuel* 158, 293–305. doi:10.1016/j.fuel.2015.05.051
- Turn, S., Kinoshita, C., Zhang, Z., Ishimura, D., Zhou, J., 1998. An experimental investigation of hydrogen production from biomass gasification. *Int. J. Hydrogen Energy* 23, 641–648.
- Udomsirichakorn, J., Salam, P.A., 2014. Review of hydrogen-enriched gas production from steam gasification of biomass: The prospect of CaO-based chemical looping gasification. *Renew. Sustain. Energy Rev.* 30, 565–579. doi:10.1016/j.rser.2013.10.013
- UK Coal, 2012. World coal statistics - UK Coal [WWW Document]. URL <http://www.ukcoal.com/world-coal-statistics.html> (accessed 7.11.14).

9. REFERENCES

- Umeki, K., Yamamoto, K., Namioka, T., Yoshikawa, K., 2010. High temperature steam-only gasification of woody biomass. *Appl. Energy* 87, 791–798. doi:10.1016/j.apenergy.2009.09.035
- UN DESA, 2015. United Nations Department of Economic and Social Affairs Population Division. *World Population Prospects: The 2015 Revision (No. ESA/P/WP.241)*. New York.
- US EPA, 2013. Coal [WWW Document]. URL <http://www.epa.gov/cleanenergy/energy-and-you/affect/coal.html> (accessed 7.14.14).
- US EPA, 2008. Polycyclic Aromatic Hydrocarbons (PAHs) [WWW Document]. URL <http://www.epa.gov/osw/hazard/wastemin/minimize/factshts/pahs.pdf> (accessed 3.24.14).
- Vakkilainen, E., Kuparinen, K., Heinimö, J., 2013. Large Industrial Users of Energy Biomass, IEA Bioenergy Task 40 Report.
- van Heek, K.H., Mühlen, H.J., 1991. Chemical Kinetics of Carbon and Char Gasification, in: Lahaye, J., Ehrburger, P. (Eds.), *Fundamental Issues in Control of Carbon Gasification Reactivity*. Springer, p. 622.
- Várhegyi, G., Mészáros, E., Antal, M.J., Bourke, J., Jakab, E., 2006. Combustion kinetics of corncob charcoal and partially demineralized corncob charcoal in the kinetic regime. *Ind. Eng. Chem. Res.* 45, 4962–4970. doi:10.1021/ie0602411
- Vascellari, M., Roberts, D.G., Hla, S.S., Harris, D.J., Hasse, C., 2015. From laboratory-scale experiments to industrial-scale CFD simulations of entrained flow coal gasification. *Fuel* 152, 58–73. doi:10.1016/j.fuel.2015.01.038
- Vassilev, S. V., Baxter, D., Andersen, L.K., Vassileva, C.G., 2010. An overview of the chemical composition of biomass. *Fuel* 89, 913–933. doi:10.1016/j.fuel.2009.10.022
- Veolia Environmental Services (UK), 2011. Sheffield's Energy Recovery Facility [WWW Document]. URL <http://www.veoliaenvironmentalservices.co.uk/Documents/Publications/Sheffield/Energy Recovery/ERF Brochure.pdf> (accessed 7.11.14).
- Wei, L., Xu, S., Zhang, L., Liu, C., Zhu, H., Liu, S., 2007. Steam gasification of biomass for hydrogen-rich gas in a free-fall reactor. *Int. J. Hydrogen Energy* 32, 24–31.
- Weisser, D., 2007. A guide to life-cycle greenhouse gas (GHG) emissions from electric supply technologies. *Energy* 32, 1543–1559.
- Westbrook, C.K., Dryer, F.L., 1984. Chemical kinetic modeling of hydrocarbon combustion. *Prog. Energy Combust. Sci.* 10, 1–57. doi:10.1016/0360-1285(84)90118-7
- Westinghouse Plasma Corp, 2013. Summary of Qualifications Westinghouse Plasma Gasification Technology.
- Wikimedia Commons, 2010. Koppers Totzek [WWW Document]. Chem. Eng. URL http://commons.wikimedia.org/wiki/File:Koppers_Totzek.svg
- World Coal Association, 2016. Coal | Coal Information | World Coal Association [WWW Document]. URL <http://www.worldcoal.org/coal/what-coal> (accessed 4.29.16).
- World Nuclear Association, 2015. Safety of Nuclear Reactors - World Nuclear Association [WWW Document]. URL <http://world-nuclear.org/information-library/safety-and-security/safety-of-plants/safety-of-nuclear-power-reactors.aspx> (accessed 4.15.16).

9. REFERENCES

- World Nuclear Association, 2014. Nuclear Power in France | French Nuclear Energy [WWW Document]. URL <http://www.world-nuclear.org/info/Country-Profiles/Countries-A-F/France/#.Uk1SrySkq6M> (accessed 7.11.14).
- World Nuclear News, 2016. Hinkley Point C will “categorically” go ahead, with FID in May [WWW Document]. World Nucl. News. URL <http://www.world-nuclear-news.org/NN-Hinkley-Point-C-will-categorically-go-ahead-with-FID-in-May-23031601.html> (accessed 4.15.16).
- Xia, W., Xie, G., 2015. Comparison of surface properties of anthracite coals before and after high temperature heating process. *Physicochem. Probl. Miner. Process.* 51, 205–212.
- Xin, F., 2013. Mathematical Modeling of Ultra-Superheated Steam Gasification. PhD Thesis. Ohio University.
- Yin, C., 2016. Effects of moisture release and radiation properties in pulverized fuel combustion: A CFD modelling study. *Fuel* 165, 252–259. doi:10.1016/j.fuel.2015.10.057
- Yoon, S.J., Lee, J.-G., 2012. Hydrogen-rich syngas production through coal and charcoal gasification using microwave steam and air plasma torch. *Int. J. Hydrogen Energy* 37, 17093–17100.
- Zhang, Y., Ashizawa, M., Kajitani, S., Miura, K., 2008. Proposal of a semi-empirical kinetic model to reconcile with gasification reactivity profiles of biomass chars. *Fuel* 87, 475–481. doi:10.1016/j.fuel.2007.04.026
- Zizak, G., 2000. Flame Emission Spectroscopy : Fundamentals and Applications, in: ICS Training Course on Laser Diagnostics of Combustion Processes. Cairo, pp. 18–22.

10 Appendix A – Details of Models

This appendix contains additional details of models and simulations described in Chapter 4.

10.1 Stoichiometric Equilibrium Model

Details of the stoichiometric equilibrium model described in Section 4.1 are given in the following tables. The independent equations are given in Equations 4-3 and 4-5. The equilibrium reactions from Equation 4-5 were solved by assuming an equilibrium temperature of 800K and using enthalpy and entropy data from the JANAF tables (National Institute of Standards and Technology, 2000). This temperature was chosen based on the reported syngas exit temperature in the previous work. The calculated values for the equilibrium constants are shown in Table 10-1.

10.1.1 Solution of Independent Equations

Using the atom balances in Equation 4-3 and the values calculated for Ke_1 , Ke_2 and Ke_3 six equations are available to solve for the six unknowns $n_1 - n_6$. The equations were solved in an iterative process one by one until all the equations were satisfied to within 1%. It was found in the first iteration that the product gas totalled 1.8 mol, which contradicted the assumption that 1 kmol of gas were produced. The input flow rates in Table 4-1 were halved to produce 0.97 mol such that the assumption that the number of moles is approximately equal to the mole fraction still holds.

Table 10-1 shows the percentage agreement between the left hand side (LHS) and right hand side (RHS) of the atom balance and equilibrium reactions. It then compares the input and output to the gasifier, such that mass must be conserved. The agreement between the mass in and out is 99.7%.

APPENDIX A – DETAILS OF MODELS

Table 10-1: Calculation of equilibrium constants for reactions R1 to R3 using data from JANAF tables (National Institute of Standards and Technology, 2000)

Considering R1:	C + CO₂ <-> 2 CO	at T=	800 K
	$dH = (hf+dh)CO - (hf+dh)C - (hf+dh)CO_2$		
dH (kJ)	172.379		
	$dS=2x S(CO)-S(C)-S(CO_2)$		
dS (J/K)	177.234		
	$dG= dH-TdS$		
dG (kJ)	30.592		
	$Ke=\exp(-dG/RT)$		
Ke1	0.995		
Considering R2:	C + H₂O <-> CO + H₂	at T=	800 K
	$dH = (hf+dh)CO + (hf+dh)H_2 - (hf+dh)C - (hf+dh)H_2O$		
dH (kJ)	135.539		
	$dS=S(CO)+S(H_2)-S(C)-S(H_2O)$		
dS (J/K)	143.174		
	$dG= dH-TdS$		
dG (kJ)	20.999		
	$Ke=\exp(-dG/RT)$		
Ke2	0.997		
Considering R3:	C + 2 H₂ <-> CH₄	at T=	800 K
	$dH = (hf+dh)CH_4 - (hf+dh)C - 2(hf+dh)H_2$		
dH (kJ)	-87.239		
	$dS=S(CH_4)-S(C)-2S(H_2)$		
dS (J/K)	-106.404		
	$dG= dH-TdS$		
dG (kJ)	-2.116		
	$Ke=\exp(-dG/RT)$		
Ke3	1.000		

In Table 10-2 the agreement between the mass in and out is 99.9%, and the agreement for the atom balance and equilibrium reactions is within 1% in each case. The number of moles of each output species is equal to its mole fraction if the total number of moles is unity (within 3% here).

This model thus predicts that the output gas would contain 33.3% hydrogen, 26.6% carbon monoxide and so forth as shown in the lower part of Table 10-2 assuming equilibrium was reached at a temperature of 800 K.

Table 10-2: Results of manually converged equilibrium model assuming equilibrium temperature of 800K

Atom Balance		LHS	RHS	Agreement
C	$a+c=n1+n3+n5+n6$	0.552	0.548	99.28%
H	$2b+a=2n2+2n4+4n6$	1.279	1.288	100.68%
O	$b+2c=n3+n4+2n5$	0.494	0.497	100.69%
Equilibrium reactions		LHS	RHS	Agreement
Ke1=CO ² /CO ₂		0.995	0.997	100.12%
Ke2=CO.H ₂ /H ₂ O		0.997	0.995	99.84%
Ke3=CH ₄ /H ₂ ²		1.000	1.001	100.07%
Input parameter	Moles	Mr	Mass (g)	
a	0.500	13	6.500	
b	0.390	18	7.013	
c	0.052	44	2.287	
Total IN		0.942		15.801
Output parameter	Moles (=mol fraction)	Mr	Mass (g)	
n1 (C)	0.100	12	1.200	
n2 (H ₂)	0.333	2	0.666	
n3 (CO)	0.266	28	7.448	
n4 (H ₂ O)	0.089	18	1.602	
n5 (CO ₂)	0.071	44	3.124	
n6 (CH ₄)	0.111	16	1.776	
Total OUT		0.97		15.816

Having demonstrated the methods used to solve an equilibrium model, the Aspen software was subsequently used to speed up the process and include all possible interactions between the reactant species using the equilibrium model, as described in Section 4.2.

10.2 CFD model parameters

Table 10-3 contains an abridged list of input parameters to the CFD model described in Section 4.4 as produced by the FLUENT software. Most are default parameters except where noted in Section 4.4.

APPENDIX A – DETAILS OF MODELS

Table 10-3: Fluent input parameters (abridged)

Fluent Input Parameters	
Version: 3d, pbns, pdf16, rke (3d, pressure-based, 16 species pdf, realizable k-epsilon)	
Release: 16.1.0	
Title:	
Models	

Model	Settings

Space	3D
Time	Steady
Viscous	Realizable k-epsilon turbulence model
Wall Treatment	Enhanced Wall Treatment
Heat Transfer	Enabled
Solidification and Melting	Disabled
Radiation	Discrete Ordinate Model
Species	Non-Premixed Combustion ((ch4 o2 h2o co co2 h h2 h2o2 ho2 hoco o oh cho hco hcooh o3) species)
Coupled Dispersed Phase	Enabled
NOx Pollutants	Disabled
SOx Pollutants	Disabled
Soot	Disabled
Mercury Pollutants	Disabled

Material Properties	

Material: anthracite (inert-particle)	

Property	Units	Method	Value(s)

Density	kg/m3	constant	300
Cp (Specific Heat)	j/kg-k	polynomial	(300 1003) (500 1593) (700 1917) (900 1925) (1100 1673) (1300 1314) (1500 1103)
Thermal Conductivity	w/m-k	constant	0.33000001
Thermophoretic Coefficient	kg-m2/s2	talbot-diffusion-coeff	#f
Particle Emissivity		constant	0.89999998
Particle Scattering Factor		constant	0.89999998
Material: pdf-mixture (mixture)			

Property	Units	Method	Value(s)

Mixture Species	names		(ch4 o2 h2o co co2 h h2 h2o2 ho2 hoco o oh cho hco hcooh o3)
Density	kg/m3	pdf	#f
Cp (Specific Heat)	j/kg-k	mixing-law	#f
Thermal Conductivity	w/m-k	constant	0.045400001
Viscosity	kg/m-s	constant	1.72e-05
Absorption Coefficient	1/m	wsggm-domain-based	#f
Scattering Coefficient	1/m	constant	0
Scattering Phase Function		isotropic	#f
Refractive Index		constant	1
Speed of Sound	m/s	none	#f
Material: steel (solid)			

APPENDIX A – DETAILS OF MODELS

Property	Units	Method	Value(s)

Density	kg/m3	constant	8030
Cp (Specific Heat)	j/kg-k	constant	502.48
Thermal Conductivity	w/m-k	constant	16.27
Absorption Coefficient	1/m	constant	0
Scattering Coefficient	1/m	constant	0
Scattering Phase Function		isotropic	#f
Refractive Index		constant	1
Material: dolomite (solid)			
Property	Units	Method	Value(s)

Density	kg/m3	constant	3100
Cp (Specific Heat)	j/kg-k	constant	1085
Thermal Conductivity	w/m-k	constant	2.5
Absorption Coefficient	1/m	constant	0
Scattering Coefficient	1/m	constant	0
Scattering Phase Function		isotropic	#f
Refractive Index		constant	1.75
Cell Zone Conditions			

Zones			
name	id	type	

solid	3	fluid	
Setup Conditions			

Condition	Value

Material Name	pdf-mixture
Specify source terms?	no
Source Terms	((mass) (x-momentum) (y-momentum) (z-momentum) (k) (epsilon) (species-0) (species-1) (species-2) (species-3) (species-4) (energy))
Specify fixed values?	no
Local Coordinate System for Fixed Velocities	no
Fixed Values	((x-velocity (inactive . #f) (constant . 0) (profile)) (y-velocity (inactive . #f) (constant . 0) (profile)) (z-velocity (inactive . #f) (constant . 0) (profile)) (k (inactive . #f) (constant . 0) (profile)) (epsilon (inactive . #f) (constant . 0) (profile)) (species-0 (inactive . #f) (constant . 0) (profile)) (species-1 (inactive . #f) (constant . 0) (profile)) (species-2 (inactive . #f) (constant . 0) (profile)) (species-3 (inactive . #f) (constant . 0) (profile)) (species-4 (inactive . #f) (constant . 0) (profile)) (temperature (inactive . #f) (constant . 0) (profile)))
Participates in radiation	yes
Deactivated Thread	no
Laminar zone?	no
Set Turbulent Viscosity to zero within laminar zone?	yes
Boundary Conditions	

Zones	
name	id type

coal_inlet	7 wall

APPENDIX A – DETAILS OF MODELS

wall-solid	1	wall
synthair_inlet	6	velocity-inlet
gas_inlet	8	velocity-inlet
outlet	9	pressure-outlet
quarl	10	wall
wall	11	wall
symmetry_x	12	symmetry
Setup Conditions		
coal_inlet		
Condition	Value	

Wall Thickness (mm)	0	
Heat Generation Rate (w/m3)	0	
Material Name	steel	
Thermal BC Type	1	
Temperature (k)	300	
Heat Flux (w/m2)	0	
Convective Heat Transfer Coefficient (w/m2-k)	0	
Free Stream Temperature (k)	300	
Enable shell conduction?	no	
Layer	(((thickness . 0) (material . steel) (qdot (constant . 0) (profile))))	
Wall Motion	0	
Shear Boundary Condition	0	
Define wall motion relative to adjacent cell zone?	yes	
Apply a rotational velocity to this wall?	no	
Velocity Magnitude (m/s)	0	

Internal Emissivity	1
External Emissivity	1
External Radiation Temperature (k)	300
Discrete Phase BC Type	2
Normal	((polynomial angle 1))
Tangent	((polynomial angle 1))
Discrete Phase BC Function	none
Impact Angle Function	((polynomial angle 1))
Diameter Function	((polynomial diameter 1.8e-09))
Velocity Exponent Function	((polynomial normal-velocity 0))
Radiation BC Type	3
X-Component of Radiation Direction	1
Y-Component of Radiation Direction	0
Z-Component of Radiation Direction	0
Theta Width of Beam (deg)	9.9923854e-07
Phi Width of Beam (deg)	9.9923854e-07
	((constant . 0) (profile)))
	((constant . 0) (profile)))
	-1
Apply Direct Irradiation Parallel to the Beam?	no
Use Beam Direction from Solar Load Model Settings	no
Use Direct and Diffuse Irradiation from Solar Load Model Settings	no
Fslip constant	0
Eslip constant	0

APPENDIX A – DETAILS OF MODELS

Surface tension gradient (n/m-k)	0
Specularity Coefficient	0
Convective Augmentation Factor	1
Enable Thermal Stabilization?	no
Scale Factor	0
Stabilization Method	1
wall-solid	
Condition	Value

Wall Thickness (mm)	0
Heat Generation Rate (w/m3)	0
Material Name	steel
Thermal BC Type	0
Temperature (k)	800
Heat Flux (w/m2)	0
Convective Heat Transfer Coefficient (w/m2-k)	0
Free Stream Temperature (k)	300
Enable shell conduction?	no
Layer	((thickness . 0) (material . steel) (qdot (constant . 0) (profile)))
Wall Motion	0
Shear Boundary Condition	0
Define wall motion relative to adjacent cell zone?	yes
Apply a rotational velocity to this wall?	no
Velocity Magnitude (m/s)	0
Internal Emissivity	0.8
External Emissivity	1

External Radiation Temperature (k)	300
Discrete Phase BC Type	2
Normal	((polynomial angle 1))
Tangent	((polynomial angle 1))
Discrete Phase BC Function	none
Impact Angle Function	((polynomial angle 1))
Diameter Function	((polynomial diameter 1.8e-09))
Velocity Exponent Function	((polynomial normal-velocity 0))
Radiation BC Type	3
X-Component of Radiation Direction	1
Y-Component of Radiation Direction	0
Z-Component of Radiation Direction	0
Theta Width of Beam (deg)	9.9923854e-07
Phi Width of Beam (deg)	9.9923854e-07
	((constant . 0) (profile))
	((constant . 0) (profile))
	-1
Apply Direct Irradiation Parallel to the Beam?	yes
Use Beam Direction from Solar Load Model Settings	no
Use Direct and Diffuse Irradiation from Solar Load Model Settings	no
Fslip constant	0
Eslip constant	0
Surface tension gradient (n/m-k)	0
Specularity Coefficient	0

APPENDIX A – DETAILS OF MODELS

Convective Augmentation Factor	1
Enable Thermal Stabilization?	no
Scale Factor	0
Stabilization Method	1
synthair_inlet	
Condition	Value

Velocity Specification Method	2
Reference Frame	0
Velocity Magnitude (m/s)	25
Supersonic/Initial Gauge Pressure (pascal)	0
Angular velocity (rad/s)	0
Temperature (k)	400
Turbulent Specification Method	1
Turbulent Kinetic Energy (m2/s2)	1
Turbulent Dissipation Rate (m2/s3)	1
Turbulent Intensity (%)	9.9999998
Turbulent Length Scale (mm)	7.6000004
Hydraulic Diameter (mm)	1000
Turbulent Viscosity Ratio	10
External Black Body Temperature Method	0
Black Body Temperature (k)	300
Internal Emissivity	1
Mean Mixture Fraction	0
Mixture Fraction Variance	0
Discrete Phase BC Type	2
Discrete Phase BC Function	none

is zone used in mixing-plane model?	no
gas_inlet	
Condition	Value

Velocity Specification Method	2
Reference Frame	0
Velocity Magnitude (m/s)	2.6
Supersonic/Initial Gauge Pressure (pascal)	0
Angular velocity (rad/s)	0
Temperature (k)	300
Turbulent Specification Method	1
Turbulent Kinetic Energy (m2/s2)	1
Turbulent Dissipation Rate (m2/s3)	1
Turbulent Intensity (%)	9.9999998
Turbulent Length Scale (mm)	3.5000002
Hydraulic Diameter (mm)	1000
Turbulent Viscosity Ratio	10
External Black Body Temperature Method	0
Black Body Temperature (k)	300
Internal Emissivity	1
Mean Mixture Fraction	1
Mixture Fraction Variance	0
Discrete Phase BC Type	2
Discrete Phase BC Function	none
is zone used in mixing-plane model?	no
outlet	
Condition	Value

APPENDIX A – DETAILS OF MODELS

Gauge Pressure (pascal)	0
Backflow Total Temperature (k)	700
Backflow Direction Specification Method	1
Turbulent Specification Method	1
Backflow Turbulent Kinetic Energy (m2/s2)	1
Backflow Turbulent Dissipation Rate (m2/s3)	1
Backflow Turbulent Intensity (%)	9.999998
Backflow Turbulent Length Scale (mm)	120.00001
Backflow Hydraulic Diameter (mm)	1000
Backflow Turbulent Viscosity Ratio	10
External Black Body Temperature Method	0
Black Body Temperature (k)	300
Internal Emissivity	0
Mean Mixture Fraction	0
Mixture Fraction Variance	0
Discrete Phase BC Type	4
Discrete Phase BC Function	none
is zone used in mixing-plane model?	no
Radial Equilibrium Pressure Distribution	no
Average Pressure Specification?	no
	0
Specify targeted mass flow rate	no
Targeted mass flow (kg/s)	1
Upper Limit of Absolute Pressure Value (pascal)	5000000
Lower Limit of Absolute Pressure Value (pascal)	1
quarl	
Condition	Value

Wall Thickness (mm)	50.000002
Heat Generation Rate (w/m3)	0
Material Name	dolomite
Thermal BC Type	0
Temperature (k)	500
Heat Flux (w/m2)	0
Convective Heat Transfer Coefficient (w/m2-k)	0
Free Stream Temperature (k)	300
Enable shell conduction?	no
Layer	((thickness . 0) (material . steel) (qdot (constant . 0) (profile)))
Wall Motion	0
Shear Boundary Condition	0
Define wall motion relative to adjacent cell zone?	yes
Apply a rotational velocity to this wall?	no
Velocity Magnitude (m/s)	0
Internal Emissivity	0.5
External Emissivity	1
External Radiation Temperature (k)	300
Discrete Phase BC Type	2
Normal	((polynomial angle 1))
Tangent	((polynomial angle 1))
Discrete Phase BC Function	none
Impact Angle Function	((polynomial angle 1))
Diameter Function	((polynomial diameter 1.8e-09))

APPENDIX A – DETAILS OF MODELS

Velocity Exponent Function normal-velocity 0))	((polynomial
Radiation BC Type	3
X-Component of Radiation Direction	1
Y-Component of Radiation Direction	0
Z-Component of Radiation Direction	0
Theta Width of Beam (deg)	9.9923854e-
07	
Phi Width of Beam (deg)	9.9923854e-07
	((constant . 0) (profile)))
	((constant . 0) (profile)))
	-1
Apply Direct Irradiation Parallel to the Beam?	yes
Use Beam Direction from Solar Load Model Settings	no
Use Direct and Diffuse Irradiation from Solar Load Model Settings	no
Rotation Speed (rad/s)	0
Fslip constant	0
Eslip constant	0
Surface tension gradient (n/m-k)	0
Specularity Coefficient	0
Convective Augmentation Factor	1
Enable Thermal Stabilization?	no
Scale Factor	0
Stabilization Method	1
wall	
Condition	Value

Wall Thickness (mm)	50.000002
Heat Generation Rate (w/m3)	0
Material Name	dolomite
Thermal BC Type	0
Temperature (k)	500
Heat Flux (w/m2)	0
Convective Heat Transfer Coefficient (w/m2-k)	0
Free Stream Temperature (k)	300
Enable shell conduction?	no
Layer	((thickness . 0)
(material . steel) (qdot (constant . 0) (profile)))	
Wall Motion	0
Shear Boundary Condition	0
Define wall motion relative to adjacent cell zone?	yes
Apply a rotational velocity to this wall?	no
Velocity Magnitude (m/s)	0
Internal Emissivity	0.8
External Emissivity	1
External Radiation Temperature (k)	300
Discrete Phase BC Type	2
Normal	((polynomial angle 1))
Tangent	((polynomial angle 1))
Discrete Phase BC Function	none
Impact Angle Function	((polynomial angle 1))
Diameter Function	((polynomial diameter 1.8e-09))

APPENDIX A – DETAILS OF MODELS

Velocity Exponent Function	((polynomial normal-velocity 0))
Radiation BC Type	3
X-Component of Radiation Direction	1
Y-Component of Radiation Direction	0
Z-Component of Radiation Direction	0
Theta Width of Beam (deg)	9.9923854e-07
Phi Width of Beam (deg)	9.9923854e-07
	((constant . 0) (profile))
	((constant . 0) (profile))
	-1
Apply Direct Irradiation Parallel to the Beam?	yes
Use Beam Direction from Solar Load Model Settings	no
Use Direct and Diffuse Irradiation from Solar Load Model Settings	no
Rotation Speed (rad/s)	0
Fslip constant	0
Eslip constant	0
Surface tension gradient (n/m-k)	0
Specularity Coefficient	0
Convective Augmentation Factor	1
Enable Thermal Stabilization?	no
Scale Factor	0
Stabilization Method	1
Solver Settings	

Equations	
Equation	Solved

Flow	yes
Turbulence	yes
Energy	yes
Discrete Ordinates	yes
Pdf	yes
Numerics	
Numeric	Enabled

Absolute Velocity Formulation	yes
Relaxation	
Variable	Relaxation Factor

Pressure	0.3
Density	0.80000001
Body Forces	1
Momentum	0.7
Turbulent Kinetic Energy	0.8
Turbulent Dissipation Rate	0.94999999
Turbulent Viscosity	1
Energy	0.94999999
Temperature	0.94999999
Discrete Ordinates	1
Mean Mixture Fraction	0.97000003

APPENDIX A – DETAILS OF MODELS

Mixture Fraction Variance	0.9		
Discrete Phase Sources	0.5		
Linear Solver			
	Solver	Termination	Residual Reduction
Variable	Type	Criterion	Tolerance

Pressure	V-Cycle	0.1	
X-Momentum	Flexible	0.1	0.7
Y-Momentum	Flexible	0.1	0.7
Z-Momentum	Flexible	0.1	0.7
Turbulent Kinetic Energy	Flexible	0.1	0.7
Turbulent Dissipation Rate	Flexible	0.1	0.7
Energy	F-Cycle	0.1	
Discrete Ordinates	Flexible	0.1	0.7
Mean Mixture Fraction	Flexible	0.1	0.7
Mixture Fraction Variance	Flexible	0.1	0.7
Pressure-Velocity Coupling			
Parameter	Value		

Type	SIMPLE		
Discretization Scheme			
Variable	Scheme		

Pressure	Second Order		

Momentum	Second Order Upwind
Turbulent Kinetic Energy	First Order Upwind
Turbulent Dissipation Rate	First Order Upwind
Energy	Second Order Upwind
Discrete Ordinates	First Order Upwind
Mean Mixture Fraction	Second Order Upwind
Mixture Fraction Variance	Second Order Upwind
Solution Limits	
Quantity	Limit

Minimum Absolute Pressure	1
Maximum Absolute Pressure	5e+10
Minimum Temperature	1
Maximum Temperature	5000
Minimum Turb. Kinetic Energy	1e-14
Minimum Turb. Dissipation Rate	1e-20
Maximum Turb. Viscosity Ratio	100000

11 Appendix B – Feedstock Material Data

This appendix contains supplementary data regarding the feedstock materials used in this work. The proximate analyses described in Section 5.2.1.1 were conducted using TGA analysis which produced curves of mass loss against temperature as shown in the following figures. The change in mass up to 110°C was associated with moisture content. Between 110 and 900°C the volatile matter was released. On addition of oxygen at 900°C the fixed carbon was reacted, with the residual mass representing ash content. Each analysis was repeated a minimum of three times; one example result is shown for each feedstock.

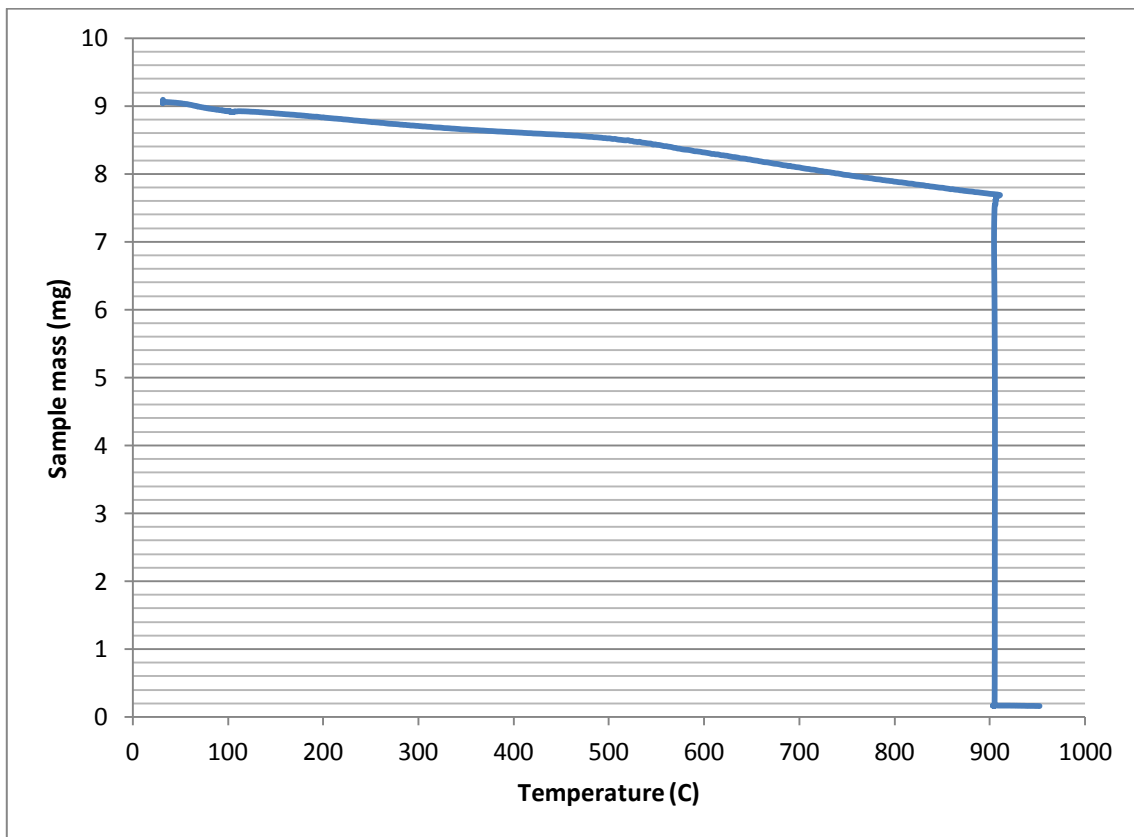


Figure 11-1: Example TGA curve for coal sample.

APPENDIX B – FEEDSTOCK MATERIAL DATA

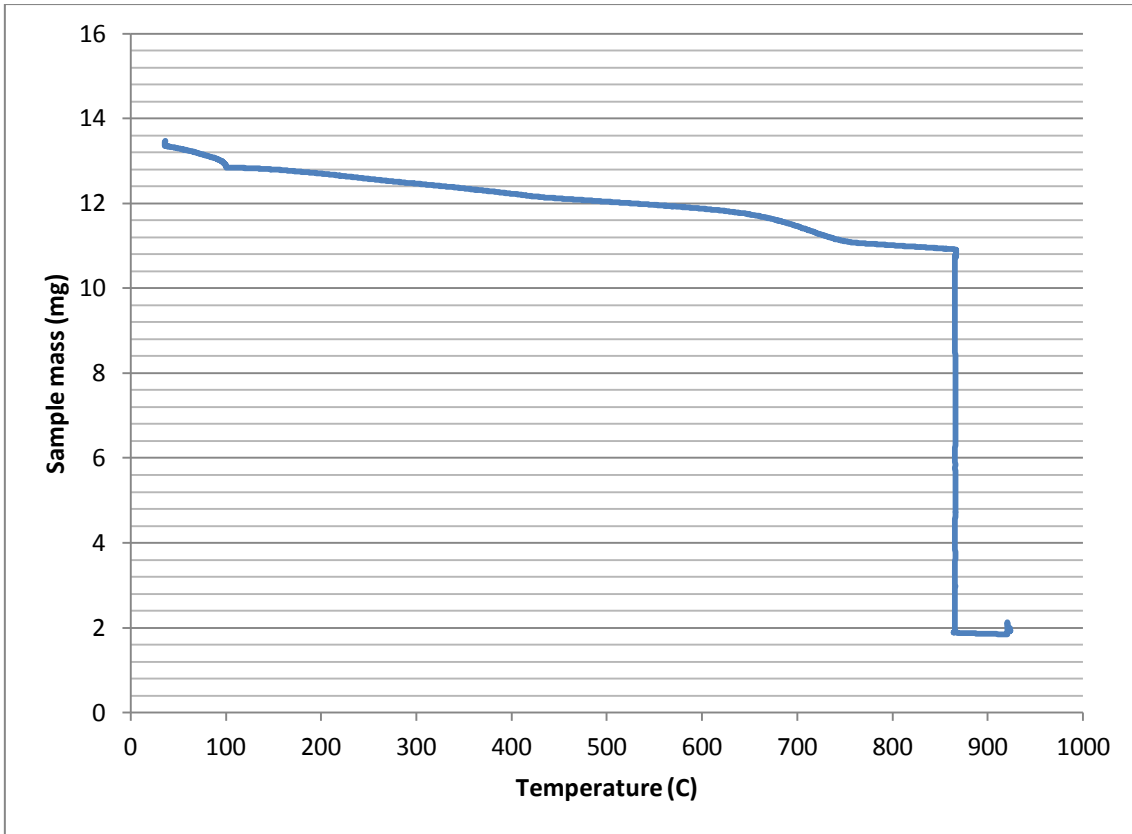


Figure 11-2: Example TGA curve for softwood char sample.

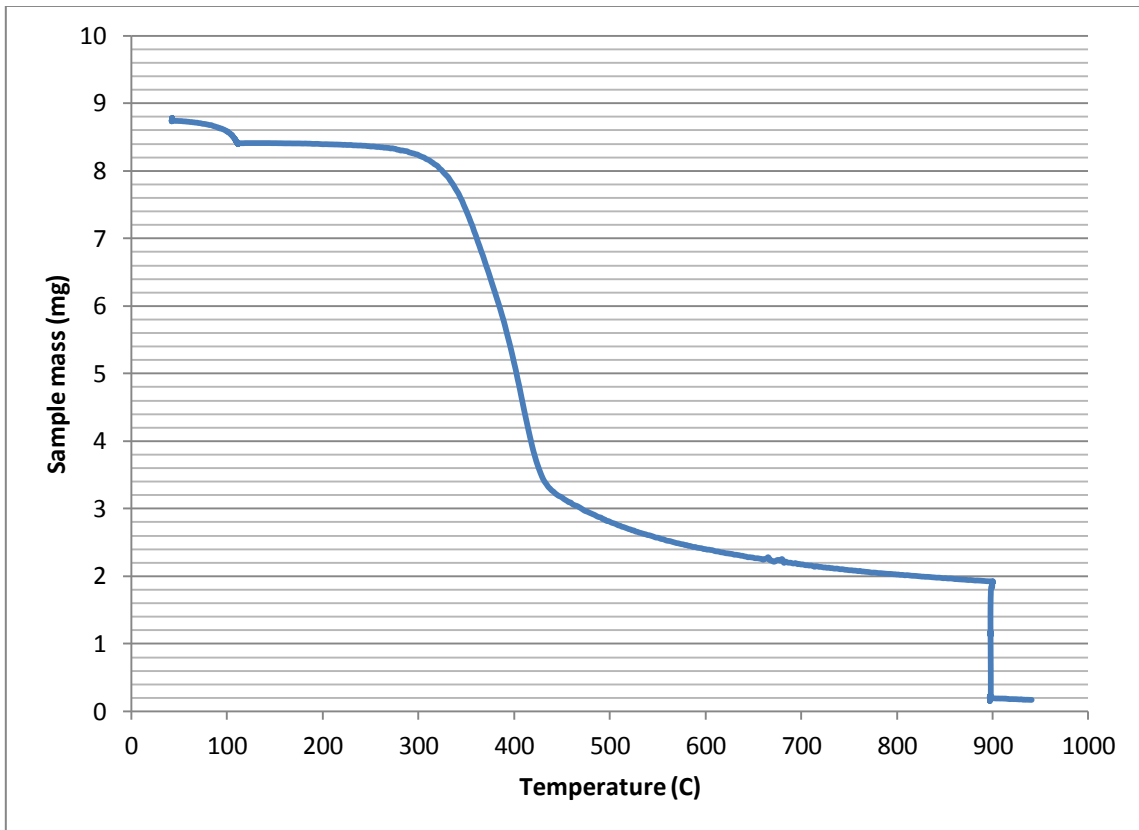


Figure 11-3: Example TGA curve for oak sawdust sample

APPENDIX B – FEEDSTOCK MATERIAL DATA

The surface area BET analysis data for coal, low ash char and high ash char are shown in Table 11-1 as presented by automated BET analyser.

Table 11-1: Surface area statistics for main gasification feedstocks

Surface Area	Coal	Softwood char	Low ash char
Single point surface area at $p/p^{\circ} = 0.300000000$, m^2/g	38.8375	289.8077	336.6561
BET Surface Area, m^2/g	47.6386	292.6159	357.7832
t-Plot external surface area, m^2/g	71.1016	179.6704	449.6946
t-Plot micropore volume, cm^3/g	-0.015273	0.058591	-0.054253

Table 11-2 shows ash analysis data for the Latvian softwood char described in Section 5.2. The softwood char was produced in an existing commercial combined heat and power (CHP) system. The CHP process is fuelled by mixed Latvian softwood species, mostly in the form of unsellable thinnings and sawmills waste. The feedstock is ground to size G30-G40 (<4 cm chips) and dried to a maximum moisture content of 15% before being fed at a rate of 45 kg/hr to the reactor. At this point the wood chips are subjected to both high and low temperature treatment zones under limited air supply to affect the oxidation and reduction reactions. This process releases the volatile gases which are cooled and filtered to remove ash and any tar, before the gas is burned in an internal combustion engine to supply a combined heat and power system (EnertecGreen, n.d.). This system provides 1 MW electrical and 2.2 MW of thermal energy, which is used for wood chip drying and to supply the district heating scheme in the town of Jekabpils, Latvia. Water for the scheme is heated to 90°C before circulation and returns at <75°C.

The residual material after devolatilisation is a char containing fixed carbon and ash components, currently produced at a rate of approximately 40 tonnes per week with planned future expansion. At the time there was no applications for this by-product due to the high ash content making it unsuitable for use as biochar for soil fertilization, however if the char can be gasified additional syngas can be produced from the fixed carbon content, which would greatly increase the fuel efficiency of the existing process.

Table 11-2 shows the very high mineral content of the tested sample; in particular the potassium content was found to be around ten times higher than typical wood chars. Other species present in high levels include magnesium and phosphorus and various aromatic species. Of particular concern is the level of PAH EPA16 in the sample tested. This classification consists of the 16 Polycyclic Aromatic Hydrocarbons (PAH) which the US Environmental Protection Agency has designated as of particular toxicological and environmental concern (Agency for Toxic Substances and Disease Registry, 1996; US EPA, 2008). The levels EPA16 found in char is usually <1mg/kg sample, though in this sample the level was over 4000 mg/kg. PAHs are formed during incomplete combustion of fossil fuels and biomass or solid waste, which means they may have been formed during the initial pyrolysis of the softwood or may have been present on the wood prior to gasification.

The presence of PAHs in high concentration also hinders the char's usability as a soil additive as PAHs such as naphthalene are harmful to worms and other organisms.

APPENDIX B – FEEDSTOCK MATERIAL DATA

Table 11-2: Latvian softwood char ash analysis. Reproduced with permission from NRM Laboratories



Report Number		25551-14		ANALYTICAL REPORT		Client JIM WATERSON	
Date Received		19-FEB-2014		R361 JIM WATERSON		HARPER ADAMS	
Date Reported		25-FEB-2014		AGRICULTURAL COLLEGE		NEWPORT	
Project		BIOCHAR		SHROPSHIRE		TF10 8NB	
Reference		JIM WATERSON					
Order Number		POCROP175					
Laboratory Reference		MANU54027					
Sample Reference		BIOCHAR 1					
Determinand		Unit		WASTE			
Dry Matter		%	97.2				
PAH EPA16		mg/kg	4206				
Total Nitrogen		% w/w	0.31				
Total Phosphorus (P)		mg/kg	4654				
Total Potassium (K)		mg/kg	25884				
Total Magnesium (Mg)		mg/kg	7720				
Total Copper (Cu)		mg/kg	15.8				
Total Zinc (Zn)		mg/kg	226				
Total Lead (Pb)		mg/kg	2.21				
Total Cadmium (Cd)		mg/kg	1.37				
Total Mercury (Hg)		mg/kg	<0.05				
Total Nickel (Ni)		mg/kg	3.82				
Total Chromium (Cr)		mg/kg	4.35				
Naphthalene		mg/kg	2263				
Acenaphthylene		mg/kg	645				
Acenaphthene		mg/kg	251				
Fluorene		mg/kg	55.7				
Phenanthrene		mg/kg	745				
Anthracene		mg/kg	81.4				
Fluoranthene		mg/kg	58.9				
Pyrene		mg/kg	42.5				
Benzo(a)anthracene		mg/kg	16.1				
Chrysene		mg/kg	24.6				
Benzo(b)fluoranthene		mg/kg	4.9				
Benzo(k)fluoranthene		mg/kg	3.3				



ANALYTICAL REPORT	
Report Number	25551-14
Date Received	19-FEB-2014
Date Reported	25-FEB-2014
Project	BIOCHAR
Reference	JIM WATERSON
Order Number	POCROP175
Laboratory Reference	MANU54027
Sample Reference	BIOCHAR 1
Determinand	Unit
Benzo(a)pyrene	mg/kg
Indeno[1,2,3-cd]pyrene	mg/kg
Dibenzof(a,h)anthracene	mg/kg
Benzo(g,h,i)perylene	mg/kg
WASTE	3.9
	4.3
	2.5
	3.7
Notes	
Analysis Notes	The sample submitted was of adequate size to complete all analysis requested. The results as reported relate only to the item(s) submitted for testing. The results are presented on a dry matter basis unless otherwise stipulated. This test report shall not be reproduced, except in full, without the written approval of the laboratory.
Document Control	
Reported by	<i>Andy Chase</i> Natural Resource Management Ltd. Coopers Bridge, Braziers Lane, Bracknell, Berkshire, RG42 6NS Tel: 01344 886338 Fax: 01344 890972 email: enquiries@nrm.uk.com

12 Appendix C - Supplementary Experimental Work

This appendix contains additional experimental work conducted during the course of this project which was not considered central to the narrative within the main text. It provides evidence of progress during the study which led to the experimental programme described in Chapters 5 and 6.

12.1 Gasification Feedstock Options

When choosing feedstock materials for comparison in the gasification system, several options were considered. Commercially available wood pellets were obtained from CPL Distribution Ltd as shown in Figure 12-1. These pellets had a diameter of 6 mm, and consisted of miscellaneous wood species from the UK. The packaging specifies <10% moisture and <0.7% ash content. They were analysed for their composition and calorific value on an as received basis, before undergoing pyrolysis to produce high quality charcoal for the gasification tests.



Figure 12-1: Wood pellets as delivered

12.1.1 Wood Pellet Pyrolysis

In order to produce a solid feedstock with maximum carbon content, the wood pellets were pyrolysed to drive off moisture and volatile matter before gasification. The apparatus used for this operation is shown in Figure 12-2.

APPENDIX C – SUPPLEMENTARY EXPERIMENTAL WORK

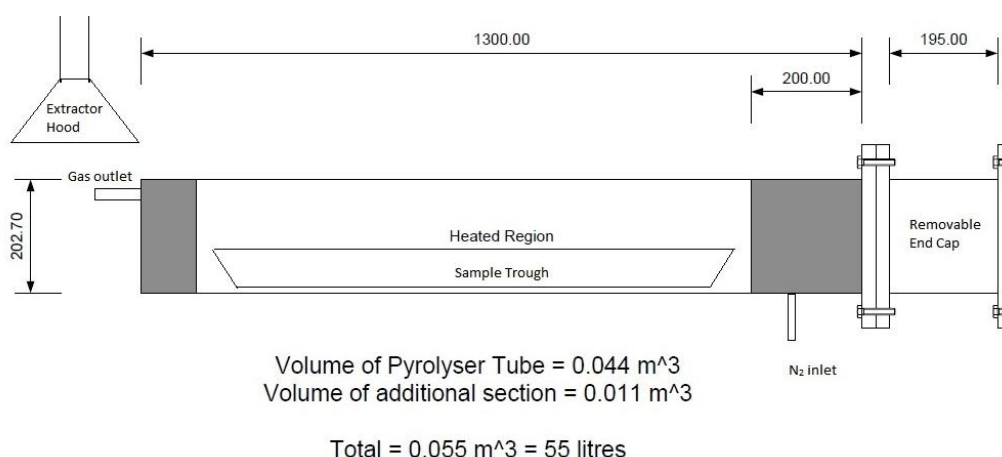


Figure 12-2: Diagram of the pyrolysis equipment (dimensions in mm)



Figure 12-3: (a) The pyrolysis unit, showing the feed trough and the end cap adjacent, (b) a sample of wood pellets after pyrolysis

Wood pellets were charged into a long trough and sealed inside the pyrolysis chamber, in batches of approximately 7 kg. The reactor was cold when the pellets were charged. The temperature in the chamber was ramped up by approximately 9°C/min. An inert atmosphere was maintained in the chamber by introducing nitrogen at 8 L/min, to prevent auto-ignition of the biomass material at elevated temperatures. The pellets were heated to a maximum temperature of 500°C or 700°C. The final temperature was maintained for 3 minutes before the material was allowed to cool inside the pyrolyser. The collected char was then pulverised using a grinder and passed through a 125 µm sieve before the analytical tests were performed, as described in the next section.

12.1.2 Feedstock Analytical Testing

The samples of coal, wood pellets and pyrolyser wood char were subject to analytical tests as described in Section 5.2.1. The results are given below, together with those from commercially available barbecue charcoal, named BBQ1 and BBQ2 to disguise the brand names. The results are presented by analysis type.

Table 12-1: Results of proximate analysis of various fuels, as received basis

	Wood Pellets	500°C Char	700°C Char	BBQ1	BBQ2
			%wt		
Moisture	8.8	1.1	0.4	4.6	8.7
Volatile matter	74.4	12.7	9.6	30.1	25.7
Fixed carbon	16.4	85.2	88.9	63.3	60.4
Ash	0.4	1.0	1.1	1.9	5.2
Gross CV (MJ/kg)	18.1	31.8	32.5	25.9	23.5

Table 12-2: Results of ultimate analysis of various fuels, as received basis

Sample	N (%wt)	C (%wt)	H (%wt)
Wood Pellets	0.05	48.40	7.26
500°C Char	0.78	87.84	2.28
700°C Char	0.64	93.98	1.39
BBQ1	0.50	82.73	4.10
BBQ2	0.07	78.16	2.66

12.1.3 Comments on Analytical Tests

Table 12-1 shows that raw wood pellets had the highest moisture and lowest fixed carbon fractions, consistent with woody biomass material. For the wood char samples the majority of the moisture and volatile matter was removed during pyrolysis, giving high fixed carbon content in excess of that observed for coal and providing for its relatively high calorific value compared to the wood pellets.

The second commercial barbecue sample, BBQ2 contained the highest ash of the samples tested. The ash content decreases the heating value of a fuel as there is a higher proportion of inert material contained per unit mass of fuel. This sample also had a high moisture fraction, comparable to that of the wood pellets, which may be due to the age of the material, as chars can absorb atmospheric moisture over time. These two factors are reflected in the reduced calorific value. In comparison, char produced through the pyrolysis of low ash wood pellets had very high calorific value due to comprising almost entirely fixed carbon owing to the low ash content of the wood pellets.

TGA technology is a relatively new method of performing proximate analysis, which means that the standard operating procedures were written before its adoption. Although the TGA allows a reduction in the time required for the tests, the different methods employed can give rise to small differences in results between TGA and the traditional standardised technique. These discrepancies were however found to be generally less than 1% (Cumming & McLaughlin, 1982). The Ultimate

analyses here were conducted prior to the device being calibrated for sulphur, meaning that the balance of the mass comprised both sulphur and oxygen.

12.1.4 Selection of Feed Materials

Following a comparison of all the materials tested, a short list was chosen for gasification tests. It was intended to select materials with a range of different properties, compositions and heating values. Further, in order to conduct a full comparison, sufficient material would be required for several gasifier runs.

It was decided that the pyrolysis of wood pellets was too inefficient to produce the volumes of char required, as each pyrolysis run took between 3-4 hours and yielded <1 kg of char from each 7 kg batch of pellets, which then had to be milled to a suitable particle size. The barbecue charcoal was also supplied in large chunks which required significant milling. The charcoal was also found to have a gross calorific value comparable to the Latvian softwood char sample which had a much greater ash content. The high ash made the softwood char a more interesting candidate for comparison, with the advantage that a sufficiently large volume was provided ready milled. This material was of low value compared to barbecue charcoal which was purchased at retail prices and was unlikely to gain value following gasification.

There is a compromise between the quality of the char produced and the energy expended in its preparation. For high quality char, significant pre-processing of the pellet material was required. This occurs both in the pellet manufacture, where the raw wood has been macerated, dried and compressed into pellet form, and subsequently in the laboratory where the pellets were pyrolysed up to 700°C for 80 minutes in a batch cycle that takes 3 hours for 7 kg of pellets. The overall efficiency of the process should take into account the degree of pre-processing required for the given gas yield.

12.2 Additional Experimental Raw Data

The experimental results presented in chapter six were produced following an extensive experimental programme which developed throughout the project. Some of the raw data from earlier experimental work is included here to highlight the extent of the efforts made in collecting the presented data and to demonstrate how the method developed as experience was gained with this system.

Table 12-3 presents some data collected during the second year of the project using propane to fuel the burner. Experiments were conducted in varying the flow rates and ratios of reactant gases without the addition of coal, following a thorough flushing of the flue line to remove any traces of residual coal dust or other material.

Table 12-4 shows data collected during a typical week of experiments. The steam flow data for the duration of each run was also collected and analysed. In this case this data was not used for the final analysis owing to fluctuations in the steam volume flow being $>\pm 10\%$ and in some cases owing to missing temperature data. Following these results the steam generator output and the pressure reducing valve were adjusted to reduce the fluctuation in steam flow to give more reproducible results.

APPENDIX C – SUPPLEMENTARY EXPERIMENTAL WORK

Table 12-3: Example raw experimental data during process development using propane fuel gas. No data available where none presented. T5= gas temperature inside gasifier. T6= gas temperature at gasifier outlet.

Run no.	C ₃ H ₈ L/min	O ₂ L/min	Steam m ³ /hr	H ₂	O ₂	N ₂	CH ₄	CO	CO ₂	Total	T5	T6
24/04/15	Propane fuelled											
#1	20	140	19.81	20.1	0.23	1.14	0.95	14.8	60.7	97.92	929.77	420.67
#2	20	140	19.93	19.6	0.24	1.70	0.78	13.7	59.3	95.33	928.21	442.18
#3	25	175	22.98	16.4	0.24	0.66	0.16	11.8	69.3	98.56	1011.94	563.39
#4	25	175	23.40	16.1	0.25	0.74	0.18	11.3	69.9	98.47	1011.13	573.41
#5	28	190	24.86	17.8	0.24	0.69	0.15	12.4	67.0	98.28	1041.83	604.67
#6	28	190	31.11	16.6	0.24	0.52	0.02	10.2	70.7	98.28	1031.74	649.92
07/05/15	Varying steam content											
#1	25	170	14.24	19.7	0.35	2.13	0.13	18.7	59	100.01	1099.00	452.89
#2	25	170	14.04	19.6	0.40	2.25	0.005	17.1	58.1	97.46	1075.09	469.99
#3	25	170	21.97	20.1	0.44	2.52	0.57	15.0	58.8	97.43	1009.27	509.48
#4	25	170	22.59	15.1	0.48	2.69	0.26	10.6	67.9	97.03	986.72	529.67
#5	25	170	30.77	19.2	0.44	2.39	0.18	10.6	65.6	98.41	949.92	570.60
#6	25	170	30.10	17.9	0.47	2.64	0.19	9.9	65.7	96.80	981.57	580.60
#7	25	170	29.26	17.4	0.49	2.91	0.17	10.6	66.7	98.27	986.90	585.38
01/07/15	Low gas flow											
#3	20	135	19.71	18.3	0.26	3.52	1.55	15.1	52.7	91.43	909.27	428.14
#4	20	135	20.17	15.6	0.43	21.0	0.73	11.9	48.5	98.16	894.69	477.03

From the experimental work represented by the tests shown in Table 12-3, it was clear that significant quantities of hydrogen and carbon monoxide, amongst other gases were produced in the burner when fuelled by propane. Later developments to the experimental rig allowed monitoring of the temperature inside the burner and recorded the temperature of the steam and oxygen entering the gasifier, for more accurate flow calculations.

Table 12-4 presents some further experimental data collected around one year later, incorporating changes to the choice of fuel gas described in Section 6.2 with regular control runs performed to demonstrate low yields of these gases without feedstock addition. Additional thermocouples linked to the data

APPENDIX C – SUPPLEMENTARY EXPERIMENTAL WORK

logger to give additional temperature data. At this stage the experimental work consistently produced high hydrogen and carbon monoxide gas yields from both coal and char feedstocks.

Table 12-4: Raw data collected during one week (abridged). No data available where none presented. Motor %= percentage of feed motor capacity, used to calculate molar carbon flow by prior calibration. LIQ = liquid collected. Resid= solids collected. T3 = steam supply temperature.

run no.	CH ₄ L/min	O ₂ L/min	Steam m ³ /hr	Motor %	Carbon kmol/hr	S/C	H ₂	O ₂	N ₂	CH ₄	CO	CO ₂	Total	LIQ ml	Resid g	Time mins	T3	T5	T6	T7	T10			
19/4				Char			%mol													°C				
#2	69.7	151	18.55	60	0.27	3.28	28.1	0.20	0.58	1.37	25.0	48.4	103.65	40	53	3.0	153.6	937.5	563.3	931.8				
#3	69.7	151	16.51	60	0.27	3.06	32.1	0.18	0.95	1.78	27.2	38.9	101.11	28	40	2.5	152.8	943.2	551.3	879.3				
#4	69.7	151	17.39	60	0.27	3.16	33.8	0.18	0.89	0.83	27.7	35.3	98.7	33	26	2.5	155.6	924.3	556.3	878.9				
#6	69.7	151	20.01	40	0.54	1.75	26.6	0.21	0.86	4.43	19.0	48.7	99.8	50	153	3.0								
				Coal																				
#7	69.7	151	18.98	25	0.36	2.58	29	0.22	0.74	2.19	18.9	47.8	98.85	53	123	3.0	143.0	968.6	545.7	946.1				
#8	69.7	151	12.19	25	0.36	2.03	29.5	0.23	0.87	0.52	22.5	47.0	100.62	42	134	3.0	131.0	971.2	544.5	814.6				
25/4				Char																				
#2	69.7	151	19.99	40	0.15	6.08	25.5	0.31	0.69	1.57	20.3	56.2	104.57	37	30	3.0	144.8	989.4	623.3	963.3	513.7			
#3	69.7	151	19	50	0.23	4.00	32.1	0.19	0.66	1.34	26.5	40.5	101.29	32	141	3.0								
#5	69.7	151	19.93	50	0.23	4.12	26.5	0.47	2.77	2.97	20.8	49.7	103.21	30	49	3.0	142.1	917.4	585.4	942.9	478.4			
#6	69.7	151	18.88	70	0.32	2.83	32.1	0.29	2.17	1.80	28.0	36.5	100.86	22	75	3.0								
#7	69.7	151	20.13	70	0.32	3.03	32.4	0.21	2.06	2.47	26.1	34.7	97.94	25	68	3.0	144.8	923.8	594.3	927.5	513.5			
#8	69.7	151	15.80	70	0.32	2.61	33.6	0.19	1.85	0.63	28.3	35.5	100.07	21	52	3.0	148.6	995.6	617.6	884.9	528.4			
26/4																								
#2	69.7	152	17.34	40	0.15	5.57	24	0.24	3.35	0.58	20.9	53.2	102.27	43	28	3.75	134.3	989.9	580.8	925.3	414.2			
#3	69.7	151	20.41	40	0.15	6.16	28.3	0.23	2.79	1.21	21.40	45.70	99.63	32	20	3.0	140.1	963.1	587.4	1015.0	440.2			
				Coal																				
#4	69.7	152	18.07	15	0.16	5.70	21.9	0.38	9.12	1.41	14.2	43.8	90.81	55	63	3.5								
#5	69.7	152	18.07	15	0.16	5.70	24.9	0.33	4.92	0.60	15.0	49.7	95.45	37	52	3.0	142.6	1013.9	570.6	969.2	485.3			
#6	69.7	155	20.40	20	0.25	3.83	25.3	0.3	3.01	0.67	16.8	54	100.08	33	125	3.5	141.1	1012.7	581.0	977.1	504.5			

12.3 Review of Flame Analysis Methods

During this project consideration was given to possible analysis methods of the steam flame, to contrast with the simulation data from the CFD model. A review of available literature on combustion system measurements was made; a much condensed version of which is included here before a description of the experimental investigation is given in the next section.

12.3.1 Temperature Measurements

Thermocouples or suction pyrometers are useful to give time averaged measurements at specific points in a flame. Light scatter techniques such as Raman and Rayleigh scatter and Laser Induced Fluorescence (LIF) have the advantage of being non-invasive so avoid any measurement bias on the flow (Chigier, 1991). Raman and Rayleigh scatter methods both require high particle concentrations and otherwise clean laboratory conditions, whereas LIF can be applied to moderately laden flows with interference from flame luminosity.

Fourier Transform Infra-Red (FTIR) spectroscopy is a method to measure the IR absorption spectrum of a sample. The technique can measure temperature and concentration of gases, particles and soot within line of sight. Separate temperatures and concentrations can be found for individual gas species and solid particles. It also can be used at low temperatures and densely charged streams; it can calculate the contributions of soot and char separately and measure particle size. This technique has been used in coal spray and coal flame analyses for CO₂, H₂O, CH₄ and particles (Chigier, 1991).

12.3.2 Species Identification

Measurement of minor species in flames, including soot and organic components is important for pollution control. Laser Induced Fluorescence (LIF) is popular due to its relatively easy implementation and large collection of existing reference databases. The radical species OH, NO, and CH are most commonly investigated in combustion systems. Radical species are difficult to measure as they are short-lived and will not survive a sampling line for external measurement; therefore they must be monitored using a non-invasive in-situ method (Kohse-Hoinghaus and Jeffries, 2002).

12.3.2.1 Absorption Spectroscopy

Emission spectra are produced when an atom or molecule in an excited state returns to the ground state by releasing energy in the form of electromagnetic radiation. Spectral emission lines are characterised by wavelength and emission intensity. The wavelengths emitted are characteristic of each species according to the energy levels through which the molecule can be excited, allowing species to be identified.

The emission intensity depends on species concentration and flame temperature. Some species such as alkali metals may ionise if heated to very high temperature. This means the valence electrons are separated from the atom and as such will not return to the ground state and emit radiation. Such species should be excited in low temperature flames to avoid this (Robinson et al., 2004).

Other investigation techniques include Laser Induced Fluorescence (LIF) and Raman Spectroscopy.

12.4 Experimental Spectrometry

Owing to the limited optical access to the gasifier, thermocouples and suction pyrometry were used for temperature measurement as described in Section 5.5.3. As a preliminary trial investigation, emission spectrometry was used to identify species in the flame, and to compare the concentrations of these species under different flame conditions. The species of interest were radicals OH, CH and C₂ having emissions commonly at 306, 431 and 516 nm respectively.

The viewport offered a limited field of view as shown in Figure 5-21. The length of the visible path is approximately 155 mm within the quartz as shown, with an additional 45 mm through the burner body to the outer surface, where a camera or fibre optic may be placed. The view field had a diameter of 25 mm as shown.

The spectrometer was an *Ocean Optics USB2000+ UV-VIS-ES*, a compact and highly portable spectrometer configured for ultraviolet and visible wavelengths between 200 and 850 nm. By contrast, the visible spectrum lies roughly between 400-700 nm. The spectrometer was fitted with a lens on a fibre optic cable which was clamped in place 20 mm from the viewport window to avoid overheating. The spectrometer settings were maintained constant at 200 ms integration time, averaged over two images in order to allow comparison between all the spectra collected. The spectra were then analysed using a reference literature source of molecular emission data (Pearse and Gaydon, 1965; Zizak, 2000).

The glass viewport used in the above experiment was tested for transmittance to ensure it would not affect the collected spectra. The glass was irradiated with a known light source and the percentage transmission shown in Figure 12-4.

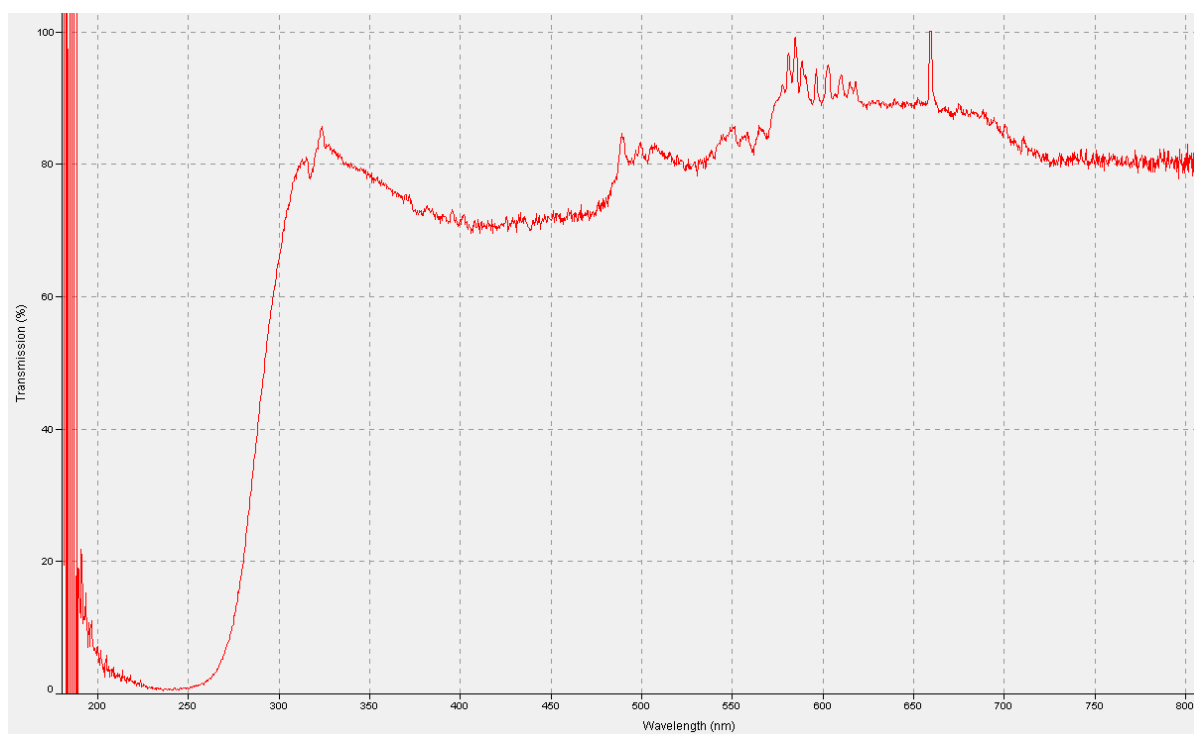


Figure 12-4: Transmission against wavelength of known light source through glass viewport

The transmission through the glass viewport was observed to be 80% on average throughout the majority of the sensitive range, though this decreases sharply at a wavelength around 310 nm. This indicated that the viewport is constructed from typical window glass, which is known to block transmission of wavelengths below 300 nm, as opposed to pure quartz glass which can be transparent to all UV wavelengths. It was noted that the glass reduced transmission, particularly near to the 306 nm wavelength of interest for detection of OH. An alternative method was investigated to protect the spectrometer from the flame and avoid use of glass.

12.4.1 Optical Probe

The ceramic probe described in Section 5.5.3.1 was designed such that the thermocouple mount could be swapped for the spectrometer lens housing. Installing the lens into the end of the probe had a number of advantages; the glass barrier could be removed without gas or flame impingement on the lens; interference from outside light sources was avoided; and the probe could be inserted into the burner to adjust the optical depth. This allowed a clearer view of the centre of the flame by effectively removing the near-side edge of the flame from view and limiting the amount of incident light from the highly luminous combustion zone. Suction was not used during spectrometry tests.

12.4.2 Spectral Results

The flames observed were a propane-air flame using 20 L/min propane and 600 L/min air (ER=1.20) and a flame using 20 L/min propane, 140 L/min oxygen and 300 L/min steam (ER = 1.25).

Figure 12-5 shows spectra from two different flames in the same position. The wavelength range spans from 180 to 870 nm, with the visible spectrum shown for reference. The emissions are largely in the visible range and the average intensity is greater for the propane-oxygen-steam (POS) flame than the propane-air (PA) flame. The higher ER and less inert gas dilution resulted in higher flame temperatures and brightness for the POS case.

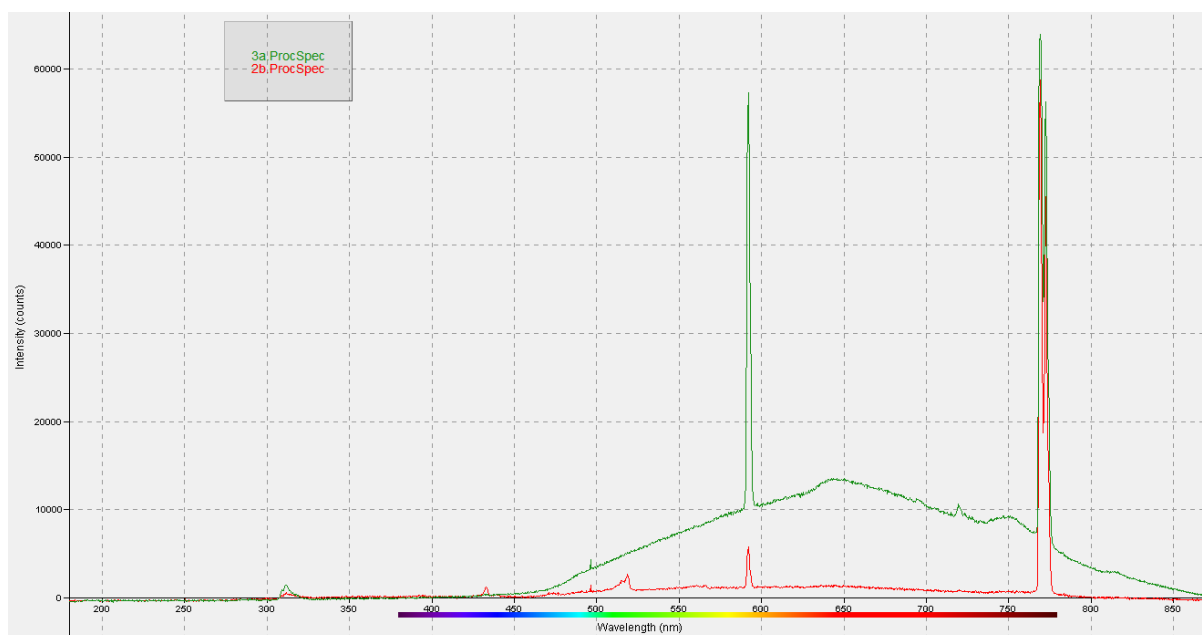


Figure 12-5: Spectra from (red) propane-air and (green) propane-oxygen-steam flames, collected with probe at outer position

The emission around 770 nm was initially weak when the flame was first ignited and grew in intensity as the burner warmed up, which is consistent with the red hot glow of the refractory within the burner. The peak at 590 nm correlates to yellow on the visible spectrum and was much more intense for the POS flame which was visibly brighter and yellow in colour.

Figure 12-6 shows a close up view of the region of interest for radical species emission. The CH and C₂ peaks at 431 and 516 nm were resolved quite clearly for the PA flame but less so for the POS flame. Conversely the OH peak at 306 nm approximately doubled in intensity in the POS spectrum. This is consistent with the additional water vapour added in the second flame, which may have suppressed the formation of CH and C₂ but promoted the formation of OH radicals. The peak at 494 nm present in both spectra could be associated to CH or possibly to atomic C.

The probe was subsequently moved to the mid insertion position, and spectra were collected for PA, POS and POS with coal flames. Gas flow rates were as above, with the coal addition made at 2 g/s.

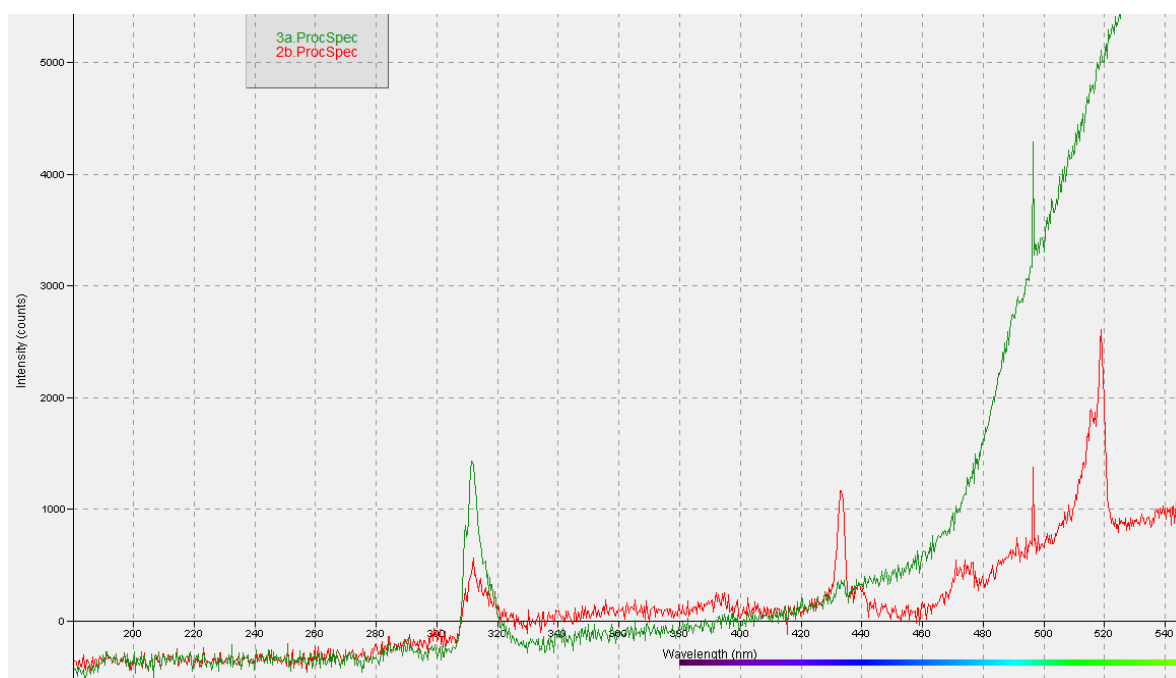


Figure 12-6: Close view of wavelengths up to 540 nm of Figure 12-5

It can be seen from Figure 12-7 that the PA and POS spectra are similar to those collected from the outer probe position in Figure 12-6. The radical peaks at 306, 431 and 516 are smaller with the probe at the mid position, with a reduced optical thickness giving less intense emission. The flame with coal addition is clearly the most luminous of the three with a higher baseline intensity across all wavelengths. The intensity across the visible range was too high to be properly resolved by the spectrometer. The OH emission peak at 306 nm is visible but the CH and C₂ emission peaks are not resolved on this spectrum. This may be due to the high baseline intensity which diluted these emissions however a small peak is visible at 405 nm which is considered to be the Comet-head C₃ emission system. Given the large addition of carbon to this flame this is not unexpected.

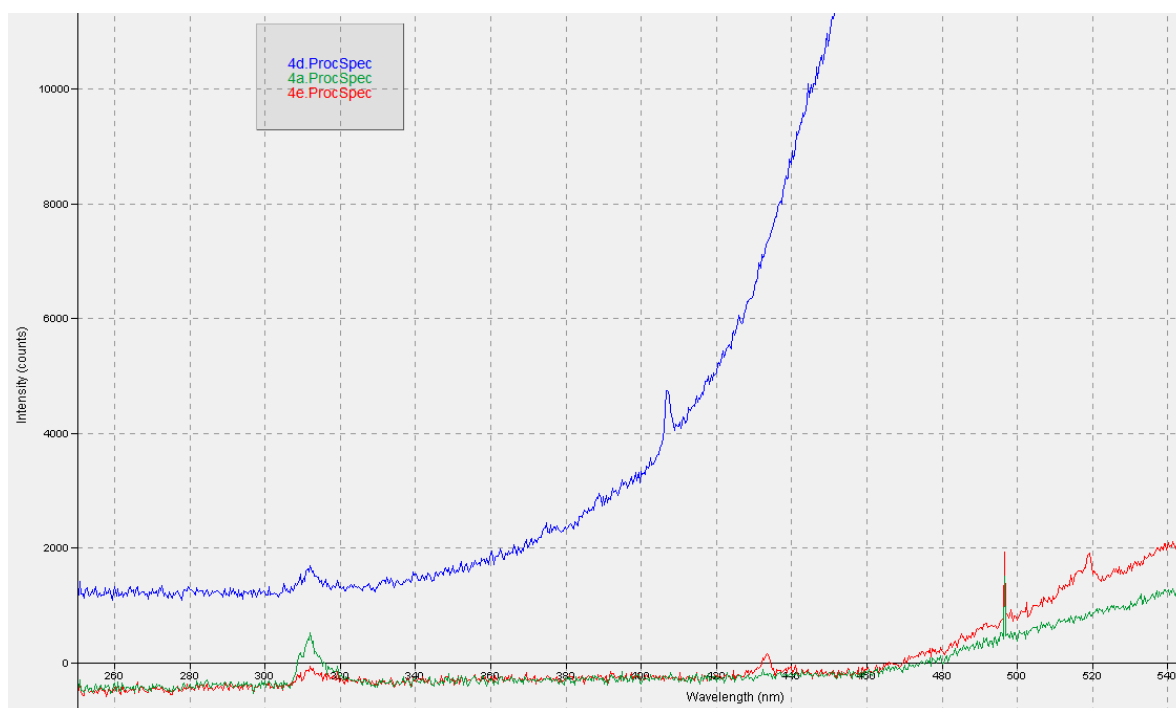


Figure 12-7: Spectra of (red) propane-air, (green) propane-oxygen-steam and (blue) propane-oxygen-steam-coal flames, collected with probe at mid position

12.5 Summary of Flame Analysis

The objective of this preliminary spectroscopy was to test the functionality of the optical analysis system in identifying significant species in the flame. In the simple propane-air flame this was successful; the expected peaks from radical species OH, CH and C₂ were identified beyond reasonable doubt. In the steam flame, CH and C₂ peaks were not visible. This may suggest that these species were no longer present in significant concentrations, or that their emission was masked by the greater background luminosity of the flame. The OH radical was found to emit at a low enough wavelength to stand out from the background flame emission. This peak was seen to increase in intensity with the combination of high steam loading and high temperature in the POS flame.

The findings of this investigation were limited to one position in the burner quarl, which was considered to be too close to the burner inlet to view the fully developed flame. Owing to the gasifier construction further measurement positions were not possible without installing additional viewports in the body, posing significant complexity and risk to the integrity of the gasifier. In future this investigation may be continued by installing the burner into a separate gasifier body which may afford greater optical access. More sophisticated flame imaging equipment, such as that developed at the University of Kent (Lu et al., 2004; Molcan et al., 2009) may be used for this purpose. An investigation of the flame region with highest concentration of radical species may indicate whether these species are prominent in the steam flame, as expected (Lewis, 2007) and how these affect gasification chemistry.

13 Appendix D - List of Publications

Conference Papers

Lakey, T.E., Sharifi, V.N., Swithenbank, J., 2016. *Entrained Flow Gasification of Coal and Biomass Char Using a Superheated Steam Flame*, in: Faaij, A.P.C., Baxter, D., Grassi, A., Helm, P. (Eds.), 24th European Biomass Conference and Exhibition, 6-9 June 2016, Amsterdam, The Netherlands. Amsterdam, NL, pp. 506–511

Oral Presentations

Entrained Flow Gasification of Coal and Biomass Char Using a Superheated Steam Flame, Postgraduate Research Conference, 29 June 2016, Sheffield, UK.

Entrained Flow Gasification of Coal and Biomass Char Using a Superheated Steam Flame, 24th European Biomass Conference and Exhibition, 6-9 June 2016, Amsterdam, The Netherlands.

Ultra Superheated Steam Gasification for Sustainable Hydrogen Production, University of Sheffield Engineering Symposium (USES), 24 June 2015, Sheffield, UK.

Sustainable Hydrogen Production, Yorkshire Postgraduate Festival, 3 July 2014, Leeds, UK.

Poster Presentations

Ultra-Superheated Steam Gasification for Sustainable Hydrogen Production, Postgraduate Research Conference, 10 June 2015, Sheffield, UK

Ultra-Superheated Steam Gasification for Sustainable Hydrogen Production, IChemE ChemEngDayUK, 8-9 April 2015, Sheffield, UK

Ultra Superheated Steam Gasification for Sustainable Hydrogen Production, University of Sheffield Engineering Symposium (USES), 24 June 2014, Sheffield, UK.

ENTRAINED FLOW GASIFICATION OF COAL AND BIOMASS CHAR USING A SUPERHEATED STEAM FLAME

Lakey, T. E., Sharifi, V. N., Swinbank, J.

Department of Chemical and Biological Engineering, University of Sheffield
 Mappin Street, Sheffield, S1 3JD. tom.lakey@sheffield.ac.uk

ABSTRACT. Biomass gasification has previously been shown to produce sustainable hydrogen rich syngas for power generation or chemical synthesis. Steam flames have the potential to combine very fast reaction rates with a reducing environment, to produce clean syngas within a short residence time. This work demonstrates the effectiveness of steam flames for rapid feedstock conversion of two high carbon feedstocks. A small scale entrained flow gasifier was used to compare gas yields from coal and a softwood biomass char with a high (~15%wt) ash content, which was produced as an industrial gasification by-product. It was found that the biomass char yielded higher concentrations of H₂ and CO in the product gas than the coal, considered to result from the higher reactivity of biomass char compared to coal. The biochar achieved high conversion in a single pass, while coal conversion was limited by the small size of the experimental reactor. No traces of tar deposition were detected on any apparatus when using coal or biomass char, and no ash sintering was observed in the high ash samples.

Keywords: biochar, coal, gasification, steam, waste

1 INTRODUCTION

The unsustainable nature of fossil fuels and slow implementation of renewable sources has spurred research into gasification for production of clean fuels. Gasification of carbonaceous materials such as coal and biomass with mixtures of steam and air has been shown historically to produce a synthetic gas or syngas rich in hydrogen (H₂) and carbon monoxide (CO). This gas can be combusted directly for power generation, used in chemical synthesis or upgraded into liquid fuels via the Fischer Tropsch process for transport applications [1,2].

More recently, the gasification of biomass and waste materials has received attention as a method for producing low carbon energy. A sustainable and cost effective method of production would allow hydrogen gas to be used as an energy vector, to be widely distributed for local electricity generation within cities and homes and benefiting from combined heat and power for maximum generation efficiency with minimal local emissions [3-5].

Much research into biomass gasification has focused on fixed bed and fluidised bed technologies. Fluid beds can handle variable quality feedstock with high throughput, but are more economical on a large scale. Fixed bed systems are economical on smaller scale but suffer from high tar production [6]. The production of tars from biomass feedstocks presents the single largest challenge in gasification commercialisation efforts [7,8]. Tar is generally understood to include largely aromatic organic species heavier than Benzene, produced from high temperature treatment of biomass [7,9]. These tars, condense on contact with reactor walls and heat transfer surfaces, causing fouling which requires costly clean up. Thermal cracking requires temperatures in excess of 1000°C to eliminate tar completely [9,10]. Steam is known to reduce high molecular weight hydrocarbons via steam reforming [11-13]. It is postulated that steam feedstocks could prove effective for converting problematic feedstocks if the concept can be proven.

The present work examines the novel application of superheated steam flames in an entrained flow configuration for syngas production in a small scale gasifier (Fig 1). Previous work has found steam flames to be combusted using a high concentration of radical species such as OH [14]. Together with the very high

temperatures, this produces an extremely reactive environment for gasification. Earlier tests with the original entrained flow gasifier system compared the performance of anthracite, bituminous coal and gas oil [15]. It was found that up to 40%wt hydrogen was produced in the dry product gas, though the degree of feedstock conversion was not reported.

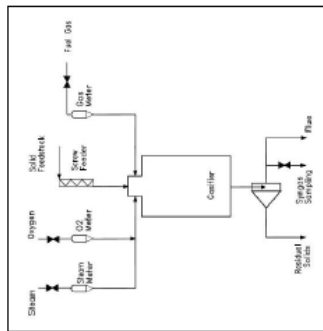


Figure 1: Schematic of steam flame gasification system.

Other works involving steam flame gasification have simulated fluidised bed systems. Data produced using Aspen Plus by T. B. Karim was cited for a model in which steam temperatures over 2200°C were achieved by supplying superheated steam to a burner together with methane and oxygen. The simulated gasification products comprised up to 40%wt H₂, 20%wt CO and 12-15%wt CO₂ on a wet basis [16]. While the assumption of adiabatic operation was not stated, the flame temperatures resemble those of a similar adiabatic, equilibrium steam flame combustion model [17]. This latter model highlighted the effect of sub-stoichiometric oxygen in steam flame generation, yielding reduced adiabatic flame temperatures and substantial

concentrations of H₂ and CO in the flame mixture. The model yielded over 50%wt H₂ in the product gas, though over half of this was present in the steam mixture before gasification of solids occurred. This can be misleading if comparing against gas yields from solid feedstock. This effect also contributed to the gas yields reported in [15].

For the present work the entrained flow experimental gasification system [15] was modified in order to compare biomass feedstock with coal (Fig 2). The aim was to compare the gas yield and feedstock conversion of charcoal against anthracite coal, using the highly reactive steam flame for a relatively short residence time. The steam flame mixture used in this work contained only minimal traces of H₂ and CO when no gasification feedstock was supplied, for easier comparison with other gasification technologies.

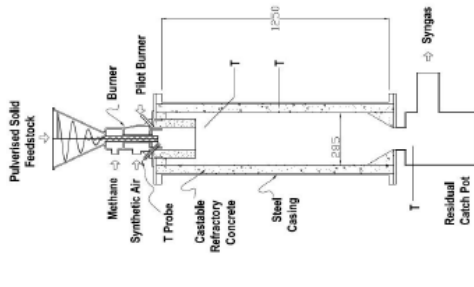


Figure 2: Diagram of gasifier showing inlets and outlets. Dimensions in mm. 'T' represents thermocouple location. Modified from [15].

2. MATERIALS AND METHODS

2.1 Experimental set up

A schematic diagram of the reaction system is shown in Fig 1, consisting primarily of a gasification chamber with a burner located in the top; fed by a steam generator, methane, oxygen and powdered feedstock from a hopper above the burner.

The gasifier consists of a downward facing burner within a cylindrical chamber of 285 mm inner diameter and 1250 mm long. The chamber is a steel shell lined with 50 mm high temperature cast refractory. The burner

is a dual fuel model modified to accept granulated solid feedstock together with fuel gas and oxidant. The burner is mounted in a cast alumina burner block ('quart') to stabilise the flame. Steam is produced by a saturated steam generator and superheated to around 140°C by rope heating elements before mixing with oxygen to produce a 'synthetic air' mixture. Solid feedstock is fed by a variable speed screw mechanism from a hopper above the burner. The powdered solid was introduced directly into the flame for maximum reaction rate and was carried through the reaction chamber by the gas flow. Below the chamber is a catch pot to collect the residual solids and a sampling point for the product gas, before the gas is vented via a flue line.

2.2 Feedstock materials

Two feedstock materials were compared in this work. The first was pulverised anthracite coal, chosen for its high fixed carbon content. The properties and sizing information are listed in Table 1. The second feedstock was a biomass char produced from mixed Larvian softwood species. This material was produced as a waste product from an existing commercial gasification plant, having been crushed complete with its bark and sand and treated at up to 1150°C, with the product gas used to fuel a combined heat and power application. This material is noted for its high ash content, which makes it unsuitable as a soil additive and difficult to treat in a fixed or fluid bed application due to risk of ash fusion caused by high concentrations of alkali metals in biomass ashes [18,19].

Table 1: Properties of feedstock materials

Property	Coal	Char
Proximate analysis, %wt (as received)		
Moisture	1.2	3.8
Volatile matter	13.2	14.1
Fixed carbon (FC)	82.9	67.4
Ash	2.7	14.6
Ultimate analysis, %wt (dry ash free)		
C	83.3	76.1
H	4.1	1.2
N	1.5	0.3
S	1.2	0.1
O (diff)	9.9	22.3
Heating value (as received)		
HHV, MJ/kg	32.1	22.4
Size (µm)	97% < 250 58% < 75	77% < 250 10% < 75

2.3 Experimental procedure

Steam and oxygen were mixed in equal parts and preheated to 120°C. This mixture was fed to the burner at a rate of 20 kg/hr to combust methane to produce the steam flame. The methane oxygen and steam flow rates were kept constant. The oxygen flow rate was set to ensure complete combustion of the fuel gas. A range of steam to carbon (S/C) ratios was achieved by varying the

Figure 13-1: Conference paper presented at EUBCE 2016

granulated solid feed rate as shown in Table II. The S/C takes into account H₂O from methane combustion as well as steam in the oxidant. Two runs were conducted for each condition. The differences in S/C ratio between the coal and char conditions are a result of the differences in carbon content (Table I) and volume density of the two materials. It was not possible to achieve identical carbon feeding rates due to limited operating range of the feeding mechanism.

Table II: Experimental conditions; A= anthracite tests, C= softwood char tests

	A1	A2	A3	C1	C2	C3
Solid feed rate (kg/hr)	3.7	5.2	6.2	3.7	4.3	5.1
S/C ratio (molar)	3.3	2.4	2.0	3.9	3.1	2.8

Once a stable steam flame was established the solid feedstock was introduced via a screw feeder. Feedstock was entered by the gas flow down the reactor length and collected in the catch pot below the gasifier, while the cooled gas flow was monitored inside the gasifier at several points. A platinum R-type thermocouple was inserted at 45° from vertical into the centre of the flame zone within a removable ceramic probe. A K-type thermocouple was inserted below the burner quartz thermocouple at the gasifier exit was recorded using another K-type thermocouple. The reactor wall temperature was also recorded halfway along the reactor length.

The test duration was approximately five minutes after establishing stable reactor flows. Gas samples were pumped through a cold finger to condense moisture before feeding to an ABB PCC1000 online gas chromatograph, which monitored gas composition (H₂, O₂, N₂, CH₄, CO, CO₂). At the end of each experiment, the residual solids were collected from the catch pot and quenched cooled before being weighed and analysed. The moisture collected by the cold finger was also weighed to establish the moisture fraction in the gas and calculate the overall mass balance (Section 3.3). The internal of the gasifier and flow lines were periodically checked for any accumulation of material.

3 RESULTS AND DISCUSSION

3.1 Temperature distribution in gasifier

A steep temperature gradient was apparent in the gasifier due to the high peak temperatures within the flame zone, the narrow geometry and relatively thin walls leading to significant heat transfer through the reactor walls. Suction pyrometry was used to measure the temperature in the flame zone within the quartz (Fig. 2). This technique extracts hot gas through a ceramic probe past a thermocouple to give a more accurate temperature reading by minimising radiative heat losses. The temperatures recorded using this technique averaged around 1350°C for the conditions described without feedstock addition. Suction pyrometry was not conducted during the gasification experiments as the removal of hot gas and particles through the probe interfered with the gas composition and flow pattern inside the burner. The

same thermocouple without the gas suction probe registered average temperatures around 150°C lower, demonstrating the effect of radiative error in thermocouples at flame temperatures. With feedstock addition, the average temperature at this point was between 1100-1150°C.

The gas temperature in the reactor below the quartz was recorded between 900-1000°C during the experimental runs. This represents a drop of 1-200°C as the gases left the narrow burner quartz and entered the wider gasification chamber. Heat was absorbed during endothermic gasification reactions as well as being lost to the cooler reactor walls, primarily by convective heat transfer. To demonstrate the influence of the gasifier wall temperature on the experimental yield, run A1 was repeated at different wall temperatures. The temperature inside the wall of the gasifier was monitored midway along its length by a thermocouple inserted into the centre of the refractory layer and plotted in Fig 3, with the corresponding gas temperatures and product yield.

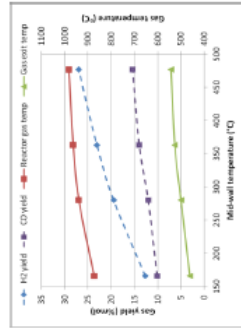


Figure 3: Gas temperature and yield with wall temperature.

The wall temperature was found to have substantial influence on the gas temperature and yield. This was considered to result from reduced heat transfer from the gas to the walls, and also the radiative interaction between the walls and the solid particles. Radiation from furnace walls is one of the major contributors to particle heating, proportional to temperature to the fourth power and particle emissivity [20]. The emissivity for black solids such as coal and soot particles is much higher than for gases, indicating that the effect of radiation on particle temperature is much greater than observed increase in gas temperature. This highlights the importance of furnace wall temperature in addition to the high gas temperatures involved in steam flame gasification.

3.2 Effect of S/C ratio

The product gas compositions are plotted against S/C in Figure 4. The balance of the gas compositions was made up of traces of oxygen and nitrogen resulting from residual air in the gasification chamber, as well as small traces of methane (~2%). Each condition was found to exhibit a high conversion of CO, primarily resulting from the balance (Section 3.3) around 69% of the observed CO₂ mass flow was estimated to originate from methane combustion.

This could be reduced by using recycled syngas to fuel the gasifier.

It was observed that reducing the S/C ratio, achieved by increasing the feedstock loading, had only a minor effect on the gas composition under the conditions tested. This was due to the small size of the gasifier giving a limited residence time which limited feedstock conversion. The small increase in H₂ and CO yields with increasing solid feed was a result of feedstock devolatilisation, which is a rapid process compared with char conversion. This is evidenced by the increasing the amount of residual unreacted feedstock collected after each test, shown in Table III.

Figure 4 shows that the softwood char consistently yielded higher H₂ and CO fractions compared to the coal feedstock, even with a lower carbon feed. This is due to the greater reactivity of biomass char than coal, which is a culmination of several factors including the material structure, surface area and the effect of mineral content. This is discussed in Section 3.4. In particular, the lower yields of CO₂ and solid carbon from biochar tests suggest the Boudouard reaction progressed to a greater extent than in coal tests, giving a greater yield of CO in the product.

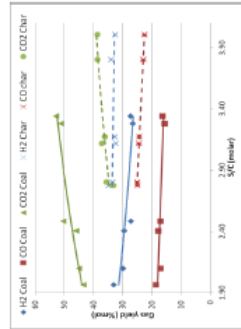


Figure 4: Dry product gas composition against S/C molar ratio. Solid lines represent coal tests, dashed lines from char tests

3.3 Mass and energy balances

The mass flow in the gasifier and products for each test are shown in Table III. The mass of residual solids was obtained from the total mass flow in the gas flow of gas. The mass flow in the gas flow and solids flows need to calculate the flows of moisture and dry gas. The moisture (H₂O) in each case exceeded that which was applied to the gasifier due to combustion of the carbon in the feed gas. From the combustion of 2.77 kg/hr of methane, up to 5.3 kg/hr mass is obtained assuming complete combustion to H₂O and CO₂.

This assumption can also give an estimate of the expected CO₂ flow in each test. For this test was estimated that at least 57% of the CO₂ in the product was produced from methane combustion. This could be compared to commercial systems by recycling syngas to provide heat to the flame, or recycling heat from the gasifier to reduce heating demand (see Fig 5). An energy balance was conducted using the mass flows from Table III. It was calculated that the calorific

value of the syngas produced from coal ranged between 5.3-6.6 MJ/Nm³. Coal conversion was more limited by the short residence time in the gasifier given its lower reactivity. This is confirmed by the amount of unreacted coal collected from the catch pot below the gasifier, which amounted to around 50% of the mass fed in each case. For the softwood char the syngas produced had a calorific value between 6.9- 8.1 MJ/Nm³. Conversion of the char was found to be more extensive than for coal, based on the higher CO yield and the fact that only around 20% of the feed mass was collected from the catch pot. Energy distributions for Runs A1 and C₁, with similar S/C ratios, are shown in Figure 5.

Table III: Mass balances for coal tests (A1-3) and char tests (C1-3). Data is mean of two runs for each case.

	A1	A2	A3	C1	C2	C3
Mass in						
CH ₄	2.4	2.4	2.4	2.4	2.4	2.4
O ₂	10.5	10.5	10.5	10.5	10.4	10.4
Steam	10.0	10.5	10.3	10.8	10.1	10.7
Coal/char	3.7	5.2	6.2	3.7	4.3	5.1
Total	26.6	28.5	29.5	27.4	27.2	28.5
Mass out						
Dry gas	13.0	14.1	14.7	16.6	16.1	17.8
Moisture	11.6	12.0	11.3	10.2	10.1	9.6
Residual solids	2.0	2.5	3.4	0.6	1.0	1.1
Total	26.6	28.5	29.5	27.4	27.2	28.5

Figure 5 highlights energy losses of around 30% of the energy input to the gasifier. These are primarily accounted for by heat losses from the gasifier wall. An estimate of heat transferred, q_c , can be made using Fourier's law of conduction through the wall of a hollow cylinder (Eq. 1);

$$q = 2 \pi k (T_i - T_o) / \ln(r_o/r_i) \quad (1)$$

Taking thermal conductivity of refractory, k , as 2.5 W/mK [15], T_i to be the mid-wall temperatures from Figure 3 and the outside surface temperature, T_o , to be around 150 K below T_i , as measured, the heat transfer through the refractory wall was estimated to be 23 kW. This also permits an estimate of the inside surface wall temperature to be made, calculated to reach up to 980 K. This heat transfer estimate equates to approximately 20% of the energy supplied to the gasifier during each experiment. This large value is due to the high temperatures produced in the flame, insufficient refractory wall thickness and the small volume of the gasifier. Other smaller system losses were found to result from small unreacted solid particles being entrained by the fine gas, and hence not accounted for in the 'PHV of solids' category. This demonstrates a compromise is required in selecting efficient particle size for this system. Smaller particles with larger total surface area provide increased reaction rate, however they stand a higher risk of being entrained and so cannot be recycled back into the system. A more comprehensive dust capture system would be necessary on a commercial system.

[18] Chan X, Tang J, Tian X, Wang L. Influence of biomass addition on Juncus cool ash fusion temperatures. *Fuel* 2015;160:14–20.

[20] Jones JM, Lee-Langdon AK, Ma L, Poutkashvina M, Williams A. *Poisons Generated by the Combustion of Solid Biomass Fuels*, vol. 4. Springer, 2014.

[21] Basu P. *Biomass Gasification and Pyrolysis: Practical Design and Theory*. Academic Press; 2010.

[22] Tsou S, Lee P-G. Hydrogen-rich syngas production through coal and charcoal gasification using microwave steam and air plasma torch. *Int J Hydrogen Energy* 2012;37:1095–100.

[23] Jones JM, Dervell LJ, Bridgeman TG, Poutkashvina M, Williams A. An investigation of the thermal and catalytic behaviour of potassium in biomass combustion. *Proc Combust Inst* 2007;31:1195–63.

[24] Nomakowaki DI, Jones JM, Byrdson RMD, Ross AB. Potassium catalysis in the pyrolysis behaviour of short rotation willow coppice. *Fuel* 2007;86:2388–402.

9 ACKNOWLEDGEMENTS

- This work was funded by the Engineering and Physical Sciences Research Council (EPSRC), UK.
- Thanks to Carbon Comfort Co. Ltd. for the provision of biomass char.

[5] McKenney P. Energy production from biomass (Part 3): Gasification technologies. *Bioresour Technol* 2002;83:35–63.

[2] Balar H, Kuray E. Hydrogen from biomass – Present scenario and future prospects. *Int J Hydrogen Energy* 2010;35:7416–20.

[3] Balar M. Potential importance of hydrogen as a future solution to environmental and transportation problems. *Int J Hydrogen Energy* 2008;33:4013–29.

[4] Srinivasan J. *Future Energy Challenges*. Acad. Publ., Helsinki Congr. Paistorni, Helsinki, Academy of Finland; 2013.

[5] Mirza UK, Ahmad N, Hanjin K, Majeed T. A vision for hydrogen economy in Pakistan. *Renew Sustain Energy Rev* 2009;13:1111–5.

[6] Wang L, Weiler CL, Jones DD, Hanna MA. Contemporary issues in thermal gasification of biomass and its application to electricity and fuel production. *Biomass and Bioenergy* 2008;32:373–81.

[7] Ehtkaga A, Lopez G, Amano M, Bilboso J, Olazar M. Steam gasification of biomass in a conical spouted bed reactor with olive and γ-alumina as primary catalyst. *Fuel Process Technol* 2013;116:592–9.

[8] Nakamura S, Shirai U, Yoshikawa K, Kinano S. Biomass Gasification using the By-products. *Energy Procedia* 2015;75:200–13.

[9] Mills TA, Evans RJ, Abuzunglun N. NREL technical report - Biomass Gasifier "Tits". Their Nature, Formation, and Conversion. NREL/TP-570-25357. 1996.

[10] Schmidt S, Giesa S, Drochner A, Vogel H. Catalytic tar removal from bio syngas—Catalyst development and kinetic studies. *Chem Today* 2011;175:442–9.

[11] Shan Y, Yoshikawa K. Recent progresses in catalytic tar elimination during biomass gasification or pyrolysis—A review. *Renew Sustain Energy Rev* 2013;21:371–82.

[12] Wei L, Xu S, Zhang L, Liu C, Zhu H, Liu S. Steam gasification of biomass for hydrogen-rich gas in a free-fall reactor. *Int J Hydrogen Energy* 2007;32:24–31.

[13] Malahat MR, Goswami DY. An experimental study of hydrogen production by gasification of biomass in the presence of a CO₂ sorbent. *Int J Hydrogen Energy* 2007;32:2803–8.

[14] Lewis FM. Generation of an ultra-supersaturated steam composition and gasification therewith. United States Patent US00729483B2, 2007.

[15] Shaibani S. An innovative coal gasifier utilizing steam raised to ultra-high temperatures. *PhD Thesis*. University of Sheffield; 2005.

[16] Pei P, Kukuru M. Modelling of Ultra-Supersaturated Steam Gasification in Integrated Gasification Combined Cycle Power Plant with Carbon Dioxide Capture. *ES2008 Proc. 2nd Int. Conf. Energy Sustain. Vol.1, ASME*; 2008, p. 763–73.

[17] Xin F. *Mathematical Modelling of Ultra-Supersaturated Steam Gasification*. PhD Thesis. Ohio University; 2013.

[18] Fang X, Jia L. Experimental study on ash fusion characteristics of biomass. *Bioresour Technol* 2012;104:768–74.

5 REFERENCES

burner jets and gasifier inside surfaces, this was dry and non-sticky and easily removed by brushing or air blowing. It was not found to be detrimental to gasifier operation.

3.5 Industrial Applications

Production of syngas from solid feedstocks can extend their versatility. Fuel gas can be used for power generation in typical installations, or in gas engines for small scale applications, or upgraded to liquid fuels or other chemicals. Gas engines or combined cycle gas turbines have a much higher efficiency of generation compared to steam turbine systems alone.

Hydrogen gas has several advantages as an urban fuel for vehicles and buildings via gas engines or fuel cells, which could meet both electrical and heating requirements. The point-of-use emissions are only water vapour, and particulate emissions associated with hydrocarbon fuels are also avoided. This has the potential to vastly improve air quality in densely populated areas.

The present work demonstrates that conversion of biochar within a small scale gasifier can be achieved for energy recovery from low value waste materials. Such a system would be most suitable on an existing industrial site to make use of low pressure steam and industrial by-products at low cost. The produced syngas can be used to offset existing fuel requirements or used for local combined heat and power needs, to reduce carbon emissions and unburnt by-products or waste materials. On a commercial system the economics of the process would be improved by optimising the gasifier scale to reduce heat loss and using recycled syngas to fuel the flame, in order to make the system self-sufficient and remove fossil fuels from the process.

4 CONCLUSIONS

Coal and biochar feedstocks were successfully gasified in a small scale entrained flow system, despite the high ash content in the biochar. No detrimental effect on equipment was observed from the ash deposition, which was easily removed by brushing or compressed air. The biochar demonstrated higher conversion and yielded richer H₂ and CO concentrations than anthracite coal. This was due to the greater reactivity of biochar compared to coal, considered to result from differences in ash content. Further work is required to confirm the catalytic effect of biomass ash on char conversion.

The reactor wall temperature was found to have a strong influence on feedstock conversion, considered to be due to the radiative interaction between walls and solid particles. This was observed to have a greater impact on product composition than the S/C ratio within the range observed.

Overall, feedstock conversion was limited by the scale of the reactor. Heat transfer through the walls limited overall efficiency, due to high temperatures and limited wall thickness. A longer reactor would allow greater residence time for reactions such as the water gas shift to play a more significant role. This with further development to increase equipment size, this technology has the potential to produce syngas on a commercial scale.

3.4 Feedstock conversion

The coal feedstock was found to undergo limited conversion in the gasifier. The mass balance in Table III shows that around 50% of the solid feed was collected from the catch pot in each coal test, not including any material which was entrained by the gas flow. The residual coal from run A1 had a HHV of around 25.5 MJ/kg which is 79% of that of the coal bed. The fixed carbon (FC) content increased from 83% to 85%, indicating that the moisture and volatile components had reacted preferentially during the short residence time in the reactor.

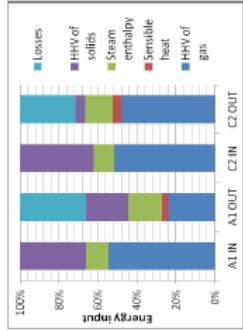


Figure 5: Energy distribution in and out of gasifier for runs A1 and C2. “HHV of gas” represents heating value of methane for infra or ultra-entrained “HHV of solids” refers to heating value of feedstock and residual solids from catch pot. “Sensible heat” includes the product gas and residual solids. “Losses” includes heat transfer through reactor wall and any entrained solids.

The char feedstock showed higher conversion than coal, with only around 30% of the feed collected in the catch pot. The C1 feedstock the highest feedstock conversion was observed, with a HHV of the residual char decreased by 53% to 11.9 MJ/kg in a single pass. The fixed carbon decreased from 87% to 60%, while the ash fraction increased from 15% to 40%, indicating high conversion. The gas yield from char was much richer in H₂ and CO than in the coal tests. These results indicate that biomass char more reactive than coal char, and biomass char reactivity is due to several factors including differences in structure and porosity. It has been previously demonstrated that the reactivity of biomass char increases with conversion, while for coal the opposite is true [21], which supports the present findings of greater biomass char conversion. A high FC ratio in the feedstock leads to a low reactivity char, requiring a greater residence time for equivalent conversion [22]. Another factor is the level of mineral content on char reactivity. Studies have demonstrated that inorganic elements, particularly potassium, have a catalytic effect on biomass densification and char burn-out, while demineralised samples exhibited very long burn-out times [23,24]. Based on these studies, the effect of the high ash content appears to be the dominant cause of greater reactivity of the biomass char compared to coal in the present work. Further investigation would be required to confirm the mechanism by characterising the mineral contents of the feedstocks. While ash deposition was observed on the



Chemical & Biological Engineering.

T. E. Lakey¹ (tom.lakey@shef.ac.uk)

Prof V. N. Sharifi¹

Prof J. Swithenbank¹

¹ Department of Chemical & Biological Engineering, University of Sheffield, UK

Ultra-Superheated Steam Gasification for Sustainable Hydrogen Production

1. Introduction

The unsustainable nature of fossil fuels and slow implementation of renewable sources has spurred research into biomass gasification for production of clean fuels. This work examines the novel aspects of Ultra Superheated Steam¹ (USS) flames using steam at around 1300°C for syngas production in a pilot scale gasifier.

The aim of this project is to explain how USS gasification can produce high concentrations of hydrogen and carbon monoxide as a clean application for coal, and increase the versatility of biomass and carbonaceous waste sources of energy.

2. Materials

Pulverised anthracite coal and Latvian softwood char from an industrial source were gasified to compare the product yields. Material properties are listed below.

Table 1: Feedstock properties

	Coal	Char
Gross CV (MJ/kg)	32.1	22.4
Moisture (%)	1.2	1.0
Volatile (%)	13.2	12.8
Fixed Carbon (%)	82.9	63.1
Ash (%)	2.7	23.1
Size (µm)	97% < 250 58% < 75	64% < 300 33% < 150



Fig 1: (above) coal, (below) char

3. Experimental Rig

The burner was fed with propane and a synthetic air mixture of oxygen and steam to create the USS flame. Feedstock was fed into the flame and entrained through the gasification chamber. Particles were removed before syngas analysis.



Fig 2: Photograph of gasifier rig

Gas inside the burner was sampled using the probe in Fig. 3, mounted at 45° in the burner roof at different insertion depths.



Fig 3: Photograph of burner probe

4. Computational Fluid Dynamics Simulation

CFD was used to predict gas composition and temperature around the burner with and without coal addition. Fig 4 shows H₂ distribution.

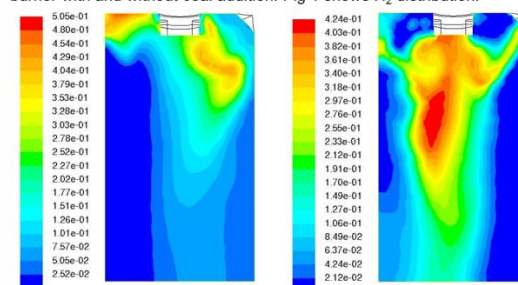


Fig 4: Molar concentration of H₂, (left) without coal; (right) with coal

5. Experimental Results

Table 2 shows gas yields from initial gasification tests. Runs I & II used coal, III & VI used char. ER = oxygen equivalence ratio.

Run No.	kg/hr			Coal/Char	Reactor Temp °C	ER	%mol				
	C ₃ H ₈	O ₂	H ₂ O				H ₂	O ₂	CH ₄	CO	CO ₂
I	3.3	15.0	14.7	6.9	1150	1.26	22.2	0.31	0.52	17.0	58.4
II	2.5	13.3	13.6	6.9	1000	1.48	17.6	0.92	1.29	14.7	63.7
III	2.8	13.3	11.5	3.3	900	1.30	19.6	0.32	1.25	19.9	57.5
VI	3.3	15.0	13.7	4.2	1050	1.26	26.5	0.26	0.85	22.8	48.6

Results of probe sample experiments are shown in Fig 5.

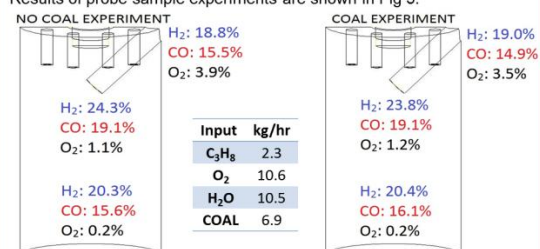


Fig 5: Molar gas composition at outer, mid and flue samples, (left) without coal, (right) with coal addition

6. Conclusions

- Char yielded a higher average syngas yield than coal.
- Greater syngas yields were obtained using higher reactant gas flows.
- The model over-predicted temperature and inlet H₂ fraction. Agreement between model and experimental results improved at lower positions.
- Tests without coal were richer in syngas than predicted, suggesting that propane-steam reforming inhibits propane combustion.
- Coal addition had little impact on gas composition, suggesting poor coal conversion.

7. Future Work

- Analysis of residual feedstock for carbon conversion fraction.
- Spectrometry used to measure distribution of radical species OH, CH and C₂ to investigate their roles in steam gasification.
- High volatile feedstock tested for comparison with high fixed carbon materials already analysed.

References

- Lewis, F.M., 2001. Generation of an ultra-superheated steam composition and gasification therewith. Patent US 7229483 B2

Acknowledgements

The authors would like to thank Carbon Compost Co. Ltd for the provision of softwood char, and EPSRC for project funding.



Figure 13-2: Poster presented at ChemEngDay UK 2015